Effects of exposure to tris (2-chloroethyl) phosphate (TCEP) on *ex ovo* chicken embryos

Ex ovo ニワトリ胚に対するリン酸トリス（2-クロロエチル）（TCEP）曝露の影響

Kazuki Kanda

2023

Table of contents

Ph.D. Dissertation 2023
Kazuki Kanda
Graduate School of Science and Engineering
Ehime University

ABSTRACT

Wild birds and their eggs are exposed to various artificial chemicals and contaminants, which places high demands on assessing chemical exposure and associated hazards. The OECD Test Guidelines have been established by the Organization for Economic Co-operation and Development (OECD) as an internationally recognized standard method for testing the safety of chemicals, which serves to assess the potential effects of chemicals on human health and the environment. However, all the OECD test guidelines for avian are for studies on adult and post-hatchling young birds and do not include studies investigating adverse outcomes on developing embryos. Therefore, we have established a novel avian embryo toxicity assay that applied a shell-less incubation method for avian embryos to the toxicity test. This test method allows temporal visualization of avian embryo development and facilitates assessment of chemical effects on the morphological changes and cardiovascular system during developmental stages. Chickens (*Gallus gallus domesticus*) were chosen as experimental animals because their genome has been fully sequenced, and eggs are readily available.

Organophosphorus flame retardants (OPFRs) are used widely in consumer and industrial products to delay the spread of fire after ignition and have been continuously increasing

because of the voluntary phase-out of traditionally used polybrominated diphenyl ether (PBDE) flame retardants. Tris (2-chloroethyl) phosphate (TCEP) is one of the pervasive OPFRs detected in the atmosphere, dust, river water, and biota, including tissues and eggs of wild birds. TCEP has been reported to have developmental toxicity, teratogenicity, neurotoxicity, carcinogenicity, reproductive toxicity, and effects on thyroid hormones based on *in vivo* or *in vitro* data. TCEP exposure to zebrafish embryos (3 to 120 hours post-fertilization (hpf)) induced embryonic development delay, vertebral deformity, and edema at 28,500 μg TCEP/L. However, even though TCEP has been detected in avian eggs, there are no studies regarding the effects of TCEP on avian embryos during the developing stage to the best of our knowledge.

The overall objective of this study is to assess the toxic effects of TCEP on avian embryos and to elucidate its molecular mechanisms. Fertilized chicken eggs were administered with low (50 nmol/g egg, TCEP-L), moderate (250 nmol/g egg, TCEP-M), and high (500 nmol/g, TCEP-H) doses of TCEP or 0.1% DMSO (vehicle control) into the air sac at Hamburger and Hamilton stage (HH) 1. After 56–60 hours of incubation, chicken embryos and internal content in eggs were transferred to shell-less incubation vessels to observe the development of chicken embryos. The first study focused on the phenotypic impact of TCEP exposure on *ex ovo* chicken embryos using a shell-less incubation system and the cardiac transcriptome using day nine hearts. Firstly, the survival rate, morphological biometrics (body length, head + bill length, forelimb

length, hindlimb length, and eye diameter), heart rate, heartbeat frequency, length and branch number of extraembryonic blood vessels, and gray value of the artery as an indicator of the number of circulating red blood cells were measured with ImageJ, an imaging analysis software, on incubation days 3–9. After collecting tissue samples, the carcasses were stained with alcian blue, and the length of the spine, bill + skull, humerus, radius, ulna, femur, and tibia were measured. The cardiac transcriptome analysis using day nine hearts was analyzed by RNA sequencing (RNA-seq) using Illumina Hiseq 2500. The total RNA solutions were pooled from three samples of each treatment group, control, TCEP-L, and TCEP-H. The log2 fold change values were calculated as the ratio of the gene expression level (FPKM; Fragments Per Kilobase of exon per Million mapped fragments) in a TCEP-treated sample to that in control. Genes with a log2 fold change value lower than -0.5 or higher than 0.5 in both TCEP-L and TCEP-H were defined as differentially expressed genes (DEGs) and further subjected to bioinformatics analyses. The gene ontology (GO) analysis, transcription factor enrichment analysis, protein-protein interaction (PPI) network analysis, and KEGG pathway analysis were carried out to predict biological processes affected by TCEP exposure. To confirm the expression levels of genes defined as DEGs by RNA-seq, the transcripts of Ca^{2+} transport-related genes (RYR2, CACNG4, CASQ2, and TRDN) and muscle filament sliding-related genes (MYL2, MYL3, MYL4, ACTC1, and TNNC1) were further quantified using qRT-PCR. Survival rates of TCEP-M and TCEP-H

were reduced from incubation day 3, the first day of observation, and were significantly reduced until day 9. This suggests that exposure to more than 250 nmol/g egg TCEP concentration poses a lethal effect on early-developing embryos. The body length was significantly shortened on days 3 and 4 in TCEP-M and days 4–9 in TCEP-H. The head + bill length was significantly reduced on days 3 in TCEP-L, days 3–8 in TCEP-M, and days 4, 5, 7, 8, and 9 in TCEP-H. The eye diameter was significantly decreased on days 4–8 in TCEP-M and days 4, 5, 8, and 9 in TCEP-H. As for the skeleton, the spine length was decreased in a TCEP concentration-dependent manner. These results suggest that TCEP exposure to more than 250 nmol/g egg induces a developmental delay in chicken embryos. The heart rate was significantly decreased on days 5 in TCEP-M and days 5–6 in TCEP-H. The heart weight to body weight ratio in embryos was significantly increased in TCEP-H. The length and branch number of extraembryonic blood vessels were significantly reduced on days 3 in TCEP-L and 3–4 in TCEP-M and TCEP-H. The digital gray value of the extraembryonic arteries as an indicator of the number of erythrocytes was significantly decreased on days 3–5 in TCEP-M and days 4–7 in TCEP-H. These results revealed that TCEP exposure induces cardiovascular dysfunction in chicken embryos. For the transcriptome analysis, the expression levels of 13378 genes were measured, and 812 genes were selected as DEGs based on the ratio of log2 fold change. GO analysis of DEGs predicted the effects on cardiac muscle contraction, ventricular cardiac muscle tissue morphogenesis, and

myoblast differentiation in the TCEP-treated chicken embryos, suggesting that altered expressions of cardiac muscle-related genes may trigger developmental and functional failures in the heart. Transcription factor enrichment analysis intimated that activation of NFKB1, SP1, SP3, SMAD4, GLI1, and CTNNB1 by TCEP exposure was a critical molecular initiating event. The investigations of KEGG pathways related to the PPI network and cardiac muscle contraction showed the dysregulation of genes related to Ca^{2+} transport and muscle filament sliding. The qRT-PCR analysis supported that the gene expression levels of RYR2 and MYL3 tended to be significantly decreased by TCEP exposure; a decrease in the expression levels of these genes may be responsible for the cardiovascular toxicity observed in chicken embryos.

The second study focused on the effects of TCEP on the cardiovascular transcriptome in *ex ovo* chicken embryos on day 5. We performed the cardiac transcriptome analysis by RNA-seq using Illumina NovaSeq 6000 system to understand the molecular mechanisms of cardiac effects caused by TCEP exposure in chicken embryos. Genes in which the TPM (Transcripts Per Million) of the TCEP-exposed groups were significantly different from that of the vehicle control (0.1 % DMSO) group were selected as DEGs and used for further analysis, such as biological function and pathway enrichment analyses. 34, 284, and 805 DEGs were found in TCEP-L, TCEP-M, and TCEP-H, respectively, and the number of DEGs increased in a TCEP concentration-dependent manner. 80% of DEGs were downregulated in TCEP-M and TCEP-H,

and the fold change of down-regulated DEGs tended to be TCEP-concentration dependent. Four GO terms associated with cardiac conduction were enriched in TCEP-M and TCEP-H groups. These GO terms contained seven genes: ATP binding cassette subfamily C member 9 (ABCC9), bridging integrator 1 (BIN1), calcium voltage-gated channel subunit alpha1 G (CACNA1G), catenin alpha 3 (CTNNA3), potassium voltage-gated channel subfamily E regulatory subunit 5 (KCNE5), Potassium inwardly-rectifying channel subfamily J member 2 (KCNJ2), and NK2 homeobox 5 (NKX2-5). NKX2-5, the transcription factor required for the development of the heart, is essential for vertebrate heart morphogenesis, myogenesis, and function. CACNA1G expresses calcium channels, while ABCC9, KCNE5, and KCNJ2 express potassium channels. In addition, several GO terms related to microtubule function, such as microtubule depolymerization, kinetochore-microtubule, and microtubule plus-end binding, were enriched in TCEP-M, and all genes involved in them were down-regulated. Microtubules transport calcium channels to BIN1-expressing regions of sarcolemma in cardiomyocytes. These results suggested that TCEP exposure causes a decrease in heart rate by reducing the expression of genes related to cardiac conduction and microtubule function. In the KEGG pathway enrichment analysis, we found that seven pathways were significantly affected, such as the regulation of the actin cytoskeleton, adherens junction, Wnt signaling pathway, and VEGF signaling pathway. Dysfunction of the actin cytoskeleton and adherens junction may have disturbed cardiomyocyte and heart morphogenesis

and induced an increase in heart weight to body weight ratio on day 9. Ingenuity Pathway Analysis (IPA) revealed 19 pathways commonly enriched in two or more TCEP-exposed groups. The epithelial-mesenchymal transition (EMT) pathway was notably affected, suggesting that TCEP exposure may suppress the EMT and inhibit cardiac development, which is supported by phenotypic observations, including decreased heart rate.

Furthermore, we measured mRNA levels of VEGF signaling-related genes in the embryonic vitelline membrane with extraembryonic blood vessels using a qRT-PCR to investigate the molecular mechanisms by which TCEP exposure inhibits vasculogenesis. Gene expression levels of fibroblast growth factor 2 (FGF2), vascular endothelial growth factor receptor 2 (VEGFR2), VEGFR3, VEGFC, hypoxia-inducible factor 1 alpha subunit (HIF1A), AKT serine/threonine kinase 1 (AKT1), phosphatidylinositol-4,5-bisphosphate 3-kinase catalytic subunit alpha (PIK3CA), and Rac family small GTPase 1 (RAC1) were significantly decreased in a TCEP concentration-dependent manner. These results suggest that TCEP exposure suppresses the vasculogenesis of extraembryonic blood vessels by downregulating these genes involved in the VEGF signaling pathway.

The third study focused on the effects of TCEP exposure on the epithelial-mesenchymal transition (EMT) in early-developing chicken embryos. Epithelial-Mesenchymal Transition (EMT) is a morphogenetic process in which cells lose epithelial characteristics such as cell

polarity and cell-cell adhesion and gain mesenchymal properties such as migration and invasion. During the gastrulation of the chicken embryo HH 4, a part of the epithelial cells forms the mesoderm by EMT. The mesoderm cells are differentiated into cardiomyocytes, hematopoietic cells, and endothelial cells that form blood vessels. In this study, to investigate whether TCEP exposure affects EMT during gastrulation of the chicken primitive streak, we measured the expression of genes involved in EMT and mesoderm in TCEP-exposed chicken embryos HH4 by qRT-PCR. Fertilized chicken eggs were treated with 50, 250, and 500 nmol/g of TCEP (TCEP-L, -M, and -H, respectively) or DMSO at day 0 (HH1). After 18 hours of incubation, HH4 chicken blastoderms were sampled, and qRT-PCR analysis was performed to measure the expression of EMT- and mesoderm-related genes (n=12/group). SNAI2 expression, a transcription factor in EMT, was significantly decreased in all TCEP exposure groups (TCEP-L, $p < 0.01$; TCEP-M, $p < 0.01$; TCEP-H, $p < 0.001$). Gene expression of TBXT (Brachyury) and TBX6, the mesoderm marker, were also significantly decreased in a TCEP exposure concentration-dependent manner. Interestingly, there was a significant positive correlation between SNAI2 and TBXT in mRNA levels ($r = 0.96$). These results suggest that TCEP suppresses EMT and delays mesoderm cell differentiation. The TCEP-H group showed increased expression of E-cadherin ($p < 0.05$) and decreased expression of N-cadherin ($p < 0.05$). Epithelial cells express E-cadherin, whereas mesenchymal cells express N-cadherin. E-cadherin expression is directly repressed by SNAI2

binding to the promoter of E-cadherin in EMT. Thus, the suppression of EMT by TCEP exposure was also supported by the altered E- and N-cadherin expressions. Among FGF signaling-related genes, FGF4 expression was significantly downregulated by TCEP exposure (TCEP-L, $p < 0.05$; TCEP-M, $p < 0.01$; TCEP-H, $p < 0.01$), and the relationship of the gene expression between FGF4 and SNAI2 ($r = 0.96$), and FGF4 and TBXT ($r = 0.94$) were significantly positively correlated. In contrast, the gene expression levels of FGF8 and FGFR1 were unchanged by TCEP exposure. FGF signaling plays a role in SNAI2-mediated EMT regulation and TBXT-mediated mesodermal induction. Therefore, the downregulation of FGF4 by TCEP may trigger the repression of SNAI2 and TBXT expression. WNT3A expression significantly increased in a TCEP exposure concentration-dependent manner ($p < 0.05$). Since the epiblast mesoderm is induced by coactivation of the FGF and Wnt signaling pathways, the increased WNT3A expression may be due to feedback regulation of FGF4 downregulated by TCEP exposure. This study found that TCEP decreased FGF4 expression and suppressed EMT progression and mesoderm cell differentiation in chicken gastrulation.

Altogether, TCEP exposed to HH1 chicken fertilized eggs suppressed EMT and interfered with mesoderm differentiation on HH4 (18–19 hours) chicken primitive streaks. Chicken embryos were consequently induced by TCEP exposure with growth retardation, reduced heart rate due to suppression of cardiac developmental transcription factors and downregulation

of cardiac conduction, and inhibition of vasculogenesis due to inhibition of FGF and VEGF signaling on HH19 (day 3) to HH35 (day 9).

ACKNOWLEDGEMENTS

First and foremost, I would like to express my deepest gratitude to my supervisor Prof. Hisato Iwata for his grateful guidance and advice on ecotoxicology in conducting this research. I am also grateful to Dr. Eun-Young Kim, Dr. Tatsuya Kunisue, Dr. Kei Nomiyama, and Dr. Mari Ochiai for their valuable and helpful advice. I am also deeply thankful to Mr. Shohei Ito and Mr. Dong-Hee Koh, who helped me with the exposure and shell-less incubation experiments.

I am deeply grateful to Mr. Yutaka Tahara and Mr. Katsuya Obara, developers of the novel shell-less culture system, for their generous technical advice on maintaining the survival rate of shell-less chicken embryos. I would like to extend my sincere thanks to my lab members, Dr. Hoa Thanh Nguyen and Dr. Mirella Kanerva, who helped me conduct transcriptome analysis and other experiments. I also want to offer my special thanks to all other Environmental Toxicology Lab members for their friendly encouragement over the years.

I would like to acknowledge the financial support from the Japan Society for the Promotion of Science (JSPS) through the Grant-in-Aid for JSPS Fellows [No. 21J15552], which was given to me. I also would like to acknowledge the financial support by Grants-in-Aid for Scientific Research (S) [No. 26220103] and Challenging Research (Exploratory) [No. 19K22912] from JSPS, which were given to Prof. Hisato Iwata. This study was also supported by the Ministry of Education, Culture, Sports, Science and Technology, Japan (MEXT), to a project on Joint Usage/Research Center – Leading Academia in Marine and Environmental Research (LaMer).

This research was also supported by the National Research Foundation of Korea (NRF) Grant (2016R1A2B4007714 and 2019R1A2C1084556) from the Ministry of Education, Science and Technology, Korea and by the Environmental Health R&D Program Grant (H117-00137-0702) from the Ministry of Environment, Korea, which were given to Prof. Eun-Young Kim.

Chapter I

Background and Introduction

1.1 Avian toxicity test assessment

Avian species are one of the most ecologically important groups of vertebrates and are distributed worldwide. Avian species are sensitive to environmental changes and generally occupy high trophic levels. Thus, avian species are sensitive indicators of aquatic and terrestrial ecosystem health. Historically in ecotoxicology, many researchers have studied birds for persistent organic pollutants (POPs), with reports continuing to follow since 2000 (Hao et al., 2021). It is known that developing vertebrate embryos, including birds, are extremely sensitive to exposure to environmental pollutants and artificial chemicals, such as endocrine disruptors (Diamanti-Kandarakis et al., 2009). These chemical's exposure during the early developmental stages can disrupt the normal pattern of tissue development and function through altered epigenetic programming (Haugen et al., 2018; Schug et al., 2011). Hence, the hazard assessment of these chemicals during the developmental stages of birds is necessary. The Organisation for Economic Co-operation and Development (OECD) Test Guidelines, the internationally accepted test guidelines for acute adult exposure to birds, are costly and time-consuming (OECD, 2016). Over several decades, the *in ovo* exposure tests as an alternative approach has been commonly used to assess embryotoxicity in birds (Peden-Adams et al., 2009). In addition, toxicity studies

have been performed combining the *in ovo* exposure testing and omics analysis, coupled with recent advances in toxicogenomics, molecular biology, and bioinformatics (Jiahua Guo et al., 2018). Omics analysis is useful for elucidating the adverse outcome pathway (AOP), a conceptual construct that allows for the integration of information spanning from effects at molecular levels to adverse outcomes at the organism level (Brockmeier et al., 2017). However, *in ovo* exposure tests can only investigate phenotypic effects at one point in the chick's life after hatching, resulting in few measurable endpoints and limited adverse outcomes, which are important events in AOP (Farhat et al., 2013; Jiahua Guo et al., 2018). On the other hand, the *ex ovo* experiment allows chronologically *in situ* observation and measurement of many phenotypic endpoints. Therefore, it is very useful to establish *ex ovo* exposure testing methods for chemicals.

1.2 *Ex ovo* culturing

Ex ovo culturing for avian embryos can apply to various fields of basic research, such as developmental biology, embryo manipulation, tumor biology, and regenerative medicine (Cloney and Franz-Odendaal, 2015; Coleman, 2008; Nowak-Sliwinska et al., 2014; Ribatti, 2014). *Ex ovo* culture is a system in which the original eggshell is removed, and the embryos are transferred to a new cultural environment, such as a surrogate eggshell and artificial incubation vessel (Borwornpinyo et al., 2005; Huang et al., 2015; C. Liu et al., 2012). Embryogenesis can be observed *in situ* (Fig. 1.1), and surgical operations such as transplantation and tumorigenesis can

be performed (Dohle et al., 2010; Zijlstra and Lewis, 2012). For example, the chicken embryo's chorioallantoic membrane (CAM), the vascular membrane responsible for gas exchange, develops at 4-5 days of incubation, and the CAM provides a platform for investigating the mechanisms of tumor vasculature formation (Pink et al., 2012). Chicken (*Gallus gallus domesticus*) has been mostly used for ex ovo culturing due to the fully sequenced genome, well-established husbandry method, and high availability with low cost in poultry markets (Sukparangsi et al., 2022). The development of chicken embryos generally can be divided into three phases: fertilization to blastoderm formation (systemI; days 0–1), embryogenesis (system II; days 1–3), and embryonic growth (system III; days 4–21) (Perry, 1988). Chicks then hatch on approximately day 21 of incubation. The developmental stage of the chicken embryo at the beginning of ex ovo culture, i.e., when the embryo is transferred to the culture environment, is key, as it causes significant changes in survival rates. The survival rate of chicken embryos transferred to artificial incubation vessels at Hamburger and Hamilton stage (HH) 15–16 was 92% until day 17, while the survival rate of chicken embryos transferred to artificial incubation vessels at HH13–14 was 0% on day 8 (Hamburger and Hamilton, 1992; Tahara and Obara, 2014). In the surrogate eggshell culture system, chicken embryos transferred at system III to turkey, guineafowl, and duck surrogate eggshells had survival rates of 55.3, 47.9, and 19.1%, respectively, on day 14. And hatchability rates were 55.3, 47.9, and 19.1%, respectively (C. Liu et al., 2012). However,

although the surrogate eggshell culture method allows observation of the chick embryo through a small eggshell window, it is difficult to observe the entire extraembryonic blood vessel formation. Transparent artificial eggshells using polydimethylsiloxane (PDMS) and polycarbonate (PC) allow observation of embryonic development and extraembryonic vessel formation on days 4-7 (Huang et al., 2015). However, these cubic artificial culture vessels were not readily available, and no data on the survival rate of chicken embryos after day 7 of incubation. Tahara and Obara (2014) established a novel *ex ovo* culture method, "a shell-less culture system," that can yield a higher survival rate. This method develops chicken embryos in polymethylpentene film with calcium lactate and distilled water; these materials are low-cost and easily available. In this shell-less culture system, Chicken embryos are preincubated for 56 hours (system II, HH15–16) and then transferred to artificial incubation vessels. The survival rate of chicken embryos on day 17 of culture was 92%, and the hatchability rate was 57.1% using the shell-less culture system (Tahara and Obara, 2014). This *ex ovo* culture method can maintain a high survival rate of chick embryos, leading to high reproducibility in chemical toxicity testing.

1.3 Organophosphorus flame retardants (OPFRs)

Organophosphorus flame retardants (OPFRs) are chemicals added to materials, including furniture, textiles, electronics, and polyurethane foams, to delay the spread of fire after ignition (EFRA, 2007). Regarding flame retardants (FRs), mainly brominated flame retardants

(BFRs), such as polybrominated diphenyl ethers (PBDEs), have been commonly used worldwide. However, due to their persistence, bioaccumulation, long-range transport, and adverse outcomes to organisms, PBDEs, including pentaBDE, octaBDE, and decaBDE, have the criteria of the Stockholm Convention on persistent organic pollutants (POPs) and have been included in the list of banned chemicals during 2009 to 2017 (http://www.pops.int/) (POPRC, 2015). Therefore, OPFRs, which have already been used for over 150 years, are considered suitable alternatives for BFRs, and the usage of OPFRs has increased (Reemtsma et al., 2008; van der Veen and de Boer, 2012). Global consumption of FRs in 2017 was 2.53 million tons, of which more than 30% were OPFRs. OPFRs accounted for 11% of total FR consumption in 2008, which means that the share of OPFRs in total FR consumption increased by 21% over about ten years (Wang et al., 2020). OPFRs whose structures vary depending on different ester linkages are classified as halogenated alkyl, non-halogenated alkyl, and aryl phosphates according to different substituents. Halogenated alkyls include chlorinated organophosphate esters (Cl-OPEs) such as tris (2-chloroethyl) phosphate (TCEP; CAS No. 115-96-8), tris (1,3-dichloropropyl) phosphate (TDCIPP; CAS No. 13674-87-8), and tris (1-chloro-2-propyl) phosphate (TCIPP; CAS No. 13674-84-5) (Fig. 1.2 and 1.3). Non-halogenated alkyls have tris (2-butoxyethyl) phosphate (TBOEP; CAS No. 78-51-3), while aryl phosphates have triphenyl phosphate (TPHP; CAS No. 115-86-6) and tricresyl phosphate (TMPP; CAS No. 1330-78-5) (Fig. 1.3). Even though OPFRs are used worldwide in a

wide range of applications, and as additives, these compounds are spread into the environment via volatilization, leaching, and abrasion due to no covalent or other chemical bonding with the product to which it is added (Marklund et al., 2003). OPFRs have been detected ubiquitously in various environmental matrices and biota, the atmosphere (Rauert et al., 2018; Saini et al., 2020; Wong et al., 2018), indoor dust (Brits et al., 2019; van den Eede et al., 2011; Wei et al., 2015), wastewater (Meyer and Bester, 2004), drinking water (Bacaloni et al., 2007; Khan et al., 2016), surface water (Guo et al., 2017; Rodil et al., 2012), foods (Gbadamosi et al., 2022), fishes (Kim et al., 2011; Sundkvist et al., 2010), human breast milk (Chen et al., 2021; Kim et al., 2014; Sundkvist et al., 2010), placenta (Ding et al., 2016), and urine (Ding et al., 2019; Hou et al., 2020). A pilot study was launched in 2018 to measure the levels of different classes of flame retardants in the atmosphere in megacities and major cities across the globe by the Global Atmospheric Passive Sampling (GAPS) network operating in five United Nations regional groups across the world. OPFRs dominated the profile at all sites with 2–5 orders of magnitude higher total concentrations than other targeted FRs such as PBDEs and new flame retardants, including Bis(2-ethyl-1-hexyl)tetrabromophthalate (BEHTEBP) (Saini et al., 2020). Furthermore, since OPFRs have been detected in various wild birds' tissues, feathers, and eggs (Greaves and Letcher, 2014; Kerric et al., 2021; Monclús et al., 2022; Verreault et al., 2018; Xie et al., 2022), it is crucial and urgent to assess the toxic effects of OPFRs on birds and avian embryos.

1.4 Tris (2-chloroethyl) phosphate (TCEP)

TCEP (CAS No. 115-96-8) is one of the pervasive OPFRs used in polyurethane foams and is mainly used in liquid unsaturated polyester resins, textiles, and furniture (Marklund et al., 2003; WHO, 1998). TCEP has a log Kow of 1.63-1.7 (Fu et al., 2021; Hou et al., 2016), which is highly hydrophilic compared to other OPFRs and has a long half-life in water ($t_{water,1/2}$; 2904 h) (Zhang et al., 2016).

1.5 TCEP concentrations in wild birds

The liver of glaucous gulls (*Larus hyperboreus*) breeding in the Eastern Canadian Arctic (Cape Dorset, Nunavut) were contaminated with 2.21 ± 2.73 ng/g ww of TCEP (Verreault et al., 2018). TCEP of 9.0 ± 2.7 ng/g dw and 6.04 ± 2.89 ng/g dw were detected in the feathers of Eurasian eagle owls (*Bubo bubo*) in Norway and cinereous vulture (*Aegypius monachus*) in Sierra Guadarrama Madrid (Spain), respectively (Monclús et al., 2022, 2018). In addition, several reports have measured the concentration of OPFRs in wild bird eggs. TCEP was detected in the eggs of night herons (*Nycticorax nycticorax*), little egrets (*Egretta garzetta*), and Chinese pond herons (*Ardeola bacchus*) at 3.34, 3.87, and 3.05 ng/g ww, respectively, in Southwest China (Huang et al., 2019). Guo *et al*. also reported that TCEP was detected at 3.27 ng/g ww in the egg of bald eagles (*Haliaeetus leucocephalus*) in the state of Michigan (Jiehong Guo et al., 2018). Another study has also investigated TCEP contamination in the egg yolk (1.38 + 0.31 ng/g ww)

and albumen (1.46 + 0.77 ng/g ww) of herring gulls (*Larus argentatus*) from a Lake Huron colony site, Laurentian Great Lake of North America (Greaves and Letcher, 2014).

1.6 Toxic effects of TCEP

The acute oral LD_{50} for TCEP was reported to be 1.23 g/kg body weight (4.31 μmol/g body weight) following a 30-day observation period in rats (WHO, 1998). While four of 18 adult White Leghorn chickens exposed to 14,200 mg/kg body weight (49.74 μmol/g body weight) TCEP died within six weeks of the first dose, the LD_{50} of TCEP for avian embryos is unknown (Sprague et al., 1981). TCEP has been categorized as a compound of high toxicological concern among 62 flame retardant chemicals based on in vivo and in vitro toxicity data (Bajard et al., 2019). TCEP has been reported to have some adverse outcomes, including developmental toxicity, reproductive toxicity, carcinogenicity, and endocrine disruption at cellular and organismal levels. TCEP exposure at concentrations (0.1–10 mg/L) that were not cytotoxic to H295R cells, a human adrenocortical carcinoma cell, significantly increased testosterone (T) and 17β-estradiol (E2) concentrations and upregulated the expression of four major steroidogenic genes (CYP11A1, CYP11B2, CYP19A1, and HSD3β2) (X. Liu et al., 2012). TCEP (22 ng/g kestrel/d) fed to adult male American kestrels (*Falco sparverius*) for 21 days significantly increased plasma-free triiodothyronine (FT3) (57%) and plasma-free thyroxine (FT4) levels (96%) (Fernie et al., 2015). Exposure to high concentrations of TCEP (14,250 and 28,500 μg/L) has been reported to cause

vertebral deformity, edema, immature spine, and delayed development in zebrafish embryos (3 to 120 hpf) (Wu et al., 2017).

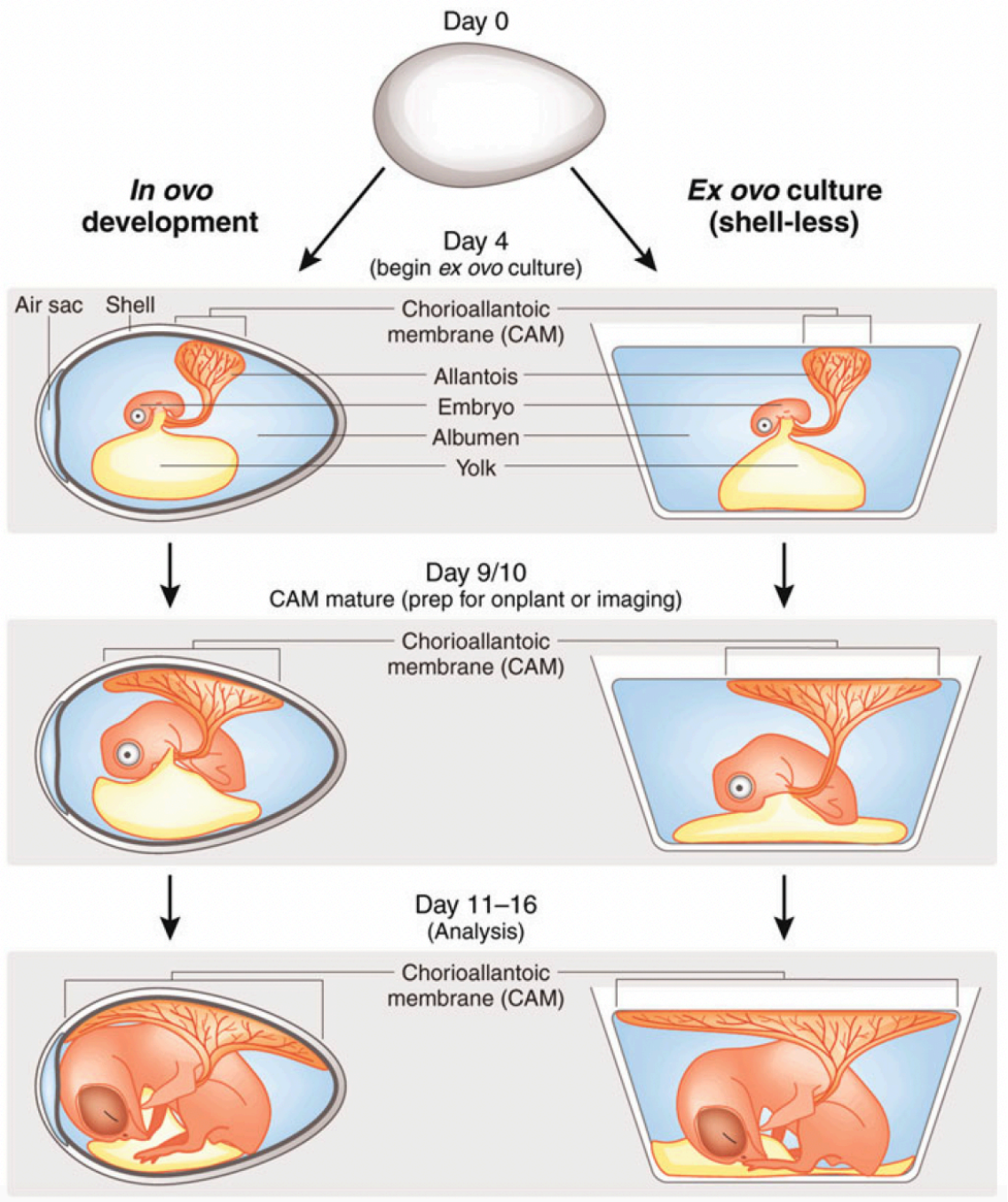

Figure. 1.1 The schematic representation of a comparison of *in ovo* and *ex ovo* chicken embryo development (adopted from Zijlstra and Lewis, 2012).

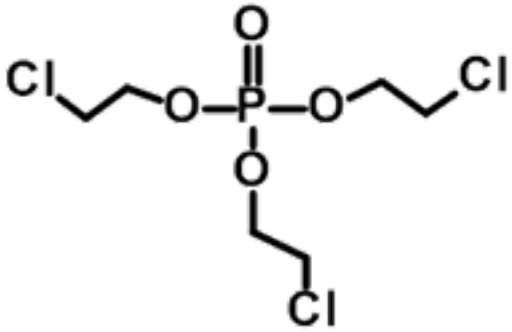

Figure. 1.2 Structural formulas of tris (2-chloroethyl) phosphate (TCEP).

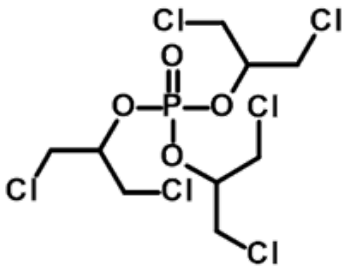

Tris (1,3-dichloropropyl) phosphate
(TDCIPP)

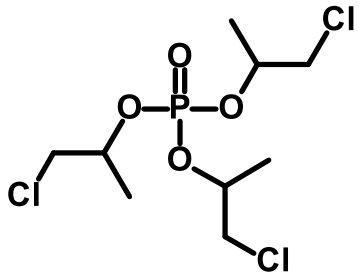

Tris (1-chloro-2-propyl) phosphate
(TCIPP)

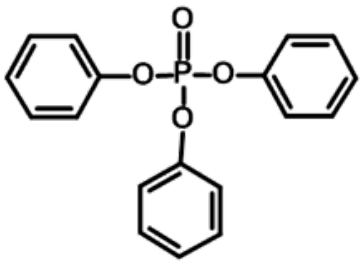

Triphenyl phosphate
(TPHP)

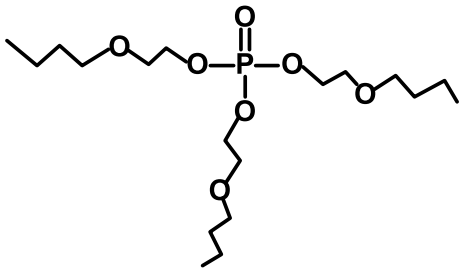

Tris (2-butoxyethyl) phosphate
(TBOEP)

Figure. 1.3 Structural formulas for other typical OPFRs

CHAPTER II

Effects of tris (2-chloroethyl) phosphate (TCEP) on the multiple phenotypes and cardiac transcriptome in *ex ovo* chicken embryos

2.1 Abstract

To uncover the phenotypic effects and its molecular mechanisms of action of tris (2-chloroethyl) phosphate (TCEP) on avian embryos, chicken embryos were exposed to low (50 nmol/g egg; TCEP-L), moderate (250 nmol/g egg; TCEP-M), and high (500 nmol/g egg; TCEP-H) doses of TCEP or Vehicle control (DMSO) from day 0 to day 9 (Hamburger and Hamilton stage (HH)1–35). Chicken embryos were observed upon shell-less incubation vessels on days 3 to 9, and 11 phenotypic endpoints were measured by image analysis with ImageJ. Embryos were dissected on day 9, and their body weight, heart weight, and liver weight were measured, and then the carcasses were stained with alcian blue, and the skeleton length was measured with ImageJ. The RNA-sequencing (RNA-seq) for the cardiac transcriptome was analyzed using an Illumina HiSeq 2500 system to identify differentially expressed genes (DEGs) by TCEP exposure. To confirm the expression level of genes defined as DEGs by the next-generation sequencing (NGS) analyses, the transcripts of Ca^{2+} transport-related genes (RYR2 CACNG4, CASQ2, and TRDN) and muscle filament sliding-related genes (MYL2, MYL3, MYL4, ACTC1, and TNNC1) were further quantified by real-time PCR.

The survival rates started to be greatly reduced from day 3 of incubation and were significantly decreased until day 9 in TCEP-M and TCEP-H groups. Morphological biometrics of chicken embryos were significantly decreased from days 3 to 9 in the TCEP-exposed group suggesting the TCEP exposure induced developmental delay in chicken embryos. The body weight was significantly decreased on day 9 in all TCEP-treated groups, and the ratio of the heart weight to the body weight was significantly higher in TCEP-H. The heart rate was significantly reduced in the TCEP-exposed group on days 4–7, and total extraembryonic vessel length and branches were reduced on days 3–4. These results revealed that TCEP exposure leads to cardiovascular dysfunction in chicken embryos. The transcriptome analysis measured the expression levels of 13378 genes using day nine heart in chicken embryos, and 812 genes were sorted as DEGs based on the ratio of $\log_2$ fold change. The GO enrichment analysis significantly affected GO terms of the cardiac muscle contraction, the ventricular cardiac muscle tissue morphogenesis, and the myoblast differentiation ($p < 0.05$). These results suggested that TCEP exposure altered expressions of cardiac muscle-related genes and may trigger developmental and functional failures in the heart. qRT-PCR analysis in the heart of day nine chicken embryos supported that the gene expression levels of RYR2 and MYL3 were significantly decreased in a TCEP concentration-dependent manner, suggesting that these downregulated genes may be responsible for the cardiovascular toxicity observed in chicken embryos.

2.2 Introduction

OPFRs have been increased usage as alternate flame retardants because brominate flame retardants such as PBDEs were voluntarily phased out (Reemtsma et al., 2008). TCEP is not chemically bonded to the products, resulting in an environmental release. TCEP has been detected worldwide in fish and wild bird eggs (Xie et al., 2022). A previous study reported that TCEP exposure to zebrafish embryos at 0.8–100 μg/L significantly increased morphological abnormalities, including pericardial edema, spinal curvature, yolk sac edema, and tail deformity (Wang et al., 2022). The toxicity of the TDCIPP and TCIPP, the Cl-OPEs, on avian embryos have been reported in ovo toxicity tests using chicken eggs (Farhat et al., 2013). 51,600 ng/g egg (158 nmol/g egg) TCIPP significantly reduced tarsus length in hatched chicks (days 20–22 of incubation). In addition, 45,000 ng/g egg (104 nmol/g egg) TDCIPP significantly reduced body weight and shortened head + bill length in hatched chicks (days 20–22 of incubation) (Farhat et al., 2013). Therefore, TCEP may also be developmentally toxic to avian embryos. However, to our knowledge, there are no studies regarding the effects of TCEP on avian embryos, and the molecular mechanisms of the toxic effects reported so far are unclear.

In "*in ovo*" exposure tests to avian embryos, *in situ* observation is difficult since avian embryos develop within non-transparent eggshells. Many efforts have thus been devoted to developing the shell-less incubation system for avian embryos. The egg contents are placed into

a plastic container that can observe the embryo's development from all directions (Perry, 1988). Tahara and Obara (2014) have recently developed a novel shell-less culture system for chicken embryos using an artificial vessel made of poly(4-methyl-1-pentene) film. A simple culture method in this incubation system was established, and more than 50% hatchability in chick embryos was achieved (Tahara and Obara, 2014). In this study, we applied this shell-less incubation system to toxicity tests to assess the effects of TCEP exposure on chicken embryos.

The objective of this study was to assess the adverse outcomes of exposure to TCEP on chicken embryos by *in situ* observation using the shell-less incubation system and to understand the key events and molecular mechanisms for phenotypic effects by transcriptome analysis.

2.3 Materials and Methods

2.3.1 Study design overview

The experimental design of this study is summarized in Fig. 2.1. Briefly, 50, 250, and 500 nmol/g egg TCEP and 0.1% DMSO (solvent control) were administered in the air sac to fertilize chicken eggs on day 0 of incubation. After 56 hours of pre-incubation, the eggshells were broken, and the embryos were transferred to shell-less incubation vessels. We performed observation and recording of images and videos for chick embryos once a day while incubation was maintained from day 3 to day 9. Image analysis was performed to measure phenotypic endpoints with ImageJ. Chicken embryos were dissected on day nine and weighed for embryonic body, heart, and liver. Heart weight to body weight and liver weight to body weight ratios were calculated. Embryo carcasses were then used for skeletal staining. In addition, cardiac transcriptome analysis was performed on the collected hearts.

2.3.2 Chemicals

TCEP (97% purity; CAS No. 115-96-8) was purchased from Sigma-Aldrich (Saint Louis, USA). Dimethyl sulfoxide (DMSO) (Wako Pure Chemical Industries) was used for preparing stock and serially diluted solutions.

2.3.3 Shell-less incubation vessel

For successful *in situ* observation of *ex ovo* chicken embryos, shell-less incubation

vessels were used in the experiment, as shown in Fig. 2.2. Poly(4-methyl-1-pentene) (PMP) films (FOR-WRAP; Riken Technos, Japan) and 430 ml polystyrene plastic cups were prepared according to the protocol reported by Tahara and Obara (2014). One hole with a diameter of approximately 1.5 cm was drilled at 4.0 cm from the bottom of the cup to allow air exchange. The hole was plugged with cotton to serve as air filters. As an antimicrobial agent, plastic cups were added with 40 ml of 0.01% benzalkonium chloride solution (Nihon Pharmaceutical, Japan). The PMP film was stretched to mimic the concave shape of an eggshell, which holds the contents of an egg. Ten aeration holes (approximately 8 mm in diameter of each aeration hole) were made in the eggshell-like PMP film with the soldering iron. This stretched film was placed on the plastic cup, and then chicken embryos and internal content in eggs were transferred into the stretched PMP film. Ten aeration holes (approximately 8 mm in diameter of each aeration hole) were made in the eggshell-like PMP film with the soldering iron. Finally, the cup was covered with another PMP film to prevent the egg contents from drying.

2.3.4 Animals and TCEP exposure experiment

Fertilized eggs of the Rhode Island Red chicken (Gallus gallus domesticus) at HH1 were purchased from Yamagishism Jikkenchi (Mie, Japan) and stored at 15℃ for seven days. The eggs were administered with 0.1 % DMSO (control, n = 38), 50 nmol/g egg (TCEP-L, n = 17), 250 nmol/g egg (TCEP-M, n = 26), and 500 nmol/g egg of TCEP (TCEP-H, n = 53) (Table 2.1). The

number of chicken embryos in each TCEP exposure group differs because unfertilized eggs and eggs with yolk spillage during the transfer of egg contents to shell-less incubation vessels were excluded. These TCEP concentrations were nominal. Before administering TCEP and DMSO, the eggs were weighed, and small holes were drilled in the eggshell above the air sac (Jiahua Guo et al., 2018). TCEP or DMSO was injected into the fertilized eggs at incubation day 0 (HH1). The injection volume ranged from 9.21 to 10.97 μL per egg, depending on the egg weight, to standardize the final doses of chemicals in each treatment group. After administration, the holes were sealed with Parafilm. The eggs were preincubated under continuous rotation (1 cycle per hour) in an incubator for 56 h at 38℃ and 60–70% humidity. After preincubation, a mark was made at a center point between the tip and blunt end of each egg. To move the blastoderm to the top of the yolk, the eggs were placed with this mark facing upward and allowed to stand for 10 min. Three hundred milligrams of calcium lactate pentahydrate powder (Wako Pure Chemical Industries, Japan) and 3 ml of sterilized distilled water were added to each incubation vessel. Each eggshell was then wiped with 70% ethanol and cracked on the side opposite the mark. Next, all internal contents, including the embryo in each egg, were transferred to a shell-less incubation vessel and covered with PMP film, as mentioned in section 2.3.3. The shell-less incubation vessels were placed at approximately 8° angles, 38℃, and 60–70% humidity. The vessels were rotated 120° clockwise twice daily. Toxicity endpoints in the chicken embryos were observed in situ;

digital images and videos were recorded daily from incubation days 3–9 using an iPhone 6 camera (Apple Inc., USA). After the observations on day 9, the embryos were euthanized following the Regulations of Animal Experiments at Ehime University. Subsequently, the embryo body, heart, and liver weights were measured. The collected heart and liver were flash-frozen in liquid nitrogen and stored at -80℃. All animal experiments were performed according to the guidelines set by the relevant animal regulatory committee of Ehime University (Matsuyama, Japan).

2.3.5 Analyses of digital images and videos

Measurable endpoints were examined to investigate the effects of TCEP exposure on the phenotype of chicken embryos, and the following 17 endpoints were measured: survival rate, body length, head + bill length, forelimb length, hindlimb length, eye diameter, heart rate, heartbeat frequency, a total number of extraembryonic blood vessels, a total length of extraembryonic blood vessels, a gray value of artery, a total distance of spontaneous movement, the maximum velocity of spontaneous movement, body weight, heart weight, liver weight, and skeletal length. The time intervals and frequency of observations for each endpoint are shown in Table 2.2. All morphological endpoints were measured only for alive chicken embryos at the observation time.

The survival rate was determined based on no visible heartbeat by direct observation of the embryos. Morphological biometrics, including the embryonic body length, head + bill length,

forelimb length, hindlimb length, and eye diameter, were measured using ImageJ imaging analysis software (Fiji, https://fiji.sc/) (Fig. 2.3). The digital measurements of forelimb length, hindlimb length, and eye diameter were performed on the right side of the embryos. The image scale was adjusted using the ImageJ toolbar, specifically "Analyze," → "Set Scale." The length of each embryonic body part was traced on its digital image and measured using the toolbar options "Segmented Line" or "Freehand Line" in ImageJ.

The length and branch number of extraembryonic blood vessels were also measured on incubation days 3 and 4 (Fig. 2.4). The extraembryonic blood vessels were traced with the "Freehand Line," and their total length was calculated. The branch number of extraembryonic blood vessels was assessed by visual inspection.

The gray value obtained by scanning the extraembryonic arteries, an indicator of the number of red blood cells, was measured (Fig. 2.5). RGB color images were converted to 8-bit grayscale images using the menu item "Image" → "Type" → "8-bit" in ImageJ. The 8-bit grayscale image is represented in 256 levels of monochrome per pixel. A straight line was drawn across each blood vessel on the 8-bit images, and the gray value chart of the line was displayed by selecting "Analyze" → "Plot Profile." To calculate the net gray value of the blood vessel, we corrected the blood vessel's minimum gray value with the background's median gray value. If the gray value of the blood vessel is low, this indicates a low number of red blood cells in the vessel.

Heart rates (beats per minute [bpm]) of the surviving embryos were measured by assessing the videos on incubation days 3–7 according to a previously described method developed for measuring heart rate in zebrafish embryos was adapted for this experiment on *ex ovo* chicken embryos (Sampurna et al., 2018). The procedure for measuring heart rate is shown in the flowchart in Figure 2.6. Briefly, the recorded videos for 20 seconds, which were visible heartbeats, were trimmed and exported using Adobe Premiere Pro software (https://www.adobe.com/jp/products/premiere.html). The 20-s video recording of the heartbeat was converted to the Audio Video Interleave format using the Virtual Dub software (http://www.virtualdub.org/). The video data were exported to ImageJ, and a time series analyzer V3 plugin was used (https://imagej.nih.gov/ij/plugins/time-series.html) to analyze the heartbeat. The ventricular region was highlighted as the region of interest (ROI) using the oval tool. Then, "Get average" was selected, and the dynamic pixel data obtained from the ROI were transferred to Microsoft Excel (Microsoft Office 365). The Peak Analyzer function in OriginPro 2020 was used to calculate the time of each contraction peak. The bmp value was obtained by dividing 60 seconds by the average time interval between peaks (in seconds).

The heartbeat frequency on days 3 and 4 was analyzed using the short-time Fourier transform tool in OriginPro 2020 (Fig. 2.7). The short-time Fourier transform was analyzed with a fast Fourier transform (FFT) length of 256, a window length of 180, an overlap of 160, and a

window function of Hanning. The dynamic pixel data obtained from the heart rate analysis was used to visualize the variation in heartbeat frequency (Hz). In addition, we investigated whether the heartbeat frequency value was changed over 20 seconds.

Spontaneous movement analysis on days 5–9 chicken embryos was performed by a particle tracking method by ImageJ (Fig. 2.8). Observational videos of chicken embryos were trimmed to 20 seconds and 30 frames per second (fps) in Adobe Premiere Pro and converted to frame-by-frame image sequences by Virtual Dub. The edited image sequence files were imported into ImageJ. The threshold color of the image sequence was converted to "Black & White," and the targeted white area was subsequently tracked for 20 seconds using the "track mate" plug-in in ImageJ (Tinevez et al., 2017). The eyes of chick embryos were tracked as trackable targets (Fig. 2.9). The x and y coordinates of the ROI tracked in the image sequence were calculated. The total distance of the spontaneous movement was calculated as

$$\sum_{t=1}^{T-1} \sqrt{(x_{t+1} - x_t)^2 + (y_{t+1} - y_t)^2}$$

where T is the total number of frames, t is time, and x and y are the image coordinates. The maximum velocity at which the coordinates of the ROI moved between the two frames was defined as the maximum velocity of spontaneous movement. The speed between frames was calculated as

$$\left(\sqrt{(x_{t+1} - x_t)^2 + (y_{t+1} - y_t)^2} \times F\right)$$

where F is the fps value of the image sequence file, 30 was substituted in this calculation. This calculation was performed for T−1 cases per image sequence, and the maximum value was obtained from all cases.

2.3.6 Staining of cartilage and bone

The cartilage and ossified bone in chicken embryos (HH 34–35) were stained with Alcian blue solution (pH 2.5) and Alizarin red S (both from Wako Pure Chemical Industries), respectively, on incubation day 9. The staining was conducted according to the method reported in a previous study (Nakane and Tsudzuki, 1999), with a slight modification as described below (Fig. 2.10). Chicken embryos were fixed in 10% formalin (Wako Pure Chemical Industries) for a week. The embryos were washed with distilled water, immersed in 70% ethanol for 24 hours, and then immersed in 95% ethanol for 24 hours. The embryos were stained in a mixture of 99% ethanol and acetate (4:1 v/v) containing Alcian blue solution for ten days. The stained embryos were neutralized in saturated sodium tetraborate solution for 24 hours and then soaked in 70% tetraborate containing 1.0% trypsin for three days. The embryos were washed with distilled water and stained for two days using 0.002% Alizarin red S in 1.0% KOH. After washing with distilled water for 1 hour, the embryos were immersed in 25% glycerol and 1.0% KOH for three days and stored in 100% glycerol.

Digital images of the stained cartilage and ossified bone were obtained using an iPhone

6 camera (Apple Inc., USA). The length of the spine, bill + skull, humerus, radius, ulna, femur, and tibia were measured using ImageJ's menu item "Segmented Line" (Fig. 2.11).

2.3.7 RNA sequencing (RNA-seq)

The procedure for the cardiac transcriptome analysis in day nine chicken embryos is shown in Figure 2.12. Total RNA solutions were extracted from approximately 5 mg of heart tissues (n=3 in each treatment group) using Direct-zol RNA miniprep kits according to the manufacturer's instructions (Zymo Research, Japan). Total RNA solutions were pooled from three samples of each treatment group of control, TCEP-L, and TCEP-H. The RNA purity and concentration were determined using a NanoDrop spectrophotometer (A260/A280 = 2.00–2.06 and A260/A230 = 1.74–2.06), and the RNA quality was assessed using Agilent 2100 Bioanalyzer (RNA integrity number; RIN > 9.0). Total RNA solutions were submitted for RNA-seq service using Illumina HiSeq 2500 (Hokkaido System Science, Japan). Image analysis, base-calling, filtering based on fluorescence purity, and output of filtered sequencing files were performed using Illumina Analysis Pipeline. The paired-end method was applied for RNA sequencing, and the read length was 101 base pairs. The mapped reads for each sample ranged from 44,186,908 to 47,667,780, and the transcriptome coverage varied from 96.06% to 96.25%. Illumina adapter sequences from sequenced reads were removed with cutadapt (v 1.1; Martin, 2011), and low-quality reads with QV < 20 were trimmed with Trimmomatic (v 0.32; Bolger et al., 2014).

Trimmed reads were mapped to reference genome Gallus gallus 5.0 (Ensembl Genes 87) using a mapping program Tophat (v 2.0.14; Trapnell et al., 2009), which is a fast splice junction mapper for RNA-seq reads. The number of fragments of genes was normalized for each sample using the transcript assembly program Cuffdiff included in the RNA-seq analysis package "Cufflinks" (v 2.2.1; Trapnell et al., 2010) to quantify the gene expression levels. Gene expression levels were calculated as fragments per kilobase of exon model per Million mapped fragments (FPKM). Genes with $\log_2$ transformed fold change (FC) at their FPKM in the TCEP treatment group relative to those in the control group were further represented. We selected genes with a $\log_2$ FC value lower than -0.5 or higher than 0.5 in both TCEP-L and TCEP-H for further bioinformatics analyses.

2.3.8 RNA-seq data analyses

To identify biological processes (BPs) in gene ontology (GO) terms and pathways affected by TCEP exposure, curated genes were individually input into Database for annotation, visualization, and integrated discovery (DAVID v6.8, https://david.ncifcrf.gov/; Huang et al., 2009). GO BP terms with $p < 0.05$ were significantly enriched. The gene regulation of up- or down-regulated genes related to cardiac muscle contraction pathway in Kyoto Encyclopedia of Gene and Genomes (KEGG) pathways were visualized using the KEGG mapper (https://www.genome.jp/kegg/mapper.html; Kanehisa et al., 2012). In the transcription factor

(TFs) enrichment analysis, TfactS (http://www.tfacts.org/; Essaghir and Demoulin, 2012) was used. TFactS predicts the associated transcription factors based on lists of upregulated and downregulated genes generated in the RNA-seq analysis. TFs with e-value < 0.05 and adjusted p-value < 0.05 were considered statistically significant. For functional protein-protein interaction (PPI) network analysis, curated genes and TFs lists were imported into Cytoscape 3.7.3, a network data integration, analysis, and visualization tool. The functional enrichment of biological pathways was analyzed using Reactome databases embedded in Reactome Functional Interaction (FI) plugin.

2.3.9 Quantitative reverse transcription polymerase chain reaction (qRT-PCR)

The cardiac mRNA expression levels of several genes selected by RNA-seq analysis results were quantified using a quantitative reverse transcription polymerase chain reaction (qRT-PCR). Total RNAs were isolated from heart tissues using the same method as RNA-seq. The RNA samples were reverse transcribed to cDNA using a High Capacity cDNA Reverse Transcription Kit (Thermo Fisher Scientific), following the manufacturer's instructions. qRT-PCR was performed using the TB green Premix Ex Taq II (Takara Co., Ltd) and StepOnePlus Real-Time PCR System (Applied Biosystems, AB). The gene expression levels of Ca2+ transport-related genes, including ryanodine receptor 2 (RYR2), voltage-dependent calcium channel gamma-4 subunit (CACNG4), calsequestrin-2 (CASQ2), and triadin (TRDN) and muscle filament sliding

related genes, including myosin regulatory light chain 2 (MYL2), myosin light chain 3 (MYL3), myosin light chain 4 (MYL4), actin alpha cardiac muscle 1 (ACTC1), and Troponin C1 were measured. Gene-specific primers for qRT-PCR were designed by Primer-BLAST (https://www.ncbi.nlm.nih.gov/tools/primer-blast/) and synthesized by Eurofins Genomics (Japan). These primers for each gene and its respective PCR conditions are listed in Table 2.3. Expression levels were normalized with the internal control mRNA, β-actin. Expression levels were normalized with the internal control mRNA, β-actin, and the data are represented as fold changes in the mRNA expression level of TCEP-exposed groups relative to the control group.

2.3.10 Protein extraction and quantification

Total cardiac protein was extracted using 0.1M Tris HCL, pH7.6 lysis buffer supplemented with 1X cOmplete mini Protease Inhibitor Cocktail (Roche). First, the lysates were homogenized at 800–1000 rpm on ice. Then, 40 µl 20% SDS was added to the homogenized lysates. The mixture solution was sonicated on ice three times. Protein quantification was performed with a BCA protein assay kit (Pierce, Rockford, IL, USA).

2.3.11 Western blotting

Western blotting quantified protein levels to confirm whether myosin light chain 2 (MLC2) and myosin light chain 3 (MYL3) protein expression was affected by TCEP exposure. Heart proteins (12.5 µg/lane) were resolved by electrophoresis on NuPAGE 4–12% Bis-Tris Gel

(Invitrogen, USA) and transferred to a polyvinylidene difluoride (PVDF) membrane with the iBlot Gel Transfer System (Invitrogen, USA). Membranes were blocked with 5% skim milk in TBST for one hour at room temperature. After that, membranes were incubated with primary antibodies against myosin light chain 2 (MLC2; abcam ab48003; 1:2000), myosin light chain 3 (MYL3; proteintech 10913-1-AP; 1:1000), beta-actin (β-actin; abcam ab8227; 1:2000) overnight at 4℃. After washing four times for 5 min with TBST, the membranes were incubated with horseradish peroxidase (HRP)-conjugate secondary antibody in 5% skim milk for one hour at room temperature. The secondary antibody was goat anti-rabbit IgG-HRP (Santa Cruz Biotechnology sc-2004; 1:2000). Detection of protein levels was performed using the enhanced chemiluminescence (ECL) Prime Western Blotting Detection Reagents (Amersham Biosciences, Little Chalfont, UK), and the signals were captured using an ImageQuant LAS 4000 mini (GE Healthcare Life Sciences, US). Densitometric analysis was performed by an ImageQuant TL (GE Healthcare Life Sciences, US), and target protein levels were normalized to the β-actin protein levels.

2.3.12 Statistical analysis

All data other than spontaneous movement results were reported as means ± standard errors (SE). Results of the spontaneous movement analysis were represented as means ± standard deviation (SD). The statistical differences in the survival rate between the control and TCEP-

exposed groups were determined using log-rank tests (GraphPad Prism 5). In addition, statistical differences in phenotypic endpoints, gene expression levels, and protein expression levels were evaluated using a one-way analysis of variance followed by Dunnett's multiple comparison tests in the R software. Results with p-value < 0.05 were regarded as statistically significant.

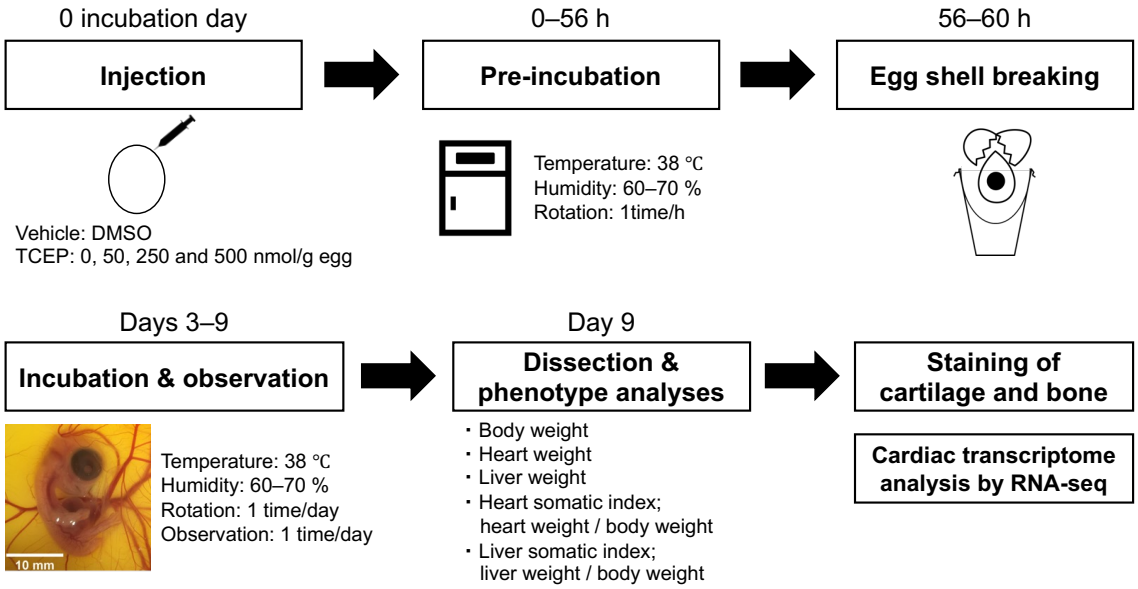

Figure. 2.1 Strategy to evaluate the effects of TCEP on chicken embryos using a shell-less incubation system.

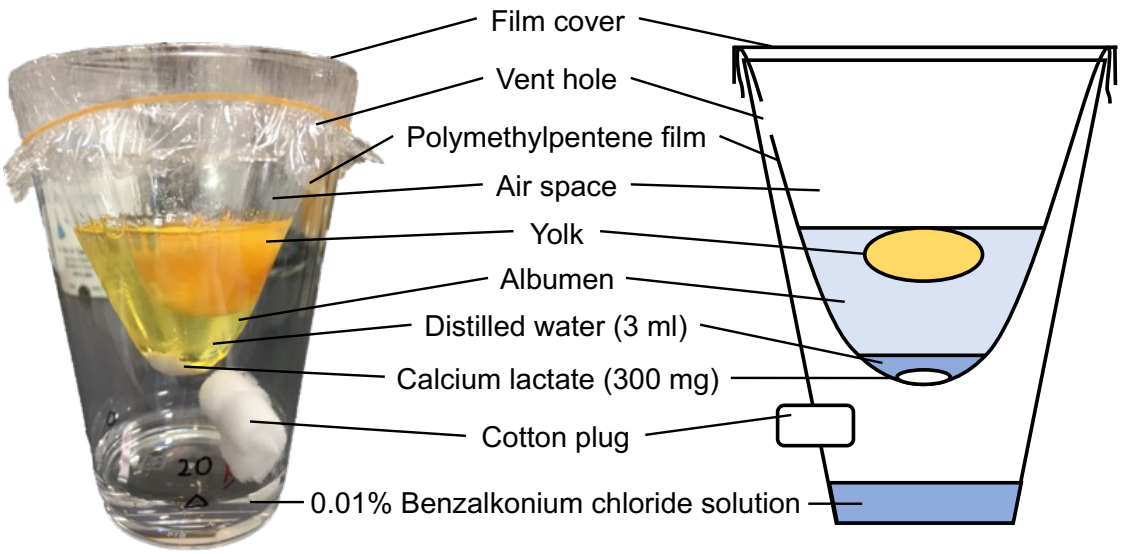

Figure. 2.2 Photograph and drawing of the shell-less incubation vessel for chicken embryos employed in this study.

Table. 2.1 Number of samples in each group.

Group	Concentration (nmol/g egg)	Sample number
Control	-	38
TCEP-L	50	18
TCEP-M	250	26
TCEP-H	500	53

Table. 2.2 The time of chicken embryonic development where each endpoint was measured.

Endpoint	Day 3	Day 4	Day 5	Day 6	Day 7	Day 8	Day 9
Survival rate	✓	✓	✓	✓	✓	✓	✓
Body length	✓	✓	✓	✓	✓	✓	✓
Head + bill length	✓	✓	✓	✓	✓	✓	✓
Forelimb length		✓	✓	✓	✓	✓	✓
Hindlimb length		✓	✓	✓	✓	✓	✓
Eye diameter		✓	✓	✓	✓	✓	✓
Heart rate	✓	✓	✓	✓	✓		
Heartbeat frequency	✓	✓					
Total number of extraembryonic blood vessels	✓	✓					
Total length of extraembryonic blood vessels	✓	✓					
Gray value of artery	✓	✓	✓	✓	✓	✓	✓
Total distance of spontaneous movement			✓	✓	✓	✓	✓
Max velocity of spontaneous movement			✓	✓	✓	✓	✓
Body weight							✓
Heart weight							✓
Liver weight							✓
Skeletal length							✓

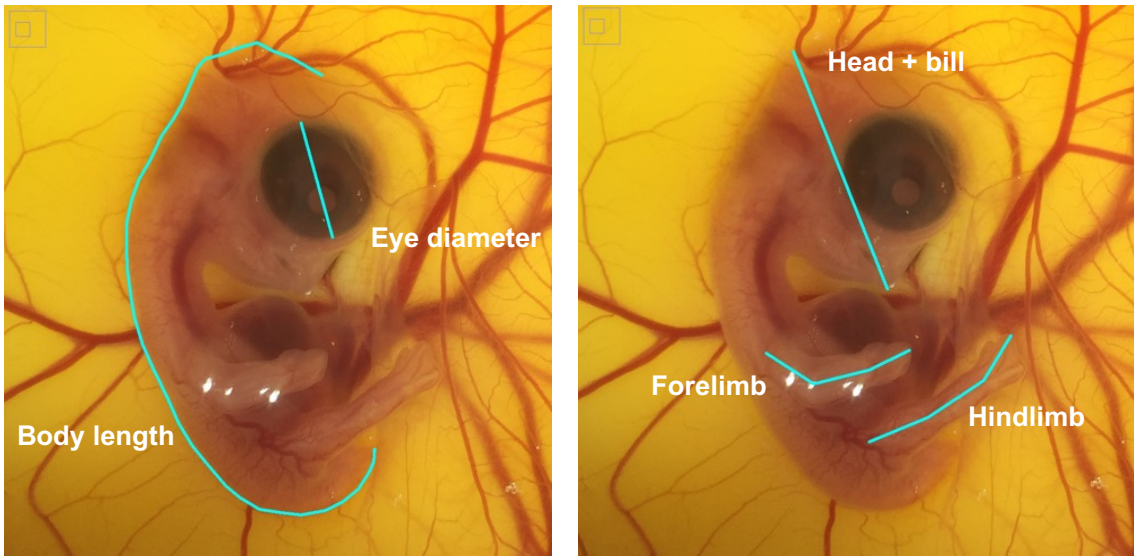

Figure. 2.3 The measurement of embryonic body parts using ImageJ. The blue line in each inset digital image indicates a representative measurement site.

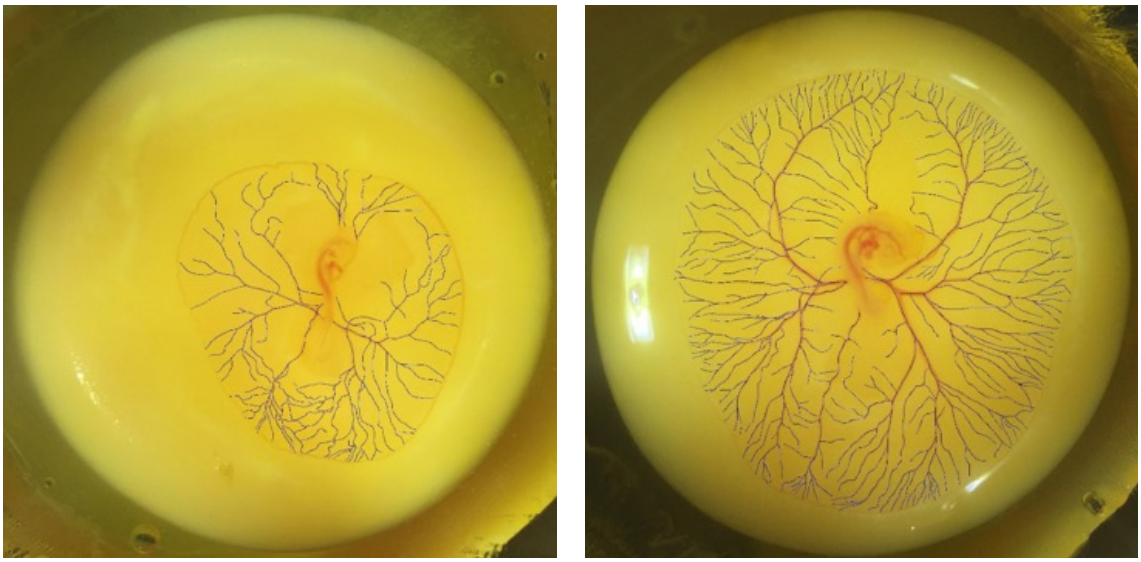

Day 3 chicken embryo **Day 4 chicken embryo**

Figure. 2.4 The measurement of the extraembryonic blood vessels on day three and day four of incubation. Blue lines tracing the blood vessels in the images indicate the measured ones.

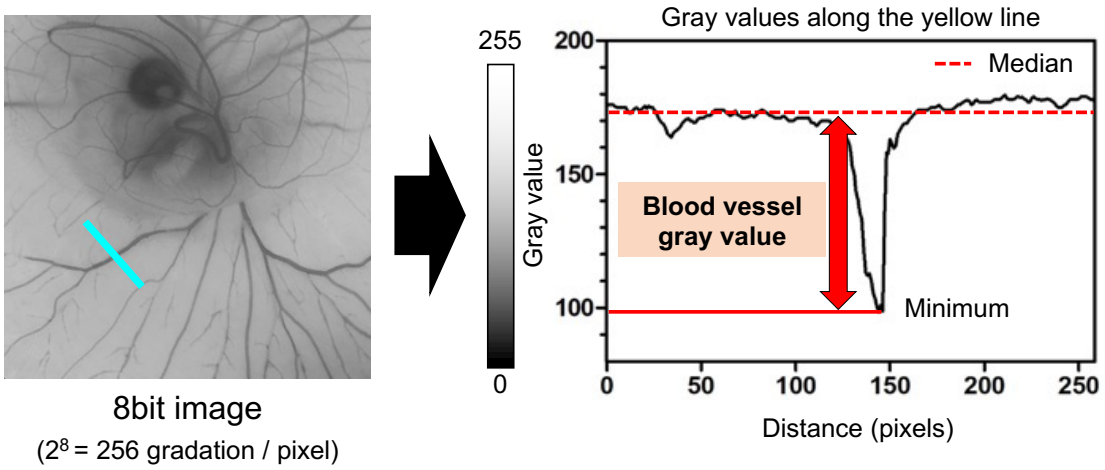

Blood vessel gray value = Background gray value − The minimum value

Figure. 2.5 The measurement of the digital gray value of the extraembryonic artery. RGB color images were converted to 8-bit grayscale images. To calculate the net gray value of the blood vessels, the minimum gray value of the blood vessels was corrected by the median gray value of the background.

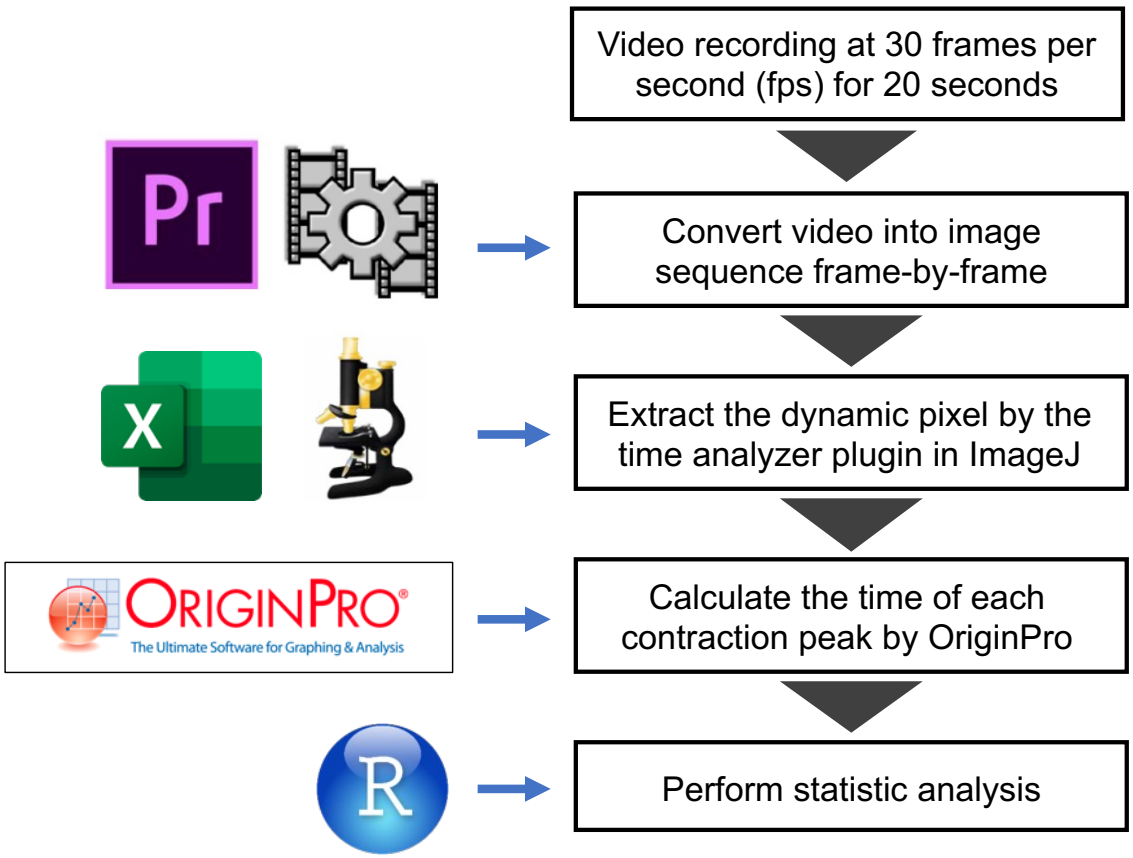

Figure. 2.6 A flowchart for analyzing heartbeat in chicken embryos using the dynamic pixel change method modified from Sampurna *et al*., 2018.

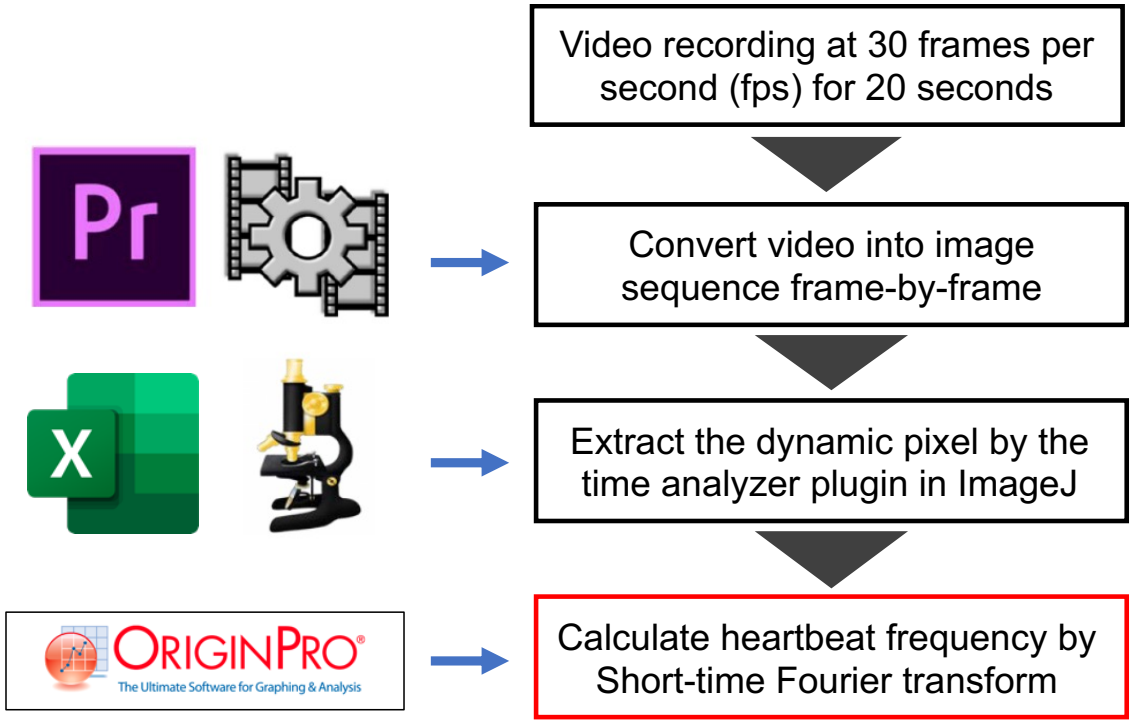

Figure. 2.7 A flowchart for analyzing heartbeat frequency (Hz) in chicken embryos by Short-time Fourier transform.

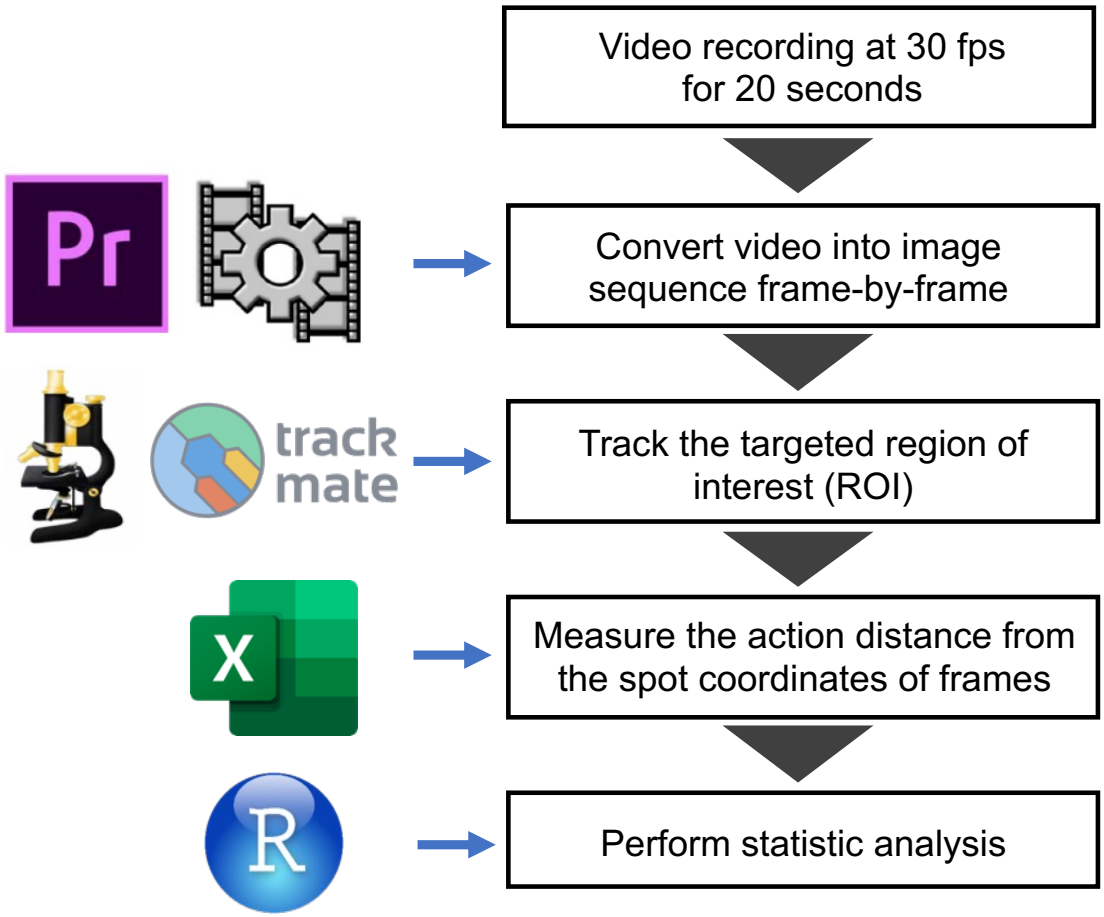

Figure. 2.8 A flowchart for analyzing spontaneous movement's total distance and velocity in chicken embryos.

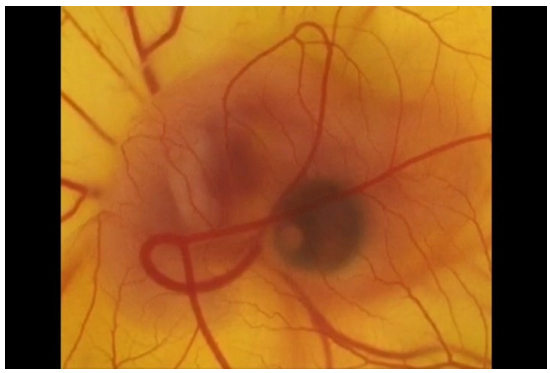

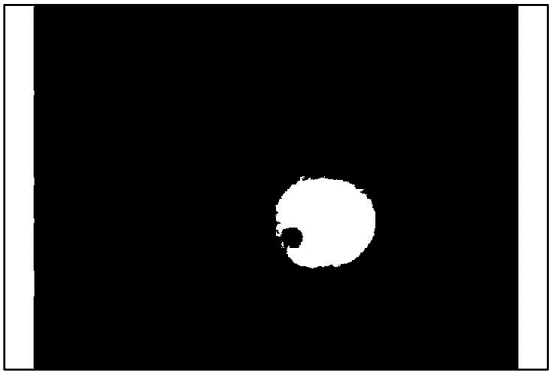

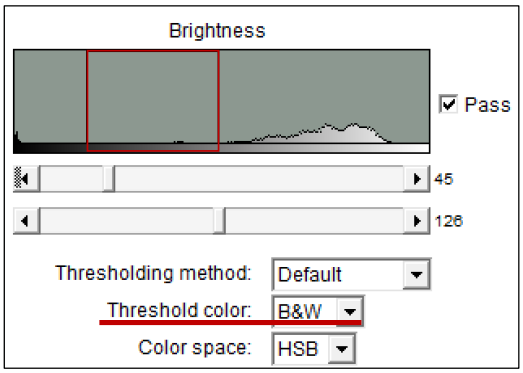

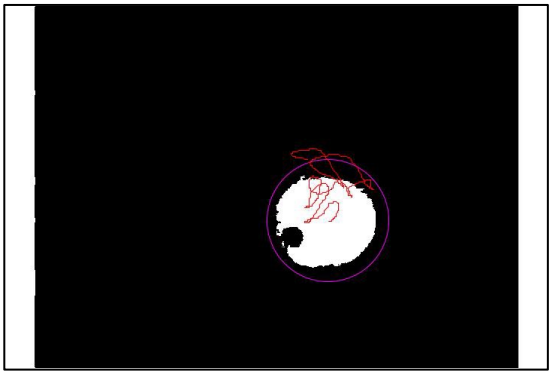

Label	POSITION_X	POSITION_Y	POSITION_T
ID74376	11.863	7.872	1
ID74516	11.863	7.872	2
ID74664	11.863	7.872	3
ID74241	11.918	7.872	4
ID74800	11.918	7.872	5
⋮	⋮	⋮	⋮
ID147240	11.087	5.599	599
ID147384	11.087	5.599	600

Figure. 2.9 The legend of editing image sequences in ImageJ and tracking analysis by TrackMate for the same chicken embryo. The threshold color in the Brightness of the image sequence was converted to B&W. Then, the eye of the chicken embryo was displayed in white and tracked using TrackMate on which white area. Tracking results were displayed in x and y coordinates and time (T) at each image sequence frame.

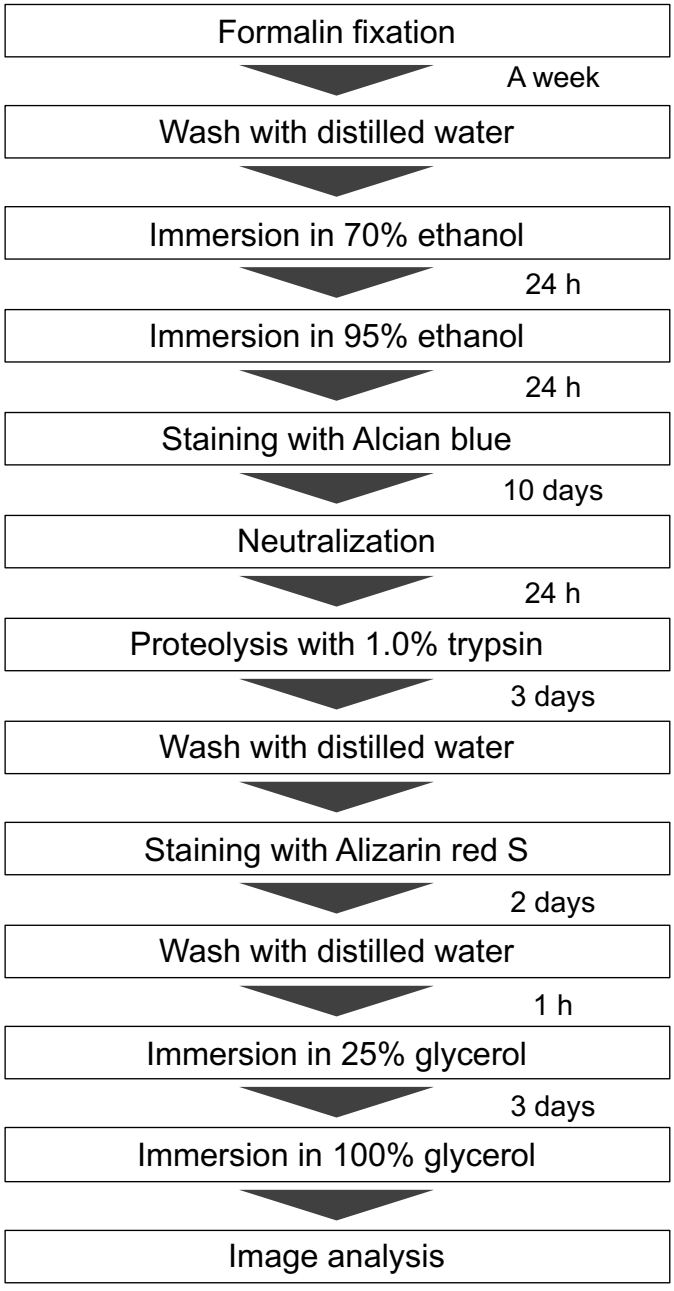

Figure. 2.10 A flowchart for staining of cartilage and bone in chicken embryos.

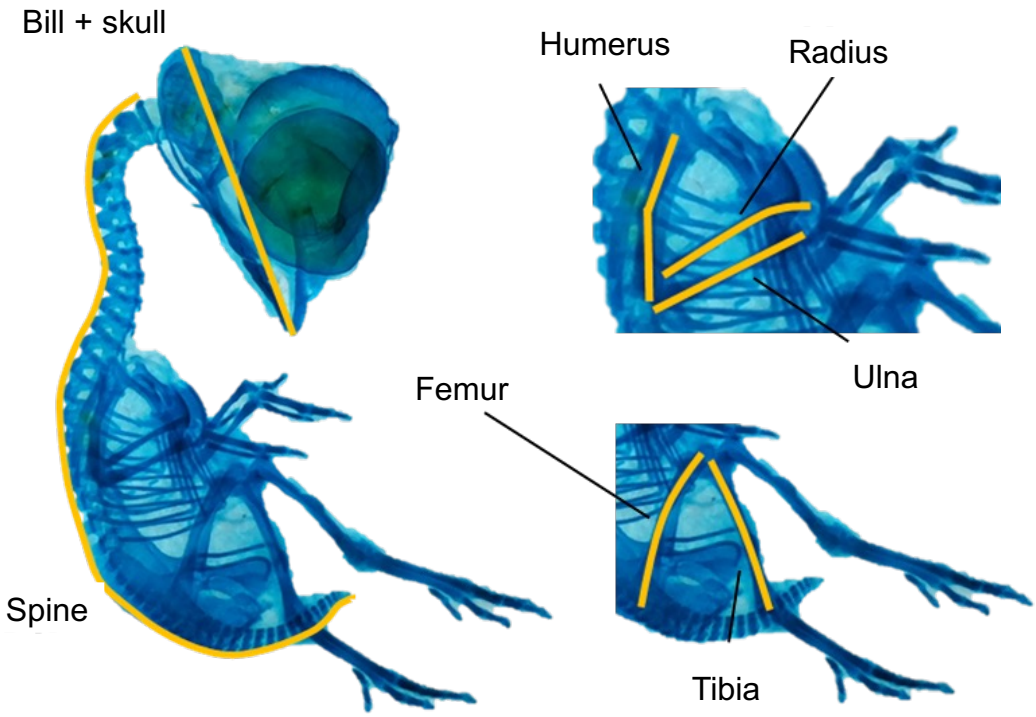

Figure. 2.11 The measurement of cartilage and bone parts using ImageJ. The yellow line in each inset digital image indicates a representative measurement site.

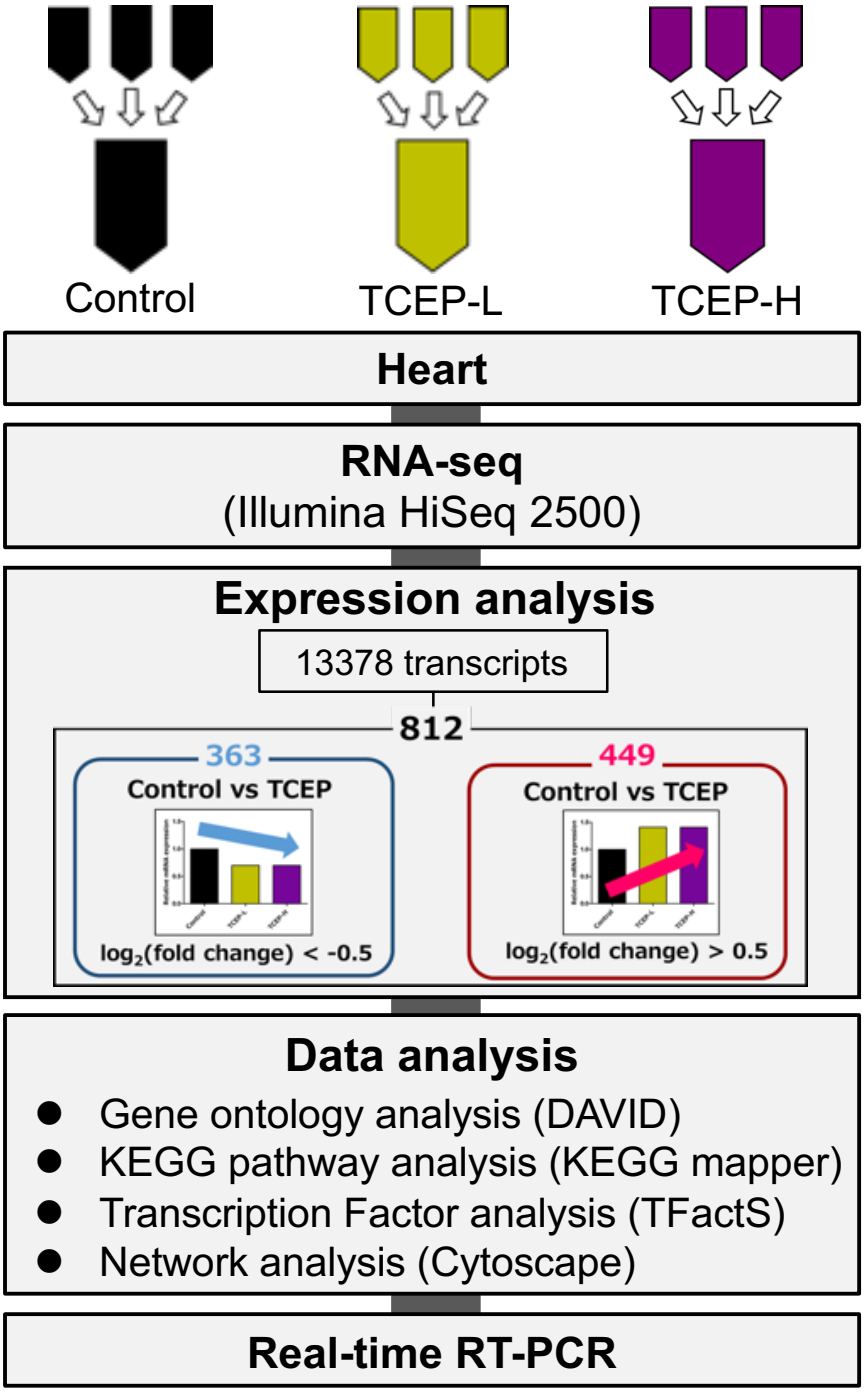

Figure. 2.12 A flowchart for the cardiac transcriptome analysis in day nine chicken embryos.

Table. 2.3 List of primers and PCR conditions applied in this study.

Symbol	Gene name	Accession number	Forward primer	Reverse primer	Tm (℃)
RYR2	Ryanodine receptor 2	XM_025149046.1	GAAGCAAAAGGAGGAGGCAA	GCTGGAGGAAACTGTAGGCAA	63
CACNG4	Calcium voltage-gated channel auxiliary subunit gamma 4	NM_204132.1	CTTCTCCGCATTGTCCGTG	GCTGTTGTAAATCCTCCCTGC	62
CASQ2	Calsequestrin 2	NM_204526.1	ACTTTCCTCTGCTCATCACTTAC	CCTCTATCCAGTCCTCCAGC	64
TRDN	Triadin	XM_015284473.2	CGAGGTTACAGCAGAAGGACG	AGAGCCACAACAAGAAGCCA	65
MYL2	Myosin light chain 2	NM_001271929.1	GCTTCATCGACAAGGCAGAC	GGATCAGCACCCTTGAGTTTC	63
MYL3	Myosin light chain 3	NM_205159.1	CTCCAGCACATTTCCAAGACA	AGTCAACCTTTCACCCAGCG	63
MYL4	Myosin light chain 4	NM_205479.3	AGACCTTCCTCCCCATCCTG	CTGTCATCTTCTCCCCCAGC	64
ACTC1	Actin alpha cardiac muscle 1	NM_001079481.1	ATGTGTGACGACGAGGAGAC	ACCATAACACCCTGGTGCCT	65
TNNC1	Troponin C1	NM_205133.1	CATCTATAAGGCGGCGGTTG	CCCAGCACGAAGATGTCGAA	63
β-actin	Beta-actin	NM_205518.1	CTGACTGACCGCGTTACTCC	GGCCCATACCAACCATCACA	63

PCR was run with the following condition: one cycle of 10 min at 95°C; 40 cycles of 15 sec at 95°C, 1 min at Tm°C; and one cycle of 15 sec at 95°C, 1 min at 60°C, and 15 sec at 95°C

Results

2.4.1 Survival rate

To assess the effect of TCEP on embryonic development, the survival of embryos was monitored during incubation. In the TCEP-M and TCEP-H groups, the survival rates started to decline greatly from incubation day 3, which was the first day of in situ observation, and significantly decreased in a dose-dependent manner (log-rank test for trend, $p < 0.001$) until incubation day 9 (Fig. 2.13A). The survival rates were 19.2% and 18.9% on day 9 in the TCEP-M and TCEP-H groups, respectively. The survival rate on day 9 in the TCEP-L group (76.5%) was not significantly different from that in the control group (71.1%). This result suggests that exposure to more than 250 nmol/g of TCEP has a lethal effect on early-developing embryos.

2.4.2 Morphological endpoints

We measured several endpoints from incubation days 3–9 to investigate the morphological effects of TCEP exposure on embryos. Here, embryos that were alive on the observation day were assessed. Compared with the control group, body length was significantly shorter on days 3 and 4 in the TCEP-M group and days 4–9 in the TCEP-H group (Fig. 2.13B). The body length in the TCEP-L group was not significantly different from that in the control group on all incubation days. Developmental delay was consistently found after the early embryonic stage in the TCEP-H exposed group. The head + bill length was significantly reduced

on day 3 in the TCEP-L group, days 3–8 in the TCEP-M group, and days 4, 5, 7, 8, and 9 in the TCEP-H group (Fig. 2.13C). Regarding eye diameter, no significant change was detected in TCEP-L compared with that in control; however, there were significant decreases in the TCEP-M and TCEP-H groups on days 4–8 and 4, 5, 8, and 9, respectively (Fig. 2.13D). The forelimb length was significantly reduced on days 5 and 6 in the TCEP-M group and on days 5 and 8 in the TCEP-H group (Fig. 2.13E). TCEP exposure significantly shortened the hindlimb length on days 6 and 8 in the TCEP-M group and day 8 in the TCEP-H group (Fig. 2.13F). These results suggest that exposure to more than 250 nmol/g egg of TCEP retards development in chicken embryos.

In addition, we analyzed the data of only chicken embryos that survived until day 9 to examine whether the data of dying embryos had affected the results. The body length was significantly shortened on days 4–9 in the TCEP-H group (Fig. 2.14A). In addition, a significant decrease in head + bill length was detected on day 3 in the TCEP-L group, days 4–6 in the TCEP-M group, and days 4, 5, and 7–9 in the TCEP-H group (Fig. 2.14B). Eye diameter was significantly decreased on days 5, 6, and 8 in the TCEP-M group and on days 4, 5, and 7–9 in the TCEP-H group (Fig. 2.14C). The forelimb and hindlimb lengths were significantly shortened on days 8 and 9 in the TCEP-M and TCEP-H groups (Fig. 2.14D and E). These results suggest that utilizing dying animals had little impact on the results of these experiments.

Furthermore, various skeletal lengths were measured in day nine chick embryos (Fig. 2.15). The spine, bill + skull, humerus, and tibia length decreased in a TCEP concentration-dependent manner. The spine and bill + skull length was significantly shortened in the TCEP-M group. In addition, there was a significant decrease in the length of the humerus and tibia in the TCEP-L group.

2.4.3 Body weight and organ weight

The embryonic body, heart, and liver weights were measured in chicken embryos on day 9 of incubation (Fig. 2.16). The embryonic body weight on day nine significantly reduced in all TCEP-exposed groups and was altered in a TCEP concentration-dependent manner. Although there was no significant difference in the heart weight between the TCEP-exposed groups and the control group, the heart weight to body weight ratio was significantly increased in the TCEP-H group and was altered in a TCEP concentration-dependent manner. The liver weight and which weight to body weight ratio in TCEP-exposed groups were not changed compared to the control group.

2.4.4 Effects on the cardiovascular system

The heart rate of chicken embryos was monitored during early developmental stages in the shell-less incubation system (Fig. 2.17). We counted the heart rates in bpm of all surviving chicken embryos daily from day 3–7, and the average heart rate was compared between groups.

The heart rate was significantly decreased in a TCEP concentration-dependent manner on days 4–6 ($p < 0.05$, Jonckheere-Terpstra test) (Fig. 2.17A). In the TCEP-M group, the heart rate was significantly decreased on days 4 and 7 compared with that of the control group; in the TCEP-H group, the heart rate was significantly decreased on days 4 and 5. Assessment of the heart rates of individual embryos indicated that most embryos with low heart rates died during their development (Fig. 2.17B). The heart rate in chicken embryos that survived until day nine was significantly reduced on day 4 in the TCEP-M and TCEP-H groups ($p < 0.05$) (Fig. 2.17C). The shift of the heart rate in TCEP-M and TCEP-H groups 0.5 days earlier than this result showed the same change in chronological heart rate as the control and TCEP-L groups (Fig. 2.17D). No alteration was detected in the heartbeat frequency (Hz) in all TCEP-treated groups, suggesting that TCEP exposure causes no arrhythmias in chicken embryos (Fig. 2.18).

During vasculogenesis and angiogenesis, the first blood vessel in chicken embryos is formed in an extraembryonic area. Therefore, we measured the length and branch number of extraembryonic blood vessels in the visible area of the embryos on days 3 and 4 to investigate the effect of TCEP on the circulatory system (Fig. 2.19). A significant reduction in the branch number of blood vessels was found on day 3 in the TCEP-L group, days 3 and 4 in the TCEP-M group, and day 4 in the TCEP-H group (Fig. 2.19A). The total blood vessel length was significantly decreased on day 3 in the TCEP-L group and days 3 and 4 in the TCEP-M and TCEP-H groups

compared with that in the control group (Fig. 2.19B). These results indicate that vasculogenesis and angiogenesis are suppressed even at the lowest TCEP dose (50 nmol/g egg).

The gray value of the extraembryonic arteries as an indicator of the number of erythrocytes was measured on days 3–9 (Fig. 2.20). The TCEP-L, TCEP-M, and TCEP-H groups had significantly lower gray values on days 3, 3–5, and 4–7, respectively, compared with the control group. In addition, the gray value of the extraembryonic arteries was significantly decreased in a TCEP concentration-dependent manner on days 3–7 (day 3, $p < 0.001$; day 4, $p < 0.001$; day 5, $p < 0.001$; day 6, $p < 0.01$; day 7, $p < 0.05$; Jonckheere-Terpstra test). These results suggest that embryo exposure to TCEP induces a decrease in erythrocytes.

2.4.5 Effects on the spontaneous activity

The total distance and maximum velocity of the spontaneous movement were measured on days 5 to 9 to confirm whether TCEP exposure affected the spontaneous activity of the chicken embryos (Fig. 2.21). The total distance of spontaneous movement was significantly reduced on days 7 and 9 in TCEP-L and on days 6 and 7 in TCEP-M compared with the control group (Fig. 2.21A). The total distance data only in chicken embryos that survived until incubation day 9 was significantly lower in the TCEP-L group on days 7 and 9 of incubation (Fig. 2.21C). Variation in the total distance for the control and TCEP-exposed groups was narrow at day 5, with SD values less than 4.0. In contrast, the variation among individuals in each group increased from day 6. In

contrast, the variability among individuals in each group increased from day 6, especially the TCEP-L group on day 9 had the highest SD value of 21.5.

The maximum velocity of spontaneous movement was significantly reduced on days 6, 7, and 9 in TCEP-L and on days 6 and 7 in TCEP-M compared with the control group (Fig. 2.21C). The maximum velocity data only in chicken embryos that survived until incubation day 9 was significantly slower on days 6, 7, and 9 in TCEP-L and on days 6 and 7 in TCEP-M (Fig. 2.21D). However, the TCEP-H exposure group did not show significant differences in the observation period. These data were consistent with the spontaneous movement distance results. These results suggest that exposure to 50 and 250 nmol/g egg TCEP on chicken embryos suppresses spontaneous activity.

2.4.6 Effects on the cardiac transcriptome on day 9

We analyzed cardiac transcriptome by RNA-seq to identify the genes which altered its expression level following TCEP exposure. RNA-seq measured the expression levels of 13378 genes. The 812 genes that fulfilled the criteria indicated in Materials and Methods (section 2.3.7) were screened from the 13378 genes as DEGs, of which 363 genes were found to be up-regulated, and 449 genes were found to be down-regulated (Fig. 2.22).

2.4.7 Gene ontology (GO) analysis of DEGs

We performed the GO enrichment analysis to gain insight into the major gene expression

patterns and identified significantly enriched GO terms to reveal the affected biological processes (BPs), cellular components (CC), and molecular functions (MF) by TCEP exposure. DAVID v6.8 carried out the GO analysis based on BP, CC, and MF. Sixty-two GO BP terms were identified as significantly enriched (Table 2.4). The top five enriched GO terms indicated cardiac muscle contraction, negative regulation of the Notch signaling pathway, inner ear development, osteoblast differentiation, and chromatin silencing. There were also 10 GO BP terms related to cardiac muscle function, including cardiac muscle contraction, negative regulation of myoblast differentiation, ventricular cardiac muscle tissue morphogenesis, cardiac muscle cell development, response to muscle activity, regulation of heart rate, muscle contraction, cardiac muscle tissue morphogenesis, regulation of myoblast differentiation, and calcium-mediated signaling. There were 22 enriched GO-CC in DEGs (Table 2.5). The top five enriched GO terms represented plasma membrane, anchoring junction, neuronal cell body, Z disc, and M band. The Z-disc and M-band are the transverse structural elements in cross-striated muscles and are involved in myocardial function. In addition, 13 GO-MF terms were significantly enriched by TCEP exposure (Table 2.6). The top five enriched GO terms indicate titin binding, ion channel binding, neuropeptide hormone activity, potassium channel regulator activity, and structural constituent of muscle.

2.4.8 Transcription factor (TF) enrichment analysis and Functional protein-protein

interaction (PPI) networks of the DEGs

To predict TFs which regulated DEGs expression, the TF enrichment analysis was performed. TF analysis demonstrated that NFKB1, FOXO1, CTNNB1, SP1, EGR1, GLI1, SP3, SMAD4, and GLI2 were enriched (Table 2.7).

We then constructed a PPI network by Cytoscape 3.7.3 to identify what DEGs are transcriptionally regulated to significantly enriched TFs and what biological functions they are involved in. The PPI network analysis was performed using the Reactome FI plugin. A total of 34 pairs of PPIs containing 290 genes were extracted. Thirty-four PPI modules containing 290 genes were extracted and focused on a network of five modules of interest (Fig. 2.23). High-density lipoprotein particle remodeling- and reverse cholesterol transport-related genes, including scavenger receptor class B member 1 (SCARB1), phosphatidylcholine-sterol acyltransferase (LCAT), apolipoprotein A-I (APOA1) constructed in module 1. BMP signaling pathway and SMAD protein signal transduction, containing mothers against decapentaplegic homolog 4 (SMAD4), mothers against decapentaplegic homolog 9 (SMAD9), growth/differentiation factor 2 (GDF2), bone morphogenetic protein 2 (BMP2), bone morphogenetic protein (BMP3) constructed in module 2. Wnt signaling pathway-related genes containing 5'-AMP-activated protein kinase catalytic subunit alpha-2 (PRKAA2), WNT4, WNT11, Wnt inhibitory factor 1 (WIF1), KREMEN1 were included in module 3. Ca2+ transport- and regulation of cardiac

conduction-related genes, including RYR2, calcium/calmodulin-dependent protein kinase II alpha (CAMK2A), voltage-dependent calcium channel gamma-7 subunit (CACNG7), cardiac phospholamban (PLN), sarcolipin (SLN) constituted module 4. Muscle filament sliding- and cardiac muscle contraction-related genes containing myosin binding protein C3, ACTC1, tropomyosin alpha-4 chain (TPM4), alpha-actinin-2 (ACTN2), MYL2, TNNC1, MYL3, troponin I, fast skeletal muscle (TNNI2) were found in module 5. Therefore, it was suggested that TCEP exposure affects some functions, such as cardiomyocyte growth and differentiation, cardiac contraction, calcium ion transport for myocardial contraction, and cholesterol transport in the heart. In the TFs, NFKB1, SP1, SP3, and SMAD4 primary regulated module 1, CTNNB1 and SMAD4 primary regulated BMP and SMAD signaling in module 2, and FOXO1 and GLI1 primary regulated DEGs in Wnt signaling in module 3. Phosphodiesterase 4B (PDE4B) and Ras protein-specific guanine nucleotide releasing factor 1 (RASGRF1), which were DEGs in module 4 involved calcium ion signaling, were found to be regulated by the TFs GLI1 and CTNNB1, respectively. In addition, module 5 DEGs (ACTC1, MYH11, and TNNC1) involved in myocardial contraction were transcriptionally regulated by NFKB1, SP1, SP3, and SMAD4.

2.4.9 Pathway analysis of cardiac muscle contraction of DEGs

We investigated KEGG pathway analysis related to cardiac muscle contraction because genes involved in cardiac muscle contraction and Ca2+ transport were altered by TCEP exposure

from the results of GO and PPI network analyses (Fig. 2.24). Up- or down-regulated genes by TCEP exposure were visualized by mapping on the KEGG pathway map, and it can know more detailed signaling and molecular interaction. The expression levels of ryanodine receptor 2 (RYR2), calcium voltage-gated channel auxiliary subunit gamma 4 (CACNG4), calcium voltage-gated channel gamma 7 (CACNG7), calsequestrin-2 (CASQ2), and triadin (TRDN) were altered in calcium signaling-related genes. We found that the expression levels of myosin regulatory light chain 2 (MYL2), myosin light chain 3 (MYL3), myosin light chain 4 (MYL4), actin alpha cardiac muscle 1 (ACTC1), tropomyosin 4 (TMP4), and troponin c slow skeletal and cardiac muscles (TNNC1) decreased in the muscle filament sliding pathway. These alterations in the cardiac muscle contraction pathway were suggested to induce a significant decrease in the heart rate of chicken embryos.

2.4.10 Validation of RNA-seq data by quantitative RT-PCR (qRT-PCR)

To quantify the mRNA expression level more accurately, cardiac muscle contraction pathways related to several genes were analyzed by qRT-PCR. Although the RYR2 expression level was not significantly different between the control and TCEP-exposed groups, there was a significantly decreasing trend in a concentration-dependent manner ($p < 0.05$) (Fig. 2.25). The expression level of MYL3 trended to significant downregulation even though it was not significantly different in each treatment group (Fig. 2.25). MYL2 and MYL4 also showed a

decrease in a dose-dependent manner, but these were not significant differences (Fig. 2.25 and 2.26). However, the mRNA expression levels of the other genes (CASQ2, TRDN, CACNG4, ACTC1, and TNNC1) were not significantly altered compared with the control group (Fig. 2.26 and 2.27).

2.4.11 Western blotting

Western blotting was performed to quantify myosin light chain 2 (MLC2) and myosin light chain 3 (MYL3) protein expression. MLC2, MYL3, and β-actin as loading control showed bands at 19 kDa, 27 kDa, and 42 kDa, respectively (Fig. 2.28A and B). The intensity of the target protein band was corrected for the intensity of the β-actin band, and the relative expression values were compared between groups, with the mean of the control group set to 1. Protein expression of MLC2 in the TCEP-L and TCEP-M groups was not significantly altered compared to the control group (Fig. 2.28C). The protein expression of MYL3 was also not significantly different in the TCEP-exposed groups (Fig. 2.28D). Therefore, the myosin light chain protein expression was inconsistent with the gene expression results.

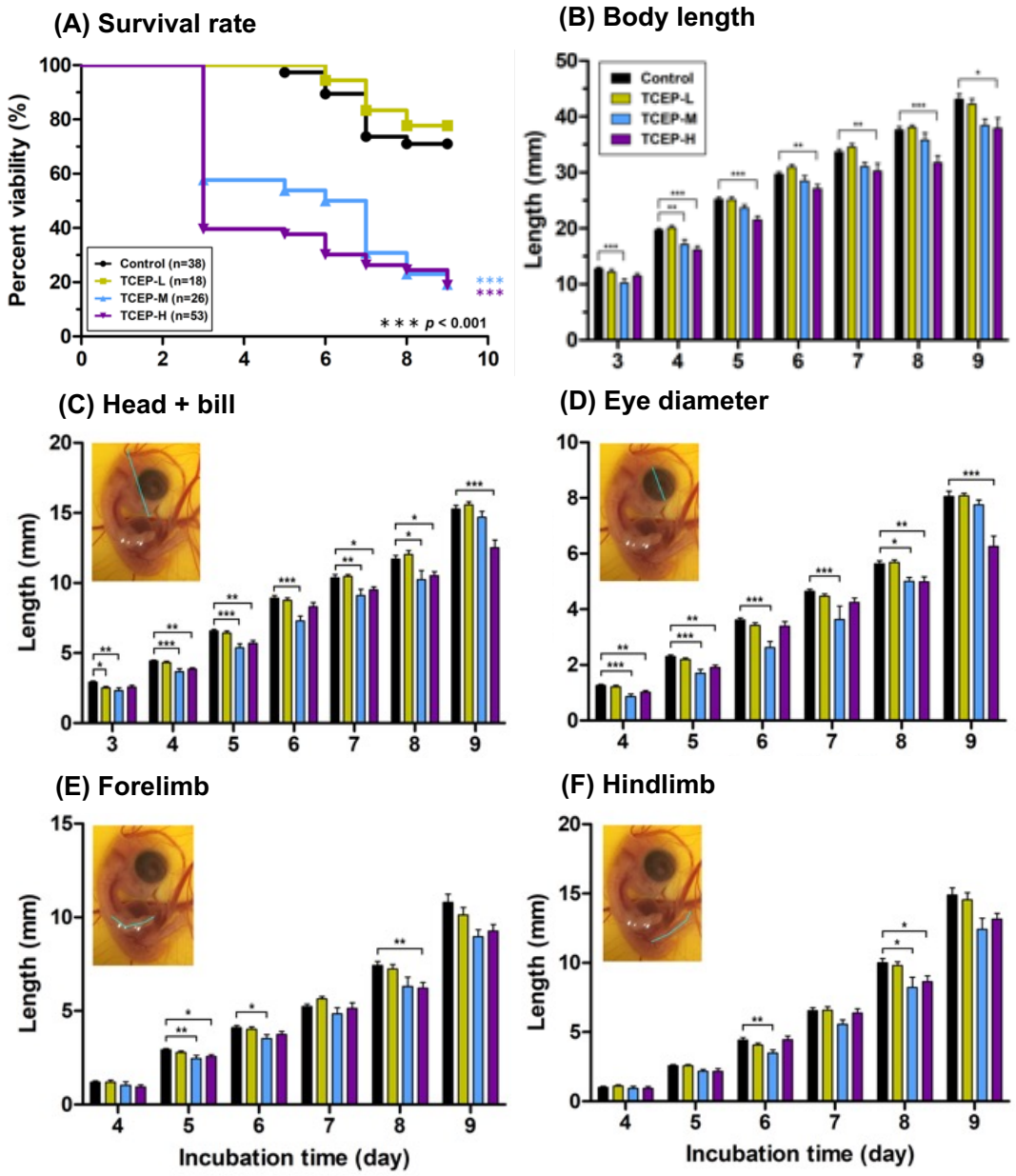

Figure. 2.13 Effects of TCEP exposure on morphological endpoints. (A) the survival rate, (B) body length, (C) head + bill length, (D) eye diameter, (E) forelimb length, and (F) hindlimb length were measured in chicken embryos (day 3 and 4: control, n = 38; TCEP-L, n = 17; TCEP-M, n = 15; TCEP-H, n = 21; day 5: control, n = 37; TCEP-L, n = 17; TCEP-M, n = 14; TCEP-H, n = 20; day 6: control, n = 34; TCEP-L, n = 16; TCEP-M, n = 13; TCEP-H, n = 16; day 7: control, n = 28; TCEP-L, n = 14; TCEP-M, n = 8; TCEP-H, n = 14; day 8: control, n = 27; TCEP-L, n = 13; TCEP-M, n = 6; TCEP-H, n = 13; day 9: control, n = 27; TCEP-L, n = 13; TCEP-M, n = 5; TCEP-H, n = 10). Data represent means ± standard errors. Asterisks indicate significant differences (*$p < 0.05$, **$p < 0.01$, ***$p < 0.001$). The blue line in each inset digital image indicates a representative measurement site.

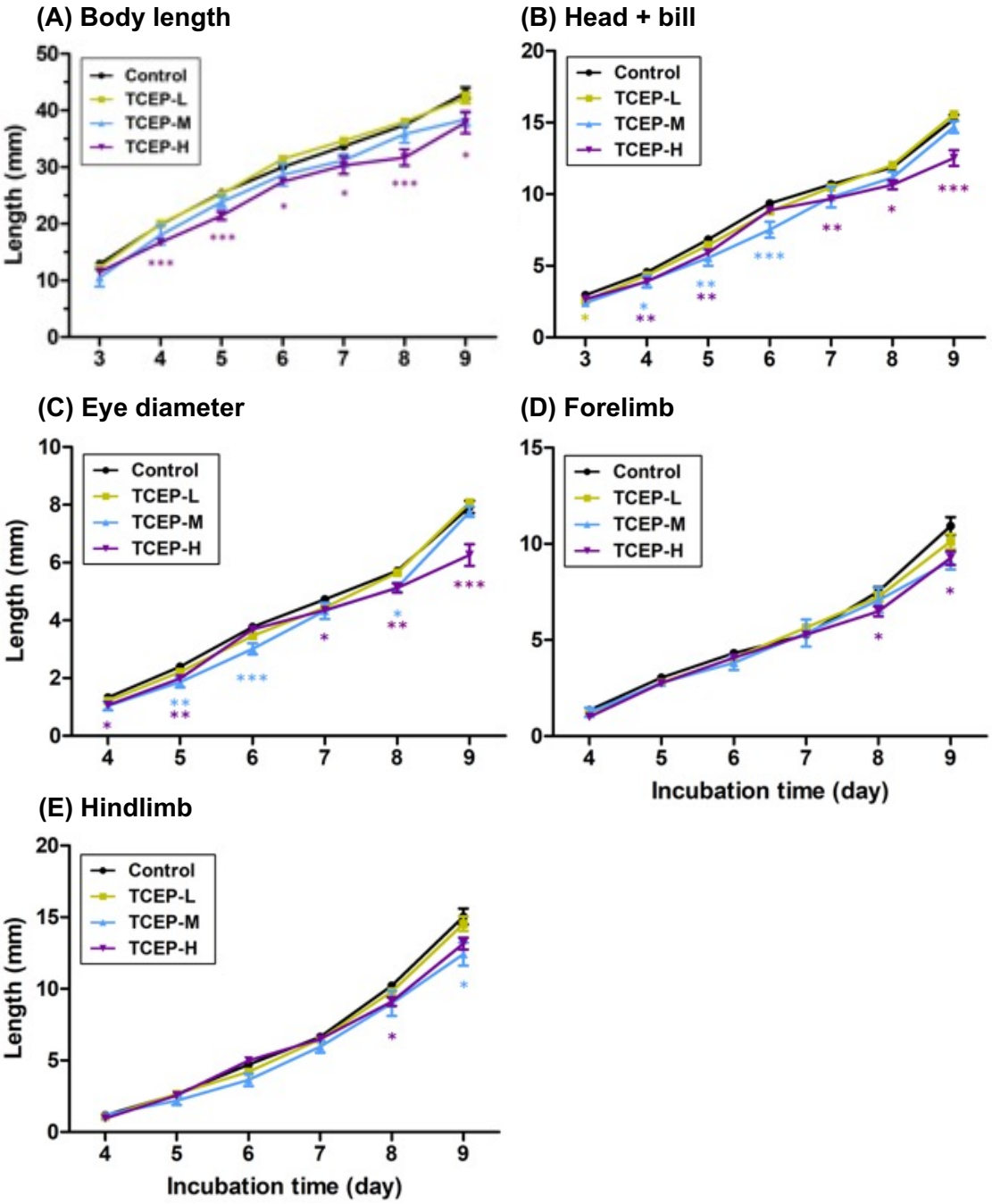

Figure. 2.14 Effects of TCEP exposure on (A) body length, (B) head + bill length, (C) eye diameter, (D) forelimb length, and (E) hindlimb length only in chicken embryos that survived until incubation day 9 (control, $n = 26$; TCEP-L, $n = 13$; TCEP-M, $n = 5$; TCEP-H, $n = 10$). Data represent means ± standard errors. Asterisks indicate significant differences (*$p < 0.05$, **$p < 0.01$, ***$p < 0.001$).

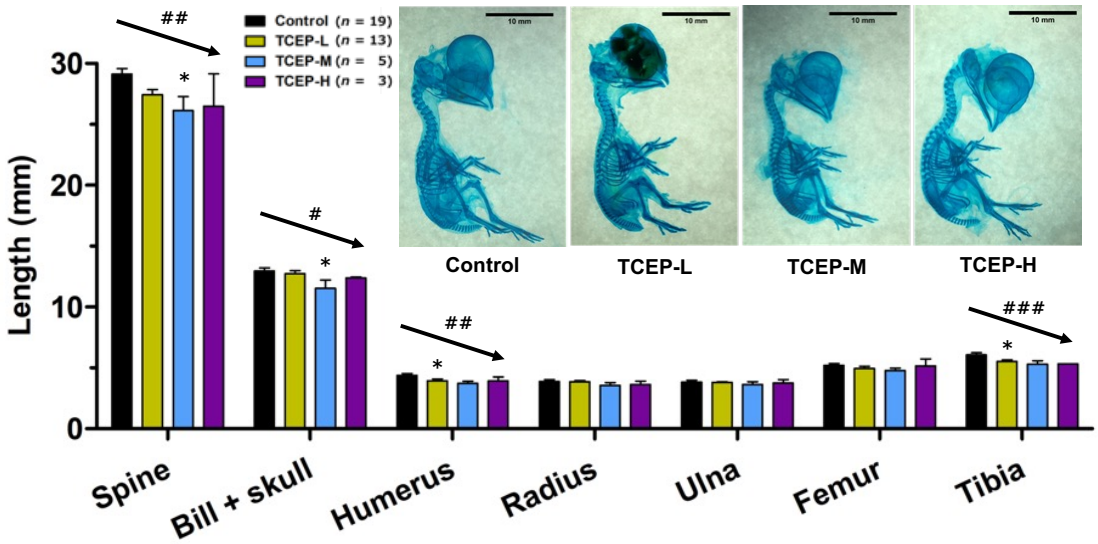

Figure. 2.15 Effects of TCEP exposure on length of the spine, bill + skull, humerus, radius, ulna, femur, and tibia in each group (control, $n = 19$; TCEP-L, $n = 13$; TCEP-M, $n = 5$; TCEP-H, $n = 3$). Data represent mean ± SE. The asterisk indicates a significant difference (*$p < 0.05$). The hash symbol and arrow indicate that the length was altered in a dose-dependent manner (# $p < 0.05$, ## $p < 0.01$, ### $P < 0.001$; Jonckheere-Terpstra test)

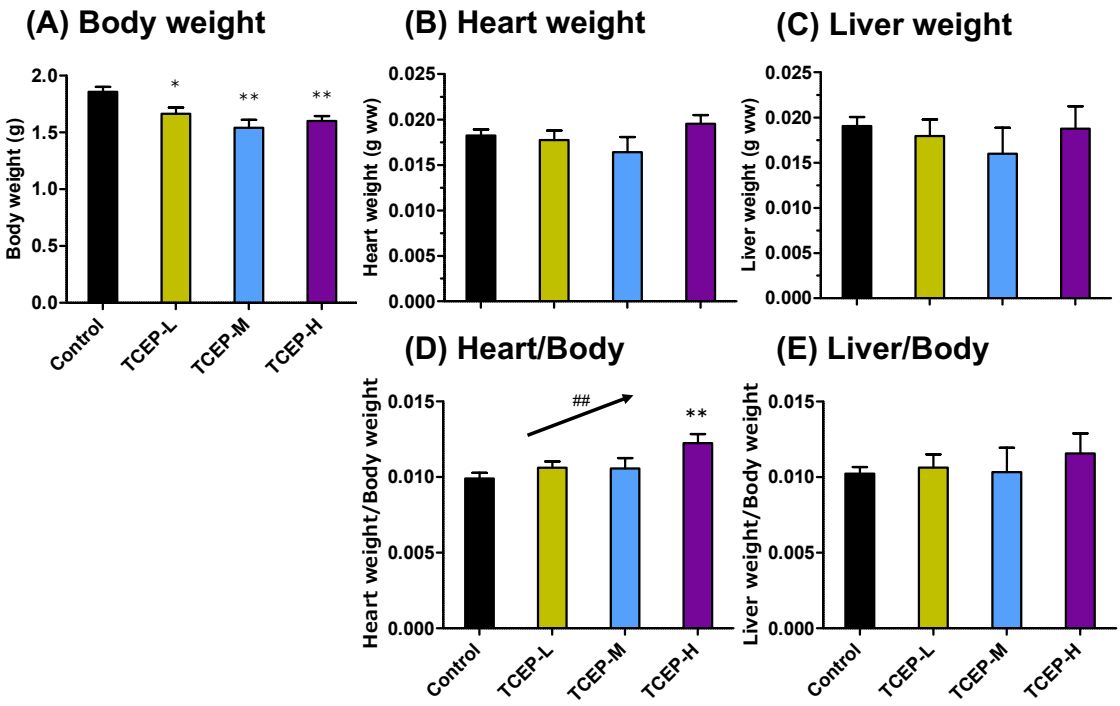

Figure. 2.16 Effects of TCEP exposure on (A) body weight, (B) heart weight, (C) liver weight, (D) heart weight relative to body weight, and (E) liver weight relative to body weight in each group (control, n = 27; TCEP-L, n = 13; TCEP-M, n = 5; TCEP-H, n = 10). Data represent mean ± SE. The asterisk indicates a significant difference (*$p < 0.05$, **$p < 0.01$). The hash symbol and arrow indicate that the length was altered in a dose-dependent manner (## $p <$ 0.01; Jonckheere-Terpstra test).

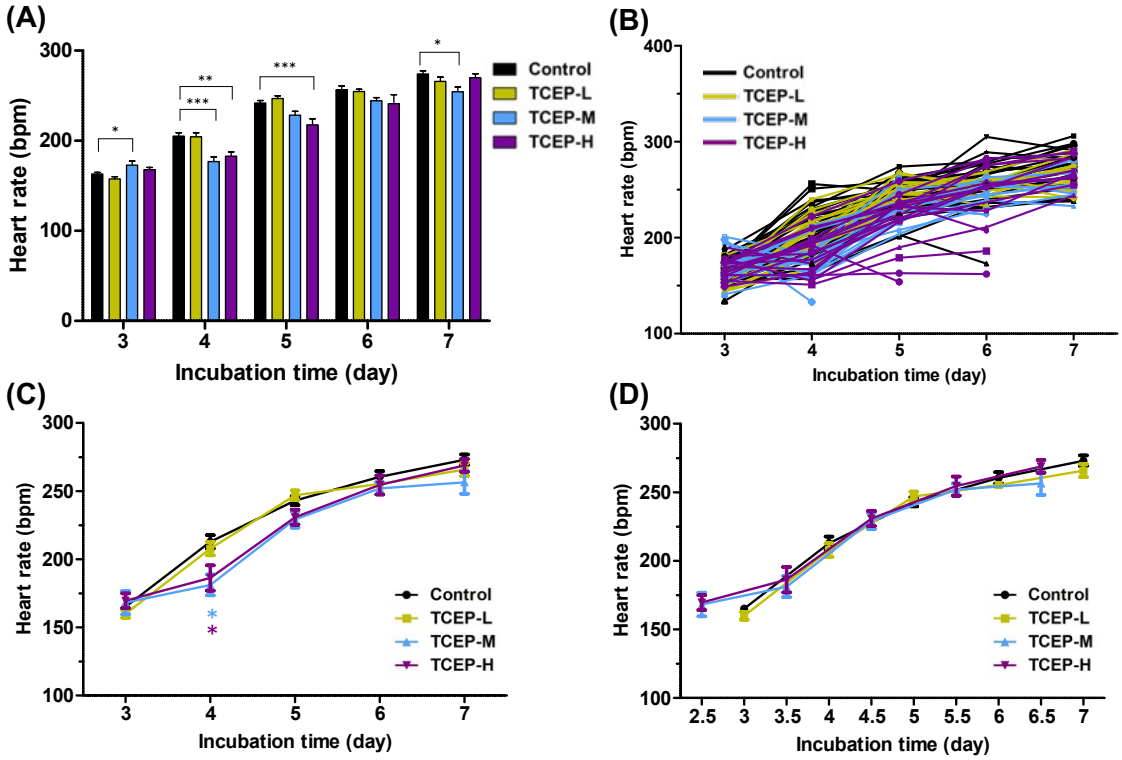

Figure. 2.17 Effects of TCEP on the chicken embryo's heart rate. (A) The average heart rate in each group. (B) The heart rate of surviving individuals. (C) The change of chronological average heart rate only in chicken embryos that survived until incubation day 9. (D) Results of shifting the average heart rate of the TCEP-M and TCEP-H groups 0.5 days earlier than graph C. Data are presented as mean ± SE. Asterisk indicates significant difference (*$p < 0.05$, **$p < 0.01$, ***$p < 0.001$).

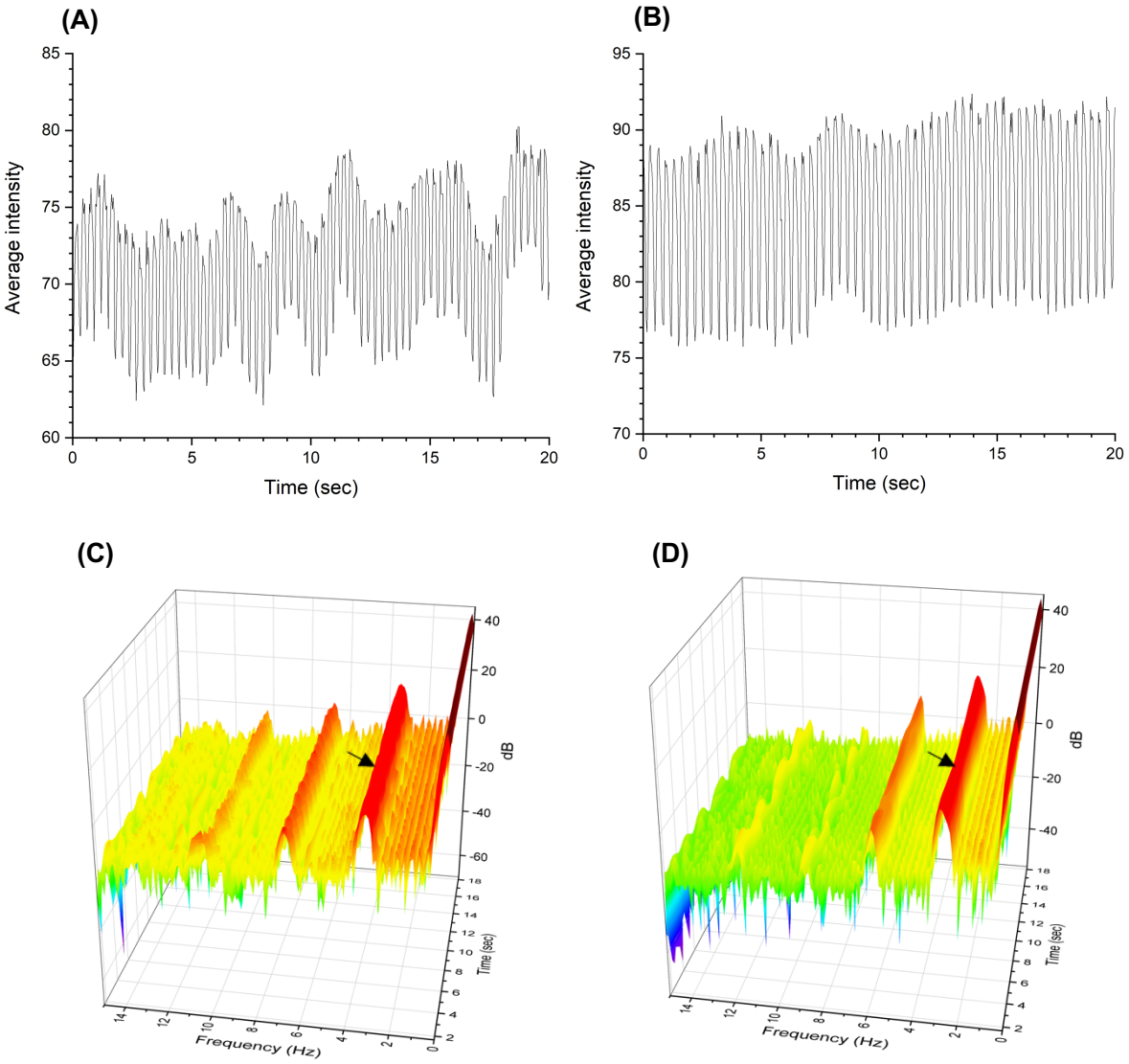

Figure. 2.18 Heart rate measured using a dynamic pixel method. Changes in the average dynamic pixel intensity for 20 s in the ventricle of (A) a control embryo and (B) a TCEP-H embryo on incubation day 4. Dynamic pixel data were converted to the heartbeat frequency (arrow) in a (C) control group and (D) a TCEP-H group by short-time Fourier transformation. The x-, y-, and z-axis indicate time (sec), heartbeat frequency (Hz), and intensity (dB), respectively.

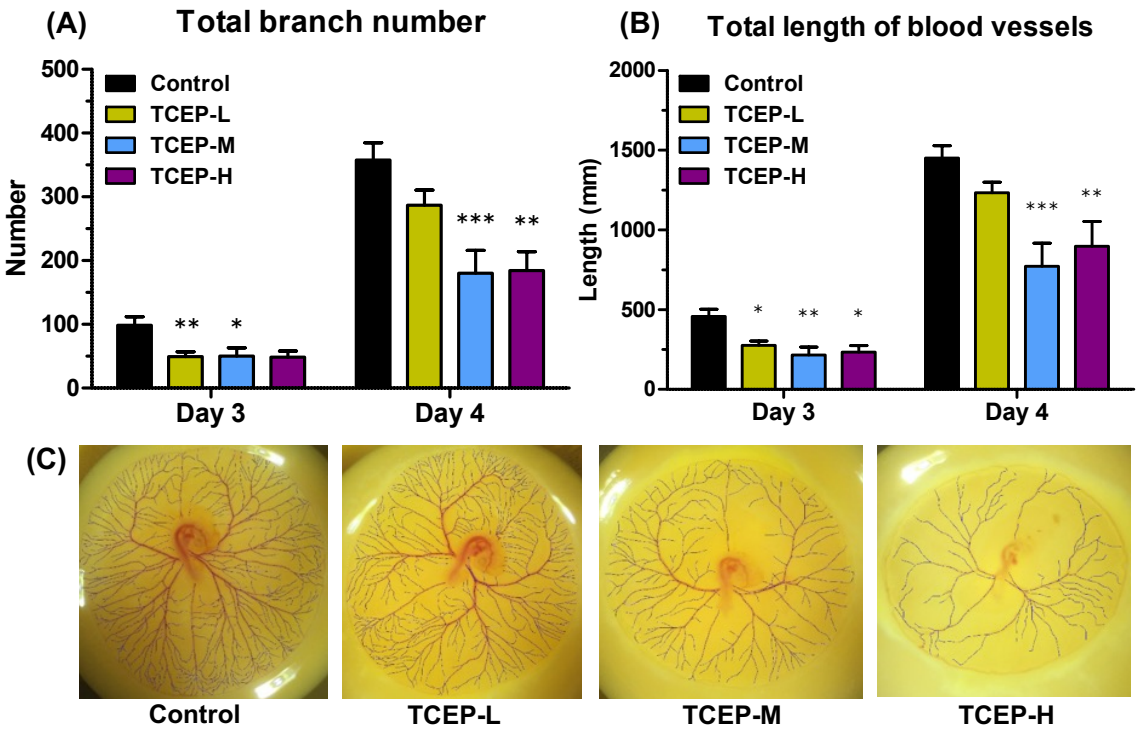

Figure. 2.19 Effects of TCEP on (A) the total branch number and (B) the total length of extraembryonic blood vessels. Data are presented as means ± standard error. Asterisks indicate significant differences (*$p < 0.05$, **$p < 0.01$, ***$p < 0.001$). (C) Representative images of extraembryonic blood vessels on day 4 in each group. Blue lines indicate the measured blood vessels.

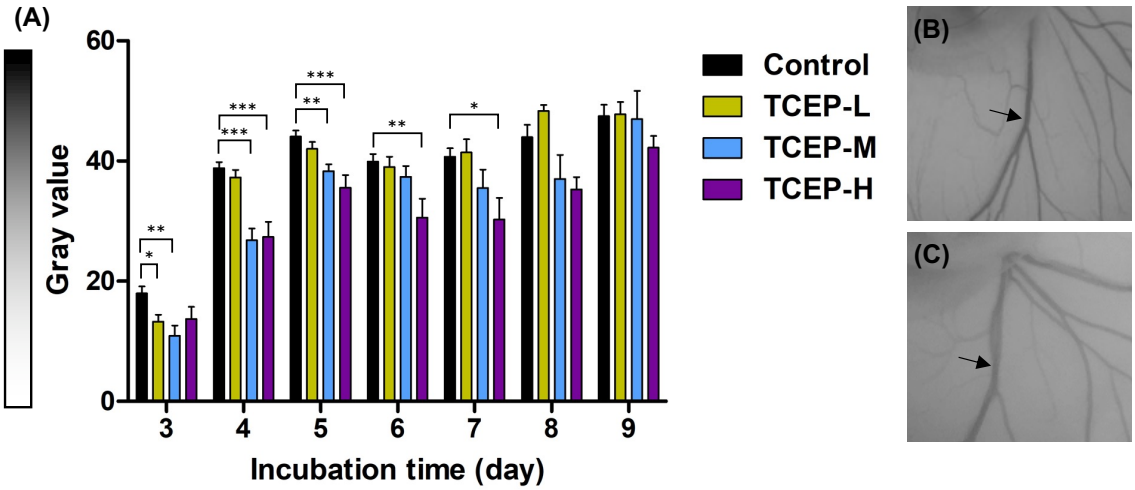

Figure. 2.20 Effects of TCEP on the gray value of extraembryonic arteries from day 3 to 9 (day 3: control, *n* = 29; TCEP-L, *n* = 18; TCEP-M, *n* = 15; TCEP-H, *n* = 8; day 4: control, *n* = 29; TCEP-L, *n* = 18; TCEP-M, *n* = 15; TCEP-H, *n* = 9; day 5: control, *n* = 29; TCEP-L, *n* = 18; TCEP-M, *n* = 14; TCEP-H, *n* = 9; day 6: control, *n* = 26; TCEP-L, *n* = 16; TCEP-M, *n* = 13; TCEP-H, *n* = 8; day 7: control, *n* = 20; TCEP-L, *n* = 14; TCEP-M, *n* = 8; TCEP-H, *n* = 5; day 8: control, *n* = 19; TCEP-L, *n* = 13; TCEP-M, *n* = 6; TCEP-H, *n* = 5; day 9: control, *n* = 19; TCEP-L, *n* = 13; TCEP-M, *n* = 5; TCEP-H, *n* = 3). (A) The net gray value of the blood vessel was calculated by correcting the blood vessel's minimum gray value with the background's median gray value. Data represent means ± standard error. Asterisks indicate significant differences (*$p < 0.05$, **$p < 0.01$, ***$p < 0.001$). Representative examples of an extraembryonic artery of (B) control and (C) TCEP-H embryo on incubation day 6. The arrow in the digital images indicates the measured extraembryonic artery.

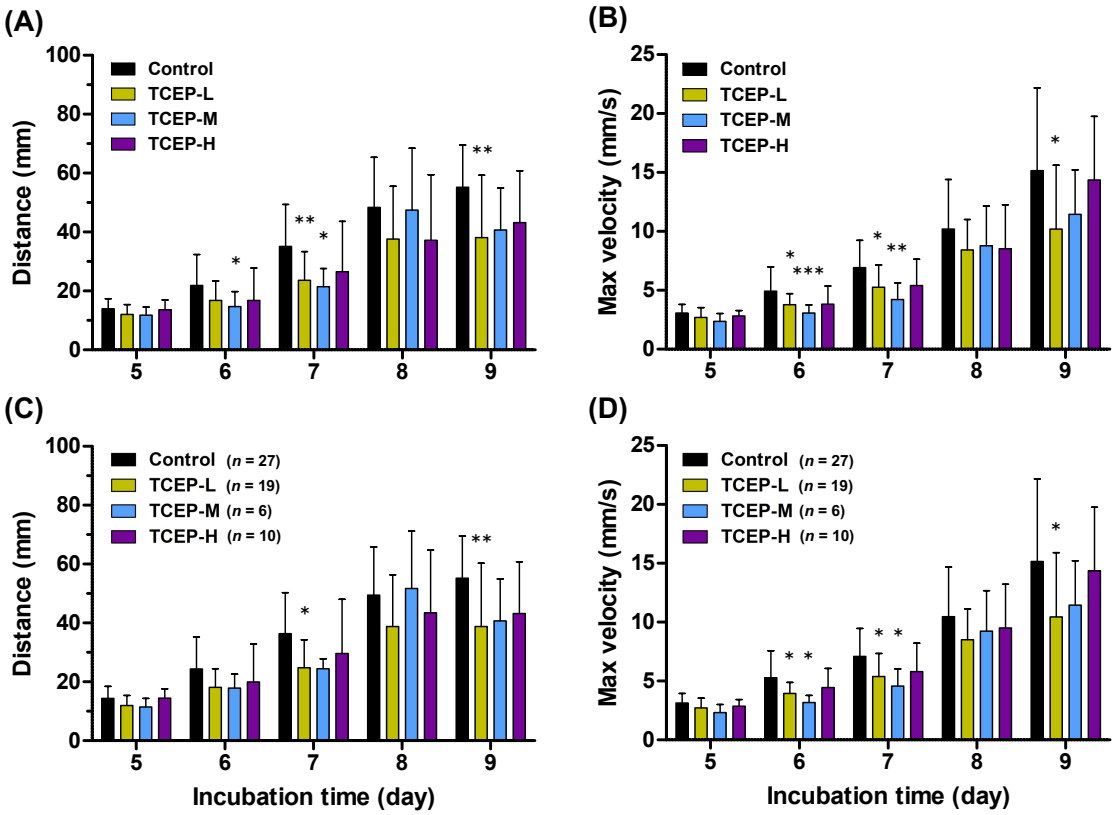

Figure. 2.21 Effects of TCEP on (A) the total distance and (B) the maximum velocity of spontaneous movement in chicken embryos. (C) the total distance and (D) the maximum velocity of spontaneous movement only in chicken embryos that survived until incubation day nine are represented. Data are presented as means ± standard deviation. Asterisks indicate significant differences (*$p < 0.05$, **$p < 0.01$, ***$p < 0.001$).

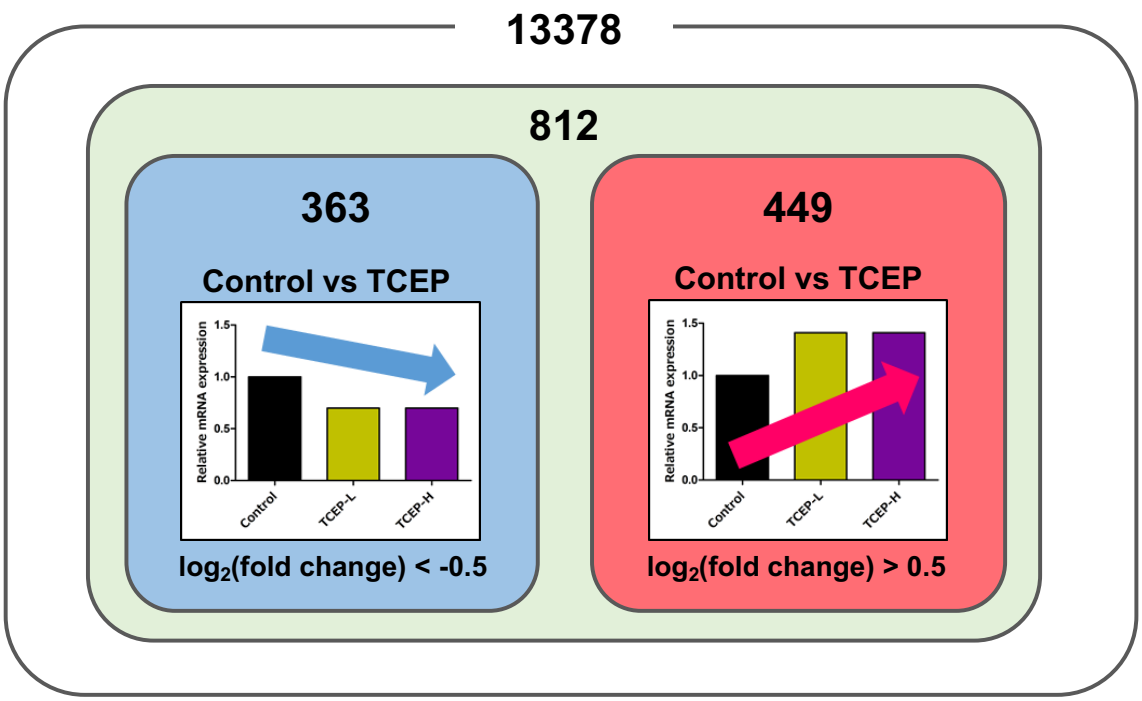

Figure. 2.22 The number of differentially expressed genes in the TCEP exposure group.

Table. 2.4 GO terms in the GO enrichment analysis's biological process (BP) using DEGs.

GO term	Count	%	P-Value
GO:0060048~cardiac muscle contraction	7	0.9	2.1E-04
GO:0045746~negative regulation of Notch signaling pathway	7	0.9	5.2E-04
GO:0048839~inner ear development	7	0.9	2.0E-03
GO:0001649~osteoblast differentiation	10	1.3	2.2E-03
GO:0006342~chromatin silencing	7	0.9	2.5E-03
GO:0060441~epithelial tube branching involved in lung morphogenesis	5	0.6	2.9E-03
GO:0006939~smooth muscle contraction	5	0.6	2.9E-03
GO:0045662~negative regulation of myoblast differentiation	5	0.6	3.9E-03
GO:0055010~ventricular cardiac muscle tissue morphogenesis	5	0.6	3.9E-03
GO:0055013~cardiac muscle cell development	5	0.6	3.9E-03
GO:0010628~positive regulation of gene expression	25	3.2	4.1E-03
GO:0090303~positive regulation of wound healing	5	0.6	5.1E-03
GO:0030308~negative regulation of cell growth	10	1.3	5.2E-03
GO:0014850~response to muscle activity	4	0.5	5.5E-03
GO:0048546~digestive tract morphogenesis	4	0.5	5.5E-03
GO:0030336~negative regulation of cell migration	10	1.3	6.3E-03
GO:0043066~negative regulation of apoptotic process	20	2.6	6.8E-03
GO:0051127~positive regulation of actin nucleation	3	0.4	7.0E-03
GO:0002931~response to ischemia	5	0.6	8.2E-03
GO:0043065~positive regulation of apoptotic process	16	2.1	8.7E-03
GO:0008285~negative regulation of cell proliferation	19	2.4	9.1E-03
GO:0000187~activation of MAPK activity	7	0.9	9.8E-03
GO:0035914~skeletal muscle cell differentiation	7	0.9	9.8E-03
GO:0001938~positive regulation of endothelial cell proliferation	7	0.9	1.3E-02
GO:0046902~regulation of mitochondrial membrane permeability	3	0.4	1.3E-02
GO:2000669~negative regulation of dendritic cell apoptotic process	3	0.4	1.3E-02
GO:0030335~positive regulation of cell migration	14	1.8	1.5E-02
GO:0045892~negative regulation of transcription, DNA-templated	19	2.4	1.7E-02
GO:0072593~reactive oxygen species metabolic process	5	0.6	1.8E-02
GO:0016126~sterol biosynthetic process	4	0.5	1.9E-02
GO:0043406~positive regulation of MAP kinase activity	7	0.9	2.0E-02

GO term	Count	%	P-Value
GO:0007611~learning or memory	5	0.6	2.1E-02
GO:0070508~cholesterol import	3	0.4	2.2E-02
GO:0010873~positive regulation of cholesterol esterification	3	0.4	2.2E-02
GO:0045766~positive regulation of angiogenesis	9	1.2	2.2E-02
GO:0030325~adrenal gland development	4	0.5	2.3E-02
GO:0009636~response to toxic substance	5	0.6	2.4E-02
GO:0030514~negative regulation of BMP signaling pathway	7	0.9	2.6E-02
GO:0002027~regulation of heart rate	4	0.5	2.9E-02
GO:0006936~muscle contraction	6	0.8	3.0E-02
GO:0042391~regulation of membrane potential	9	1.2	3.0E-02
GO:0042493~response to drug	8	1.0	3.1E-02
GO:0045606~positive regulation of epidermal cell differentiation	3	0.4	3.2E-02
GO:0061549~sympathetic ganglion development	3	0.4	3.2E-02
GO:0003334~keratinocyte development	3	0.4	3.2E-02
GO:0003151~outflow tract morphogenesis	5	0.6	3.2E-02
GO:0030032~lamellipodium assembly	5	0.6	3.2E-02
GO:0032526~response to retinoic acid	5	0.6	3.2E-02
GO:0060173~limb development	6	0.8	4.1E-02
GO:0032148~activation of protein kinase B activity	4	0.5	4.1E-02
GO:0032720~negative regulation of tumor necrosis factor production	5	0.6	4.1E-02
GO:0045214~sarcomere organization	5	0.6	4.1E-02
GO:0043583~ear development	3	0.4	4.3E-02
GO:2000279~negative regulation of DNA biosynthetic process	3	0.4	4.3E-02
GO:0006002~fructose 6-phosphate metabolic process	3	0.4	4.3E-02
GO:0055008~cardiac muscle tissue morphogenesis	3	0.4	4.3E-02
GO:0045661~regulation of myoblast differentiation	3	0.4	4.3E-02
GO:0040008~regulation of growth	5	0.6	4.6E-02
GO:0006695~cholesterol biosynthetic process	4	0.5	4.8E-02
GO:0030318~melanocyte differentiation	4	0.5	4.8E-02
GO:0048709~oligodendrocyte differentiation	4	0.5	4.8E-02
GO:0019722~calcium-mediated signaling	6	0.8	4.9E-02

Table. 2.5 GO terms in the GO enrichment analysis's cellular component (CC) using DEGs.

GO term	Count	%	P-Value
GO:0005886~plasma membrane	125	16.0	9.1E-04
GO:0070161~anchoring junction	11	1.4	1.1E-03
GO:0043025~neuronal cell body	16	2.1	1.1E-03
GO:0030018~Z disc	11	1.4	1.4E-03
GO:0031430~M band	5	0.6	1.7E-03
GO:0005615~extracellular space	65	8.3	2.9E-03
GO:0030424~axon	19	2.4	4.6E-03
GO:0030672~synaptic vesicle membrane	8	1.0	5.0E-03
GO:0005576~extracellular region	39	5.0	6.7E-03
GO:0031674~I band	4	0.5	6.8E-03
GO:0009986~cell surface	24	3.1	7.1E-03
GO:0008076~voltage-gated potassium channel complex	9	1.2	8.5E-03
GO:0005901~caveola	7	0.9	9.9E-03
GO:0005737~cytoplasm	161	20.6	1.6E-02
GO:0030016~myofibril	5	0.6	2.0E-02
GO:0033017~sarcoplasmic reticulum membrane	4	0.5	2.5E-02
GO:0016324~apical plasma membrane	15	1.9	3.4E-02
GO:0005783~endoplasmic reticulum	37	4.7	3.6E-02
GO:0016328~lateral plasma membrane	6	0.8	3.7E-02
GO:0005887~integral component of plasma membrane	47	6.0	3.9E-02
GO:0071944~cell periphery	4	0.5	4.9E-02
GO:0031463~Cul3-RING ubiquitin ligase complex	5	0.6	4.9E-02

Table. 2.6 GO terms in the GO enrichment analysis's molecular function (MF) using DEGs.

GO term	Count	%	P-Value
GO:0031432~titin binding	4	0.5	1.9E-03
GO:0044325~ion channel binding	12	1.5	2.3E-03
GO:0005184~neuropeptide hormone activity	6	0.8	3.8E-03
GO:0015459~potassium channel regulator activity	6	0.8	4.6E-03
GO:0008307~structural constituent of muscle	5	0.6	7.1E-03
GO:0005515~protein binding	13	1.7	1.2E-02
GO:0005246~calcium channel regulator activity	5	0.6	1.5E-02
GO:0030234~enzyme regulator activity	5	0.6	1.8E-02
GO:0005509~calcium ion binding	40	5.1	2.1E-02
GO:0016918~retinal binding	3	0.4	4.0E-02
GO:0019841~retinol binding	3	0.4	4.0E-02
GO:0003779~actin binding	16	2.1	4.1E-02
GO:0008157~protein phosphatase 1 binding	4	0.5	4.3E-02

Table. 2.7 Enriched transcription factors (TFs) in DEGs by TCEP exposure.

Transcription Factor	TFactS		
	Overlap	P.value	E.value
NFKB1	14/141	0.00E+00	0.00E+00
FOXO1	15/161	0.00E+00	0.00E+00
CTNNB1	27/306	0.00E+00	0.00E+00
SP1	32/428	0.00E+00	0.00E+00
EGR1	11/91	0.00E+00	0.00E+00
GLI1	12/124	1.00E-05	1.19E-03
SP3	11/132	1.00E-04	1.19E-02
SMAD4	6/45	3.30E-04	3.93E-02
GLI2	9/107	4.00E-04	4.76E-02
GLI3	2/2	4.40E-04	5.24E-02
SOX10	3/10	9.90E-04	1.18E-01
SMAD1	4/22	1.04E-03	1.24E-01
PPARG	5/41	1.59E-03	1.89E-01
SMAD3	6/63	2.01E-03	2.39E-01
USF2	7/86	2.16E-03	2.57E-01

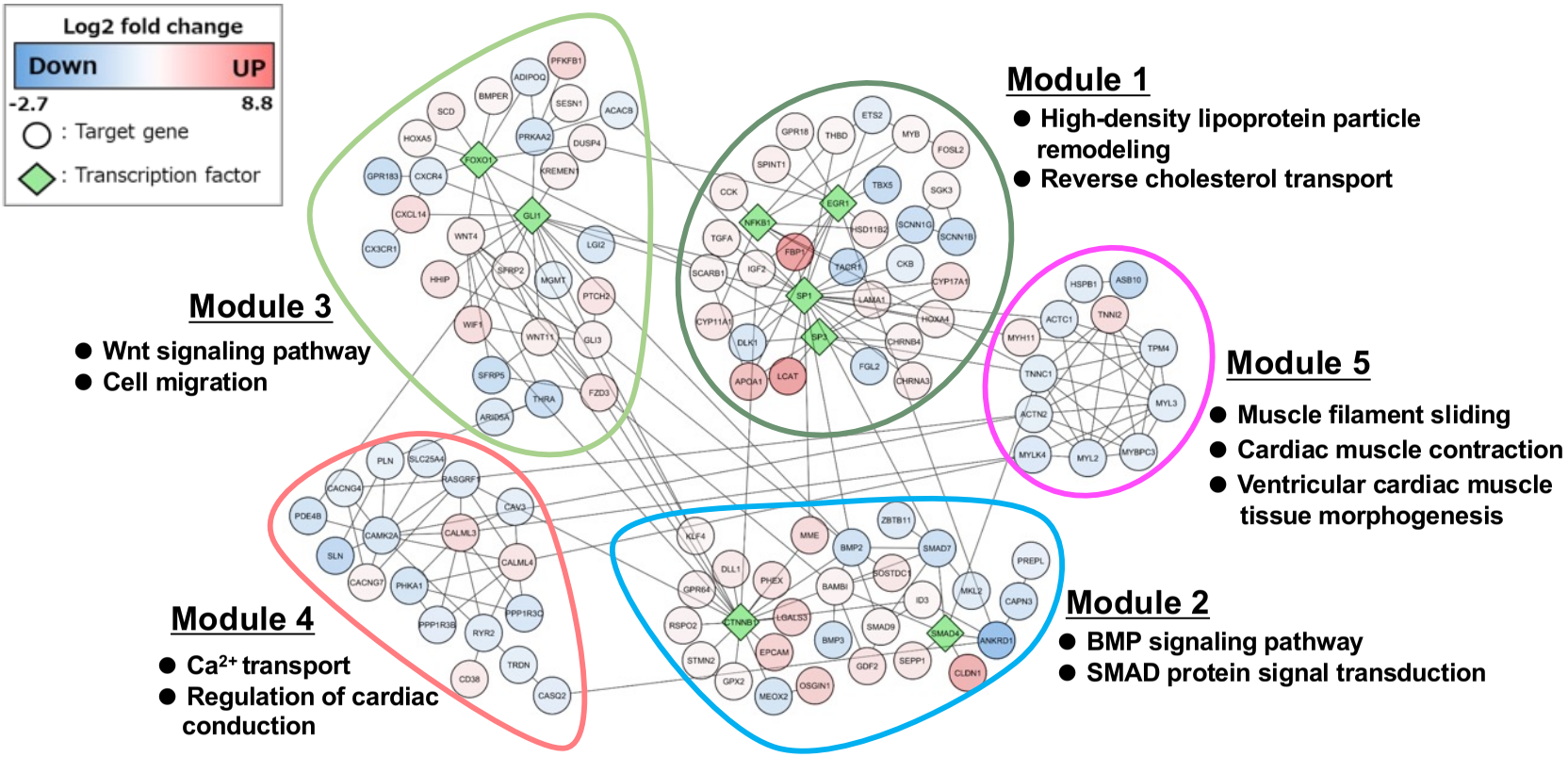

Figure. 2.23 The most common transcription factors and affected genes found in comparisons between the control and TCEP-H groups.

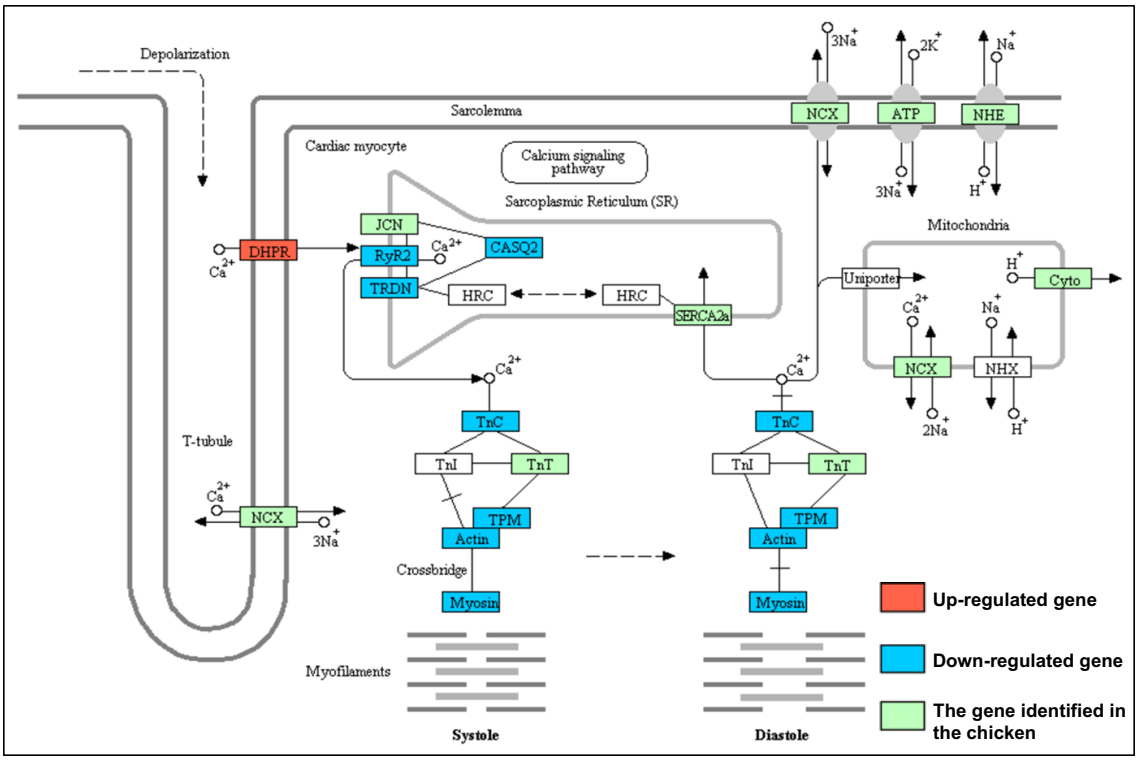

Figure. 2.24 Effect of TCEP exposure on the cardiac muscle contraction pathway. All DEGs in the TCEP-H group were mapped by the KEGG mapper tool. Red-colored genes and blue-colored genes indicate DEGs of up-regulated and down-regulated, respectively.

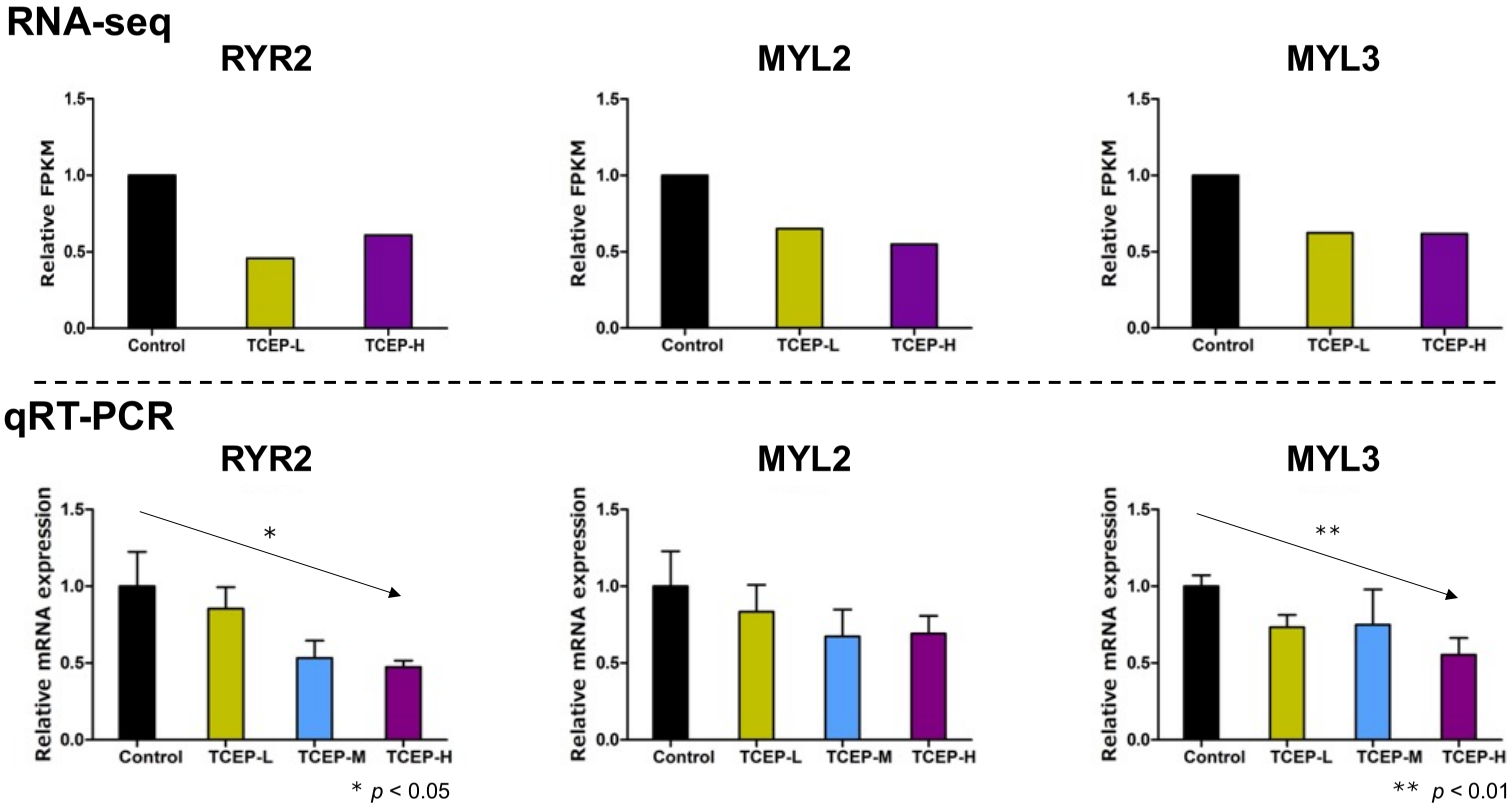

Figure. 2.25 Relative mRNA expression levels of RNA-seq and qRT-PCR in RYR2, MYL2, and MYL3. Data represent mean ± SE. The asterisk symbol and arrow indicate that the mRNA level was altered dose-dependent (* $p < 0.05$, ** $p < 0.01$; Jonckheere-Terpstra test).

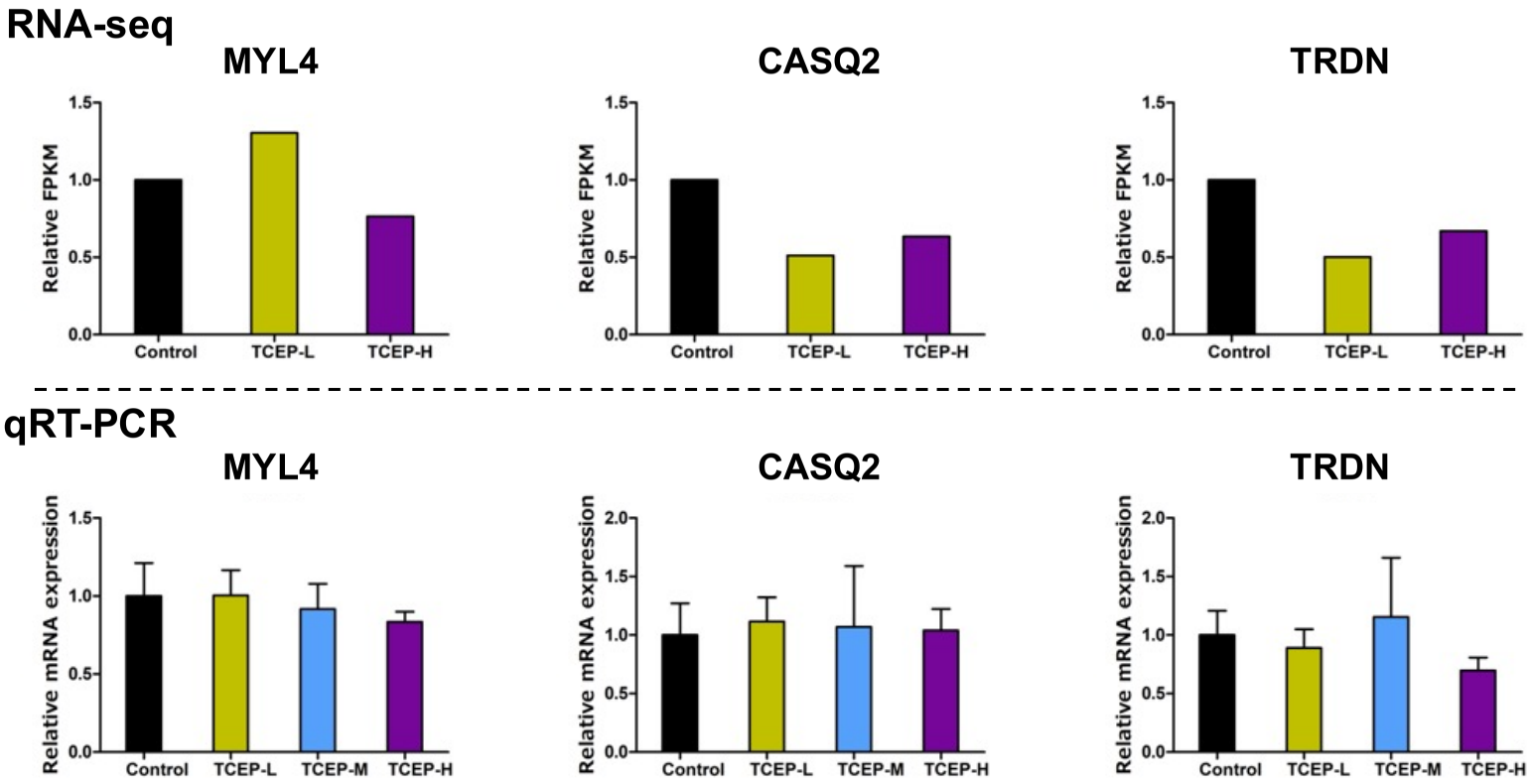

Figure. 2.26 Relative mRNA expression levels of RNA-seq and qRT-PCR in MYL4, CASQ2, and TRDN. Data represent means ± standard error.

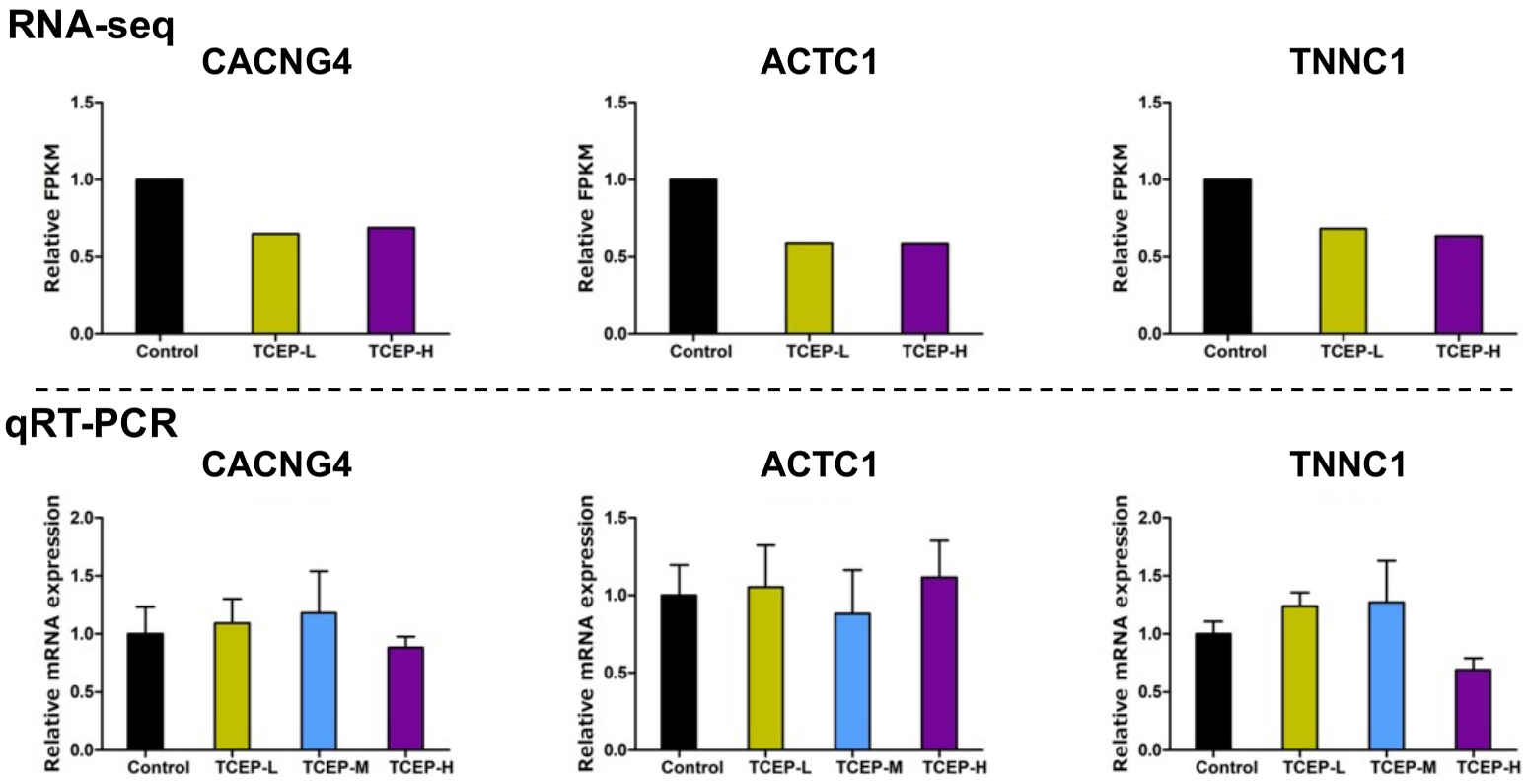

Figure. 2.27 Relative mRNA expression levels of RNA-seq and qRT-PCR in CACNG4, ACTC1, and TNNC1. Data represent means ± standard error.

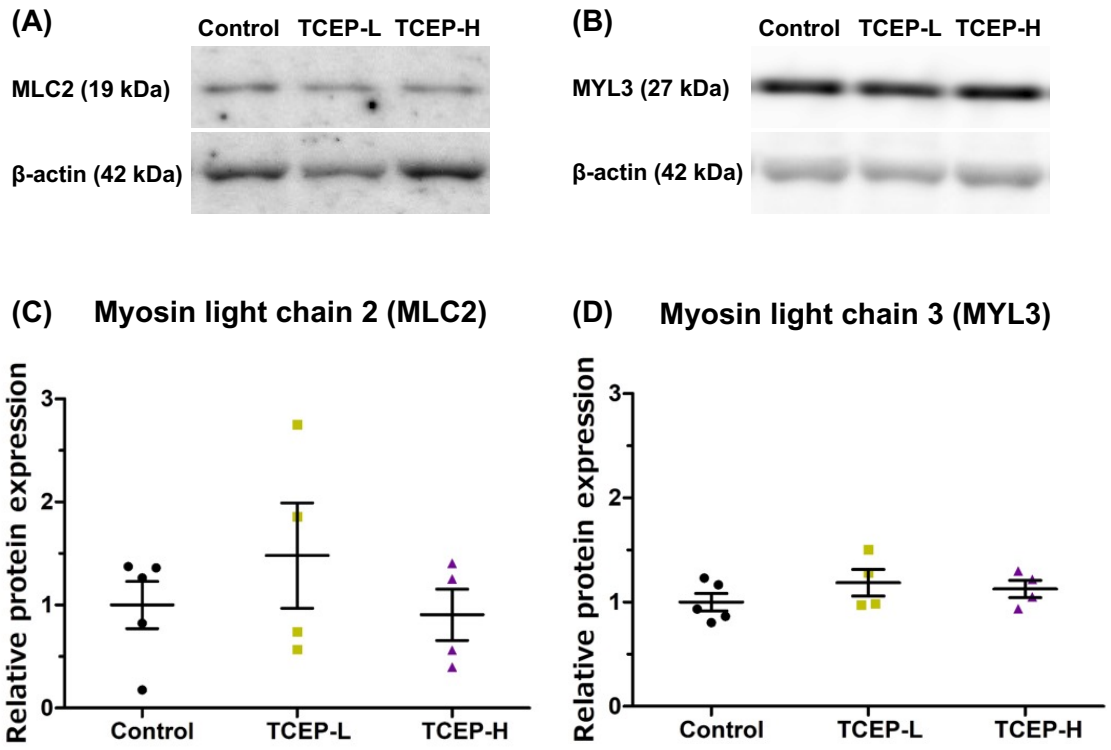

Figure. 2.28 Effects of TCEP on protein expression in the heart. Images of (A) myosin light chain 2 (MLC2) and (B) myosin light chain 3 (MYL3) protein bands by western blot. Relative (C) MLC2 and (D) MYL3 protein expression from two independent experiments were expressed as a value relative to the control group after normalization by β-actin. Data represent means ± standard error.

Discussion

We established a novel toxicity assessment method using a shell-less culture system to investigate the effects of TCEP on early chicken embryos. This approach allowed for the measurement of more than 17 phenotypic endpoints, and we were able to examine the toxic effects of TCEP from various perspectives. There was a significant difference in the survival of chicken embryos between 50 nmol/g egg and 250 nmol/g egg. It is suggested that the LD50 of TCEP for chicken embryos is within the range of 50 nmol/g egg to 250 nmol/g egg. Embryonic body length, body parts length, skeletal length, and body weight showed that TCEP above 250 nmol/g retarded the growth of chicken embryos. It has been reported that exposure of 3- to 120-h post-fertilization (hpf) zebrafish embryos to TCEP (14,250 and 28,500 μg/L) delays their development (Wu et al., 2017). Therefore, it was suggested that TCEP inhibits the growth of avian embryos and fish embryos. TCIPP and TDCIPP, major Cl-OPEs similar in chemical structure to TCEP, delayed pipping in chicken embryos at doses of 28 nmol/g egg and 18 nmol/g egg, respectively. Higher levels of TCIPP (158 nmol/g egg) and TDCIPP (104 nmol/g egg) significantly reduced the tarsus length and body mass at pipping (Farhat et al., 2013). Thus, exposure of early embryos to TCEP may delay hatching time and cause the hatching of premature chicks. In the skeletal results, no skeletal malformation was observed in the chicken embryos, although a previous study demonstrated that exposure to TCEP induced vertebral deformities such as the immature spine,

tail deformation, and spinal curvature in zebrafish embryos (Wang et al., 2022; Wu et al., 2017). These results suggest that the mechanism of TCEP-induced effects on skeletal formation in chicken embryos may be different from that in zebrafish.

The heart rate was significantly decreased in a TCEP concentration-dependent manner on days 4 to 6 (Fig. 2.17A). These results are consistent with those in previous studies, in which exposure to OPFRs, including tris (methylphenyl) phosphate (TMPP), TPHP, and TDCIPP, resulted in significant reductions in the heart rate of zebrafish (Alzualde et al., 2018; Du et al., 2015). However, the heart rate in chicken embryos that survived until day nine was significantly reduced on only day 4 (Fig. 2.17C). The results of heart rate values for the TCEP-M and TCEP-H groups were then shifted by 0.5 days and showed similar heart rate changes as the control group (Fig. 2.18D). In addition, no alteration was detected in the heartbeat frequency (Hz) in all TCEP-treated groups, suggesting that TCEP exposure causes no arrhythmias in chicken embryos. Previous studies exposing zebrafish embryos to TCEP showed no significant changes in heart rate (Alzualde et al., 2018; Wu et al., 2017). In vitro cardiotoxicity assessment using human induced pluripotent stem cells (iPSCs)-derived cardiomyocytes, TCEP exposure did not alter the Ca^{2+} flux in cardiomyocytes and did not induce cardiotoxicity (Sirenko et al., 2017). Therefore, decreased heart rate may be associated with TCEP-induced growth retardation. On the other hand, the heart weight to body weight ratio was significantly increased in the TCEP-H group (Fig. 2.16D). The

reduction in body weight in the TCEP-treated groups indicates a delay in development (Fig. 2.16A). Therefore, the heart weight in the TCEP-treated groups should have decreased if the heart development was delayed. However, there was no significant difference in heart weight. This result suggests that TCEP exposure induces cardiac hypertrophy in chicken embryos. In previous studies, exposing zebrafish to TDCIPP and TPHP significantly increased the pericardial area in a concentration-dependent manner (Dasgupta et al., 2018; Isales et al., 2015). Consequently, our results indicate that TCEP may also induce cardiac hypertrophy.

In the primary vasculogenesis of chicken embryos, the blood island becomes visible in the proximal region of the yolk sac, the area vasculosa at HH6 (23–25 hours). In the blood island, the blood travels from the embryo to the yolk sac and transports partly digested yolk to the embryo (Sheng, 2010). TCEP-exposed groups decreased the length and branch number of extraembryonic blood vessels on days 3–4 and reduced the number of erythrocytes on days 3–7 compared to the control group (Fig. 2.19 and 2.20). To the best of our knowledge, there are no reports of studies regarding the effects of TCEP on angiogenesis or hematopoietic function. However, TDCIPP, a Cl-OPEs, has been reported to affect the circulatory system. Zhong et al. (2019) reported that exposure of zebrafish embryos (2 hpf) to 0.7 and 1.2 μM TDCIPP delayed the formation of intersegmental vessels and common cardinal veins and decreased gene expression of Vegfa, Vegfr1, Vegfr2, and Hif1a, which are involved in angiogenesis. Exposure to 30 μM TDCPP has

been reported to cause pericardiac edema and reduction of blood flow in trunk vessels in zebrafish embryos. Also, 1.56 μM and 3.12 μM TDCIPP-treated zebrafish embryos showed a significant concentration-dependent decrease in hemoglobin levels from 0.75 to 72 hpf, and transcriptome analysis using zebrafish embryos suggested that the cause of this effect is the downregulation of mesoderm development (Dasgupta et al., 2018). Therefore, TCEP may also affect mesoderm development and VEGF signaling, and molecular mechanisms in TCEP's effects on the circulatory system need further investigation.

To investigate the molecular mechanisms of toxicity of TCEP exposure on chicken embryo hearts, transcriptome analysis was performed using day nine hearts. GO enrichment analysis revealed that the function of cardiac muscle contraction was significantly affected by TCEP exposure (Table 2.4). KEGG pathway analysis showed that TCEP altered the expression of nine genes involved in cardiac muscle contraction (Fig. 2.24). In addition, the expression of these nine genes was measured by qRT-PCR, and mRNA levels of RYR2, MYL2, and MYL3 were found to be reduced in a TCEP concentration-dependent manner (Fig. 2.25). RYR2 plays an important role in myocardial contraction. In the cardiomyocyte, activating a cluster of RYRs, and consequent mobilization of Ca^{2+} from the sarcoplasmic reticulum produces an elementary Ca^{2+} release signal (Marks, 2013). Troponin c (TnC) binding with Ca^{2+} causes a conformational change in associated Troponin I (TnI). This enables troponin/a-tropomyosin (Tn/Tm) to slide into the

groove between actin monomers, allowing the thick myosin filament to bind actin, thus forming a cross-bridge (Fearnley et al., 2011). Caldwell et al. (2008) used cultured H9c2, rat cardiac myocyte cell line, to demonstrate that trichloroethylene disrupted the Ca^{2+} homeostasis following repressed RYR2 transcripts. It has been reported that mouse embryonic stem (ES) cell-derived cardiomyocytes with a functional knockout (KO) of the RYR2 showed a slowing of the rate of spontaneous diastolic depolarization and an absence of calcium sparks and decreased heart rate (Yang et al., 2002). Thus, the trend of decreasing RYR2 expression in the heart by TCEP exposure may perturb calcium signaling and induce heart rate deduction. Also, in previous studies, the disruption of the inter-domain interactions, such as the destabilization of the interaction between N-terminal and central domains, within the RyR2, caused cardiomyocyte hypertrophy (Hamada et al., 2009; Oda et al., 2005). Accordingly, it is possible that downregulated expression of RYR2 induced cardiac hypertrophy.

Myosin light chains have important functions in myocardial contraction. The cardiac sarcomere comprises thick filaments containing the molecular motor myosin and thin filaments containing polymerized actin with its associated regulatory proteins tropomyosin and troponin. The binding of Ca2+ to the troponin complex results in the movement of troponin/tropomyosin from an inhibitory state, exposing myosin binding sites on actin, thus permitting actin-activation of myosin ATPase activity and ensuing contractions to occur (Chang et al., 2016).

Phosphorylation of the myosin light chain activates the actin-activated myosin ATPase to regulate muscle contraction (Sheikh et al., 2014). It has been reported that the inactivation of the myosin light chain 2 (Mlc2a) gene resulted in diminished atrial contraction and consequent embryonic lethality in mice (Huang et al., 2003). MYL 3 is the myosin light chain 3 of cardiac and type I skeletal muscle fibers and is a biomarker for cardiac and skeletal muscle toxicity (Bodié et al., 2016; Tonomura et al., 2012). The decreased expression of myosin light chain-related genes may affect contractile and relaxing functions in the myocardium. However, MLC2 and MYL3 protein expression were not changed by TCEP exposure (Fig. 2.28). The correlation between mRNA and protein abundance depends on various biological and technical factors (Maier et al., 2009). In addition, it is not expected that induced transcription immediately leads to increased protein levels because maturation, export, and mRNA translation take some time. Thus, there is a delay between transcriptional induction and protein level increases (Liu et al., 2016). Decreased gene expression of myosin light chain and ryanodine receptor due to TCEP exposure may affect the heart of chicken embryos after day 9.

In conclusion, we administered TCEP to fertilized chicken eggs and performed a novel avian embryonic toxicity study investigating the phenotypic effects, including the morphology and cardiovascular system, by a shell-less incubation system. We could successfully measure a variety of phenotypic endpoints. This method can also monitor the effects of other chemicals on

avian-developing embryos successively. All the OECD Test Guidelines for birds are for testing of adult and post-hatchling young birds, not for the effects on embryos. Therefore, toxicity testing using our shell-less incubation system could be a new method. We found that chicken embryos exposed to TCEP at above 250 nmol/g egg induced lethal effects, growth retardation, reduced heart rate, cardiac hypertrophy, and suppressed blood vessel formation. Cardiac transcriptome analysis in chicken embryos on day 9 revealed decreased expression of MYL2–4, a cardiac muscle contraction-related gene, and RYR2, a Ca^{2+} transport-related gene. These expression variation genes were predicted to be regulated by the transcription factors NFKB1, SP1, SP3, SMAD4, GLI1, and CTNNB1. MYLs and RYR2 changed gene expressions could have induced heart failure, cardiac arrest, and cardiac hypertrophy (Fig. 2.29). However, the heart rate could not be measured in day nine chicken embryos because a chorioallantoic membrane covers the heart, and it is unknown whether the heart rate was reduced to the down-regulation of RYR2 and MYLs genes in day nine chicken embryos. Therefore, transcriptome analysis of days 4–5 hearts with dramatically reduced heart rate may reveal a reliable cause for the reduced heart rate.

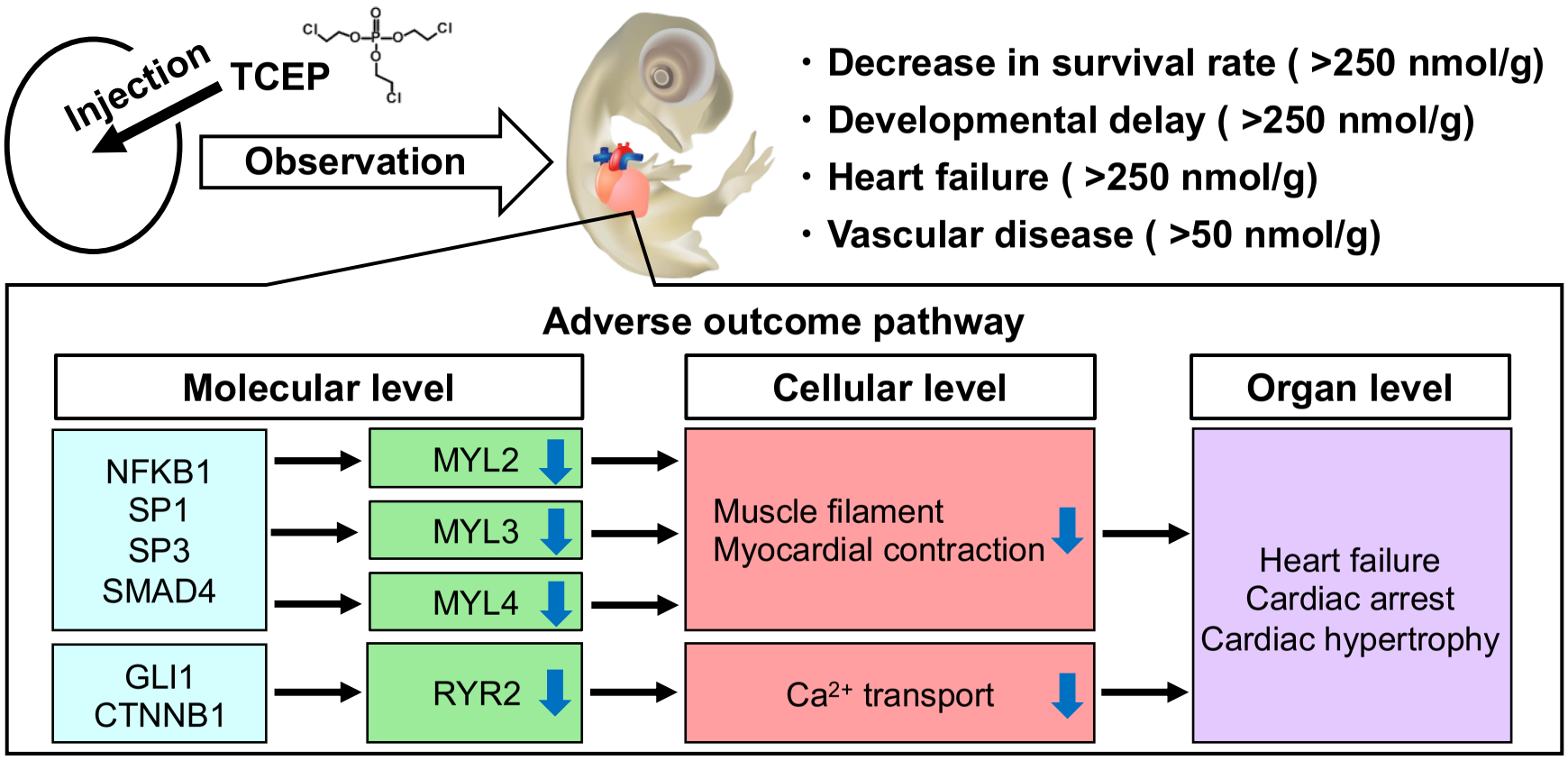

Figure. 2.29 The adverse outcome pathways predicted by TCEP exposure in chicken embryos.

CHAPTER III

Effects of TCEP on the cardiovascular transcriptome in *ex ovo* chicken embryos on day 5

3.1 Abstract

We have established a novel avian embryonic toxicity test method using a shell-less incubation system. A TCEP exposure study was conducted using this toxic test and found that TCEP exposure of more than 250 nmol/g egg induced growth delay, decreased heart rate, cardiac hypertrophy, inhibition of vasculogenesis, and decreased blood cells in chicken embryos. Cardiac transcriptome analysis using chicken embryo hearts on day 9 of incubation found that expression of cardiomyocyte contraction- and Ca^{2+} transport-related genes were affected by TCEP exposure. However, since the heart rate was critically affected by TCEP only on days 4-5, cardiac transcriptome analysis needs to be performed at an earlier developmental stage than day 9 to understand the molecular mechanisms of heart rate reduction. TCEP exposure inhibited vasculogenesis and angiogenesis in extraembryonic blood vessels in chickens, but this mechanism of action is unknown.

In this study, we investigated the mechanisms of cardiovascular toxicity of TCEP in chicken embryos on day 5. Fertilized chicken eggs were treated with 50, 250, and 500 nmol/g of TCEP (TCEP-L, -M, -H, respectively) or DMSO at Hamburger and Hamilton stage (HH) 1, and

measured cardiovascular phenotypic endpoints, including the heart rate, the heartbeat frequency, the ventricular surface area to body weight ratio, and the length of extraembryonic blood vessels on days 3 to 5 by the shell-less incubation system. RNA-seq for transcriptome analysis was performed with the hearts on day 5. In addition, vitelline membranes containing extraembryonic blood vessels on day 5 of incubation were sampled, and expression levels of genes related to vasculogenesis were measured by qRT-PCR.

The heart rate was significantly decreased in the TCEP-H group on days 3–5, particularly in all TCEP exposure groups on day 4 (TCEP-L, $p < 0.05$; TCEP-M, $p < 0.001$; TCEP-H, $p < 0.001$). In addition, the ventricular surface area to body weight ratio was significantly increased in a TCEP concentration-dependent manner ($p < 0.05$). Total extraembryonic vessel length was significantly decreased on day 4 in TCEP-M and TCEP-H groups ($p < 0.05$) and significantly reduced on day 5 in a TCEP concentration-dependent manner. The cardiac transcriptome analysis showed four enriched GO terms associated with cardiac conduction in TCEP-M and TCEP-H. Expression levels of BIN1, CACNA1G, CTNNA3, KCNE5, KCNJ2, and NKX2-5 related to cardiac conduction were significantly decreased. Therefore, TCEP exposure may cause a decrease in heart rate by reducing the expression of these genes. In addition, the adherens junction, actin cytoskeleton regulation, and Wnt signaling pathway were significantly enriched in KEGG pathway analysis. Since these pathways are involved in cardiomyocyte

morphogenesis, TCEP exposure may induce abnormal cardiac morphology. IPA revealed 19 pathways commonly enriched in two or more TCEP-exposed groups. The epithelial-mesenchymal transition (EMT) pathway was notably affected, with 17 genes, including SNAI2 and FOXC2, downregulated. As EMT is involved in differentiating cardiac fibroblasts and smooth muscle cells from epicardial-derived progenitor cells, TCEP exposure may affect the EMT and inhibit cardiac development, which is supported by phenotypic observations, including decreased heart rate. qRT-PCR analyses of genes in vitelline membranes showed that gene expression levels of FGF2, VEGFR2, VEGFR3, VEGFC, HIF1A, AKT, PIK3CA, and RAC1 were significantly decreased in a TCEP concentration-dependent manner. These results suggest that TCEP exposure suppresses the vasculogenesis of extraembryonic blood vessels by downregulating these genes involved in the VEGF signaling pathway.

3.2 Introduction

We have previously established a novel developmental toxicity test method using a shell-less incubation system for chicken embryos that enable theirs *in situ* temporal observation. In this previous study, exposure to TCEP (250 and 500 nmol/g egg) in chicken embryos was found to be significantly shorter in the body length, head + bill length, forelimb length, hindlimb length, and eye diameter during early developmental stages up to day nine incubation, suggesting that TCEP induces a developmental delay in chicken embryos. It is also interesting that TCEP exposure (≥ 50 nmol/g egg) to chick embryos significantly reduced the heart rate (day 4–7, $p < 0.05$), increased the ratio of heart weight to body weight (day 9, $p < 0.05$), inhibited the extraembryonic angiogenesis (day 3 and 4, $p < 0.05$), and reduced the production of erythrocytes (day 3–7, $p < 0.05$). It has been reported that TDCIPP, one of the chlorinated OPFRs, has also induced the formation of pericardial edema, reduced heart rate, suppression of intersegmental vessels, and common cardinal vein formation decreased hemoglobin levels and reduction in blood flow in trunk vessels in zebrafish embryos (Dasgupta et al., 2018; Lee et al., 2020; Zhong et al., 2019). Therefore, TCEP exposure may also cause cardiovascular toxicity in chicken embryos. In the chapter II study, Cardiac transcriptome analysis using hearts on day 9 of incubation indicated that expression of cardiomyocyte contraction- and Ca^{2+} transport-related genes were affected by TCEP exposure. However, this transcriptome analysis used only one pooled sample per TCEP

exposure group and did not determine the differentially expressed genes (DEGs) by the statistical test. qRT-PCR analysis to more accurately quantify mRNA expression levels revealed TCEP concentration-dependent trend changes in MYL3 and RYR2 expression, but their expression in the TCEP-exposed group was not significantly different than in the control group. Therefore, understanding the molecular mechanism of the reduced heart rate requires cardiac transcriptome analysis at an earlier developmental stage than day 9, when the effect of TCEP on heart rate was significant.

The present study aims to reveal the cardiovascular effects of TCEP on chicken embryos by investigating the phenotypic effects of heart and extraembryonic blood vessels and changes in the cardiac transcriptome profiles and mRNA levels of angiogenesis-related genes in chicken embryos on day 5. The experimental design of this study is summarized in Fig. 3.1. First, we measured phenotypic endpoints in the heart and vitelline membrane of chicken embryos over time using the shell-less incubation system. We then performed the transcriptome analyses, including RNA sequencing (RNA-seq) of the heart and qRT-PCR of some genes in the vitelline membrane, and tried to identify genes of which the expression levels are altered by TCEP exposure. Finally, based on the combination of phenotypic effects and the pathways in which the differentially expressed genes by TCEP exposure are enriched, we attempted to predict the mechanism of TCEP-induced toxicity in chicken embryos.

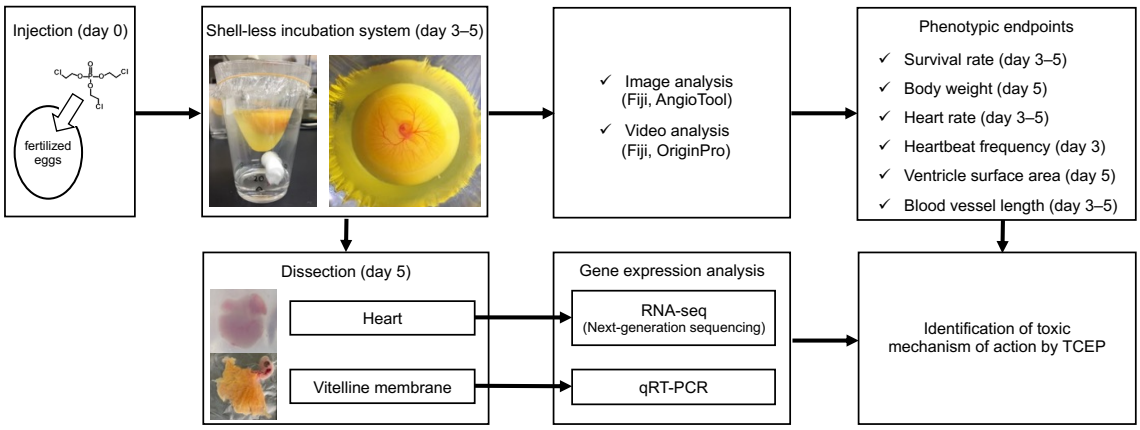

Figure. 3.1 Overview of experimental design.

3.3 Materials and Methods

3.3.1 Chemicals

TCEP (97% purity; CAS No. 115-96-8) was purchased from Sigma-Aldrich (Saint Louis, USA). Dimethyl sulfoxide (DMSO) (Wako Pure Chemical Industries) was used for preparing stock and serially diluted solutions.

3.3.2 Chemical injection and chicken embryo incubation

TCEP exposure experiments were conducted using shell-less incubation vessels as in the Chapter II experiment method. Briefly, fertilized chicken eggs at HH1 were divided into four groups: vehicle control (0.1% DMSO, n = 5), TCEP-L (50 nmol/g egg, n = 6), TCEP-M (250 nmol/g egg, n = 20), TCEP-H (500 nmol/g egg, n = 21) (Table. 3.1). On incubation day 0 (HH1), TCEP was injected into the air sac through a small hole in the eggshell. Embryos were pre-incubated at 38℃ and 70% humidity for 56 hours under rotation of 1 time/hour in the incubator. After the pre-incubation, the whole internal contents in eggs were transferred to the shell-less incubation vessels. Incubation vessels were installed at approximately 8° angle and were incubated in an incubator (temperature 38℃; humidity 70％; rotation 120° clockwise once a day). Cardiovascular endpoints in the chicken embryos were observed *in situ*; digital images and videos were recorded once daily from incubation days 3–5 using a Sony Alpha 6000 camera fitted with a Sony SEL30M35 lens (30 mm, F3.5, Macro; Sony, Japan). After the observations on day 5, the

embryos were euthanized. The heart and vitelline membrane samples were collected and stored at -80℃ until use.

3.3.3 Analyses of cardiovascular endpoints

The endpoint analyses in images and videos recorded during the embryo incubation were performed as Chapter II described. The survival rate was determined based on the heartbeat and developmental progression by in situ observation of the embryos.

The embryos' heart rate (beats per minute [bpm]) was measured by analyzing the videos on incubation days 3–5. The 30-s video data of the heartbeat was exported to ImageJ Fiji (https://fiji.sc/). The heart rate was calculated as the mean pixel intensity with a time series analyzer V3 plugin (https://imagej.nih.gov/ij/plugins/time-series.html). The Peak Analyzer function in OriginPro 2021 software (Originlab Corporation) was used to calculate the time of mean pixel intensity peaks at a heartbeat. The bpm value was obtained by dividing 60 s by the average time interval between peaks. We counted the heart rates of all surviving chicken embryos daily from day 3–5, and the heart rate was compared between groups. Heartbeat frequency on chicken embryos at day 3 of incubation was analyzed using the short-time Fourier transform tool in OriginPro 2021. The short-time Fourier transform was analyzed with a fast Fourier transform (FFT) length of 256, a window length of 180, an overlap of 160, and a window function of Hanning.

To explore the effects of TCEP on vasculogenesis and angiogenesis in chicken embryos, the total length of extraembryonic blood vessels on 3, 4, and 5 days of incubation were measured by AngioTool (Zudaire et al., 2011). AngioTool is software that automatically recognizes blood vessels in images. The images of chicken extraembryonic blood vessels, which were converted to 8-bit images, were imported into AngioTool to detect a skeletal representation of the vascular network and measure the length of extraembryonic blood vessels (Fig. 3.2). The parameters of AngioTool were as follows; low threshold value: 3, high threshold value: 255, vessel thickness value: 4, and small particles value: 320. Since there was a significant positive correlation between vessel lengths measured by AngioTool and those traced and measured using ImageJ's "Freehand Line," the quantified blood vessel lengths are highly accurate (Fig. 3.3). The weight of the chick embryos was measured at the time of dissection on day 5 of incubation. After the dissection, the ventricular surface area of chick embryos was measured using the "Freehand selections" tool in ImageJ.

3.3.4 RNA-seq analysis

Since the heart rate of chicken embryos on day 5 of incubation was significantly affected in a TCEP concentration-dependent manner, we used the heart from day five chicken embryos for RNA-seq. Total RNA was extracted from the heart (n = 3/ treatment group; Table. 3.1) using NucleoSpin® RNA (Takara, Kusatsu, Shiga, Japan) according to the manufacturer’s protocol. The

purity and concentration of extracted RNA solution were determined by an ND-1000 NanoDrop (Thermo Fisher Scientific, Waltham, MA, USA). RNA purity was confirmed by A260/A280 and A260/A230 ratios of >2.1 and >1.4, respectively. Each sample's RNA integrity number (RIN) was measured using a bioanalyzer (Agilent, Santa Clara, CA, USA). The RNA samples with a threshold RIN >9.5 were subjected to further analyses. A strand-specific library was obtained from total RNA using the Poly(A) mRNA Magnetic Isolation Module (New England Biolabs, Ipswich, MA, USA) and NEBNext Ultra II Directional RNA Library Prep Kit for Illumina (New England Biolabs, Ipswich, MA, USA). Next-generation RNA sequencing (RNA-seq) was carried out by Rhelixa Co., Ltd. (Tokyo, Japan) using Illumina NovaSeq 6000 (Illumina, San Diego, California) to produce 150 base pair-end reads. The sequenced data were analyzed according to the flow shown in Fig. 3.4. RNA-seq fastq data were trimmed to remove the Illumina adapter sequence and low-quality value regions by PRINSEQ++ v1.2.4 (https://github.com/Adrian-Cantu/PRINSEQ-plus-plus). The trimmed reads were mapped to the reference genome of Gallus gallus (GRCg6a) using STAR v2.7.9a (Dobin et al., 2013). Transcript quantification was performed using RSEM v1.3.3 (Bo and Colin, 2011). A total of 196.2 million raw reads were obtained (16.4 ± 1.3 million reads per sample). 90.9 ± 0.59% of the reads were mapped onto the chicken reference genome GRCg6a. Transcript abundance was reported as Transcripts Per Million (TPM) (Wagner et al., 2012). Because transcript data with low TPM values may reflect noise

rather than low expressed genes, we omitted transcript data that showed less than 1 TPM (Cockrum et al., 2020). Differentially expressed genes (DEGs) between the TCEP-treated and vehicle control samples were determined based on a false discovery rate (FDR) < 0.05, using the default parameters in EdgeR (Robinson et al., 2010).

3.3.5 Bioinformatics analyses

To investigate the biological function of genes affected by TCEP exposure, we used the ClueGO v2.5.8, a plug-in embedded in Cytoscape v3.8.2, to perform a gene ontology (GO) enrichment analysis (Bindea et al., 2009). GO terms with p-value < 0.05 were regarded as enriched GO terms. A Kyoto Encyclopedia of Gene and Genomes (KEGG) pathway enrichment analysis were performed by clusterProfiler (Yu et al., 2012). The transcriptomic data set, including Ensembl gene IDs, fold changes, and FDR of the total quantified gene, was submitted to Ingenuity Pathway Analysis (IPA) for core analysis (QIAGEN Redwood City, CA, www.qiagen.com/ingenuity).

3.3.6 qRT-PCR analysis

Quantitative RT-PCR (qRT-PCR) was conducted to confirm the mRNA expression levels of several DEGs related to phosphoinositide 3-kinase and AKT serine/threonine kinase (PI3K-AKT) signaling (PIK3CA, PIK3R3, and AKT1) from the heart samples including the same samples as those provided for RNA-seq. For the heart samples that were used for RNA-seq

analysis, an aliquot of total RNA solution was used for qRT-PCR. The mRNA levels of 13 genes associated with vasculogenesis and angiogenesis in the vitelline membrane, including extraembryonic blood vessels, were also measured by qRT-PCR. For heart samples that were not used for RNA-seq analysis and vitelline membrane samples, total RNA was extracted using NucleoSpin® RNA (Takara, Kusatsu, Shiga, Japan) according to the manufacturer's protocol. Total RNA from each sample was reverse transcribed to cDNA using a High Capacity cDNA Reverse Transcription Kit (Thermo Fisher Scientific), following the manufacturer's instruction.

qRT-PCR was performed using TB Green® Premix Ex Taq™ II (Takara, Kusatsu, Shiga, Japan) in a StepOnePlus Real-Time PCR system (Thermo Fisher Scientific). Each gene-specific primer for qRT-PCR was designed to span exon boundaries by Primer-BLAST (https://www.ncbi.nlm.nih.gov/tools/primer-blast/index.cgi) and synthesized by Eurofins Genomics (Tokyo, Japan). The sequences of the primers and their respective PCR conditions are listed in Table 3.2. Gene expression levels were normalized to those of an internal control mRNA, GAPDH. The mRNA expression data were expressed as fold changes of normalized values from TCEP-exposed groups relative to that from the vehicle control group.

3.3.7 Protein extraction and quantification

The heart tissues and vitelline membrane samples were extracted using 0.1M Tris HCL, pH7.6 lysis buffer supplemented with 1X cOmplete mini Protease Inhibitor Cocktail (Roche).

First, the lysates were homogenized at 800–1000 rpm on ice. Then, 40 μl 20% SDS was added to the homogenized lysates. The mixture solution was sonicated on ice three times. Protein quantification was performed with a BCA protein assay kit (Pierce, Rockford, IL, USA).

3.3.8 Western blotting

Western blotting was performed to determine the expression of the proteins involved in the PI3K-Akt pathway in the heart and vitelline membranes of chicken embryos on day 5. We detected the protein expression of AKT, phospho-AKT, PI3K, and phospho-PI3K, which gene expression was affected by TCEP exposure. Heart proteins (15 μg/lane) and vitelline membrane proteins (30 μg/lane) were resolved by electrophoresis on NuPAGE 4–12% Bis-Tris Gel (Invitrogen, USA) and transferred to a polyvinylidene difluoride (PVDF) membrane with the iBlot Gel Transfer System (Invitrogen, USA). Membranes were blocked with Blocking Reagent -Chemically Defined- (COSMO BIO Co., LTD., Japan) for three hours at room temperature. After that, membranes were incubated with primary antibodies against AKT (proteintech 10176-2-AP; 1:2000), phospho-Akt (Cell Signaling #9271; 1:500), PI3K (proteintech 27921-1-AP; 1:250), Phospho-PI3K (Affinity AF3242; 1:100), GAPDH (proteintech 10494-1-AP; 1:2000) overnight at 4℃. After washing four times for 5 min with TBST, the membranes were incubated with horseradish peroxidase (HRP)-conjugate secondary antibody in IMMUNO SHOT -Platinum- (COSMO BIO Co., LTD., Japan) for one hour in room temperature. The secondary antibody was

goat anti-rabbit IgG-HRP (Santa Cruz Biotechnology sc-2004; 1:2000). Detection of protein levels was performed using the enhanced chemiluminescence (ECL) Prime Western Blotting Detection Reagents (Amersham Biosciences, Little Chalfont, UK), and the signals were captured using an ImageQuant LAS 4000 mini (GE Healthcare Life Sciences, US). Densitometric analysis was performed by an ImageQuant TL (GE Healthcare Life Sciences, US), and target protein levels were normalized to the GAPDH protein levels.

3.3.9 Statistical analyses

All data are reported as means ± standard errors. All data were assumed to be normally distributed. The statistical differences in the survival rate between the control and TCEP groups were determined using log-rank tests (GraphPad Prism 5, La Jolla, CA, USA). Statistical differences in other measurements were evaluated using a one-way analysis of variance followed by Dunnett's multiple comparison tests in the R software. The TCEP dose-dependency for some endpoints was assessed using the Jonckheere-Terpstra test in the R software. A Spearman's correlation analysis was conducted to examine the relationship between gene expression levels between RNA-seq and qRT-PCR assays. Results with $p < 0.05$ were regarded to be statistically significant.

Table. 3.1 Number of samples in each group

Treatment	Control	TCEP-L	TCEP-M	TCEP-H
Incubation start day0	5	6	20	21
Body weight	5	5	7	4
Heart rate (day3–5)	5	5	7	4
Heartbeat frequency	5	5	7	4
Ventricle surface area	5	5	7	4
Total of extraembryonic blood vessel length on day 3	5	5	7	4
Total of extraembryonic blood vessel length on day 4	5	5	6	4
Total of extraembryonic blood vessel length on day 5	5	5	6	4
RNA-seq	3	3	3	3
qRT-PCR (heart)	3	3	3	3
qRT-PCR (vitelline membrane)	5	5	7	4

In the total of extraembryonic blood vessel length on days 4 and 5, one sample of TCEP-M was not measured because the whole extraembryonic blood vessels could not be observed.

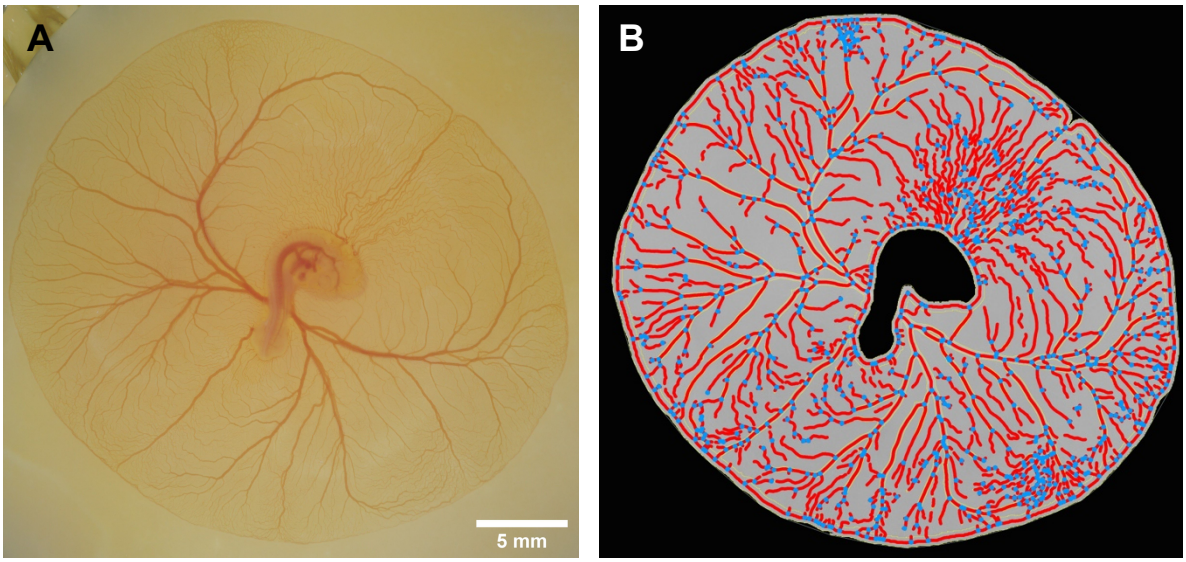

Figure. 3.2 Measurement of the total length of extraembryonic blood vessels by AngioTool. (A) Representative a chicken embryo and an extraembryonic blood vessel on day 3. (B) Result image after analysis of the extraembryonic blood vessel shown in (A) by AngioTool. The outline of the vasculature is shown in yellow, the skeleton representation of the vasculature is in red, and the branching points are blue.

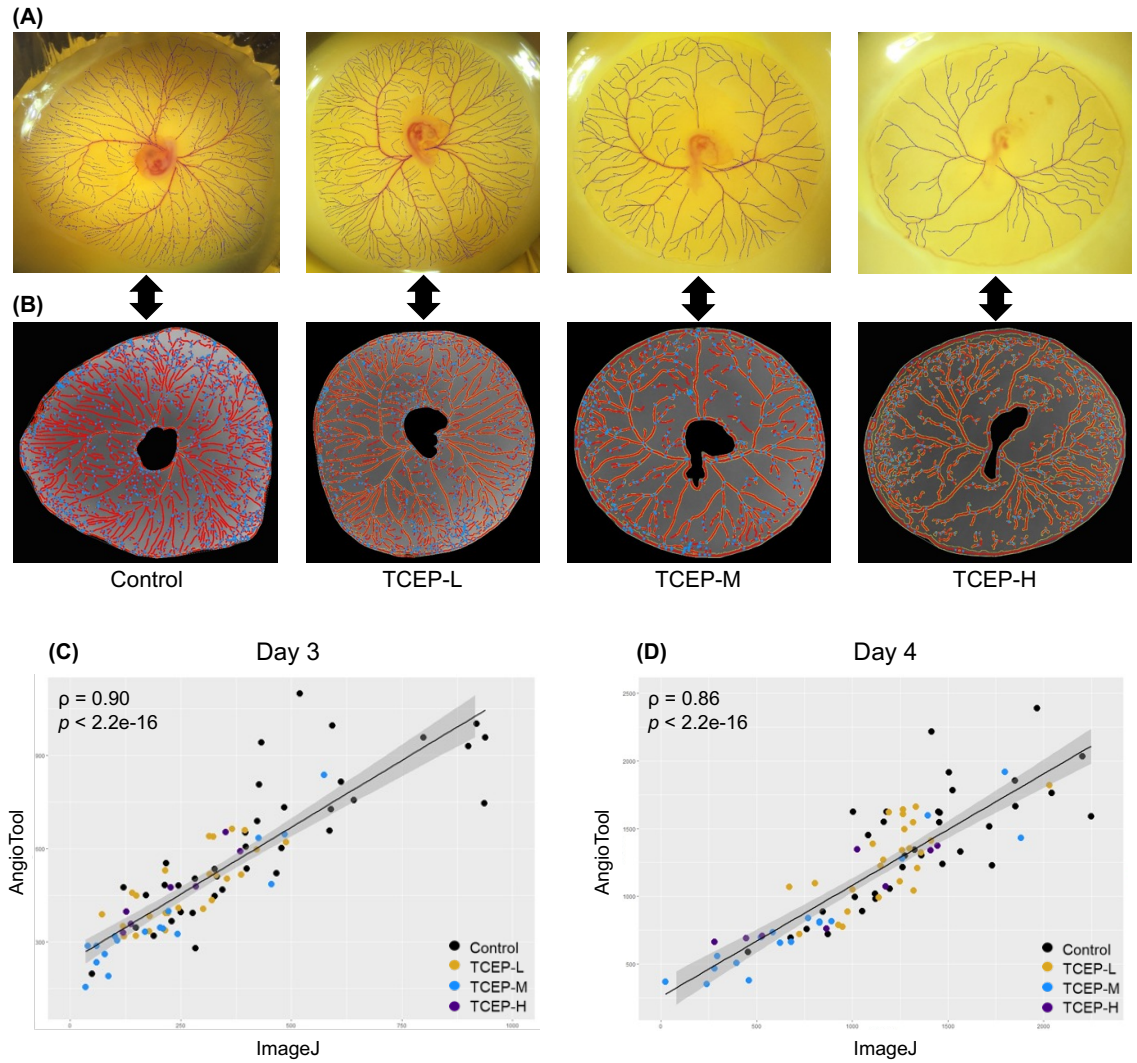

Figure. 3.3 Comparison of embryonic extracorporeal vessel lengths measured with AngioTool and ImageJ. (A) is an image of blood vessels traced by "Freehand Line" in ImageJ (blue lines). (B) is an image of blood vessels recognized and measured by AngioTool (red lines). Relationship between extraembryonic blood vessel lengths measured by AngioTool and ImageJ in chicken embryos on (C) days three and (D) four of incubation.

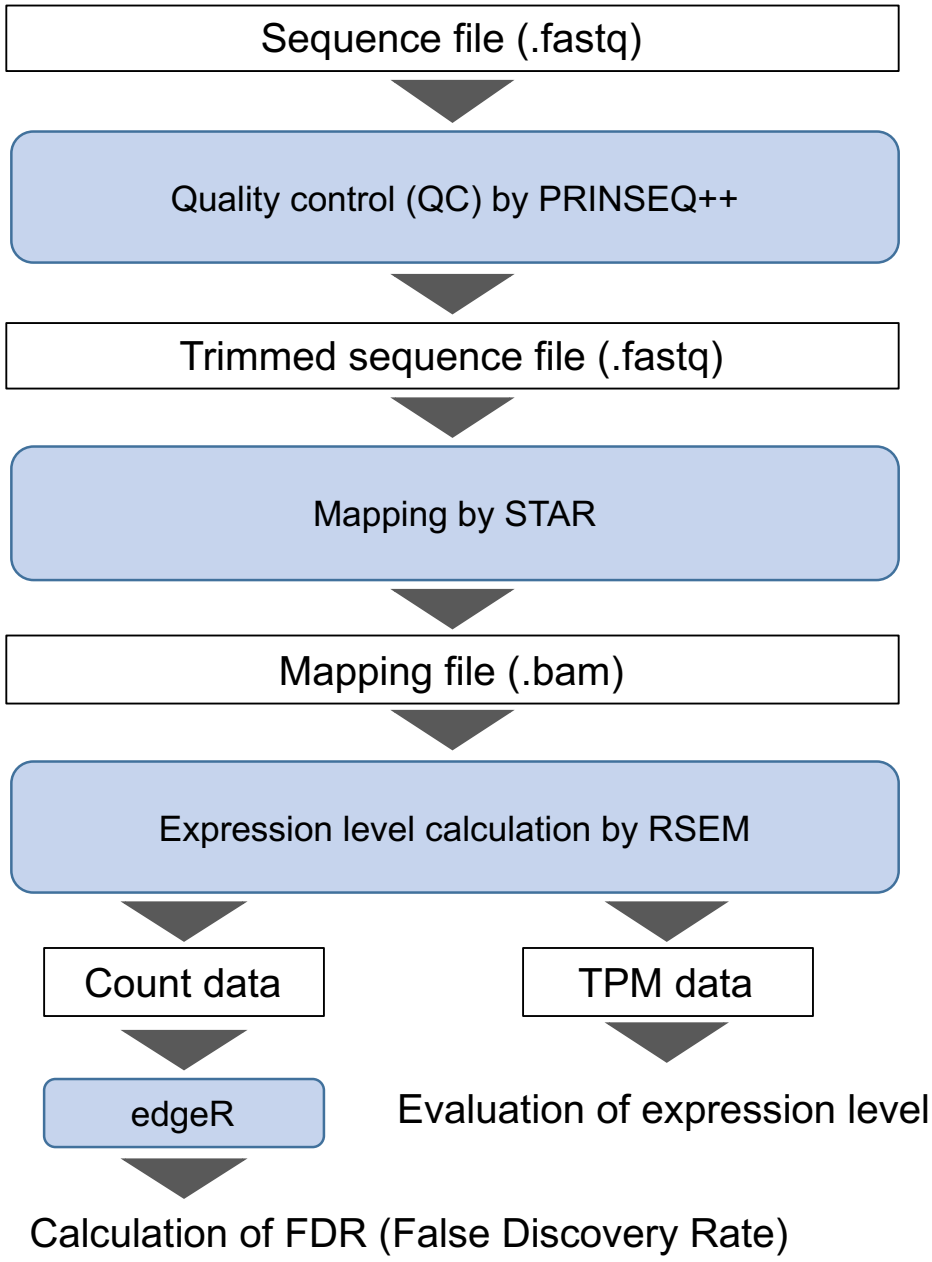

Figure. 3.4 A procedure for RNA-seq analysis.

Table. 3.2 List of primers and PCR conditions applied in this study.

Symbol	Gene name	Forward primer	Reverse primer	Tm (°C)
AKT1	AKT serine/threonine kinase 1	CCGGCTCCCTTTCTACAATCA	GGACCGCCTCCTAACCTTTG	62
PIK3CA	phosphatidylinositol-4,5-bisphosphate 3-kinase catalytic subunit alpha	GCTATGCGGGACTGAGTAACA	CTGTGGCTCCAGAGGAAGTC	62
PIK3R3	phosphoinositide-3-kinase regulatory subunit 3	GCCTGTTCTGTGGTAGCTGA	GCAAGCCTGACATTGAGGGA	62
FGF2	fibroblast growth factor 2	AAGCGGCTCTACTGCAAGAAC	TGAAGCTGCAGTTTGATGTGCG	62
FGFR1	fibroblast growth factor receptor 1	ATCTTCACGTTGGGTGGTTCG	CGCATCATCATGTACAGCTCG	60
HIF1A	hypoxia inducible factor 1 alpha subunit	GGCGTCACCGACAAGAAGA	GTCTCTAGCTCACCAGCATCC	66
RAC1	rho family, small GTP binding protein Rac1	ACTACGCCCACTCTCCTACC	CGCACCTCAGGATACCACTTA	63
VEGFA	vascular endothelial growth factor A	TACAAACCACCCAGCTTTCAC	CCTTCTTTTCCGCTGCTCAC	64
VEGFC	vascular endothelial growth factor C	TCACCTTGGAGATTCTGACACG	AGCGGATGATGTTTGGGACA	62
VEGFD	vascular endothelial growth factor D	GTCAAATACCCAGCGTCACCA	TCGTAAAGGGACAACCATCTTC	62
VEGFR1 (FLT1)	fms related receptor tyrosine kinase 1	AGTGGACACTCTTTGGCATGA	GACTCGCTGAGTTGGTCACA	66
VEGFR2 (KDR)	kinase insert domain receptor	GATTGGACAGCATCACGAGC	AGGTCTTCAGAACCAGCGTC	66
VEGFR3 (FLT4)	fms related tyrosine kinase 4	GGAGGGACGGAACAAGACAG	CTTCTGAGGGCTGGGATTCG	60
GAPDH	glyceraldehyde-3-phosphate dehydrogenase	GTCGGAGTCAACGGAT	GGCCACCACTTGGACT	63

PCR was run with the following condition: one cycle of 10 min at 95°C; 40 cycles of 15 sec at 95°C, 1 min at Tm°C; and one cycle of 15 sec at 95°C, 1 min at 60°C, and 15 sec at 95°C

Table. 3.3 Effects of TCEP exposure on body weight, heart rate, ventricle surface area, and extraembryonic blood vessel length in chicken embryos.

Treatment	Control	TCEP-L	TCEP-M	TCEP-H	
Body weight (mg)	449.34 ± 14.23	437.47 ± 11.97	391.22 ± 33.26	320.48 ± 40.17*	#
Heart rate on day 3 (bpm)	178.2 ± 3.0	164.8 ± 3.1	158.4 ± 4.1**	159.8 ± 5.1*	##
Heart rate on day 4 (bpm)	236.4 ± 1.2	221.8 ± 4.1*	206.3 ± 2.3***	188.3 ± 5.4***	###
Heart rate on day 5 (bpm)	262.0 ± 3.8	264.6 ± 7.2	256.9 ± 5.3	237.5 ± 2.4*	##
Ventricle surface area (mm^2)	2.94 ± 0.11	2.59 ± 0.12	2.83 ± 0.14	2.48 ± 0.30	
Heart weight (mg)	8.30 ± 0.93	12.07 ± 2.95	10.86 ± 1.54	11.10 ± 3.75	
Ventricle surface area/Body weight	0.00656 ± 0.00026	0.00593 ± 0.00027	0.00754 ± 0.00067	0.00798 ± 0.00078	#
Heart weight/Body weight	0.0185 ± 0.0020	0.0275 ± 0.0066	0.0297 ± 0.0054	0.0327 ± 0.0089	
Total of extraembryonic blood vessels length on day 3	2155.8 ± 117.1	1503.8 ± 153.1	1826.6 ± 325.7	2087.0 ± 480.0	
Total of extraembryonic blood vessels length on day 4	4395.2 ± 145.7	3570.1 ± 221.0	2922.6 ± 385.6*	2949.6 ± 468.1*	##
Total of extraembryonic blood vessels length on day 5	4579.2 ± 105.3	4274.4 ± 137.6	3906.8 ± 329.3	3591.4 ± 324.6	##

Data are expressed mean ± SEM.

Significant difference by Dunnet test, * $p < 0.05$; ** $p < 0.01$; *** $p < 0.001$

Significant trend in a TCEP concentration-dependent manner by Jonckheere-Terpstra test, # $p < 0.05$; ## $p < 0.01$; ### $p < 0.001$

3.4 Results

3.4.1 Effects on survival rate and phenotypes

We measured the survival rate and body weight to assess the effect of TCEP on embryonic development. The survival rate of chicken embryos was decreased in a TCEP dose-dependent manner (Fig. 3.4A). In the TCEP-M and TCEP-H groups, the survival rates started to decline greatly from incubation day 3, which was the first day of in situ observation, and significantly decreased (log-rank test for trend, TCEP-M; $p < 0.05$, TCEP-H; $p < 0.01$). The survival rates on day 5 in the control, TCEP-L, TCEP-M, and TCEP-H groups were 100%, 83.3%, 35.0%, and 19.0%, respectively. The survival rate on day 5 in TCEP-L showed no significant difference compared to the control group. The body weight on day 5 (Fig. 3.4B, Table 3.3) showed a significant trend of concentration-dependent decrease with TCEP exposure ($p < 0.01$), and the TCEP-H group had a significant decrease as compared to the control group (Control; 449.3 ± 14.2 mg, TCEP-H; 320.5 ± 40.2 mg).

We then evaluated the cardiac effects of TCEP in chicken embryos on days 3–5. The heart weight and the ratio of heart weight to body weight on day 5 had no significant change in the TCEP-treated groups, but some TCEP-treated samples showed higher values than the control samples (Fig. 3.4C and E, Table 3.3). As for the ventricle surface area of chicken embryos on day 5, no significant difference was observed in the TCEP-exposed groups compared to the control

group (Fig. 3.4D, Table 3.3), while the ratio of ventricular surface area to body weight tended to increase in a concentration-dependent manner ($p < 0.05$; Jonckheere-Terpstra test) (Fig. 3.4F, Table 3.3). The mean heart rate of each group was then measured on days 3–5 of incubation (Fig. 3.5A, Table 3.3). The mean heart rates in TCEP-M and TCEP-H groups were significantly decreased on day three compared to the control group. The mean heart rates of the control, TCEP-L, TCEP-M, and TCEP-H groups on day 4 were 236.4 ± 1.2, 221.8 ± 4.1, 206.3 ± 2.3, and 188.3 ± 5.4 bpm, respectively, indicating a significant concentration-dependent decrease in TCEP-exposed groups. Furthermore, the heart rate on day five was significantly decreased in the TCEP-H group (90.6%, $p < 0.05$), whereas there were no significant differences in TCEP-L and TCEP-M groups. There was a positive correlation between the body weight and heart rate in chicken embryos on day 5 ($\rho = 0.75$, $p < 9.1e\text{-}05$), indicating that the growth of embryos with a weak heartbeat is retarded (Fig. 3.6). To investigate whether TCEP induces cardiac arrhythmia, the alteration in heartbeat frequency (Hz) was measured on day three of chicken embryos by short-time Fourier transform. However, there was no change in the heartbeat frequency in all control and TCEP-treated groups, suggesting that TCEP does not induce cardiac arrhythmia in chicken embryos (Fig. 3.7). The total extraembryonic blood vessel length on days 3-5 of incubation was measured to confirm the effect of TCEP on vasculogenesis and angiogenesis in chicken embryos using AngioTool (Fig. 3.5B, Table 3.3). The total extraembryonic blood vessel length was not

changed on day 3 in all TCEP exposure groups, although the length on day four was significantly decreased in TCEP-M (66.5%) and TCEP-H groups (67.1%). The total extraembryonic blood vessel length on day 5 was also significantly decreased in a TCEP concentration-dependent manner ($p < 0.01$).

3.4.2 Effects on cardiac transcriptome

We applied the RNA-seq approach to explore changes in the cardiac transcriptome of day five chicken embryos exposed to TCEP. We detected a total of 23,884 transcripts. To determine DEGs (FDR < 0.05), we compared the expression level of each transcript in TCEP-exposed groups to that of the control group. The volcano plot showed that DEGs were abundant with much lower adjusted p-values (FDR) in Control vs. TCEP-H, Control vs. TCEP-M, and Control vs. TCEP-L (Fig. 3.8A–C). The expression levels of 34 (24 up- and 10 down-regulated), 284 (57 up- and 227 down-regulated), and 805 (164 up- and 641 down-regulated) genes were significantly altered in TCEP-L, TCEP-M, and TCEP-H, respectively. The number of DEGs increased in a TCEP concentration-dependent manner. Seven DEGs were common among all TCEP-exposed groups (Fig. 3.8D). There were 206 common DEGs between the TCEP-M and TCEP-H groups, representing 72.5% of the DEGs in the TCEP-M group (Fig. 3.8D). The heatmap represents the $\log_2$ fold change of the TPM in the TCEP-exposed embryos relative to the mean TPM of the control group in each DEG (Fig. 3.9). The up- or down-regulated relative expression

of many DEGs was common in TCEP-exposed embryos, and the fold changes of down-regulated DEGs tended to be TCEP-concentration dependent.

To confirm the RNA-seq data, we performed qRT-PCR for AKT1, PIK3CA, and PIK3R3 genes. Significant correlations between TPM values by RNA-seq and the expression levels normalized by GAPDH levels by qRT-PCR were observed (Fig. 3.10, Spearman's rank correlation coefficient, $\rho \geq 0.79$, $p \leq 0.004$).

3.4.3 Gene Ontology (GO) enrichment analysis

GO enrichment analysis was performed to classify TCEP-affected genes according to the biological processes (BP), cellular components (CC), and molecular functions (MF) and to identify DEGs associated with cardiovascular function. The top 10 significant GO terms of BP, CC, and MF in each group are shown in Fig. 3.11–3.13. There were no significantly enriched GO terms in TCEP-L, whereas we identified significantly enriched GO terms which were 54 and 85 for BP, 8 and 25 for CC, and 19 and 12 for MF in TCEP-M and TCEP-H, respectively. Among the significantly enriched GO terms, three terms in TCEP-M and seven in TCEP-H had direct linkages with the cardiovascular biological processes such as cardiac conduction, regulation of heart rate, cell migration involved in sprouting angiogenesis, and regulation of angiogenesis (Table 3.4). As for genes with GO terms related to cardiac contraction, ATP binding cassette subfamily C member 9 (ABCC9) was upregulated by TCEP exposure, and bridging integrator 1

(BIN1), calcium voltage-gated channel subunit alpha1 G (CACNA1G), catenin alpha 3 (CTNNA3), potassium voltage-gated channel subfamily E regulatory subunit 5 (KCNE5), Potassium inwardly-rectifying channel subfamily J member 2 (KCNJ2), and NK2 homeobox 5 (NKX2-5) were downregulated by TCEP exposure, all of which showed TCEP concentration-dependent changes (Table 3.4 and Fig. 3.14). Interestingly, the TPM value of these genes was found to correlate strongly with the heart rate of chicken embryos on day 5 ($\rho < 0.70$; Fig. 3.15). A total of 20 DEGs were included in the enriched GO term associated with angiogenesis, of which 16 gene expression was reduced in a TCEP concentration-dependent manner (Table 3.4 and Fig. 3.16). Several GO terms related to microtubule function, such as microtubule depolymerization, kinetochore-microtubule, and microtubule plus-end binding, were enriched in BP, CC, and MF of TCEP-M (Fig. 3.11–13). Expression levels of adenomatous polyposis coli (APC), calcium and integrin binding family member 1 (CIB4), cytoplasmic linker associated protein 1 (CLASP1), and kinesin family member 18A (KIF18A) listed as DEGs involved in microtubule depolymerization were significantly decreased in a TCEP concentration-dependent manner (Fig. 3.17).

3.4.4 KEGG pathway analysis

We then performed the KEGG pathway enrichment analysis to predict the effects on the pathways in which genes affected by TCEP exposure are involved. Significantly enriched KEGG pathways ($p < 0.05$) in all TCEP-treated groups are shown in Fig. 3.18 and Table 3.5. Nine

pathways were enriched in TCEP exposure groups, and DEGs in all enriched pathways except the Wnt signaling pathway were mostly downregulated (> 75%). In regulating the actin cytoskeleton, 17 gene expressions were significantly altered in all TCEP exposure groups, of which the expressions were downregulated (Fig. 3.19). Nine DEGs associated with adherens junction were significantly downregulated by TCEP (Fig. 3.20). The expression of 13 genes in the Wnt signaling, including the Wnt family (WNT2B and WNT10A), and Frizzled (FZD6), the receptor for Wnt, was composed of up- and downregulation (Fig. 3.21). In addition, the expression of genes in the enriched VEGF signaling pathway, including vascular endothelial growth factors (VEGFs) and their receptor interactions (AKT1, PIK3CA, PIK3R2, PIK3R3, PIK3R5, RAC1, RAC3, PPP3R1, and PLA2G4EL2) was altered in a TCEP concentration-dependent manner (Fig. 3.22). The VEGF ligands and receptors (VEGFRs) are critical regulators of vasculogenesis, angiogenesis, and vascular permeability in vertebrates (Shibuya and Claesson-Welsh, 2006). Notably, several genes were commonly involved in multiple gene ontologies and pathways. For example, RAC1 and RAC3 regulate the actin cytoskeleton, Wnt signaling, adherens junction, and VEGF signaling pathways. PIK3CA, PIK3R3, and PIK3R2 regulate the actin cytoskeleton and VEGF signaling pathway. APC is in the regulation of microtubule depolymerization actin cytoskeleton and Wnt signaling pathway.

3.4.5 Ingenuity Pathway Analysis (IPA)

We further performed an Ingenuity Canonical Pathway analysis using IPA. Nine, 24, and 167 pathways were shown to be significantly affected in the TCEP-L, TCEP-M, and TCEP-H groups, respectively ($p < 0.05$). There were 19 common pathways in two or more TCEP-treated groups (Fig. 3.23). Actin cytoskeleton signaling was significantly enriched in TCEP-M and TCEP-H, which was identical to the result in the KEGG pathway analysis. Twenty-one genes involved in this actin cytoskeleton signaling were altered by TCEP treatment, and 85.7% (18/21) of these DEGs were downregulated (Fig. 3.24 A and B).

3.4.6 Angiogenesis gene expression in vitelline membranes

Cardiac transcriptome analysis found that VEGF signaling, which is involved in vasculogenesis and angiogenesis, is affected by TCEP exposure. Thus, to investigate whether perturbation of VEGF signaling is associated with suppression of extraembryonic blood vessel formation, we measured mRNA levels of VEGF signaling-related genes in embryonic vitelline membranes with extraembryonic blood vessels by qRT-PCR (Fig. 3.25). Among VEGF-related genes, mRNA levels of VEGFC, VEGFR2 (KDR), and VEGFR3 (FLT4) indicated a significant TCEP concentration-dependent decreasing trend, and VEGFC expression in the TCEP-H group was significantly decreased compared to the control group. Gene expression levels of hypoxia-inducible factor 1 alpha subunit (HIF1A), AKT1, PIK3CA, and RAC1 were significantly

decreased in a TCEP concentration-dependent manner. AKT, PI3K, and RAC are key mediators to induce vascular permeability in VEGF signaling (Eriksson et al., 2003). HIF1 is a transcriptional factor that regulates the transcriptional activation of VEGF, and HIF1 expression depends on the activation of the PI3K-AKT pathway (Iyer et al., 1998; Laughner et al., 2001). Furthermore, the fibroblast growth factor 2 (FGF2) mRNA level was significantly decreased in the TCEP-M and TCEP-H groups. FGF 2-mediated signaling is essential for hemangioblast proliferation, differentiating into hematopoietic and endothelial cells (Faloon et al., 2000).

3.4.7 Expression of proteins involved in the PI3K-AKT signaling

The expression of the four proteins, including AKT, p-AKT, PI3K, and p-PI3K, were quantified in the heart and vitelline membrane samples exposed to TCEP. In the heart on day 5, AKT, p-AKT, PI3K, and p-PI3K proteins were detected at 56, 60, 110, and 84 kDa, respectively. However, these protein expressions were not altered by TCEP exposure (Fig. 3.26). In the vitelline membrane containing the extraembryonic blood vessel on day 5, four proteins were also detected in the same location, while these protein expressions were not significantly changed by TCEP exposure (Fig. 3.27).

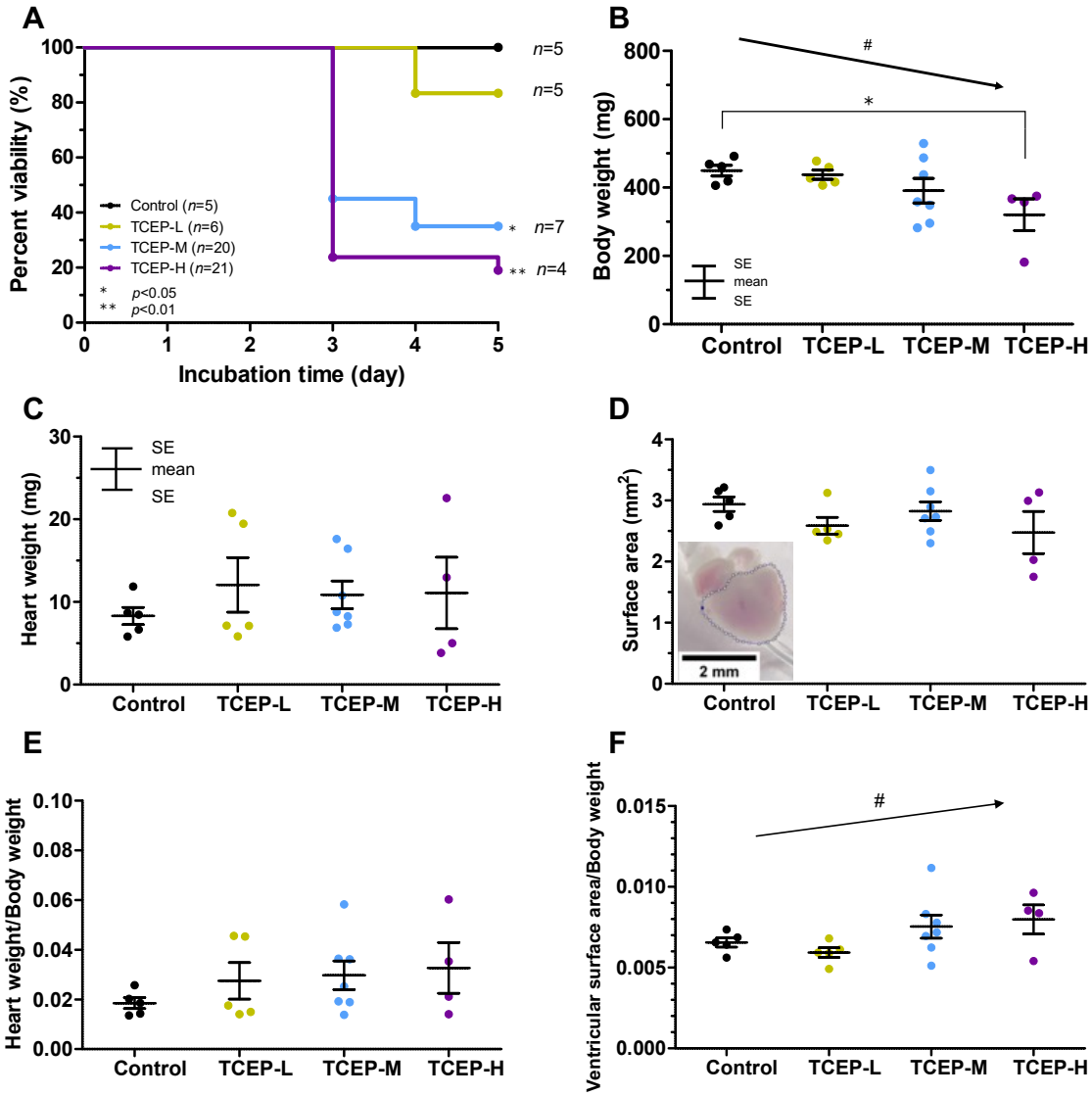

Figure. 3.4 Effect of TCEP exposure on (A) survival rate; (B) body weight on day 5; (C) heart weight on day 5; (D) ventricular surface area on day 5; (E) heart weight to body weight ratio; and (F) ventricular surface area to body weight ratio in chicken embryos. Data represent means ± standard error of the mean (SEM). The asterisks indicate significant differences (*$p < 0.05$; **$p < 0.01$) in each measurement in a TCEP-treated group compared with that in the respective control. Hash symbols with arrows indicate a significant trend in a concentration-dependent manner (#$p < 0.05$) in control and TCEP-treated groups, which were determined by the Jonckheere-Terpstra test.

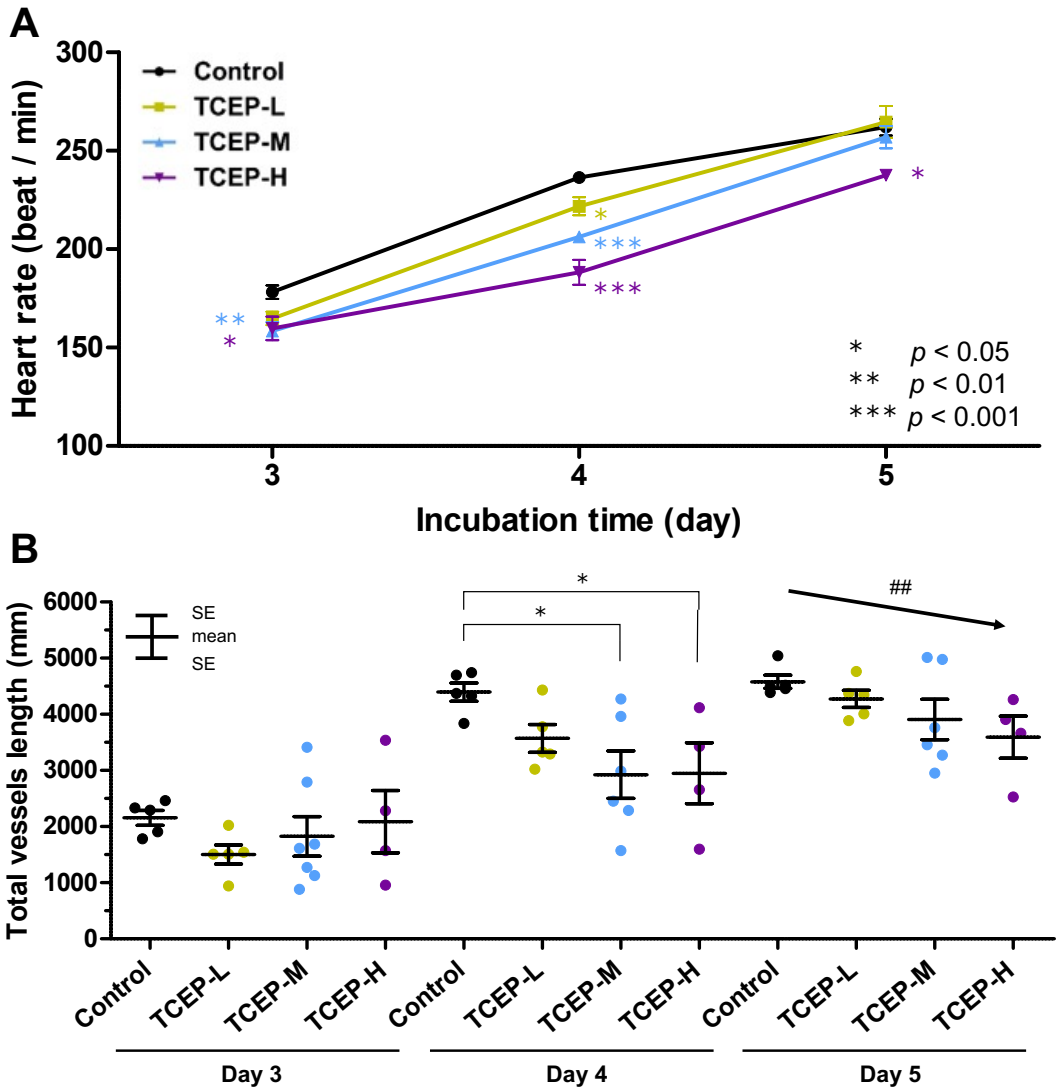

Figure. 3.5 Effect of TCEP exposure on (A) heart rate; (B) a total extraembryonic blood vessel length in chicken embryos on days 3–5. Data represent means ± standard error of the mean (SEM). The asterisks indicate significant differences (*$p < 0.05$; **$p < 0.01$; *** $p < 0.001$) in each measurement in a TCEP-treated group compared with that in the respective control. Hash symbols with arrows indicate a significant trend in a concentration-dependent manner (##$p <$ 0.01) in control and TCEP-treated groups, which were determined by the Jonckheere-Terpstra test.

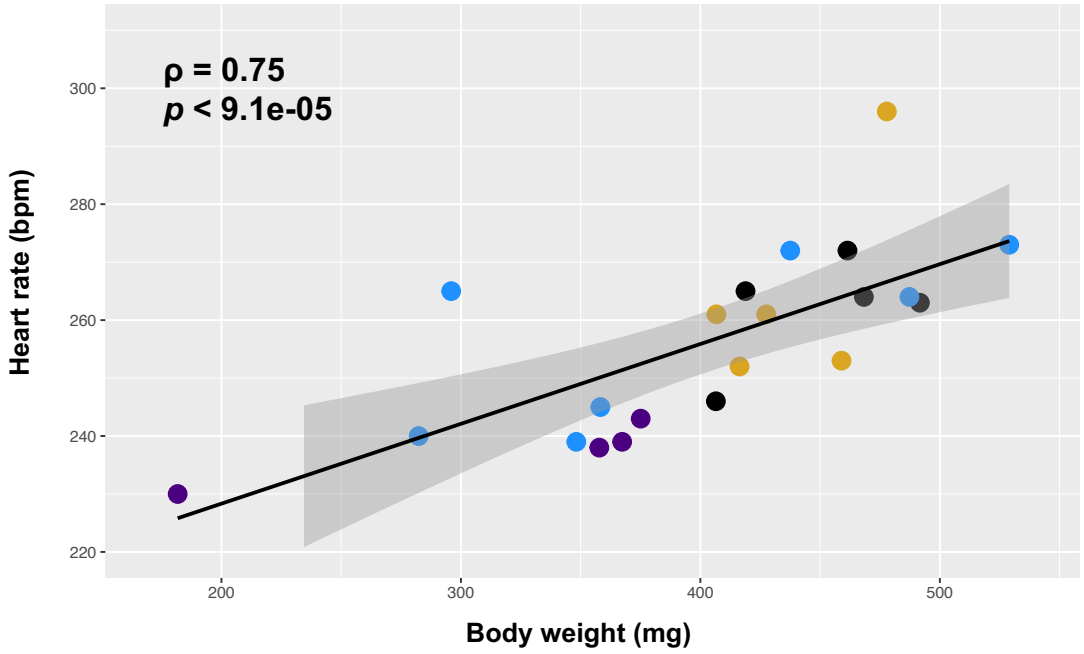

Figure. 3.6 Relationship between body weight and heart rate in chicken embryos on day 5 of incubation. Rho indicates the correlation coefficient. Control, TCEP-L, TCEP-M, and TCEP-H samples are shown as black, yellow, blue, and purple plots, respectively. The black line represents the regression line, and the gray range represents the 95% confidence

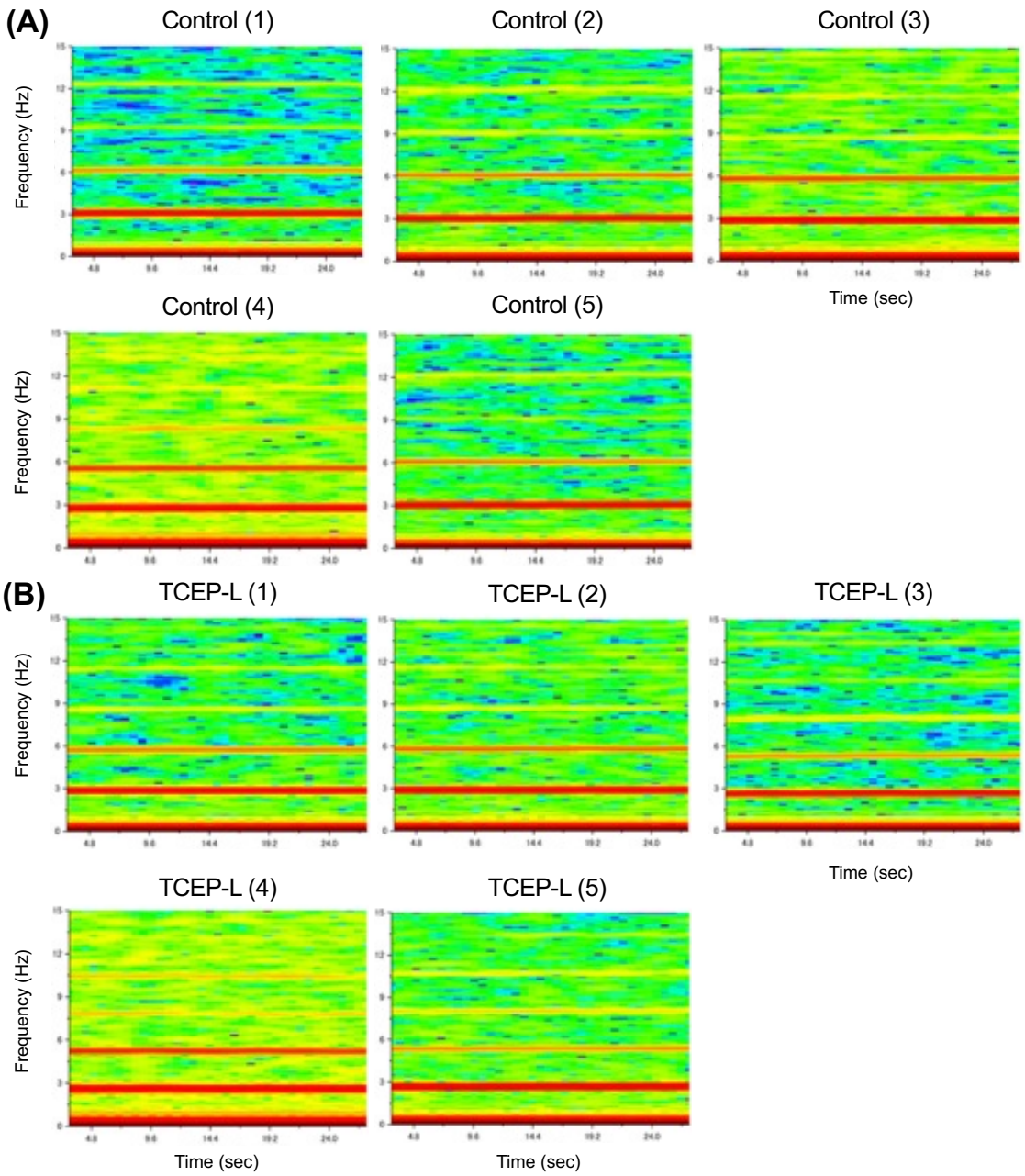
(A)
Control (1)
Control (2)
Control (3)
Frequency (Hz)
Time (sec)
Control (4)
Control (5)
Frequency (Hz)
(B)
TCEP-L (1)
TCEP-L (2)
TCEP-L (3)
Frequency (Hz)
Time (sec)
TCEP-L (4)
TCEP-L (5)
Frequency (Hz)
Time (sec)
Time (sec)

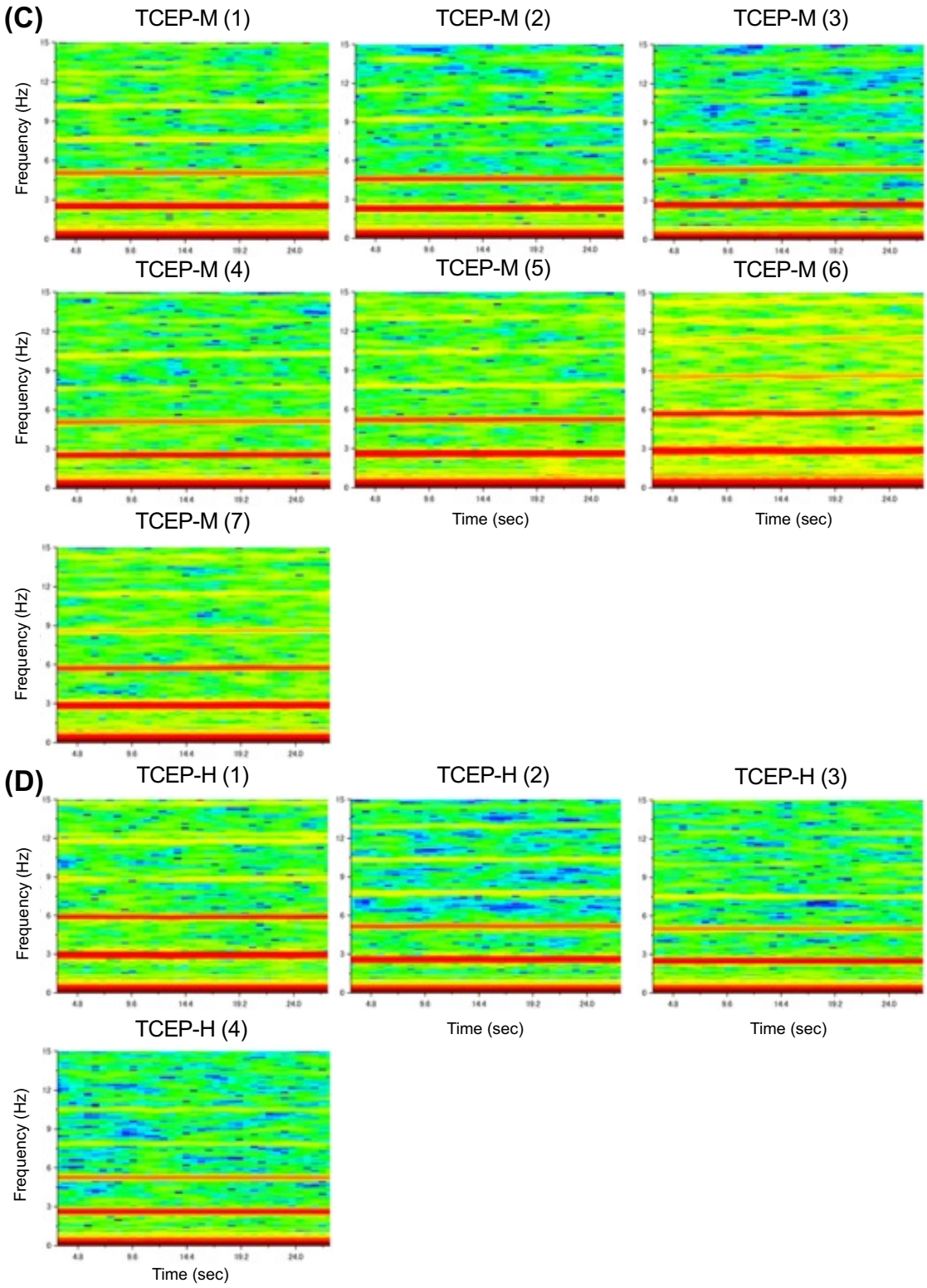

Figure. 3.7 Heartbeat frequency (Hz) was detected by short-time Fourier transformation for the (A) control (n = 5), (B) TCEP-L (n = 5), (C) TCEP-M (n = 7), and (D) TCEP-H (n = 4) groups of chicken embryos on day 3.

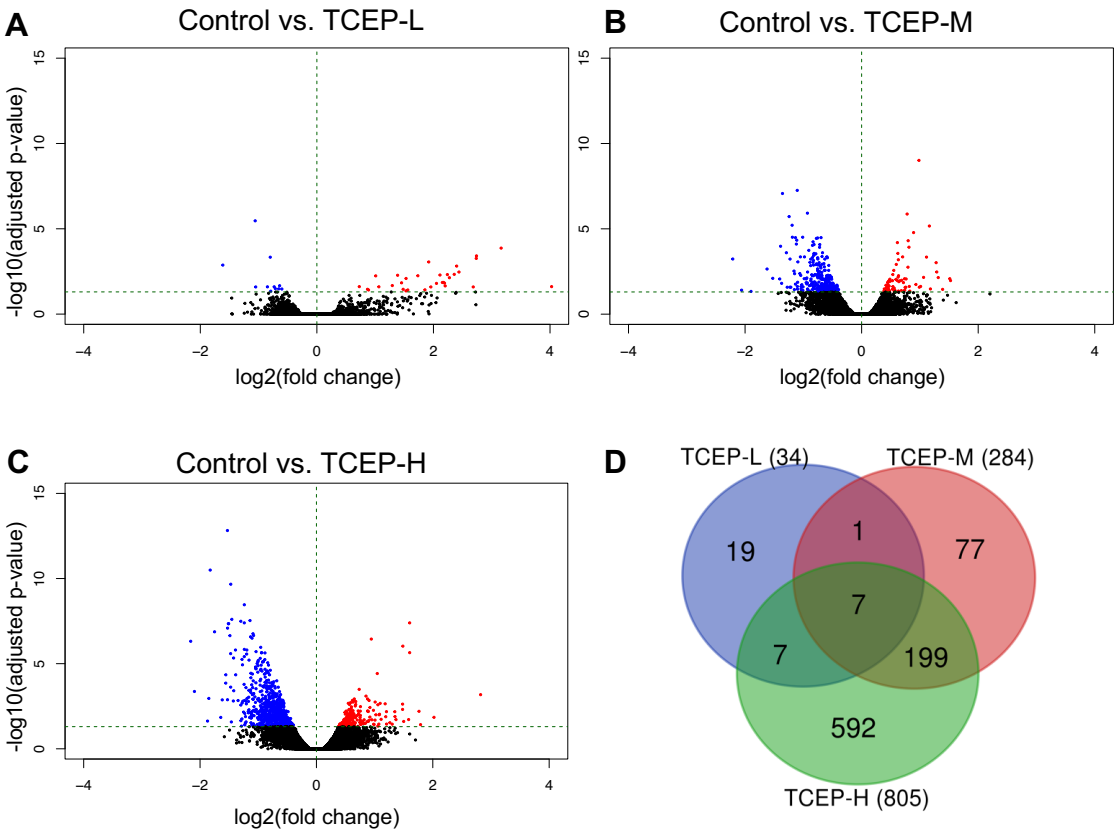

Figure. 3.8 Transcriptomic differences in the hearts from control, TCEP-L, TCEP-M, and TCEP-H chicken embryos on day 5. (A) The TCEP-L, (B) TCEP-M, and (C) TCEP-H groups volcano plot showing the log2 fold change and the minus log10 adjusted p-value of each gene compared to the control group in the differential expression analysis. Genes with a significant expression change are highlighted as red (up-regulation) and blue (down-regulation) dots. (D) Venn diagram representing the number of significant differentially expressed genes (DEGs).

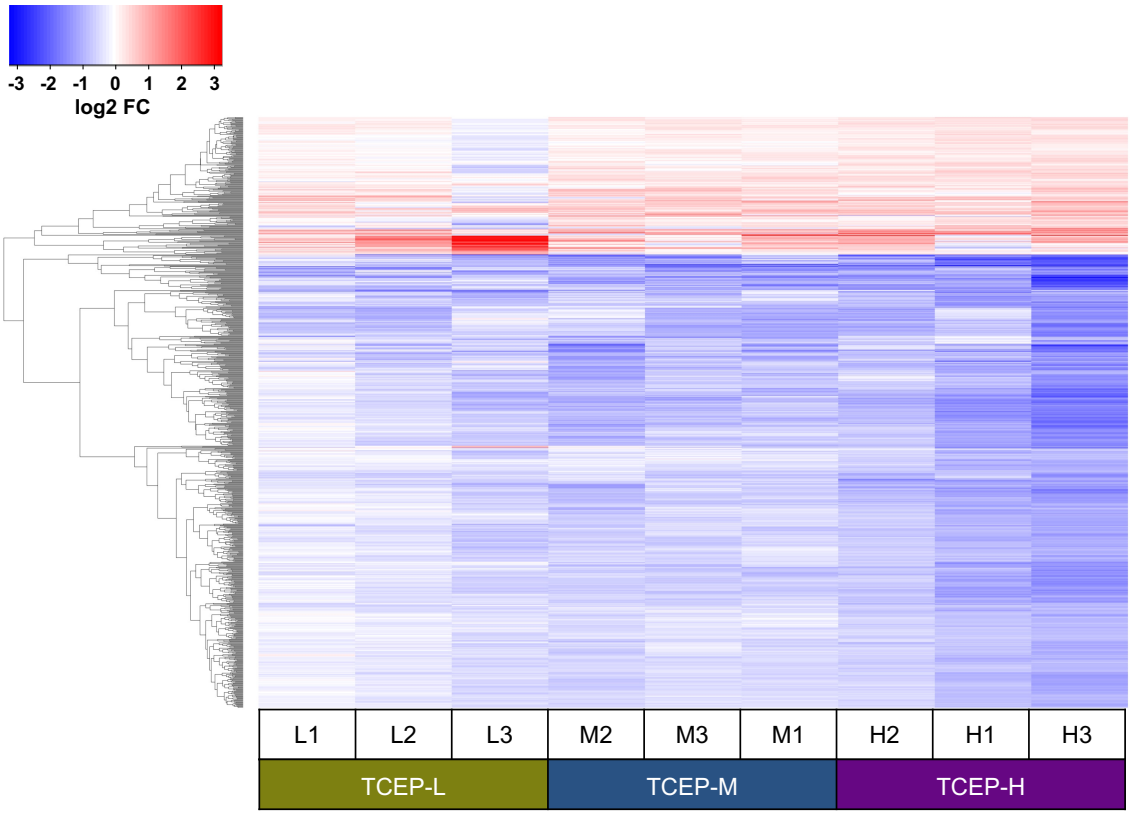

Figure. 3.9 The heatmap shows the log2 fold change of transcripts per million (TPM) of the TCEP exposed sample relative to the mean TPM of the control group in each DEG.

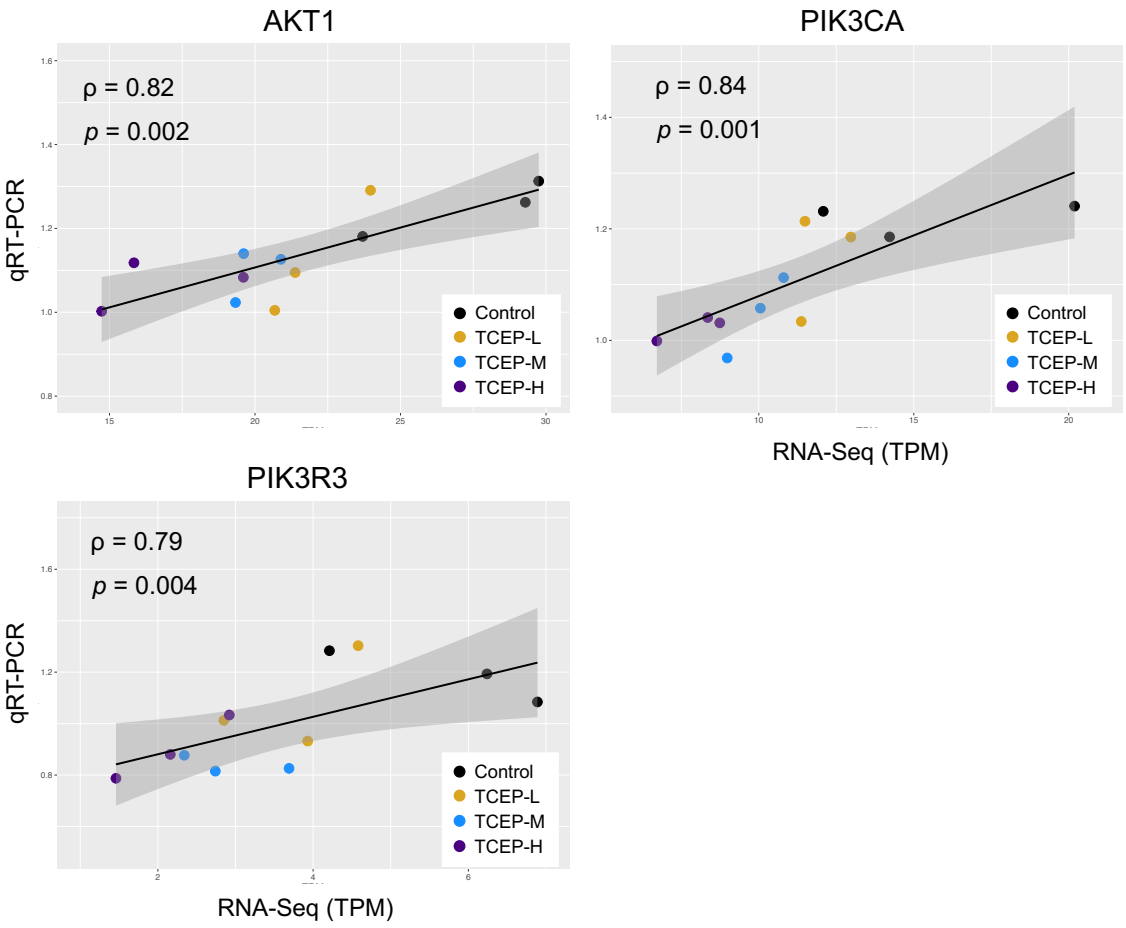

Figure. 3.10 Correlation of mRNA expression levels of examined genes between RNA-seq (TPM values) and qRT-PCR (the relative expression to GAPDH) in chicken embryos.

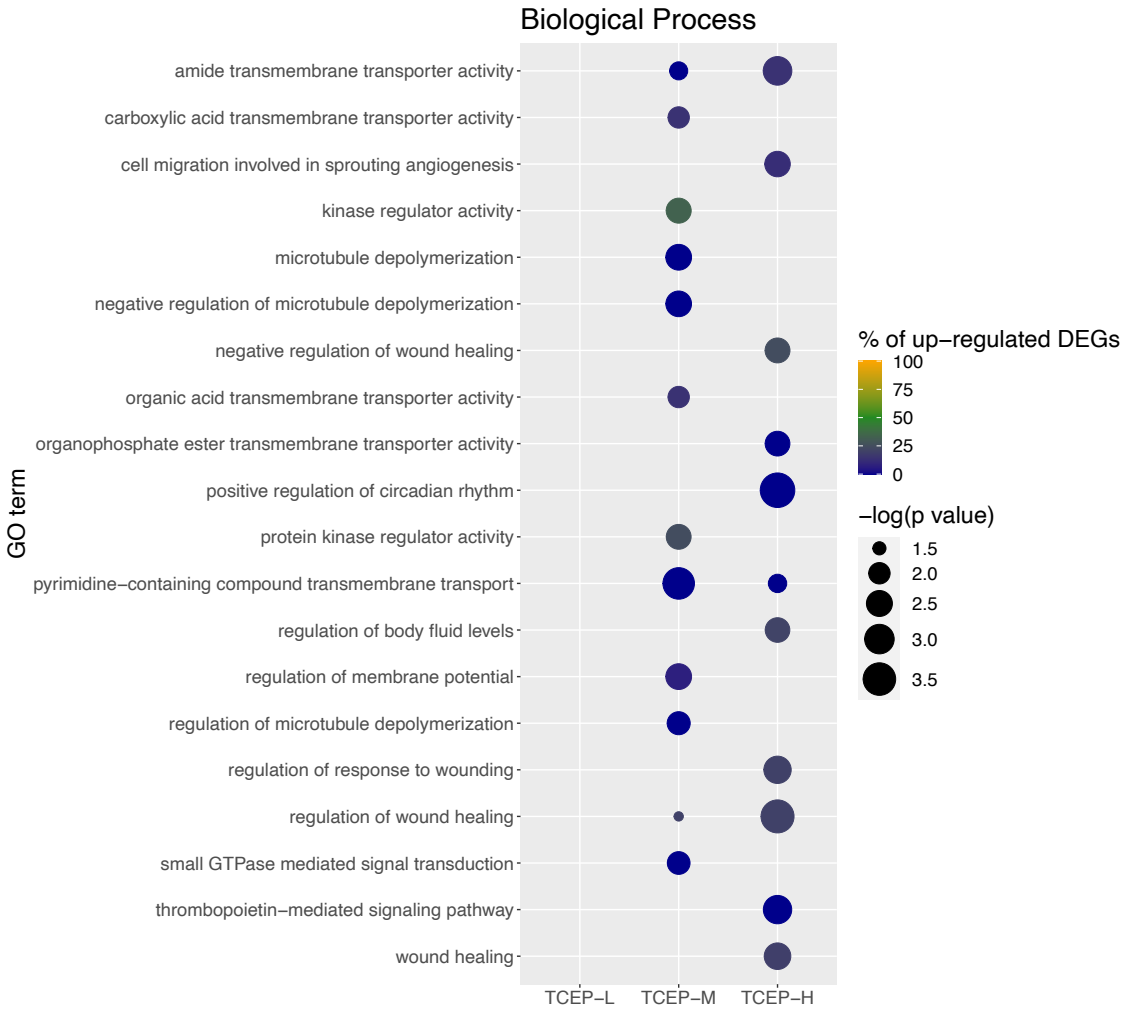

Figure. 3.11 Enrichment analysis for the biological process (BP) of Gene Ontology (GO) using ClueGO. The top 10 GO terms were significantly enriched in the TCEP-L, TCEP-M, and TCEP-H exposure groups. The circle size shows the degree of significance (log-transformed p-value multiplied by -1). The circle's color indicates the percentage of significantly upregulated genes in the GO term.

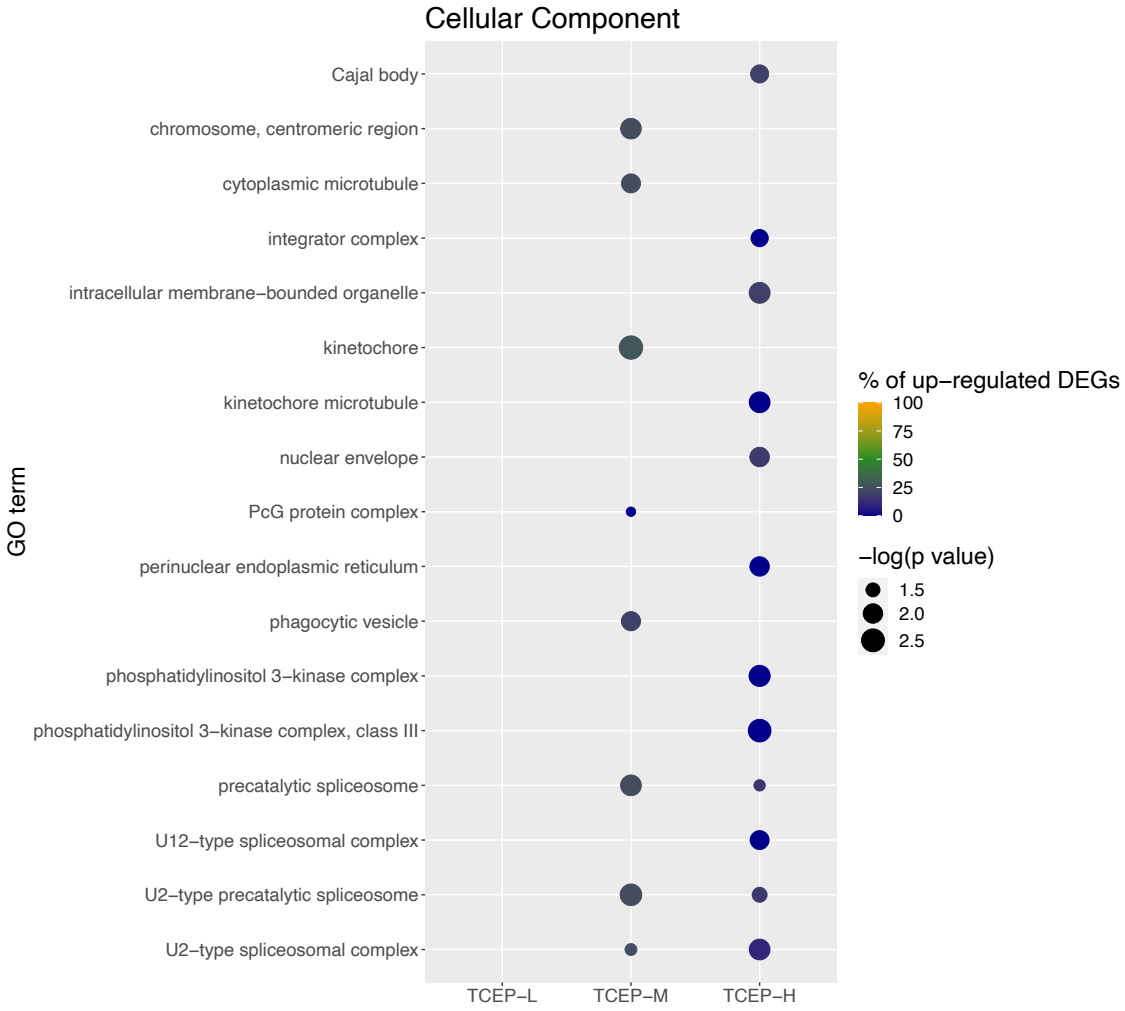

Figure. 3.12 Enrichment analysis for the cellular component (CC) of Gene Ontology (GO) using ClueGO. The top 10 GO terms were significantly enriched in the TCEP-L, TCEP-M, and TCEP-H exposure groups. The circle size shows the degree of significance (log-transformed p-value multiplied by -1). The circle's color indicates the percentage of significantly upregulated genes in the GO term.

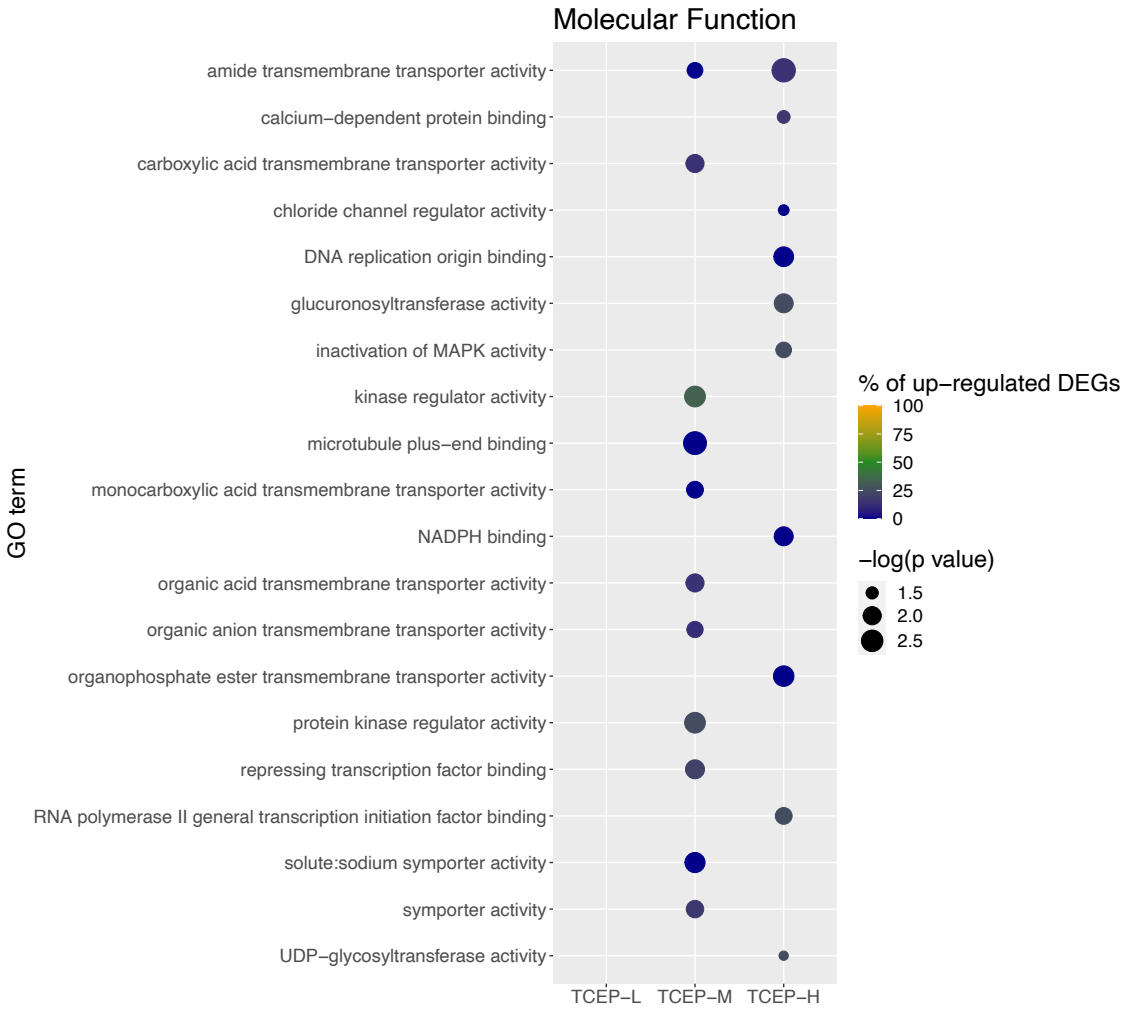

Figure. 3.13 Enrichment analysis for the molecular function (MF) of Gene Ontology (GO) using ClueGO. The top 10 GO terms were significantly enriched in the TCEP-L, TCEP-M, and TCEP-H exposure groups. The circle size shows the degree of significance (log-transformed p-value multiplied by -1). The circle's color indicates the percentage of significantly upregulated genes in the GO term.

Table. 3.4 Results of chicken-specific Gene Ontology (GO) enrichment analysis related to cardiac and angiogenesis function.

GO term	Control vs.	Up-regulated genes	Down-regulated genes	p-value
cell migration involved in sprouting angiogenesis	TCEP-H	MIA3	AKT1, ANXA1, CIB4, ITGB1BP1, MAP3K3, MEOX2, PLK2	0.004
positive regulation of angiogenesis	TCEP-H	STAT3	ANXA1, CHRNA7, CIB4, ERAP1, GATA6, MAP3K3, MTDH, MYDGF, PLK2, SMAD1, TGFBR2, XBP1	0.008
regulation of cell migration involved in sprouting angiogenesis	TCEP-H		ANXA1, CIB4, ITGB1BP1, MAP3K3, MEOX2, PLK2	0.011
regulation of angiogenesis	TCEP-H	EGLN1, STAT3, TNMD	ANXA1, CHRNA7, CIB4, ERAP1, GATA6, ISM1, ITGB1BP1, MAP3K3, MEOX2, MTDH, MYDGF, PLK2, SMAD1, TGFBR2, XBP1	0.017
positive regulation of cell migration involved in sprouting angiogenesis	TCEP-H		ANXA1, CIB4, MAP3K3, PLK2	0.018
cardiac conduction	TCEP-H	ABCC9	BIN1, CACNA1G, CTNNA3, KCNE5, KCNJ2, NKX2-5	0.022
regulation of heart rate by cardiac conduction	TCEP-H		BIN1, CACNA1G, CTNNA3, KCNE5, KCNJ2	0.036
regulation of heart rate by cardiac conduction	TCEP-M		BIN1, CACNA1G, KCNJ2	0.018
cardiac muscle cell action potential involved in contraction	TCEP-M		BIN1, CACNA1G, KCNJ2	0.029
cardiac muscle cell action potential	TCEP-M		BIN1, CACNA1G, KCNJ2	0.039

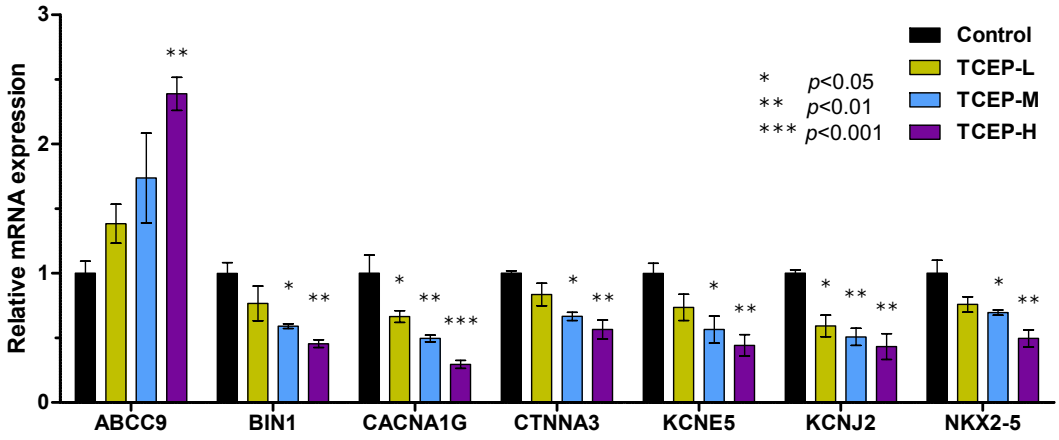

Figure. 3.14 Results for relative mRNA expression levels of differentially expression genes (FDR < 0.05) included in the enriched Gene Ontology (GO) term (p < 0.05) associated with cardiac contraction. The y-axis represents the fold change compared to the control group. Asterisk signs (* p <0.05; ** p <0.01; *** p <0.001) indicate the significantly different levels in TCEP exposure groups compared with control group by RNA-seq, which were determined by Dunnett's test.

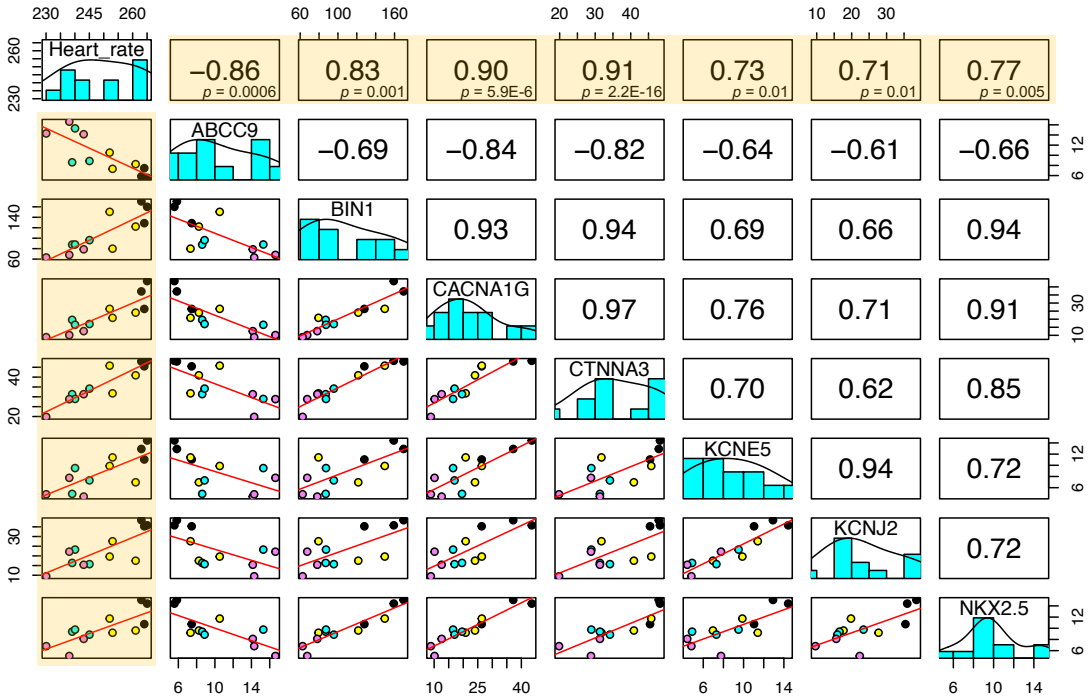

Figure. 3.15 Relationship between the TPM value of DEGs included in the GO term associated with cardiac contraction and heart rate in chicken embryos on day 5 of incubation. The numbers indicate the respective correlation coefficients (Spearman's rank correlation coefficient). Control, TCEP-L, TCEP-M, and TCEP-H samples are shown as black, yellow, blue, and purple plots, respectively. The red line represents the regression line.

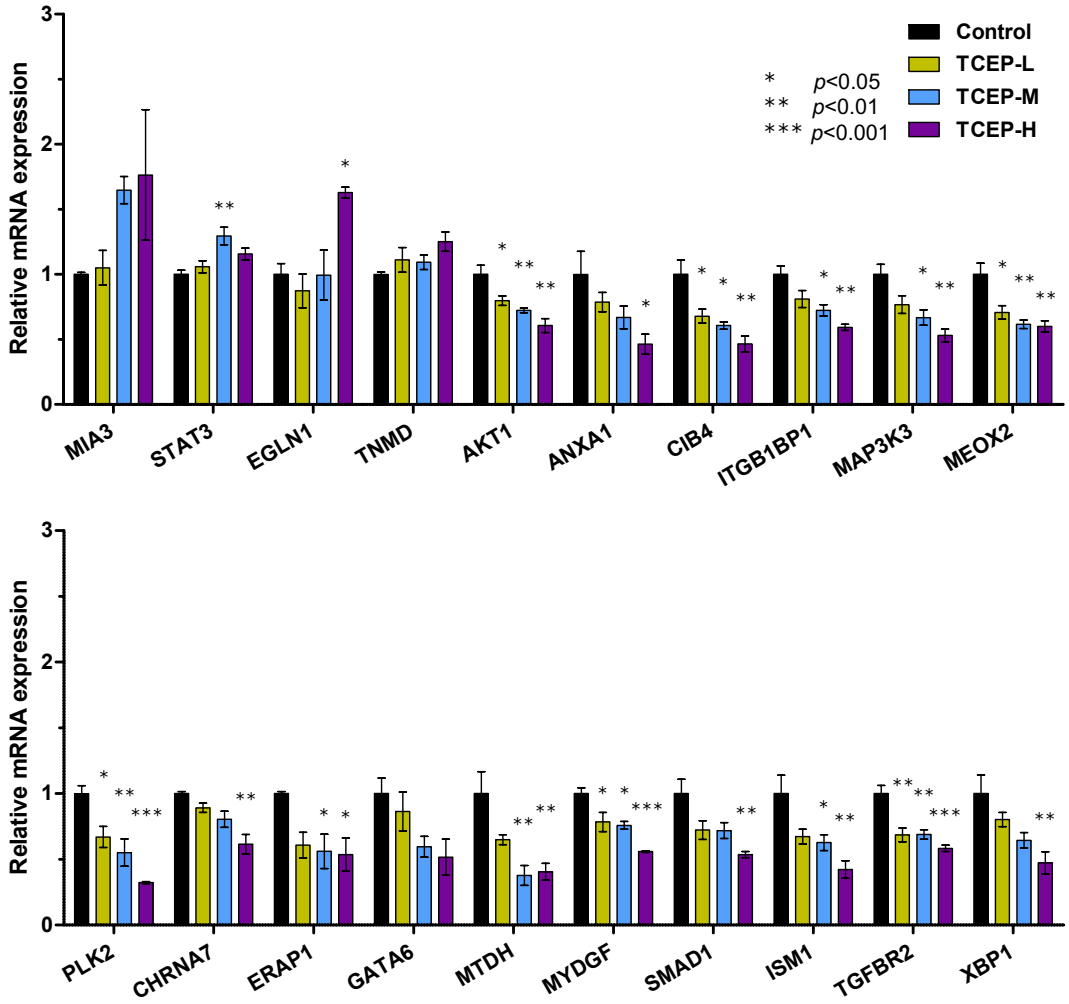

Figure. 3.16 Results for relative mRNA expression levels of differentially expressed genes (FDR < 0.05) included in the enriched Gene Ontology (GO) term ($p < 0.05$) associated with angiogenesis. The y-axis represents the fold change compared to the control group. Asterisk signs (* p <0.05; ** p <0.01; *** p <0.001) indicate the significantly different levels in TCEP exposure groups compared with the control group by RNA-seq, which were determined by Dunnett's test. MIA3: MIA family member 3, ER export factor; STAT3: signal transducer and activator of transcription 3; EGLN1: egl-9 family hypoxia inducible factor 1; TNMD: tenomodulin; AKT1: AKT serine/threonine kinase 1; ANXA1: annexin A1; CIB4: calcium and integrin binding family member 1; ITGB1BP1: integrin subunit beta 1 binding protein 1; MAP3K3: mitogen-activated protein kinase kinase kinase 3; MEOX2: mesenchyme homeobox 2; PLK2: polo like kinase 2; CHRNA7: cholinergic receptor nicotinic alpha 7 subunit; ERAP1: endoplasmic reticulum aminopeptidase 1; GATA6: GATA binding protein 6; MTDH: metadherin; MYDGF: myeloid derived growth factor; SMAD1: SMAD family member 1; ISM1: isthmin 1; TGFBR2: transforming growth factor beta receptor 2; XBP1: X-box binding protein 1.

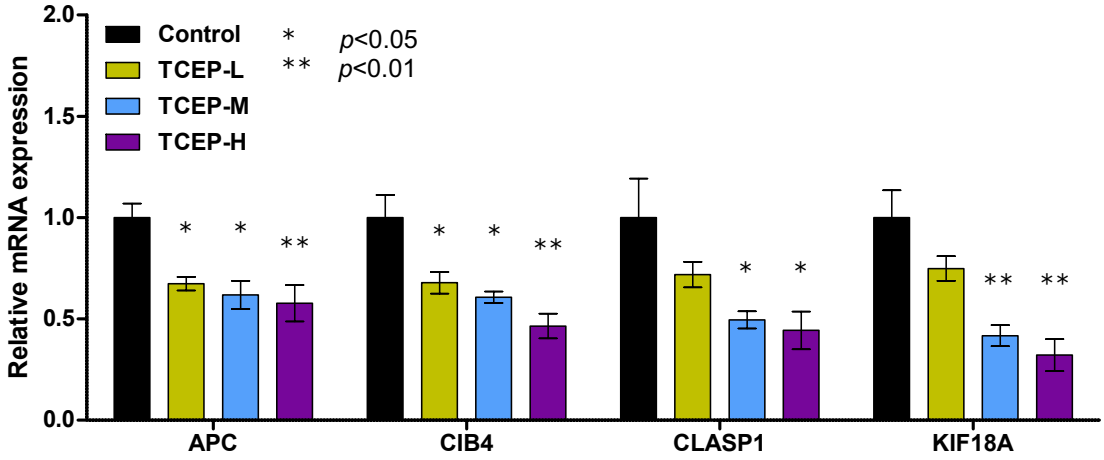

Figure. 3.17 Results for relative mRNA expression levels of differentially expressed genes (FDR < 0.05) included in the enriched Gene Ontology (GO) term (p < 0.05) associated with microtubule depolymerization. The y-axis represents the fold change compared to the control group. Asterisk signs (* p <0.05; ** p <0.01; *** p <0.001) indicate the significantly different levels in TCEP exposure groups compared with the control group by RNA-seq, which were determined by Dunnett's test. APC: Adenomatous polyposis coli; CIB4: calcium and integrin binding family member 1; CLASP1: cytoplasmic linker associated protein 1; KIF18A: kinesin family member 18A.

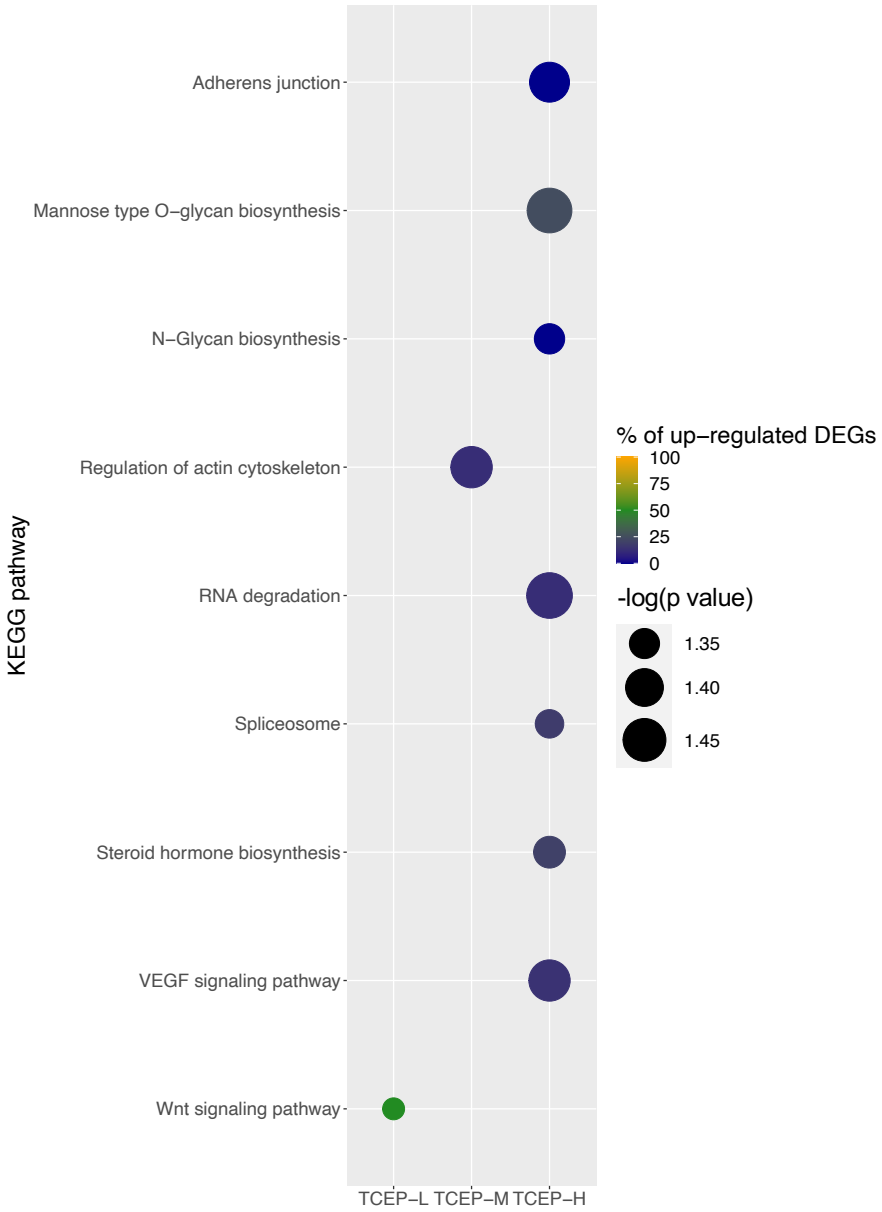

Figure. 3.18 Enrichment analysis for KEGG pathways. Pathways that were significantly enriched in the TCEP-L, TCEP-M, and TCEP-H exposure groups. The circle size shows the degree of significance (log-transformed p-value multiplied by -1). The circle's color indicates the percentage of significantly upregulated genes in the pathway.

Table. 3.5 Results of KEGG pathway enrichment analysis from DEGs in TCEP exposure groups.

Description	GeneRatio	BgRatio	pvalue	qvalue	Nr. Genes	Genes
TCEP-L						
Wnt signaling pathway	2/12	148/5042	0.047	0.274	2	RSPO1, ROR2
TCEP-M						
Regulation of actin cytoskeleton	8/99	195/5042	0.037	0.879	8	PIK3R2, APC, ITGA7, FGF20, NCKAP1, ARHGEF12, WASF1, BDKRB1
TCEP-H						
RNA degradation	8/275	69/5042	0.033	0.849	8	ENO2, TTC37, PABPC1L, HSPA9, EDC4, XRN2, LSM4, DCP2
Mannose type O-glycan biosynthesis	4/275	23/5042	0.034	0.849	4	B3GAT1, TMEM5, B3GAT1L, LARGE1
VEGF signaling pathway	7/275	58/5042	0.037	0.849	7	PPP3R1, AKT1, RAC3, RAC1, PIK3CA, PLA2G4EL2, PIK3R3
Adherens junction	8/275	71/5042	0.038	0.849	8	TGFBR2, RAC3, RAC1, PARD3, CTNNA3, FER, WASF1, SNAI2
Steroid hormone biosynthesis	5/275	36/5042	0.044	0.849	5	SRD5A1, HSD17B12, CYP3A4, COMT, CYP21A1
N-Glycan biosynthesis	6/275	48/5042	0.045	0.849	6	ALG3, MAN1A1, MAN2A1, DPM2, MGAT5, MGAT4A
Spliceosome	11/275	114/5042	0.045	0.849	11	PRPF4, SRSF6, FUS, PLRG1, EIF4A3, SF3B6, SF3B1, LSM4, SNRPD1, PHF5A, RBM22

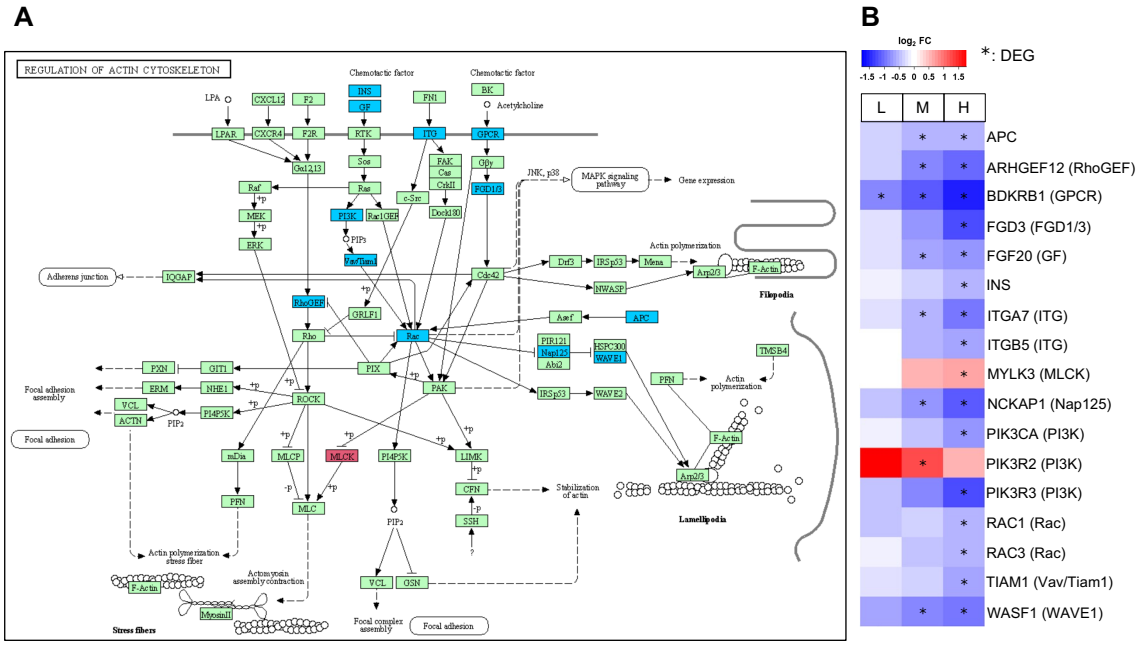

Figure. 3.19 Overview of the effect of exposure to TCEP on the regulation of actin cytoskeleton. (A) DEGs in the regulation of actin cytoskeleton. All DEGs were mapped using the KEGG mapper tool. Red-colored genes and blue-colored genes indicate DEGs of up-regulated and down-regulated, respectively. (B) A heatmap of the regulation of actin cytoskeleton-related DEGs. Each column represents a single group (L: TCEP-L; M: TCEP-M; H: TCEP-H), and each row represents a single DEG. The blue and red colors indicate DEG, which was down- and up-regulated in the group. Asterisks denote DEGs.

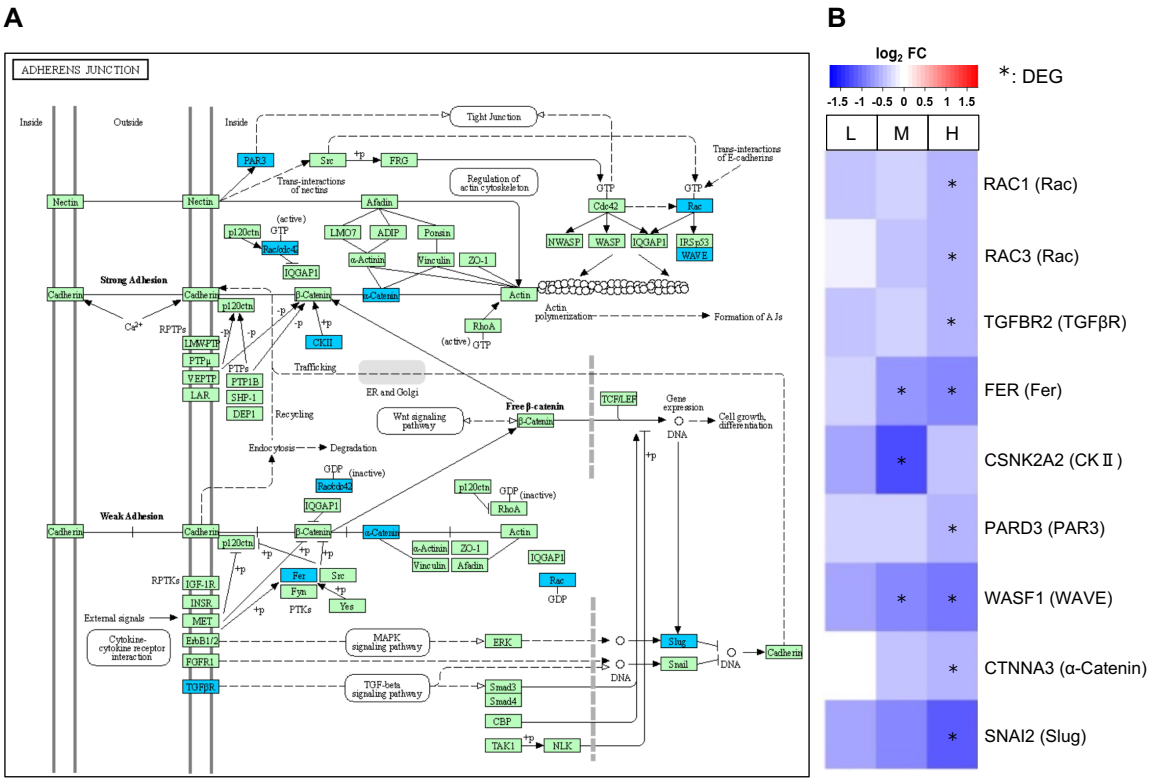

Figure. 3.20 Overview of the effect of exposure to TCEP on the adherens junction. (A) DEGs in the adherens junction. All DEGs were mapped using the KEGG mapper tool. Red-colored genes and blue-colored genes indicate DEGs of up-regulated and down-regulated, respectively. (B) A heatmap of the adherens junction-related DEGs. Each column represents a single group (L: TCEP-L; M: TCEP-M; H: TCEP-H), and each row represents a single DEG. The blue and red colors indicate DEG, which was down- and up-regulated in the group. Asterisks denote DEGs.

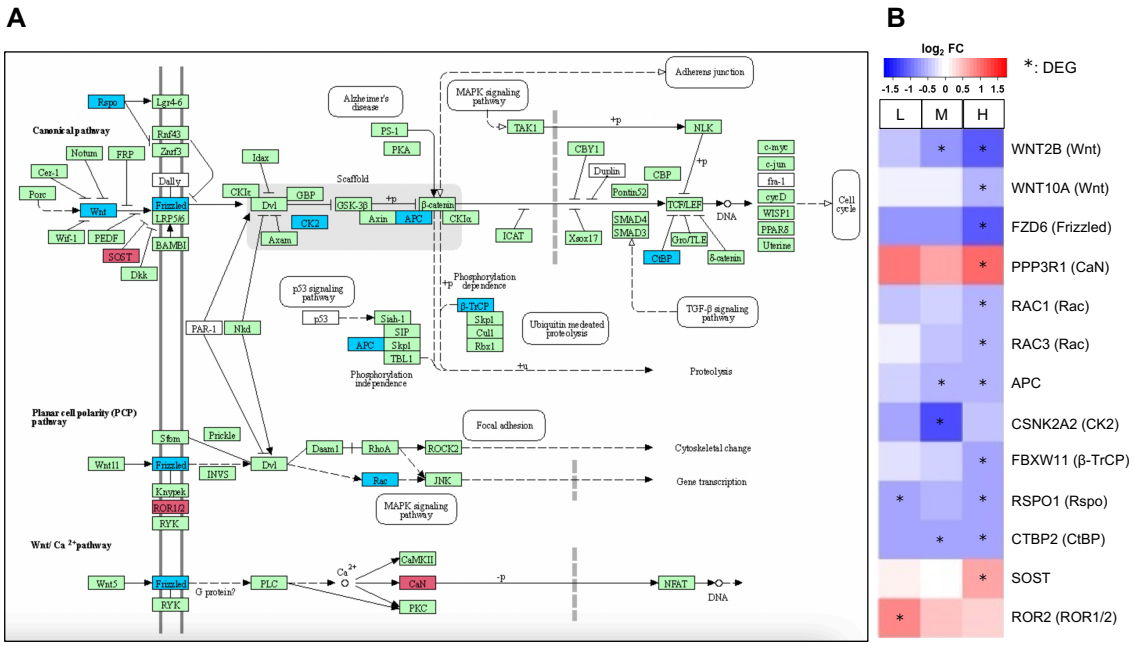

Figure. 3.21 Overview of the effect of exposure to TCEP on the Wnt signaling pathway. (A) DEGs in the Wnt signaling pathway. All DEGs were mapped using the KEGG mapper tool. Red-colored genes and blue-colored genes indicate DEGs of up-regulated and down-regulated, respectively. (B) A heatmap of the Wnt signaling-related DEGs. Each column represents a single group (L: TCEP-L; M: TCEP-M; H: TCEP-H), and each row represents a single DEG. The blue and red colors indicate DEG, which was down- and up-regulated in the group. Asterisks denote DEGs.

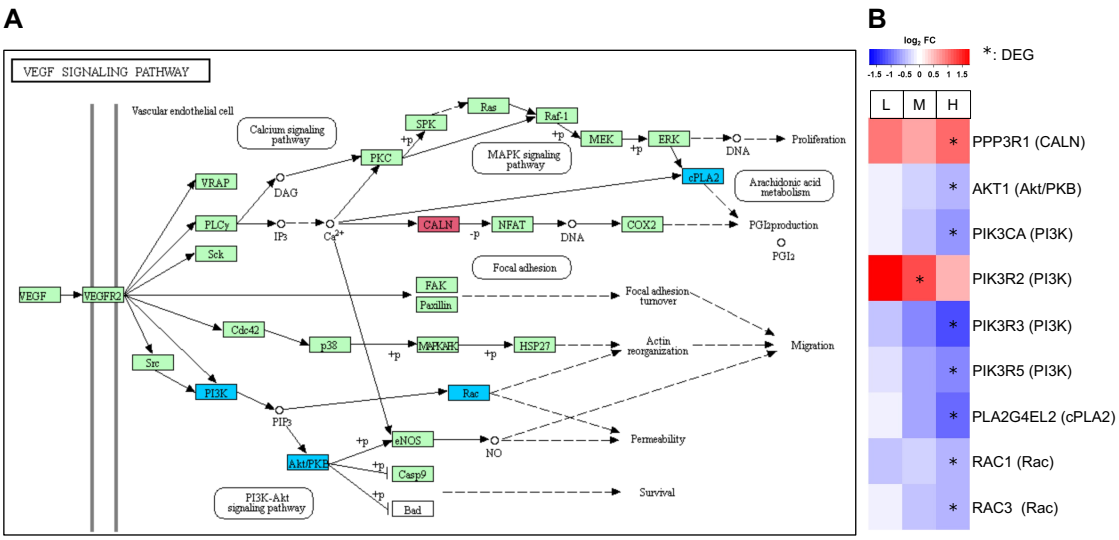

Figure. 3.22 Overview of the effect of exposure to TCEP on the VEGF signaling pathway. (A) DEGs in the VEGF signaling pathway. All DEGs were mapped using the KEGG mapper tool. Red-colored genes and blue-colored genes indicate DEGs of up-regulated and down-regulated, respectively. (B) A heatmap of the VEGF signaling-related DEGs. Each column represents a single group (L: TCEP-L; M: TCEP-M; H: TCEP-H), and each row represents a single DEG. The blue and red colors indicate DEG, which was down- and up-regulated in the group. Asterisks denote DEGs.

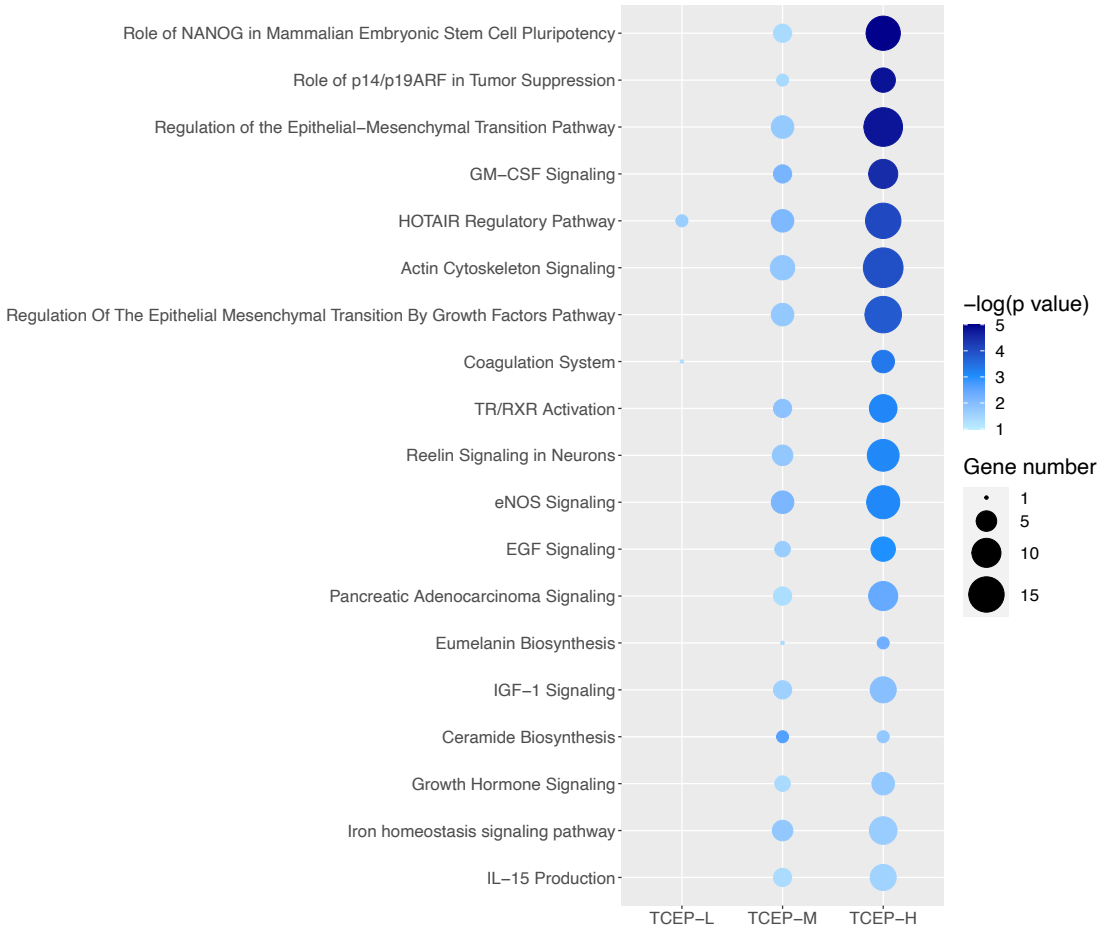

Figure. 3.23 Scatter plot for enriched canonical pathways results by IPA. Only pathways common to two or more groups in the TCEP treatment group are represented. The size of the circle shows the degree of gene number annotated in this pathway. The circle's color indicates the degree of significance (log-transformed p-value multiplied by -1).

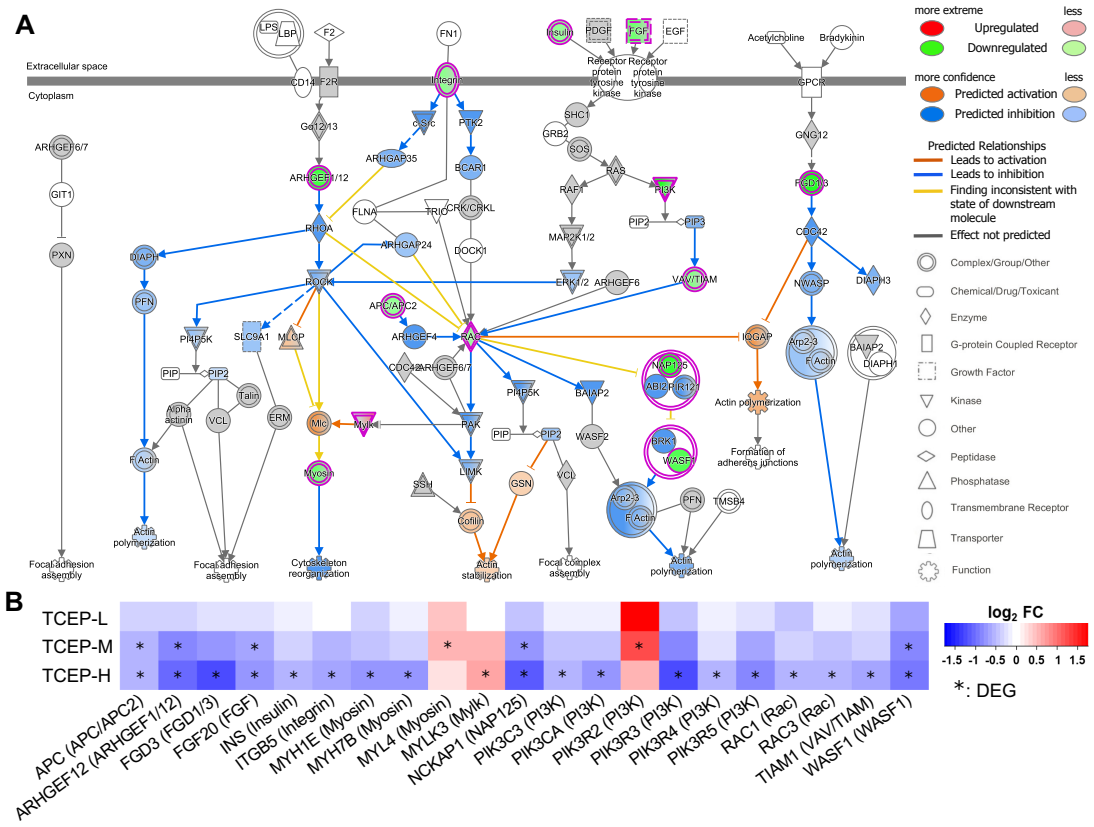

Figure. 3.24 Enrichment analysis for IPA. (A) Actin cytoskeleton signaling pathway in the TCEP-H group identified by IPA. The shapes represent the molecular classes of the proteins. In the figure, red represents upregulation, green, downregulation, and color intensity represent the relative magnitude of change in protein expression. (B) A heatmap of the actin cytoskeleton signaling related DEGs. Each column represents a single DEG, and each row represents a single TCEP exposure group. The blue and red colors indicate DEG, which was down- and up-regulated in the group. Asterisks denote DEGs.

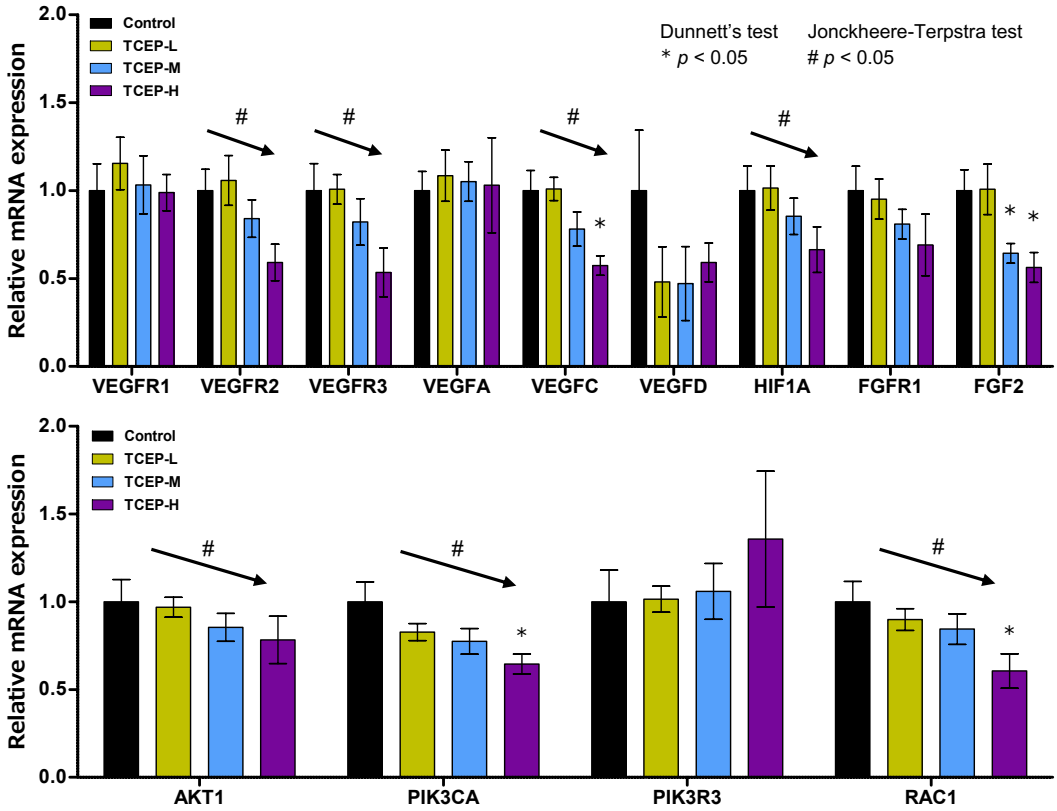

Figure. 3.25 Relative expression levels of angiogenesis-related genes compared to the control group by qRT-PCR in the vitelline membrane containing extraembryonic blood vessels of chicken. Data represent means ± standard error of the mean (SEM). Asterisks indicate significant differences (*p < 0.05) in each measurement in a TCEP-treated group compared with that in the respective control, which was determined by Dunnett's test. Hash symbols with arrows indicate the significant trends in a concentration-dependent manner (#p < 0.05) in control and TCEP-treated groups, which were determined by the Jonckheere-Terpstra test.

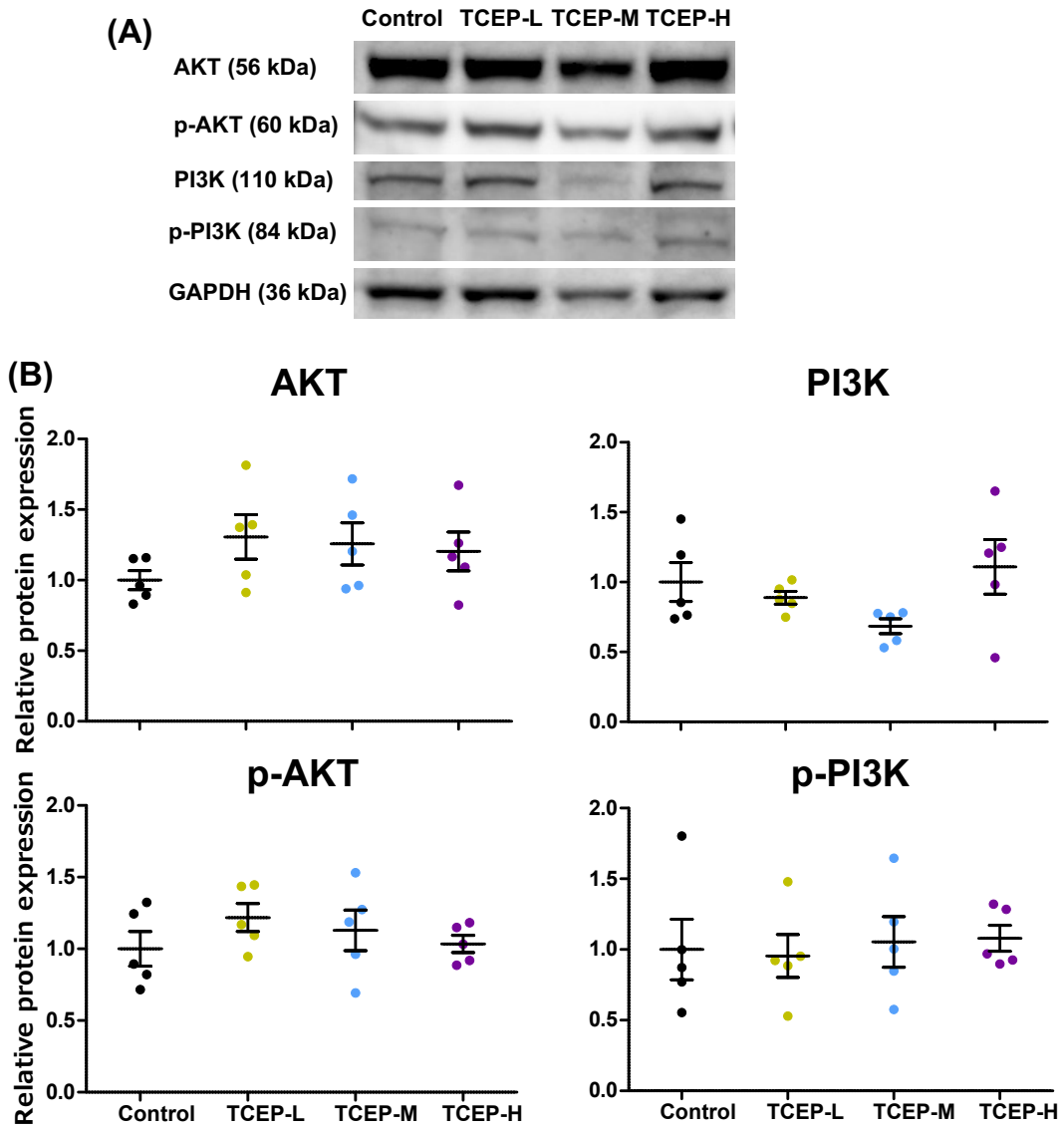

Figure. 3.26 Effects of TCEP on protein expression in the heart of chicken embryo on day 5. (A) Images of PI3K, p-PI3K, AKT, p-AKT, and GAPDH protein bands by western blot. (B) Relative each protein expression was expressed as a value relative to the control group after normalization by GAPDH. Data represent means ± standard error.

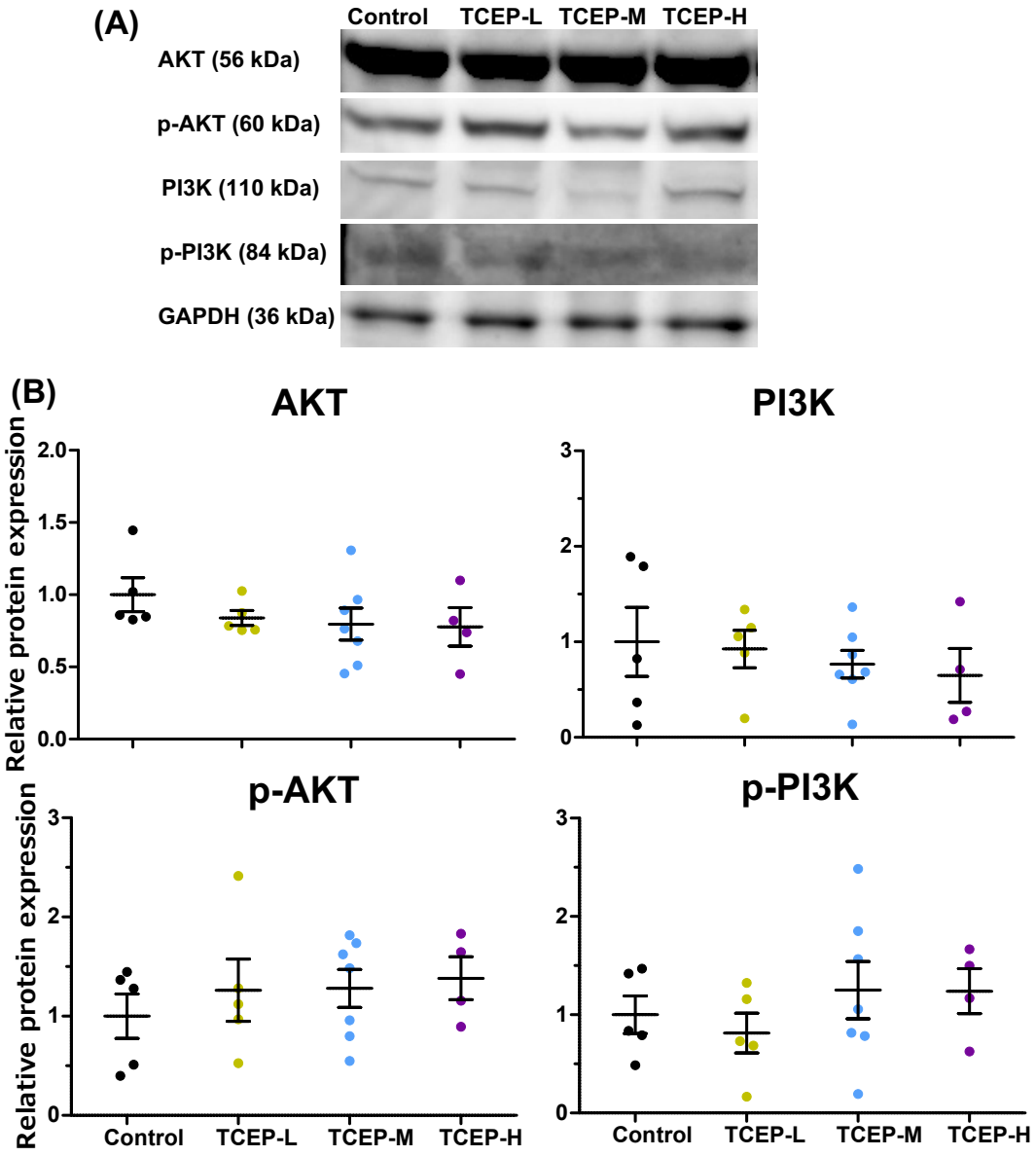

Figure. 3.27 Effects of TCEP on protein expression in the vitelline membrane of the chicken embryo on day 5. (A) Images of PI3K, p-PI3K, AKT, p-AKT, and GAPDH protein bands by western blot. (B) Relative each protein expression was expressed as a value relative to the control group after normalization by GAPDH. Data represent means ± standard error.

3.5 Discussion

This study aims to investigate TCEP exposure's effects on cardiac and vascular development in chicken embryos on day five from a phenotypic endpoint and transcriptomic perspective. We first performed a quantitative comparison of the phenotypic endpoints of day five survivors in each treatment group by in situ observation and image analysis. The body weight of embryos on day 5 decreased in a TCEP concentration-dependent manner, consistent with the results for body weight on day 9 of the study in Chapter I (Kanda et al., 2021). The heart rate was significantly reduced by TCEP exposure, especially on day 4, when the heart rate decreased in a TCEP concentration-dependent manner. The heart rate of the chicken embryo reaches an upper maximum on the fifth day of incubation and maintains a constant heart rate until hatching (J. Bogue, 1932). Because the heart rate of the control group on day five may have reached the upper limit in this study as well, it is considered that the heart rate of the TCEP-L and TCEP-M groups increased with a delay, and there were not different compared to the control group on day 5. According to the study by Alzualde et al. (2018), exposure to TDCIPP (30 and 100 μM) in zebrafish embryos significantly reduced heart rate. However, TDCIPP was not considered cardiotoxic since lethality was also caused at the same doses at which bradycardia was detected (Alzualde et al., 2018). In our study, the following two points that (1) there was a significantly strong correlation between embryo weight and heart rate (Fig. 3.6), and (2) the heartbeat

frequency was undisturbed, indicating no arrhythmias were observed in all treated groups (Fig. 3.7) are suggested that the lower heart rate of chicken embryos in the TCEP exposure group maybe not a cardiac-specific effect but an effect associated with growth retardation.

To understand the molecular mechanisms leading to cardiac effects following TCEP exposure, we analyzed differences in the cardiac transcriptome between TCEP-exposed embryos and vehicle-exposed embryos. The significantly enriched cardiac conduction GO term included five genes (ABCC9, BIN1, CACNA1G, KCNE5, and KCNJ2) involved in calcium and potassium ion channels. Down-regulation of BIN1 is consistent with that observed in TDCIPP-treated zebrafish embryos (Dasgupta et al., 2018). In the mouse heart, the T-type Cav3.1 Ca^{2+} channel encoded by cacna1g is highly expressed in the sinoatrial node (SAN) (Mangoni et al., 2006). The CACNA1G gene has been expressed in embryonic chicken hearts sinoatrial myocardium for at least HH21 (3.5 days) (Vicente-Steijn et al., 2017). Furthermore, a strong correlation was observed between the heart rate and the expression of these genes (Fig. 3.15); thus, the decrease in heart rate in chicken embryos by TCEP exposure may be directly related to a decrease in this ion channel expression. GO analysis showed that TCEP exposure significantly reduced mRNA expression of genes involved in the regulation of microtubule depolymerization (APC, CIB4, CLASP1, and KIF18A). The contract function in cardiomyocytes involves calcium channel localization, the trafficking by microtubules, and BIN1 expression (Hong et al., 2014; Shaw et al.,

2007). In the mammalian ventricular myocytes, the cardiac transverse tubule (t-tubule) is a highly branched invagination of cardiomyocyte sarcolemma rich in ion channels important for excitation-contraction (EC) coupling (Dibb et al., 2009). The function of t-tubules is regulation of cardiac EC coupling by concentrating voltage-gated L-type calcium channels (LTCCs) and positioning them close to calcium sense and release channels, ryanodine receptors (RyRs), at the junctional membrane of sarcoplasmic reticulum (jSR) (Hong and Shaw, 2017). Microtubules transport new LTCCs from the Golgi to the T-tubules, and the membrane scaffolding protein BIN1 localizes LTCCs to T-tubule membrane structures (Hong et al., 2010). Although nonmammalian cardiomyocytes, including avian, do not have T-tubule membranes, there is crosstalk between LTCC and RyR in the quail heart, confirming a functional connection between the sarcolemma and SR membranes (Filatova et al., 2020; Shiels and Galli, 2014). Therefore, suppression of microtubule function and downregulation of the BIN1 in the chicken embryo heart is suspected of disrupting the normal expression and localization of calcium channels in the sarcolemma and inhibiting cardiac contractile function (Fig. 3.28).

NKX2-5, the transcription factor required for the development of the heart, is essential for vertebrate heart morphogenesis, myogenesis, and function (Akazawa and Komuro, 2003; Lyons et al., 1995). NKX2-5 knockout mice demonstrate reduced cardiac contraction, conduction defects, cardiac hypertrophy, and reduced expression of multiple NKX2-5 downstream transcripts,

including T-type Ca2 channels (Pashmforoush et al., 2004; Terada et al., 2011). Triphenyl phosphate (TPHP) and Cresyl diphenyl phosphate (CDP) in OPFRs induce significant downregulation of mRNA expression of transcription factors involved in heart development, including NKX2-5, reduced heart rate, formation of pericardial edema, and disorders of cardiac looping in zebrafish embryos in a previous study (Du et al., 2015). Thus, the present study suggests that reduced expression of NKX2-5 by TCEP exposure may cause developmental delay of the cardiac conduction system and reduced heart rate. The KEGG pathway analysis showed that TCEP disrupts the Wnt signaling pathway (Fig. 3.18 and 21, Table 3.5). Wnt signaling regulates NKX2-5 to induce cardiac mesoderm differentiation and embryonic heart development (Cambier et al., 2014; Liu et al., 2009; Peng et al., 2020). Thus, TCEP may have suppressed NKX2-5 expression by disrupting Wnt signaling, inhibiting myocardial development. Pathway analysis revealed that TCEP significantly downregulates gene expression regulating the actin cytoskeleton and adherens junction in the embryonic chicken heart on day 5 (Fig. 3.19, 3.20, and 3.24). The actin cytoskeleton undergoes dynamic assembly and disassembly during cell crawling, which regulates protrusion formation, focal adhesion assembly/disassembly, and contractile filament organization (Tang and Gerlach, 2017). Cell migration is initiated or enhanced by activating receptors that cause cytoskeletal remodeling and subcellular organelles reordering. Relevant receptors include a wide variety of G-protein coupled receptors (GPCR), receptor

tyrosine kinases (RTK), and matrix adhesive proteins such as integrins (Gerthoffer, 2008). TCEP downregulated gene expression of Insulin and FGF20, ligands for RTKs; ITGB5, an integrin; and BDKRB1, involved in GPCR. In addition, gene expression of PI3K (PIK3CA, PIK3R3, PIK3R4, and PIK3R5) and Rac family small GTPase (RAC1 and RAC3), which are activated by RTK signaling, was significantly reduced by TCEP exposure (Fig. 3.19 and 3.24). Phosphoinositide 3-kinase (PI3K) plays a key role in chemotaxis, regulating cell motility by controlling the actin cytoskeleton in mammalian cells. Phosphatidylinositol (3,4,5)-trisphosphate [PtdIns(3,4,5)P_3], produced by PI3K, acts via diverse downstream signaling components, including the GTPase Rac, Arf-GTPases, and the kinase Akt (PKB) (Kölsch et al., 2008). The small G proteins (Ras, Rho, Rac, Cdc42) are very early elements in signaling pathways that promote cell migration. Both RTKs and GPCRs activate several small G proteins via the regulation of guanine nucleotide exchange factors (GEFs) and GTPase-activating proteins (Gerthoffer, 2007). Rac1 and Rac2 activate p21-activated protein kinases (PAKs), and PAK mediates cell migration via its effects on the cytoskeleton (Weber et al., 2004). Cell morphogenesis and cell migration have important roles in heart development in the embryo. Avians, including chickens, have a cardiac loop process during heart development. The process of cardiac looping in the chick embryo occurs at HH9-34 (30 hours–day 8 of incubation) (al Naieb et al., 2013; Christoffels et al., 2000; Martinsen, 2005). Cardiac looping bending and rotation are caused by changes in cardiomyocyte morphology due

to alterations in cytoskeletal regulation and cell adhesion (Itasaki et al., 1989; Linask and VanAuker, 2007). We found that TCEP exposure increased chicken embryos' ventricular surface area to body weight ratio on day 5 (Fig. 3.4). Zebrafish embryos exposed to TDCIPP have been reported to be affected by pericardial edema, cardiac looping defects, and reduced heart rate(Dasgupta et al., 2018; Zhong et al., 2019). Therefore, it is suggested that TCEP exposure induced abnormal heart morphogenesis in the chicken embryo heart by altering gene expression related to the cytoskeleton and cell adhesion.

In the IPA analysis, two pathways that regulate epithelial-mesenchymal transition (EMT) are significantly enriched in TCEP-M and TCEP-H, suggesting that TCEP may inhibit EMT in early chicken embryos (Fig. 3.23). EMT is a process by which epithelial cells lose their cell polarity and cell-cell adhesion and gain migratory and invasive properties to become mesenchymal stem cells. EMT is regulated by diverse pathways, including RTK signaling, transforming growth factor beta (TGF-β) signaling, and Wnt signaling involving growth factors (Thiery et al., 2009). In cardiac development, epicardial-derived progenitor cells (EPDCs) arise from the epicardial layer through an EMT event that initiates after Hamburger-Hamilton stage 18 in chicks, and EPDCs contribute to various cardiac lineages such as cardiac fibroblasts (CFs), smooth muscle cells (SMCs) and pericytes (PCs) (Quijada et al., 2020). In the IPA analysis, 19 differentially expressed genes were involved in EMT, of which TCEP decreased the expression

of 17 genes (Fig. 3.28 and 3.29). The expression of TGFBR2, a receptor for TGF-β, and WNT10A, WNT2B, and FZD6 in WNT signaling and FGF20 were significantly decreased. In addition, SNAI2, a key EMT transcription factor expressed in the cytoplasm and nucleus, was down-regulated (Zhou et al., 2019). Suppression of EMT impedes the differentiation of cardiac-related cells from epicardial-derived progenitor cells, suggesting that it suppresses cardiac development by TCEP exposure. Furthermore, the earliest EMT in development occurs during gastrulation, a process that generates mesoderm and endoderm from the ectoderm (HH4 [18–19h]) (Nakaya and Sheng, 2009). Accordingly, TCEP may cause EMT function suppression and mesoderm differentiation inhibition in chicken embryos, inducing developmental delay.

KEGG pathway analysis showed that gene expression in the vascular endothelial growth factor (VEGF) signaling pathway was significantly altered (Fig. 3.22). In particular, the expression of genes involved in PI3K (PIK3CA, PIK3R3, and PIK3R5), AKT serine/threonine kinase 1 (AKT), and RAC (RAC1 and RAC3) of the VEGF signaling pathway was significantly decreased. Interaction with VEGF and VEGFR induces PI3K and AKT phosphorylation, which promotes angiogenesis (Melincovici et al., 2018; van der Ploeg et al., 2021). We measured protein levels of AKT, PI3K, phosphorylated AKT (p-AKT), and phosphorylated PI3K (p-PI3K), but TCEP did not affect their protein expression. Discrepancies between mRNA and protein expression levels can have many causes. In a previous study, a systematic quantitative proteome

dataset revealed that a considerable fraction of genes shows mRNA-protein expression level discrepancy (Wang et al., 2019). The first cause is the complicated transcription and translation process. Multiple-level processes, including histone modification, DNA methylation, and transcription factor regulations in transcriptional regulation and RNA binding protein, RNA modification, and microRNA regulations after transcription intensively regulate gene expression (Klutstein et al., 2016; Li et al., 2016; Mohr and Mott, 2015). Therefore, differences in mRNA and protein levels can occur during these processes. The second cause is the time of translation and protein synthesis. These processes may cause proteins not to reflect simultaneous mRNA expression levels (Liu et al., 2016). In developing embryos, mRNA and protein expression changes following cellular differentiation and morphological changes. Thus, gene and protein quantification using day five hearts collected simultaneously may be a discrepancy. However, since many genes in the pathway were downregulated, the mRNA-level results from the transcriptome analysis can be trusted. Because there was a significant correlation between changes in mRNA levels and phenotypic endpoints, biological functions and pathways statistically significantly affected by TCEP exposure are likely responsible for causing adverse outcomes in chicken embryos.

The formation of extraembryonic blood vessels was inhibited by TCEP exposure (Fig. 3.5B). Since cardiac transcriptome analysis showed that the VEGF signaling pathway was

disturbed by TCEP exposure, gene expression involved in VEGF signaling in extraembryonic blood vascular vessels was measured to investigate whether disturbance of VEGF signaling is responsible for the inhibition of vasculogenesis and angiogenesis. Gene expression levels of VEFR2, VEGFR3, VEGFC, HIF1A, FGF2, AKT, PIK3CA, and RAC1 showed a downward trend in a TCEP concentration-dependent manner (Fig. 3.25). Circulatory system development begins immediately after gastrulation, concomitant with somite formation (Risau et al., 1988). The early vascular plexus forms from mesoderm by differentiation of angioblasts, which subsequently generate primitive blood vessels. Mesoderm-inducing factors of the FGF family are crucial in the mesoderm to form angioblasts and hematopoietic cells (Risau, 1997). Downregulation of FGF2 by TCEP exposure suggests that TCEP may suppress mesoderm differentiation into hemangioblasts by inhibiting FGF. The VEGF family consists of five peptide ligands (VEGFA–D and placental growth factor) and three receptors (VEGFR1–3) (Karaman et al., 2018). VEGFR1–3 all have roles in vasculogenesis and angiogenesis, with VEGFR1 interacting most strongly with VEGFs, and VEGFC is a ligand that interacts specifically with VEGFR2 and VEGFR3 (Monaghan et al., 2021). Therefore, it is suggested that TCEP exposure decreased the gene expression of VEGFR2, VEGFR3, and VEGFC and suppressed angiogenesis.

On the other hand, even high-concentration TCEP exposure did not completely suppress angiogenesis. This may be due to the maintenance of VEGFR1 and other VEGFs expressions.

Because AKT1 and PI3CA, involved in VEGF signaling, were downregulated by TCEP exposure, protein levels of AKT and PI3K were measured by western blot. However, the respective protein levels were unchanged by TCEP. Discrepancies between mRNA and protein results are noted above. In a previous study, TDCIPP exposed to zebrafish embryos decreased the expression of VEGF-related genes and inhibited the remodeling of common cardinal veins (Zhong et al., 2019). Our study is similar to the previous study, revealing that TCEP inhibits angiogenesis by disrupting VEGF signaling. However, TCEP also downregulated FGF2, a marker of mesoderm that differentiates into angioblasts, suggesting that TCEP may already be interfering at the mesoderm stage, and further assessment of the effects of TCEP in the early stages of chicken embryos is needed.

The cardiovascular effects on chicken embryos on days 3–5 was summarized in Fig. 3.30. In conclusion, TCEP may disturb Wnt signaling and microtubule function, suppresses cardiac conduction, and reduces heart rate in chicken embryos. And TCEP exposure may cause abnormal cardiac morphology by downregulation of genes involved in receptor tyrosine kinase signaling and dysfunction of actin cytoskeleton regulation and adherens junction. It is suggested that TCEP exposure downregulates VEGF signaling-related genes and induces suppression of angiogenesis in embryonic extraembryonic blood vessels. In addition, TCEP exposure may suppress EMT in the heart.

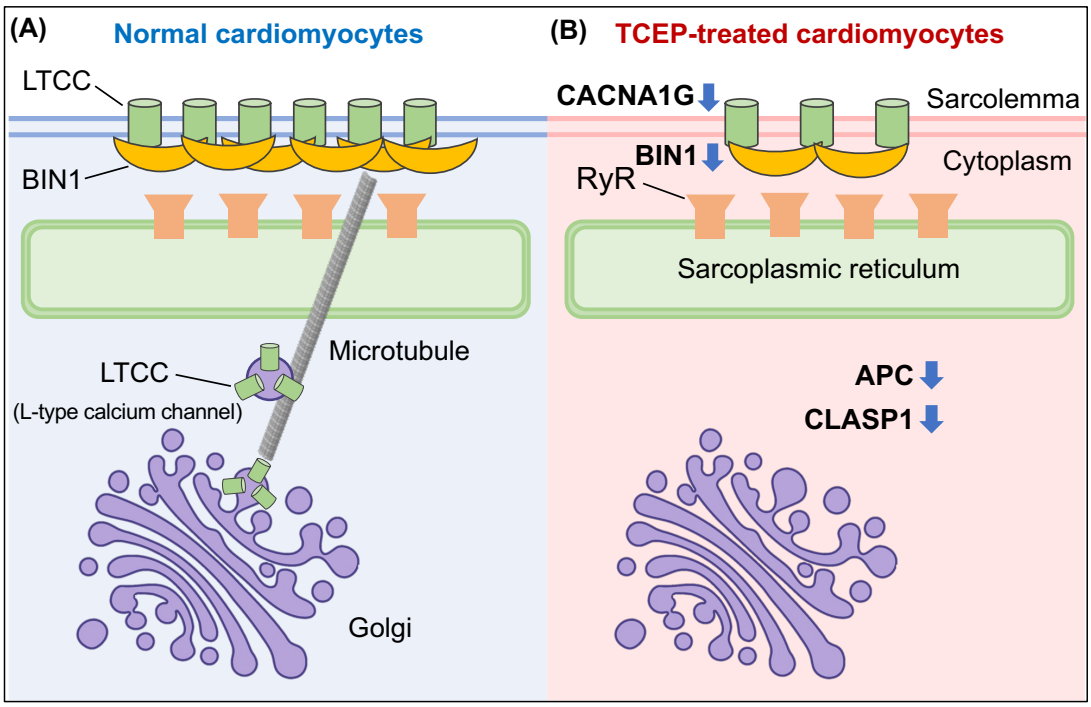

Figure. 3.28 Schematic of the cardiomyocyte structure components in chicken embryos. (A), In normal cardiomyocytes, L-type calcium channels (LTCCs) are transported from the Golgi to the sarcolemma by microtubules, and BIN1 promotes LTCC localization and clustering at the sarcolemma. (B), TCEP-treated cardiomyocytes suppress the gene expression of CLASP1 involved in microtubule function, LTCC (CACNA1G), and BIN1, subsequently causing inhibition of cardiac conduction and contraction.

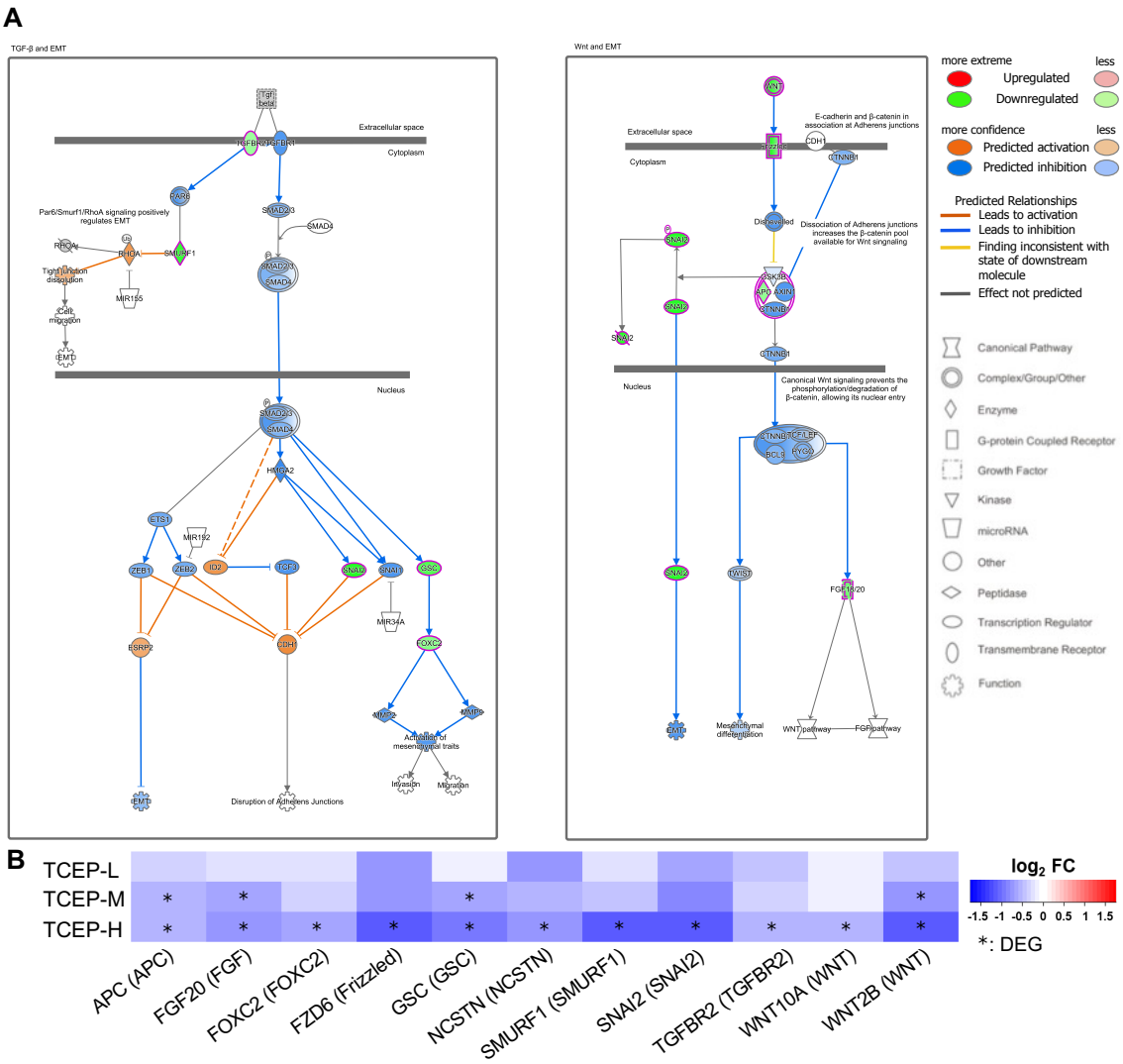

Figure. 3.28 Regulation of the Epithelial-Mesenchymal Transition (EMT) pathway in the TCEP-H group identified by IPA. (A) The shapes represent the molecular classes of the proteins. In the figure, red represents upregulation, green, downregulation, and color intensity represent the relative magnitude of change in protein expression. (B) A heatmap of the regulation of the EMT pathway-related DEGs. Each column represents a single DEG, and each row represents a single TCEP exposure group. The blue and red colors indicate DEG, which was down- and up-regulated in the group. Asterisks denote DEGs.

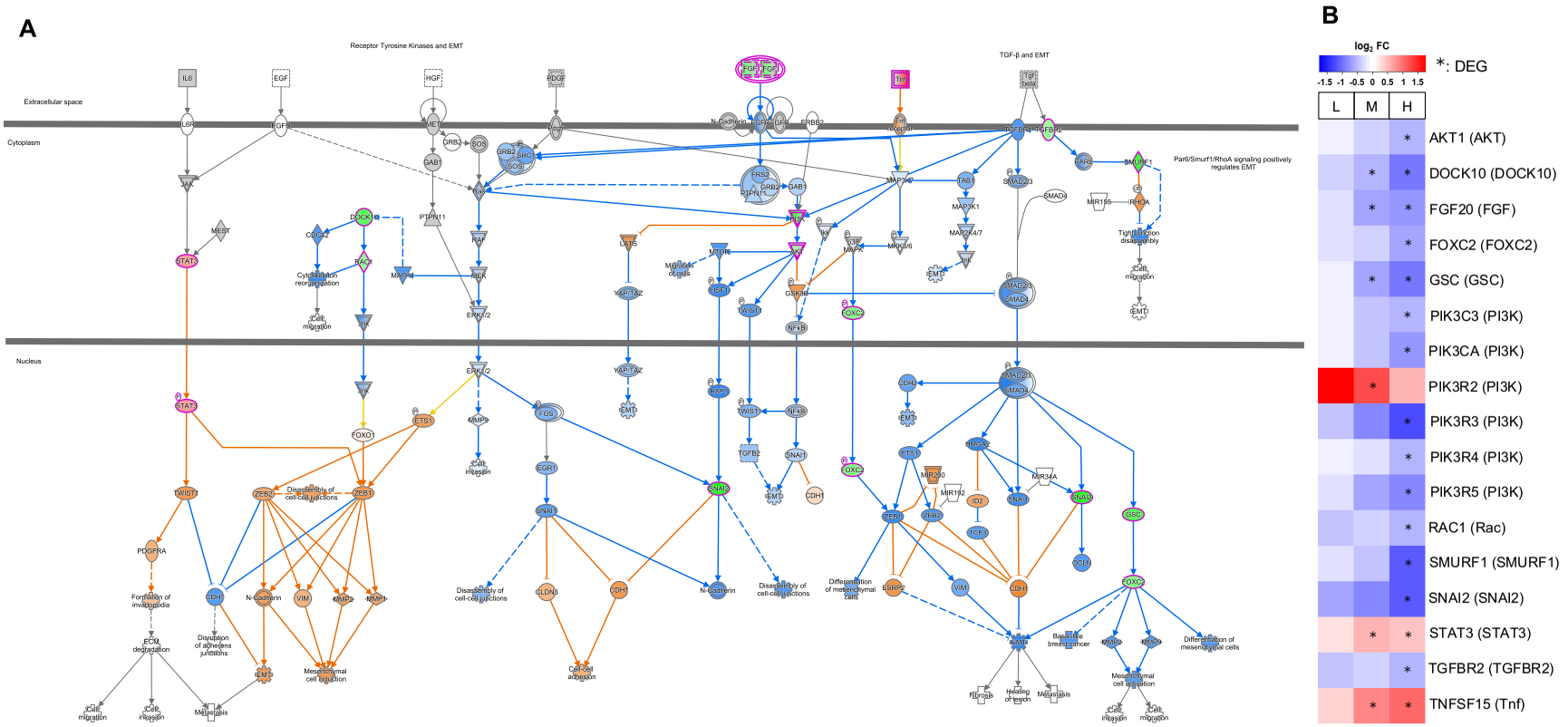

Figure. 3.29 Regulation of t the EMT by growth factors pathway in the TCEP-H group identified by IPA. (A) The shapes represent the molecular classes of the proteins. In the figure, red represents upregulation, green, downregulation, and color intensity represent the relative magnitude of change in protein expression. (B) A heatmap of the regulation of the EMT pathway-related DEGs. Each column represents a single DEG, and each row represents a single TCEP exposure group. The blue and red colors indicate DEG, which was down- and up-regulated in the group. Asterisks denote DEGs.

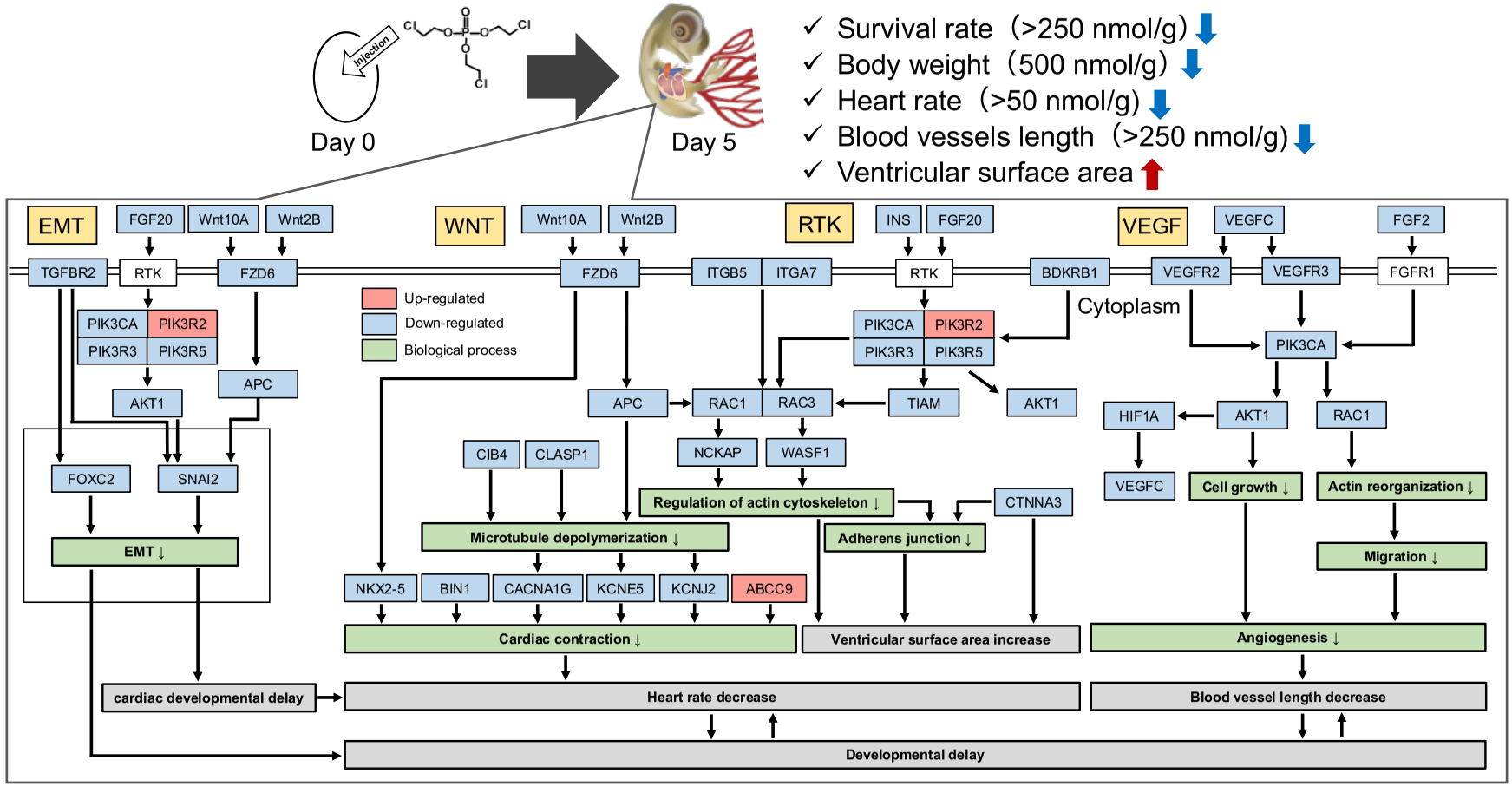

Figure. 3.30 Proposed adverse outcome pathways (AOPs) for the cardiovascular effects of TCEP exposure in chicken embryos on day 5.

CHAPTER IV

Effects of TCEP exposure on the epithelial-mesenchymal transition (EMT) in early-developing chicken embryos

4.1 Abstract

We have previously found that exposure to TCEP above 250 nmol /g egg already had lethal effects on day three of chicken embryos. Furthermore, cardiac transcriptome analysis found that TCEP exposure may significantly affect the epithelial-mesenchymal transition (EMT) signaling pathway in the heart of chicken embryos on day 5. Epiblast cells undergo an EMT during the gastrulation to form mesoderm and endoderm in the primitive streak. The formed mesoderm cells subsequently differentiate into various cells with specific characteristics, such as cardiomyocytes, vascular endothelial cells, and hematopoietic cells. We, therefore, hypothesized that TCEP disrupts EMT and mesoderm differentiation during protoderm formation and ultimately affects the cardiovascular system. To investigate whether TCEP exposure affects EMT in gastrulation, a developmental event of earlier avian embryos, the fertilized chicken eggs were exposed to 50, 250, and 500 nmol/g egg of TCEP (TCEP-L, -M, and -H, respectively) or 0.1% DMSO (vehicle control) from Hamburger and Hamilton stage (HH) 1 to 4. We sampled HH4 chicken blastoderms and performed the gene expression analysis using qRT-PCR. Gene expression of SNAI2, a transcription factor of EMT, and TBXT and TBX6, mesoderm markers,

was significantly decreased in a TCEP concentration-dependent manner. The TCEP-H group showed increased expression of E-cadherin ($p < 0.05$) and decreased expression of N-cadherin ($p < 0.05$). Because SNAI2 directly represses E-cadherin expression during EMT, the higher E-cadherin expression in the TCEP-exposed group compared with the control group supported the suppression of EMT by SNAI2 downregulation. The expression of FGF4, one of the FGF ligands, was significantly decreased by TCEP exposure. There was a significant positive correlation between FGF4, SNAI2, and TBXT in mRNA levels. FGF signaling plays a role in SNAI2-mediated EMT regulation and TBXT- mediated mesodermal induction. Thus, the downregulation of FGF4 by TCEP may trigger the repression of SNAI2 and TBXT expression. This study found that TCEP decreased FGF4 expression and suppressed EMT progression and mesoderm cell differentiation in chicken gastrulation. These effects may induce developmental delays and cardiovascular dysfunction in chicken embryos exposed to TCEP.

4.2 Introduction

Survival data showed that TCEP exposure (250 and 500 nmol/g egg) already had lethal effects on chicken embryos by day 3 of incubation. TCEP also induced developmental delays, such as significantly shortened body length, and suppressed the cardiovascular system, such as reduced heart rate and suppressed vasculogenesis during developmental stages between days 3 and 9. Therefore, TCEP may be causing adverse outcome events in the earlier developmental stages of the chicken embryo.

Ingenuity Pathway Analysis (IPA) canonical pathway analysis on the cardiac transcriptome using chicken embryos on day 5 showed that TCEP affected the epithelial-mesenchymal transition (EMT) signaling pathway. EMT is a morphogenetic process in which cells lose epithelial characteristics such as cell polarity and cell-cell adhesion and gain mesenchymal properties such as migration and invasion (Thiery et al., 2009). In addition, the cardiac transcriptome analysis indicated that expression of the Snail family transcriptional repressor 2 (SNAI2) gene was significantly decreased in the EMT signaling pathway. SNAI2 is a transcription factor of EMT and directly represses E-cadherin transcription, which is involved in mechanisms regulating cell-cell adhesions of epithelial cells (Yang and Weinberg, 2008). In amniotes (reptiles, birds, and mammals), EMT is generally considered a critical component of the developmental process to generate the mesoderm and endoderm from the ectoderm, namely

gastrulation (Nakaya and Sheng, 2008). In the case of the chick embryo, the primitive streak (streak), the site of EMT, is specified at the posterior part of the area pellucida by an earlier dorsal/ventral patterning event at stage HH1, and elongation of the streak anterior-ward occurs from HH2 to HH4 (Voiculescu et al., 2007). Gastrulation is initiated at HH4 (18-19 hours incubation), and a part of the epithelial cells forms the mesoderm by EMT (Nakaya and Sheng, 2009) (Fig. 4.1). The mesoderm cells are then differentiated into cardiomyocytes, hematopoietic cells, and endothelial cells that form blood vessels (Acloque et al., 2009; Marziano et al., 2021).

Therefore, we hypothesized that TCEP affects EMT and gastrulation of chicken primitive streak at HH4 and that cardiac development and angiogenesis are inhibited (Fig. 4.2). Thus, this study aimed to investigate whether TCEP exposure affects EMT during gastrulation of the chicken primitive streak.

We administered TCEP to HH1 chicken fertilized eggs and examined expression changes of 13 EMT- and mesoderm-related genes in the primitive streak and blastoderm at HH4. Snail family transcriptional repressor 2 (SNAI2) was selected because it is an important transcription factor for EMT during chicken gastrulation. EMT is associated with changes in cadherin expression. Expression of the three cadherins involved in EMT was also measured. Epithelial cells express E-cadherin (CDH1, Cadherin 1), mesenchymal cells express N-cadherin (CDH2, Cadherin 2), and both cells express P-cadherin (CDH3, Cadherin 3) (Dady et al., 2012;

Moly et al., 2016). If TCEP affects EMT, cadherin expression may also be altered. T-box transcription factor T (TBXT, [Brachyury or T]) and T-box transcription factor 6 (TBX6) are known as mesoderm markers because they are specifically expressed in mesoderm cells (Chapman et al., 1996; Wilkinson et al., 1990). TBXT and TBX6 expression is regulated by FGF signaling (Ciruna and Rossant, 2001). We measured FGF signaling-related genes, fibroblast growth factor 4 (FGF4), fibroblast growth factor 8 (FGF8), fibroblast growth factor receptor 1 (FGFR1), and AKT serine/threonine kinase 1 (AKT1), which are highly expressed in chicken embryos at HH4. In addition, mRNA levels of Wnt family member 3A (WNT3A), Bone morphogenetic protein 4 (BMP4), and Notch 1 (NOTCH1), which are associated with Wnt, BMP, and NOTCH signaling that regulate EMT, were also quantified (Thiery et al., 2009).

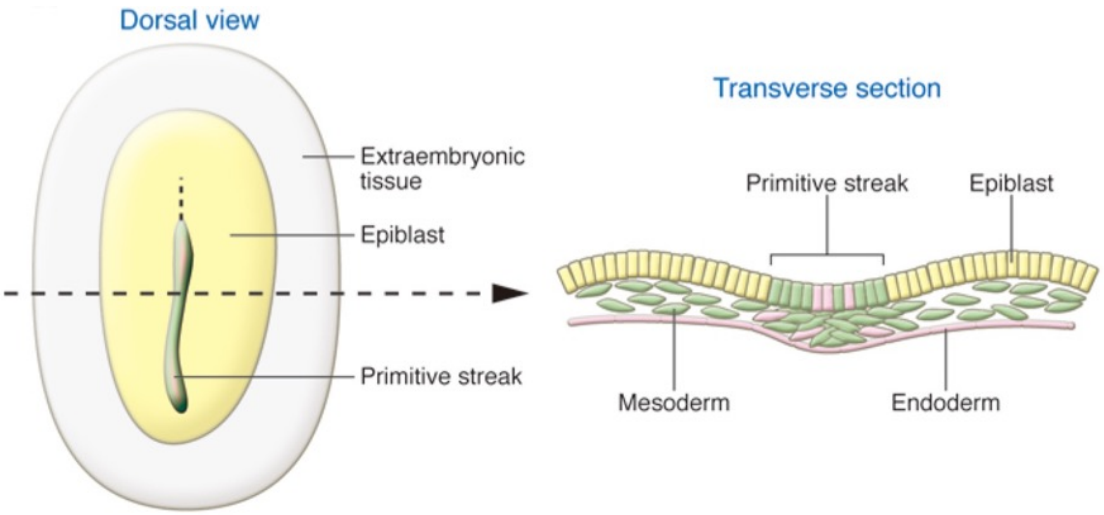

Figure. 4.1 The schematic representation of embryonic layers of chicken embryos during gastrulation at HH4. Mesoderm (green) and endoderm (pink) are generated from the ectoderm (yellow) via EMT during gastrulation (adopted from Acloque *et al*., 2009).

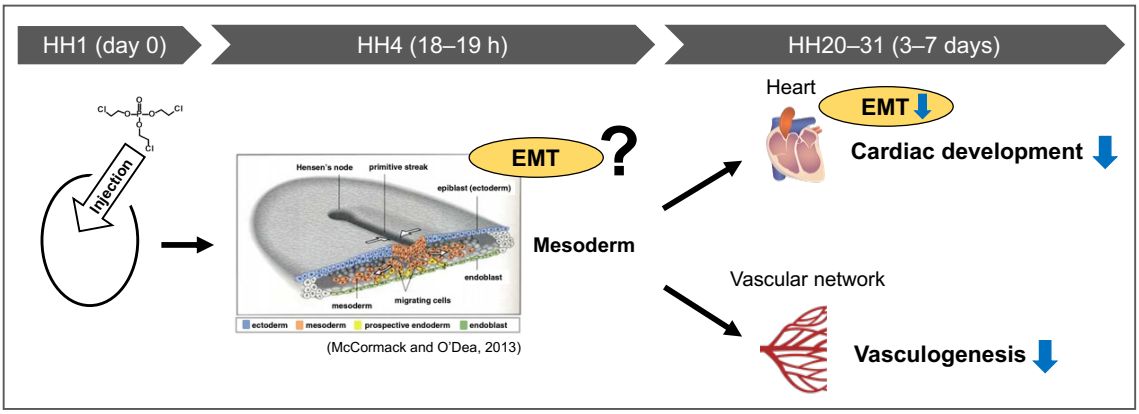

Figure. 4.2 Schematic diagram of the hypotheses in this study.

4.3 Materials and Methods

4.3.1 Chemicals

TCEP (97% purity; CAS No. 115-96-8) was purchased from Sigma-Aldrich (Saint Louis, USA). Dimethyl sulfoxide (DMSO) (Wako Pure Chemical Industries) was used for preparing stock and serially diluted solutions.

4.3.2 Animals and administration experiments

Fertilized eggs of the Rhode Island Red chicken (*Gallus gallus domesticus*) were purchased from Yamagishism Jikkenchi (Mie, Japan). The chicken eggs were categorized into four groups: vehicle control (control, receiving DMSO, $n = 14$), low-TCEP (TCEP-L; 50 nmol/g egg, $n = 13$), moderate-TCEP (TCEP-M; 250 nmol/g egg, $n = 13$), and high-TCEP (TCEP-H; 500 nmol/g egg, $n = 12$) groups. TCEP or DMSO was injected into the air sac of fertilized eggs at HH1 (day 0 of incubation), and these eggs were then incubated under continuous rotation of 1 cycle per hour in an incubator for 18–19 hours at 38℃ and 60% humidity. After 18-19 hours of incubation, the eggshells were cut with scissors, and the blastoderms at HH4 were transferred to petri dishes containing PBS solution with diethylpyrocarbonate (DEPC). A primitive streak approximately 2 mm long and 0.1 mm wide was found (Fig. 4.3). The yolk attached to the blastoderm was carefully removed, and blastoderms were immediately flash-frozen in liquid nitrogen stored at -80°C until RNA extraction.

4.3.3 RNA extraction and cDNA synthesis

Total RNA was extracted from 12 blastoderm samples from each treatment group using NucleoSpin RNA (Takara, Kusatsu, Japan) according to the manufacturer's protocol. Total RNA from each sample was reverse transcribed to cDNA using a High Capacity cDNA Reverse Transcription Kit (Thermo Fisher Scientific), following the manufacturer's instruction.

4.3.4 Quantitative reverse transcription polymerase chain reaction (qRT-PCR)

qRT-PCR was conducted to measure the mRNA expression levels of 13 EMT- and mesoderm-related genes. qRT-PCR was performed using TB Green® Premix Ex Taq^{TM} II (Takara, Kusatsu, Japan) in a StepOnePlus Real-Time PCR system (Thermo Fisher Scientific). Each gene-specific primer for qRT-PCR was designed to span exon boundaries by Primer-BLAST (https://www.ncbi.nlm.nih.gov/tools/primer-blast/) and synthesized by Eurofins Genomics (Tokyo, Japan). The sequences of the primers and their respective PCR conditions are listed in Table 4.1. Gene expression levels were normalized to those of an internal control mRNA, GAPDH. The mRNA expression data were expressed as fold changes of normalized values from TCEP-exposed groups relative to that from the vehicle control group.

The hearts, vitelline membranes containing the extraembryonic blood vessels, and heart-removed embryonic bodies of chicken embryos on day five, sampled in Chapter III, were also used for qRT-PCR analysis. These samples were performed for total RNA extraction and cDNA

synthesis according to the methods described in Chapter III.

4.3.5 Statistical analyses

All data were reported as means ± standard errors (SE). Differences in mRNA expression levels between TCEP treatment and control groups in qRT-PCR were statistically determined using a one-way ANOVA followed by Dunnett's multiple comparison tests in the R software. TCEP concentration-dependent trend changes in gene expression levels were assessed using the Jonckheere-Terpstra test with R software. Pearson's correlation analysis was performed to confirm the relationship between mRNA levels in each gene. Results with p-value < 0.05 were regarded as statistically significant.

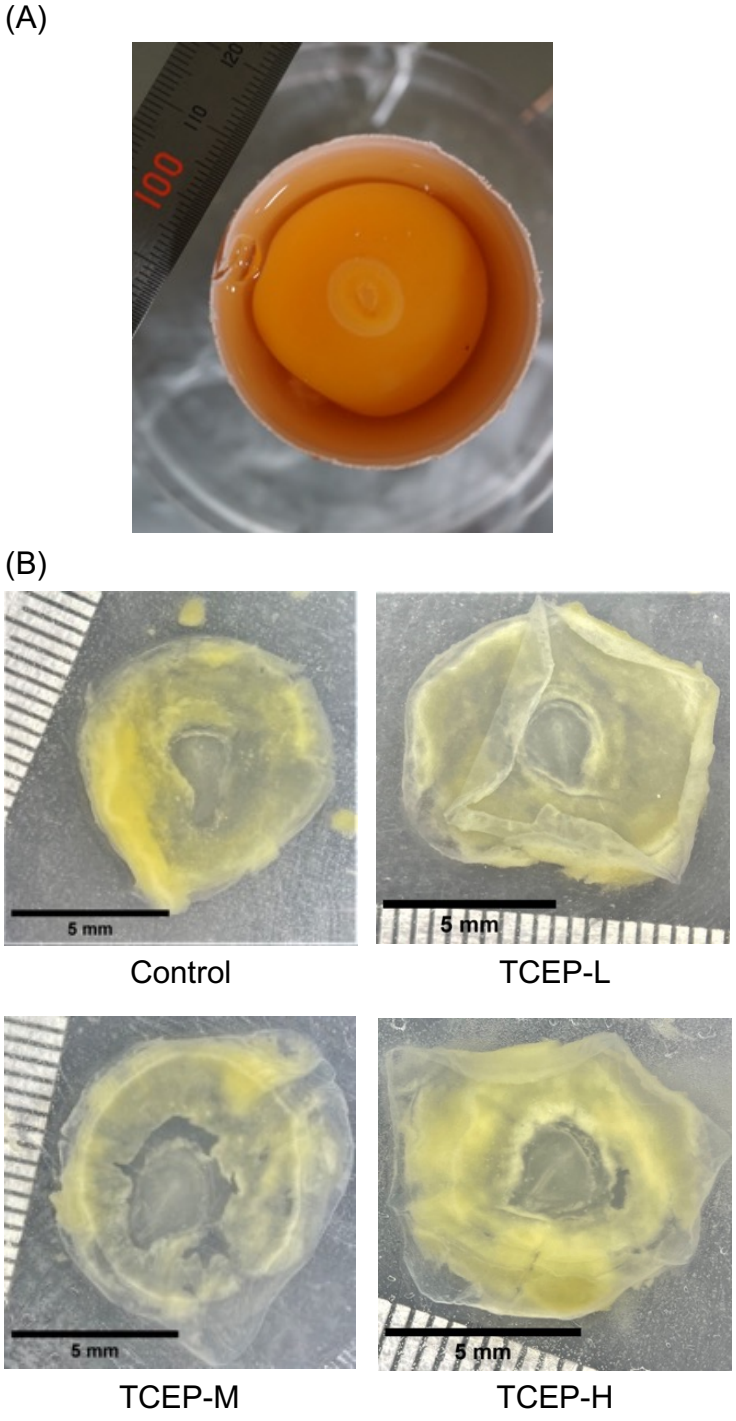

Figure. 4.3 The blastoderm and primitive streak at 18–19 hours of incubation. (A) The blastoderm on yolk before sampling. (B) Primitive streaks were collected in each treatment group—length: approximately 2 mm; width: approximately 0.1 mm.

Table. 4.1 List of primers and PCR conditions applied in this study

Symbol	Gene name	Forward primer	Reverse primer	Tm (°C)
SNAI2	Snail family transcriptional repressor 2	CCCTATCATACCGCAGCCAG	ACCGCTGTGATCTTTGGAGG	62
TBXT	T-box transcription factor T (Brachyury, T)	AGAAACAACTCACCAACAGCTT	CTCATGGGCAGCATAGTCGT	62
TBX6	T-box transcription factor 6	TCTTCACTTCTGTTACTGCCTACCA	TTGGCTCGTCCTTCCCTTCG	62
CDH1	Cadherin 1 (E-cadherin)	AGGACAAGGAGTCTAAGGTGT	GTGGGAGAAGAGGGTGTAGC	62
CDH2	Cadherin 2 (N-cadherin)	ACCTCTGCTCAATGTGAGGTTT	CTGTGAATGCTGGTTCAGGG	62
CDH3	Cadherin 3 (P-cadherin)	GGAGGCAGAAGAGGGATTGG	GCATGGGAGTAGAGGTGGT	62
FGF4	Fibroblast growth factor 4	GATCCACAGCGAGAACCGAT	GCACTCATCATTGAAATGGGTAGAT	62
FGF8	Fibroblast growth factor 8	GGGAAACTGATCGGCAAGAGTA	CGCCGTGTAGTTGTTCTCCA	62
FGFR1	Fibroblast growth factor receptor 1	ATCTTCACGTTGGGTGGTTCG	CGCATCATCATGTACAGCTCG	60
WNT3A	Wnt family member 3A	CGCCTCGGAAGAAAGGAAAGT	CCAATCGCCAAGGACCACCA	63
NOTCH1	Notch 1	GTATCCTATGTATGTGGTGGTGGC	AAGCATTTTTGAGGGGTTTCAGTC	62
BMP4	Bone morphogenetic protein 4	AAATCAGCCGTCATCCCCAG	GCTCTCCAGGTGCTCTTCAT	65
AKT1	AKT serine/threonine kinase 1	CCGGCTCCCTTTCTACAATCA	GGACCGCCTCCTAACCTTTG	62
GAPDH	glyceraldehyde-3-phosphate dehydrogenase	GTCGGAGTCAACGGAT	GGCCACCACTTGGACT	63

PCR was run with the following condition: one cycle of 10 min at 95°C; 40 cycles of 15 sec at 95°C, 1 min at Tm°C; and one cycle of 15 sec at 95°C, 1 min at 60°C, and 15 sec at 95°C

4.4 Results

4.4.1 Effects of TCEP exposure on the expression of genes

To examine whether TCEP exposure perturbed the EMT progress and mesodermal differentiation, we measured mRNA levels by qRT-PCR (Fig. 4.4). SNAI2 expression, a transcription factor in EMT was significantly decreased in all TCEP exposure groups (TCEP-L, $p < 0.01$; TCEP-M, $p < 0.01$; TCEP-H, $p < 0.001$). Gene expression levels of SNAI2 in the heart, the vitelline membrane containing extraembryonic blood vessels, and heart-removed embryonic bodies in 5-day-old chicken embryos were also analyzed (Fig. 4.5). SNAI2 mRNA levels in the heart showed a non-significant but TCEP-concentration-dependent decrease trend. In contrast, gene expression of SNAI2 in the vitelline membrane and embryonic body was unchanged in all TCEP-treated groups. TBXT, the mesoderm marker, was significantly decreased in TCEP-M and TCEP-H groups and was changed in a TCEP concentration-dependent manner (TCEP-M, $p < 0.05$; TCEP-H, $p < 0.001$). Gene expression of TBX6 was also significantly decreased in TCEP-L and TCEP-H groups (TCEP-L, $p < 0.05$; TCEP-H, $p < 0.001$). E-cadherin (CDH1) expression was significantly increased in TCEP-H ($p < 0.05$) and upregulated in a TCEP concentration-dependent manner ($p < 0.01$, Jonckheere-Terpstra test), while N-cadherin (CDH2) expression was significantly decreased in TCEP-H ($p < 0.05$) and downregulated in a TCEP concentration-dependent manner ($p < 0.01$, Jonckheere-Terpstra test). In P-cadherin (CDH3), mRNA levels were

not altered in TCEP-exposed groups compared to the control group, but there was a TCEP concentration-dependent increasing trend ($p < 0.05$, Jonckheere-Terpstra test). Among FGF signaling-related genes, FGF4 expression was significantly downregulated in all TCEP exposure groups (TCEP-L, $p < 0.05$; TCEP-M, $p < 0.01$; TCEP-H, $p < 0.01$). On the other hand, the gene expression levels of FGF8 and FGFR1 were unchanged by TCEP exposure. Gene expression of AKT1, which is involved in the FGF signaling process, was not significantly altered in the TCEP-exposed group but was slightly increased in a TCEP concentration-dependent manner ($p < 0.01$, Jonckheere-Terpstra test). WNT3A expression significantly increased in a TCEP exposure concentration-dependent manner ($p < 0.05$, Jonckheere-Terpstra test). However, MNP4 and NOTCH1 mRNA levels were not changed between treatment groups.

4.4.2 Correlation of expression levels among genes

We analyzed the correlation between the mRNA levels of each gene to examine the relationship between the differential expressed genes, and the results of those correlations are shown in Fig. 4.6. Interestingly, there was a significantly positive correlation between SNAI2 and TBXT in mRNA levels ($r = 0.96$). Another mesoderm marker, TBX6, showed a moderate positive correlation with SNAI2 ($r = 0.65$) and TBXT ($r = 0.69$). FGF4 had a very high positive correlation with SNAI2 ($r = 0.96$) and TBXT ($r = 0.94$) and a moderate correlation with TBX6 ($r = 0.53$). Among cadherins, E-cadherin only had a significant positive correlation with WNT3A ($r = 0.63$)

but not SNAI2. On the other hand, N-cadherin indicated a very strong positive correlation with SNAI2 (r = 0.93), TBXT (r = 0.93), and FGF4 (r = 0.92) and a moderate positive correlation with TBX6 (r = 0.65). P-cadherin showed a significant but not strong positive correlation with WNT3A and E-cadherin.

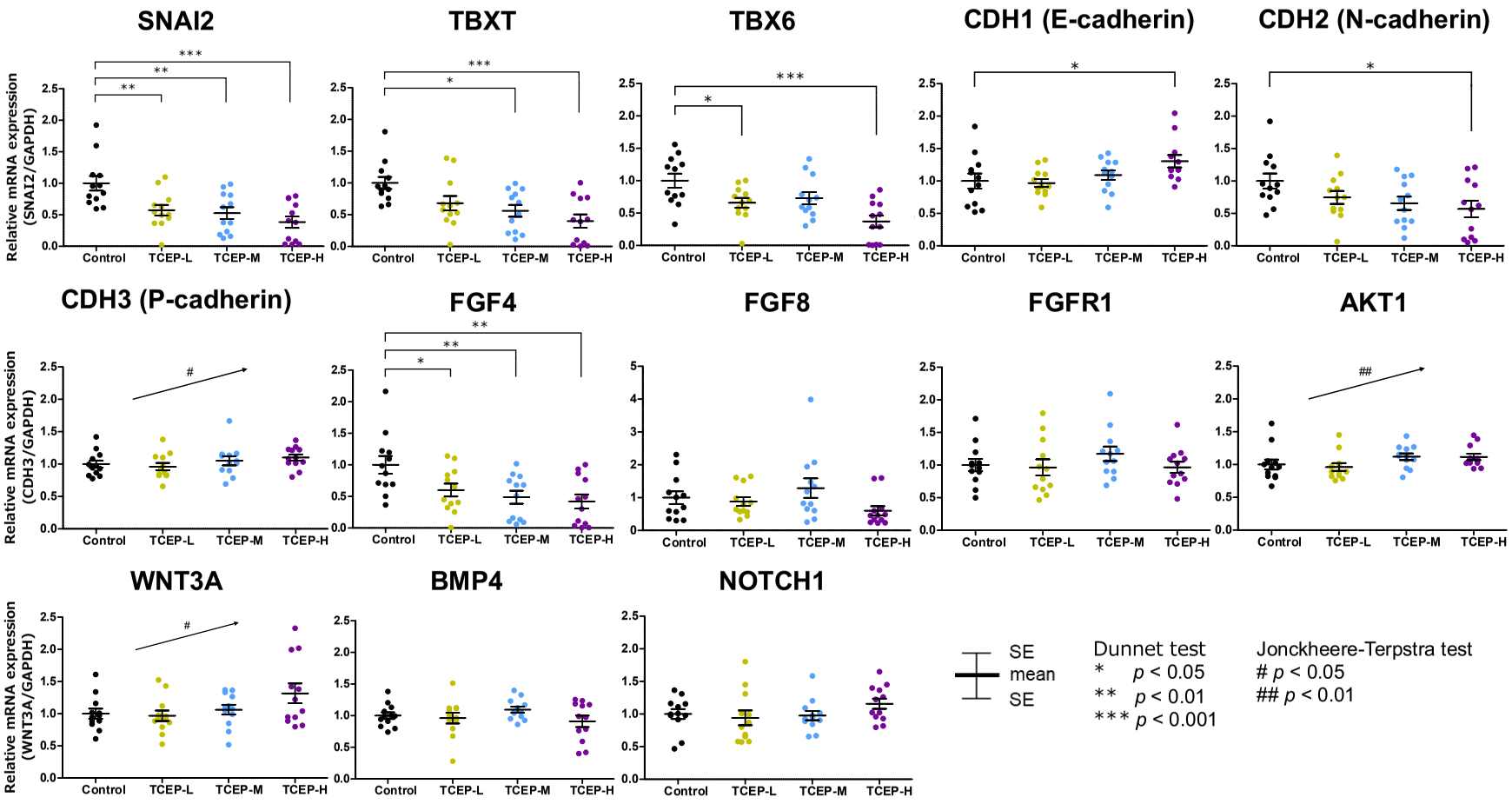

Figure. 4.4 Relative expression levels of epithelial-mesenchymal transition (EMT)- and mesoderm-related genes compared to the control group by qRT-PCR in chicken blastoderms at HH4 (n = 12/group). Data represent means ± standard error (SE). Asterisks indicate significant differences (*p < 0.05, **p < 0.01, ***p < 0.001) in each TCEP-exposed group compared with the control group by Dunnett's test. Hash symbols and arrows indicate that the mRNA level was altered dose-dependent (# p < 0.05, ## p < 0.01; Jonckheere-Terpstra test).

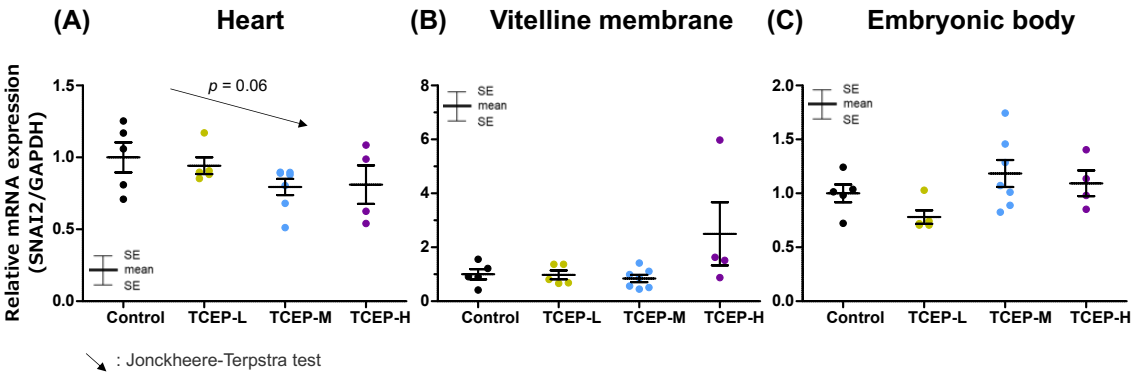

Figure. 4.5 Comparison of SNAI2 gene expression in heart, yolk membrane containing extraembryonic blood vessels, and heart-removed embryonic body in day five chicken embryos. Data represent means ± standard error (SE). The *p*-value upon the arrow indicates the result of the statistical trend test by the Jonckheere-Terpstra test.

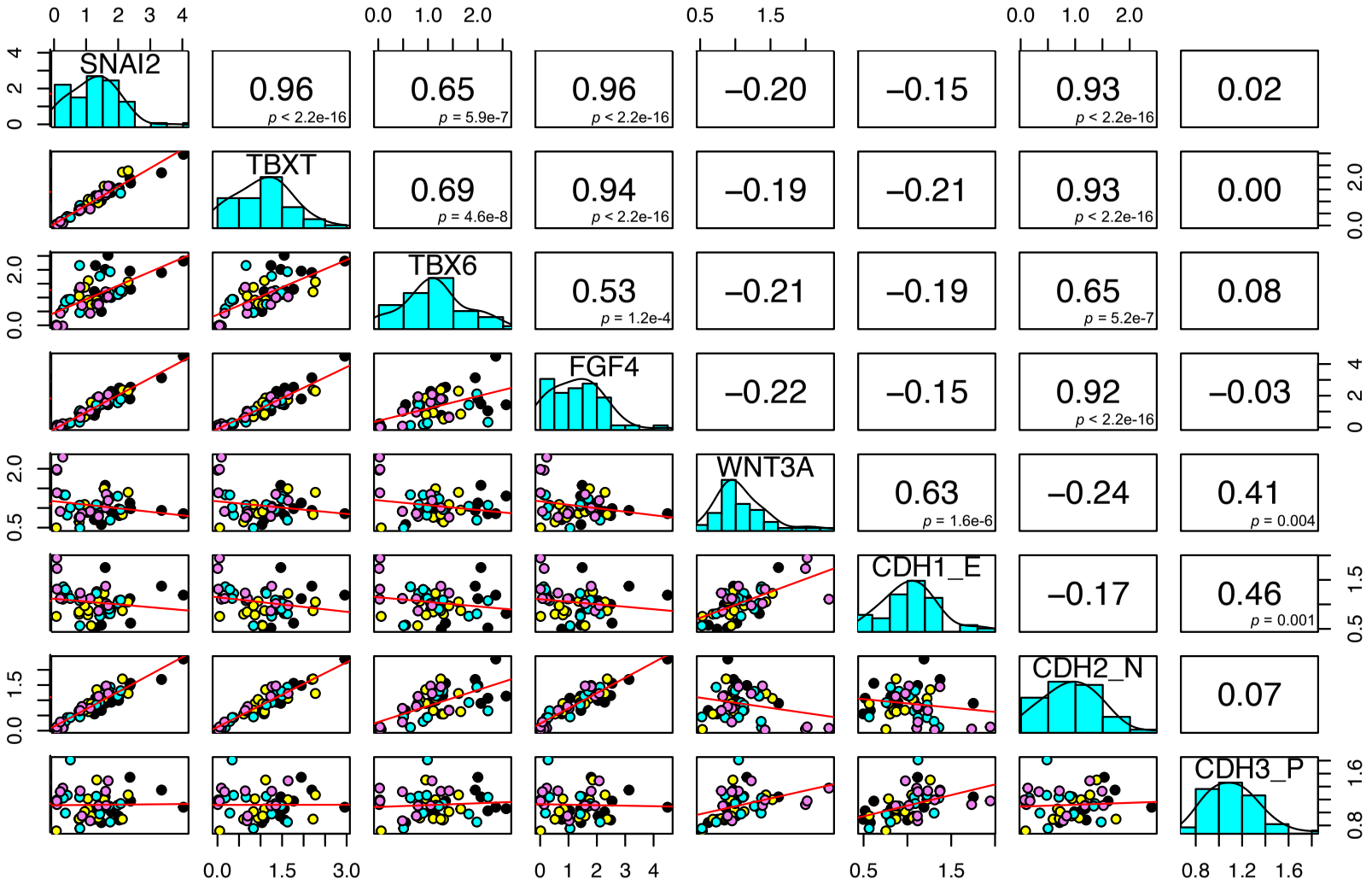

Figure. 4.6 Relationship between the mRNA level of EMT- and mesoderm-related genes in chicken blastoderms at HH4. The numbers indicate the respective correlation coefficients (Spearman's rank correlation coefficient). Control, TCEP-L, TCEP-M, and TCEP-H samples are shown as black, yellow, blue, and purple plots, respectively. The red line represents the regression line.

4.5 Discussion

The developmental toxicity of chlorinated organophosphate esters (Cl-OPEs), including TCEP, has been widely reported to be associated with thyroid hormone disturbance (Farhat et al., 2013; Wang et al., 2022, 2013). On the other hand, it has been reported that TCEP above 14,250 μg/L delays gastrulation in zebrafish embryos (Wu et al., 2017). However, the mechanism of TCEP toxicity on gastrulation is not clear. In a previous study, TDCIPP exposure to zebrafish embryos at the 2-cell stage (0.75 hpf) significantly reduced the expression of mesoderm development-related genes (tbx6l, tbx6, tbx16) and induced pericardial edema, heart looping defects, and reduced hemoglobin levels (Dasgupta et al., 2018). The authors in this previous study focused on BMP signaling as a cause of mesoderm development inhibition, but the expression of BMP-related factors was not altered by TDCIPP exposure. Therefore, the mechanism of action responsible for Cl-OPEs-induced inhibition of gastrulation and mesoderm development remains unknown. We found that TCEP exposure may significantly affect the EMT of chicken embryo hearts on day five by the cardiac transcriptome analysis.

To investigate whether TCEP exposure affects EMT during gastrulation of the chicken primitive streak, TCEP was administered, and changes in the expression of EMT and mesoderm-related genes in HH4 were examined. SNAI2 expression in HH4 chicken primitive streaks was significantly reduced in a TCEP concentration-dependent manner, while SNAI2 expression in the

vitelline membranes and embryonic bodies on day 5 of incubation was unchanged between TCEP exposure groups and the control group (Fig.4.4 and 4.5). Like the primitive streak, SNAI2-mediated EMT is triggered in the epicardium, the atrioventricular, and the outflow tract cardiac cushions during cardiac development (Niessen et al., 2008; Smith et al., 2011). SNAI2 showed a TCEP concentration-dependent decreasing trend in the heart on day 5, but it was a weaker gene expression change of SNAI2 at the primitive streak (Fig. 4.5). Thus, it is suggested that SNAI2 expression is most affected by TCEP exposure during gastrulation. In the study of Chapter I, TCEP exposure (250 and 500 nmol/g egg) already had lethal effects on chicken embryos by day 3 of incubation and arrested development in over 40% of individuals. Many individuals in the TCEP-H group that was dead at the time of observation on day 3 of incubation had stopped developing in the form of primitive streaks and had not developed into HH20–23 (day 3) chicken embryos (Fig. 4.7). It has been reported that the snail knockout mouse embryo (E7.5) is smaller than the wild type, are defective in mesoderm formation, maintain E-cadherin expression, and finally die during gastrulation (Carver et al., 2001). Therefore, TCEP may have lethal effects during gastrulation in chicken embryos by decreasing SNAI2 expression. EMT proceeds when transcription factors such as Snail1/2 bind to the promoter of E-cadherin and repress its transcription. EMT then causes epithelial cells to acquire a mesenchymal phenotype, such as cell migration, in which E-cadherin is not expressed (Batlle et al., 2000; Cano et al., 2000; Herranz et

al., 2008). N-cadherin is specifically expressed in mesenchymal cells in the chick primitive streak in contrast to E-cadherin. The loss of E-cadherin expression and gain of N-cadherin expression through EMT is called "Cadherin switching" (Dady et al., 2012; Maeda et al., 2005; Nakagawa and Takeichi, 1995; Wheelock et al., 2008). We found that TCEP-exposed groups had higher expression of E-cadherin and lower expression of N-cadherin than the control group (Fig. 4.4). These results suggest that the TCEP exposure decreases the SNAI2 expression, suppresses the cadherin switching, and inhibits EMT progression during gastrulation. Gene expression of P-cadherin was not significantly altered in TCEP exposure groups. P-cadherin has been reported to be repressed by SNAI2 in HH4 chicken embryos but is independent of gastrulation EMT (Acloque et al., 2017; Moly et al., 2016). It is suggested that E-cadherin and N-cadherin are particularly affected by TCEP in cadherins.

We analyzed the quantification of TBXT (T, Brachyury) and TBX6 gene expression, a mesoderm marker gene, to investigate whether TCEP decreased mesoderm cells with concomitant effects on EMT. As anticipated, TBXT and TBX6 expression was significantly reduced in a TCEP concentration-dependent manner (Fig. 4.4). Furthermore, the trends of SNAI2 and TBXT expression with TCEP exposure were remarkably similar (r = 0.96) (Fig. 4.5). SNAI2 and TBXT are strongly expressed in the same regions of the streak, axial mesoderm, and intermediate mesoderm in HH4 chicken embryos (Hardy et al., 2011). These results suggested that TCEP

exposure inhibits both EMT and mesoderm differentiation.

The EMT program is regulated by numerous signaling pathways, including FGF, Wnt, Notch, and TGF-β/BMP, and mesoderm induction is involved with FGF and Nodal/TGFβ signaling. (de Robertis and Kuroda, 2004; Heisenberg and Solnica-Krezel, 2008; Thiery et al., 2009; Yamashita et al., 2002; Yang and Weinberg, 2008). To determine the cause of TCEP inhibits EMT and mesoderm induction, we measured the expression levels of relevant genes in these signaling pathways. Among FGF signaling-related genes, HH4 chicken embryos express FGF4, FGF8, and FGFR1 around the primitive streak and in mesenchyme cells (Hardy et al., 2011). In a previous study, FGFR1-deficient mouse embryos were found to have suppressed Snail and TBXT (Brachyury) expression in the primitive streak (Ciruna and Rossant, 2001). TCEP exposure significantly reduced FGF4 expression while not altering FGF8, FGFR1, and AKT1 expression in HH4 chick embryos (Fig. 4.4). Notably, FGF4 mRNA levels were positively correlated with SNAI2 ($r = 0.96$) and TBXT ($r = 0.94$) mRNA levels (Fig. 4.5). FGF4 promotes up-regulation of the EMT transcription factors Snail, Slug, and Twist and down-regulation of E-cadherin in Human lung adenocarcinoma cell lines (Qi et al., 2016). It has been reported that FGF4 induces migratory mesoderm cells by expression Bra (TBXT) and Snai2 in the streak and the marginal zone of the chicken embryo. Therefore, it is suggested that decreased FGF4 expression induces delayed EMT due to decreased SNAI2 expression and inhibition of mesoderm cell differentiation due to

decreased TBXT expression.

WNT3A mRNA levels showed an increasing trend in a TCEP concentration-dependent manner (Fig. 4.4). Wnt3a is expressed in the superficial and middle layers of the primitive streak in the chicken (Baranski et al., 2000). And Wnt3a expression is associated with EMT and promotes colon cancer progression (Qi et al., 2014). In addition, Wnt3a regulates TBXT expression during paraxial mesoderm specification, and it has been reported that administration of FGF4 and Wnt3a into the subgerminal cavity of HH1 chick embryos artificially increases TBXT and Tbx6 expression more than administration of FGF4 alone. It has been demonstrated that E-cadherin can sequester free β-catenin to the cell membrane and prevent its association with LEF/TCF proteins, and E-cadherin expression could attenuate a Wnt signaling response (Ciruna and Rossant, 2001; Orsulic et al., 1999). Thus, WNT3A expression may have increased due to feedback regulation of TBXT downregulation.

BMP4 and NOTCH are a factor that promotes EMT via EMT transcription factor such as SNAI2 (Kar et al., 2019; Richter et al., 2014; Timmerman et al., 2004). However, the gene expression of BMP4 and NOTCH1 was not altered by TCEP exposure. These results suggest that the suppression of SNAI2 expression by TCEP exposure is independent of BMP4 and NOTCH1 expression.

In summary, TCEP exposure decreased gene expression of FGF4 and downregulated

expression of SNAI2, an EMT transcription factor, and the mesoderm markers TBXT and TBX6 during gastrulation in HH4 chick embryos (Fig. 4.8). E-cadherin expression was maintained, accompanying the downregulation of SNAI2. These gene expression results suggest that TCEP inhibits the EMT program during protoderm formation and delays mesoderm cell differentiation. These effects consequently may induce developmental delays and cardiovascular dysfunction in chicken embryos exposed to TCEP. The ventricular surface area to body weight ratio was also increased by disturbance of RTK signaling such as FGF and integrins.

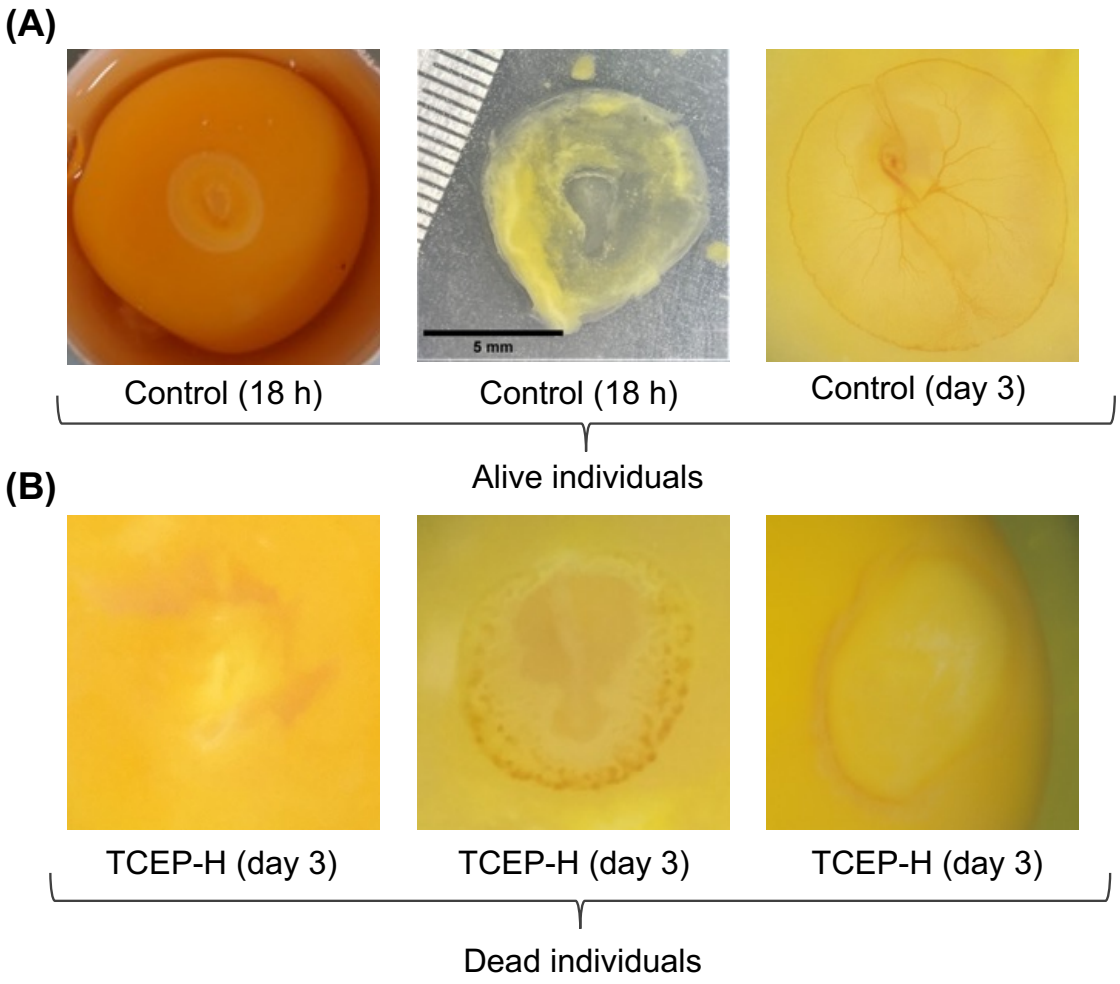

Figure. 4.7 Images of individuals in control and TCEP-H groups at observation. Parentheses indicate observed incubation times. (A) is surviving individuals in the control group. (B) indicates individuals in the TCEP-H group that had stopped developing at the time of observation on day 3.

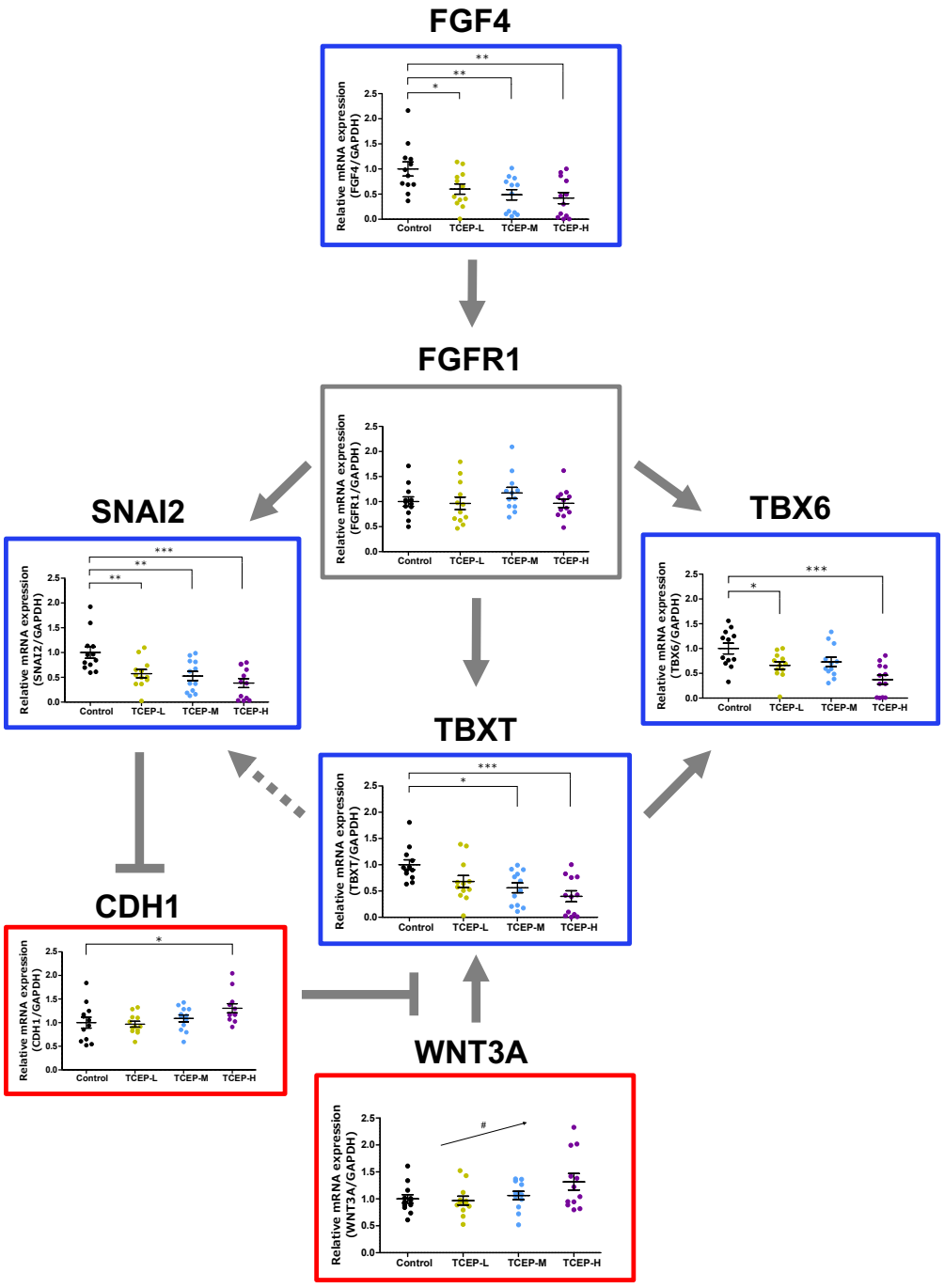

Figure. 4.8 A pathway of effects of TCEP exposure on the expression of EMT- and mesoderm-related genes during gastrulation in HH4 chicken embryos. Blue and red indicate genes down- and up-regulated by TCEP exposure, respectively.

Conclusion

In the present study, we combined a novel toxicity test using a shell-less incubation system with transcriptome analysis and elucidated the various phenotypic effects of TCEP exposure and its molecular mechanisms of action in chicken embryos. A summary of the chronological adverse outcome pathways (AOPs) for TCEP toxicity identified in this study is shown in Fig. 5.1. TCEP exposure decreased gene expression of FGF4, SNAI2, TBXT, and TBX6 on HH4 chicken embryos. Downregulation of SNAI2 is suggested to delay EMT progression and downregulation of TBXT and TBX6 to suppress mesoderm differentiation. These effects caused suppression of cardiac development, vascular formation, and embryonic development on day 5. At day 5 of incubation, TCEP resulted in decreased expression of Wnt signaling and NKX2-5, a cardiac developmental transcription factor, following delayed mesoderm differentiation. Downregulation of NKX2-5, CACNA1G, KCNE5, KCNJ2, and BIN1 induced heart rate reduction by reducing cardiac conduction function. In the extraembryonic blood vessels on day 5, expression of FGF2, which is important in the early formation of angiogenesis, was downregulated. FGF2 is expressed in mesoderm cells that differentiate into primordial endothelial cells (Marcelo et al., 2013). Therefore, the delay in mesoderm differentiation during HH4 may trigger the downregulation of FGF2. Decreased gene expression associated with VEGF signaling and PI3K-AKT signaling inhibited vasculogenesis and angiogenesis, and the formation of

extraembryonic vessels was suppressed. In addition, gene expression of myosin light chain and ryanodine receptors involved in myocardial contraction and calcium transport was reduced by TCEP exposure at day 9 of incubation. These effects may induce heart failure and cardiac arrest. Cardiac hypertrophy in the TCEP-exposed group on day nine was caused by possibly due to disturbance of the actin cytoskeleton and the microtubule on day 5. This is the first study to find that TCEP affects EMT and mesoderm differentiation in early chicken embryos (HH4), inducing growth retardation and neovascular system inhibition by combining *in situ* observations and omics analysis.

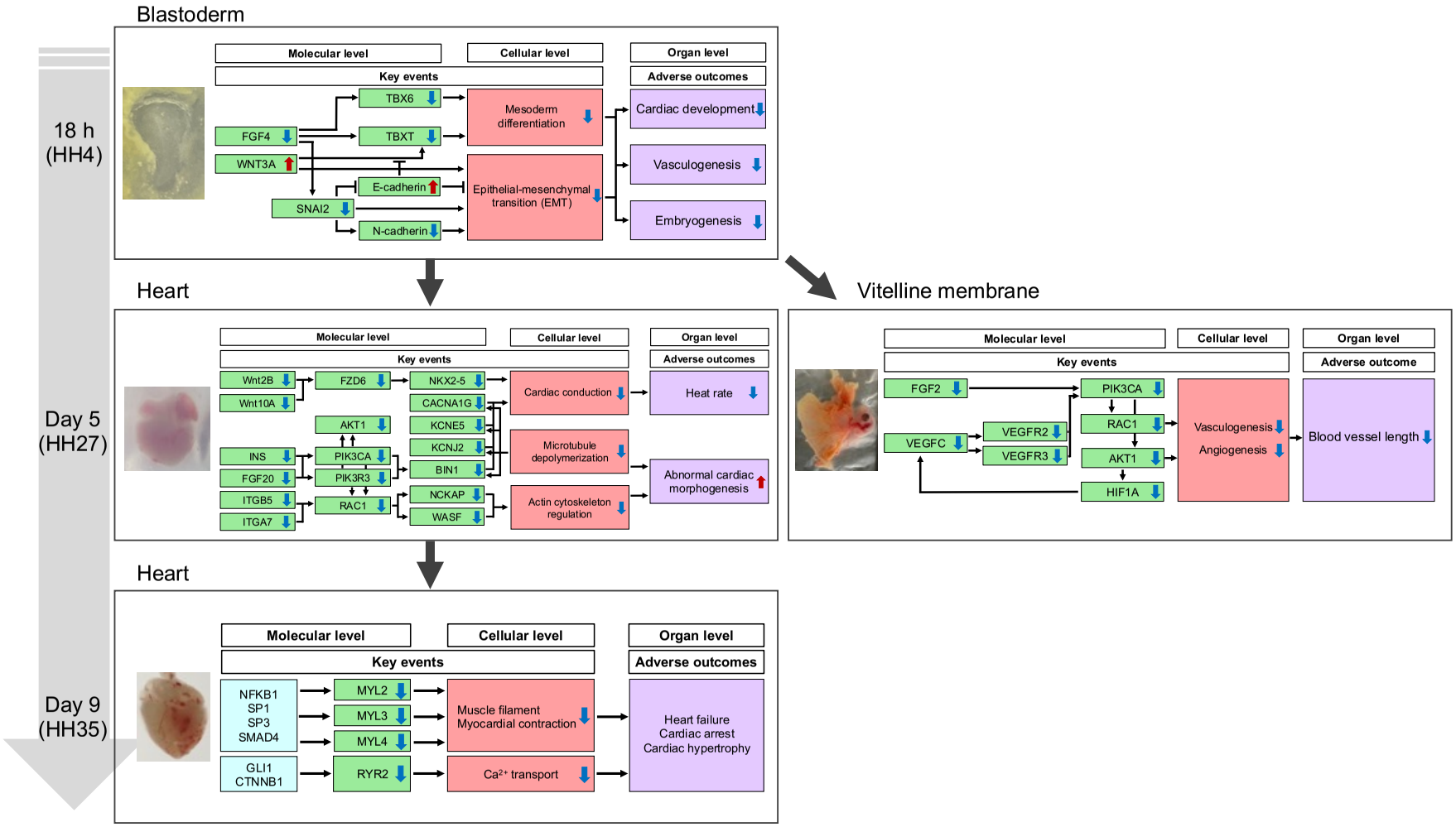

Figure. 5.1 Proposed chronological adverse outcome pathways (AOPs) for the toxicity of TCEP in HH4, HH27, and HH35 chicken embryos.

REFERENCES

Acloque, H., Adams, M.S., Fishwick, K., Bronner-Fraser, M., Nieto, M.A., 2009. Epithelial-mesenchymal transitions: The importance of changing cell state in development and disease. Journal of Clinical Investigation 119, 1438–1449. https://doi.org/10.1172/JCI38019

Acloque, H., Ocaña, O.H., Abad, D., Stern, C.D., Nieto, M.A., 2017. Snail2 and Zeb2 repress P-cadherin to define embryonic territories in the chick embryo. Development (Cambridge) 144, 649–656. https://doi.org/10.1242/dev.142562

Akazawa, H., Komuro, I., 2003. Roles of cardiac transcription factors in cardiac hypertrophy. Circ Res 92, 1079–1088. https://doi.org/10.1161/01.RES.0000072977.86706.23

Alzualde, A., Behl, M., Sipes, N.S., Hsieh, J.H., Alday, A., Tice, R.R., Paules, R.S., Muriana, A., Quevedo, C., 2018. Toxicity profiling of flame retardants in zebrafish embryos using a battery of assays for developmental toxicity, neurotoxicity, cardiotoxicity and hepatotoxicity toward human relevance. Neurotoxicol Teratol 70, 40–50. https://doi.org/10.1016/j.ntt.2018.10.002

Bacaloni, A., Cavaliere, C., Foglia, P., Nazzari, M., Samperi, R., Laganà, A., 2007. Liquid chromatography/tandem mass spectrometry determination of organophosphorus flame retardants and plasticizers in drinking and surface waters. Rapid Communications in Mass Spectrometry 21, 1123–1130. https://doi.org/10.1002/rcm.2937

Bajard, L., Melymuk, L., Blaha, L., 2019. Prioritization of hazards of novel flame retardants using the mechanistic toxicology information from ToxCast and Adverse Outcome Pathways. Environ Sci Eur. https://doi.org/10.1186/s12302-019-0195-z

Baranski, M., Berdougo, E., Sandler, J.S., Darnell, D.K., Burrus, L.W., 2000. The dynamic expression pattern of frzb-1 suggests multiple roles in chick development. Dev Biol 217, 25–41. https://doi.org/10.1006/dbio.1999.9516

Batlle, E., Sancho, E., Francí, C., Domínguez, D., Monfar, M., Baulida, J., García De Herreros, A., 2000. The transcription factor Snail is a repressor of E-cadherin gene expression in epithelial tumour cells. Nat Cell Biol 2, 84–89.

Bindea, G., Mlecnik, B., Hackl, H., Charoentong, P., Tosolini, M., Kirilovsky, A., Fridman, W.H., Pagès, F., Trajanoski, Z., Galon, J., 2009. ClueGO: A Cytoscape plug-in to decipher functionally grouped gene ontology and pathway annotation networks. Bioinformatics 25, 1091–1093. https://doi.org/10.1093/bioinformatics/btp101

Bo, L., Colin, D., 2011. RSEM: accurate transcript quantification from RNA-Seq data with or without a reference genome. BMC Bioinformatics 12, 1471–2105. https://doi.org/https://doi.org/10.1186/1471-2105-12-323

Bodié, K., Buck, W.R., Pieh, J., Liguori, M.J., Popp, A., 2016. Biomarker evaluation of skeletal muscle toxicity following clofibrate administration in rats. Experimental and Toxicologic Pathology 68, 289–299. https://doi.org/10.1016/j.etp.2016.03.001

Bolger, A.M., Lohse, M., Usadel, B., 2014. Trimmomatic: A flexible trimmer for Illumina sequence data. Bioinformatics 30, 2114–2120.

Borwornpinyo, S., Brake, J., Mozdziak, P.E., Petitte, J.N., 2005. Culture of Chicken Embryos in Surrogate Eggshells. Poult Sci 84, 1477–1482.

Brits, M., Brandsma, S.H., Rohwer, E.R., de Vos, J., Weiss, J.M., de Boer, J., 2019. Brominated and organophosphorus flame retardants in South African indoor dust and cat hair. Environmental Pollution 253, 120–129. https://doi.org/10.1016/j.envpol.2019.06.121

Brockmeier, E.K., Hodges, G., Hutchinson, T.H., Butler, E., Hecker, M., Tollefsen, K.E., Garcia-Reyero, N., Kille, P., Becker, D., Chipman, K., Colbourne, J., Collette, T.W., Cossins, A., Cronin, M., Graystock, P., Gutsell, S., Knapen, D., Katsiadaki, I., Lange, A., Marshall, S., Owen, S.F., Perkins, E.J., Plaistow, S., Schroeder, A., Taylor, D., Viant, M., Ankley, G., Falciani, F., 2017. The role of omics in the application of adverse outcome pathways for chemical risk assessment. Toxicological Sciences 158, 252–262. https://doi.org/10.1093/toxsci/kfx097

Caldwell, P.T., Thorne, P.A., Johnson, P.D., Boitano, S., Runyan, R.B., Selmin, O., 2008. Trichloroethylene disrupts cardiac gene expression and calcium homeostasis in rat myocytes. Toxicological Sciences 104, 135–143. https://doi.org/10.1093/toxsci/kfn078

Cambier, L., Plate, M., Sucov, H.M., Pashmforoush, M., 2014. Nkx2-5 regulates cardiac growth through modulation of Wnt signaling by R-spondin3. Development 141, 2959–2971. https://doi.org/10.1242/dev.103416

Cano, A., Pérez-Moreno, M.A., Rodrigo, I., Locascio, A., Blanco, M.J., del Barrio, M.G., Portillo, F., Angela Nieto, M., 2000. The transcription factor Snail controls epithelial-mesenchymal transitions by repressing E-cadherin expression. Nat Cell Biol 2.

Carver, E.A., Jiang, R., Lan, Y., Oram, K.F., Gridley, T., 2001. The Mouse Snail Gene Encodes a Key Regulator of the Epithelial-Mesenchymal Transition. Mol Cell Biol 21, 8184–8188. https://doi.org/10.1128/mcb.21.23.8184-8188.2001

Chang, A.N., Kamm, K.E., Stull, J.T., 2016. Role of myosin light chain phosphatase in cardiac physiology and pathophysiology. J Mol Cell Cardiol 101, 35–43. https://doi.org/10.1016/j.yjmcc.2016.10.004

Chapman, D.L., Agulnik, I., Hancock, S., Silver, L.M., Papaioannou, V.E., 1996. Tbx6, a Mouse T-Box Gene Implicated in Paraxial Mesoderm Formation at Gastrulation. Dev Biol 180, 534–542.

Chen, X., Zhao, X., Shi, Z., 2021. Organophosphorus flame retardants in breast milk from Beijing, China: Occurrence, nursing infant's exposure and risk assessment. Science of the Total Environment 771. https://doi.org/10.1016/j.scitotenv.2021.145404

Ciruna, B., Rossant, J., 2001. FGF Signaling Regulates Mesoderm Cell Fate Specification and Morphogenetic Movement at the Primitive Streak. Dev Cell 1, 37–49. https://doi.org/10.1016/s1534-5807(01)00017-x

Cloney, K., Franz-Odendaal, T.A., 2015. Optimized Ex-ovo Culturing of Chick Embryos to Advanced Stages of Development. Journal of Visualized Experiments. https://doi.org/10.3791/52129

Cockrum, C., Kaneshiro, K.R., Rechtsteiner, A., Tabuchi, T.M., Strome, S., 2020. A primer for generating and using transcriptome data and gene sets. Development 148. https://doi.org/10.1242/dev.193854

Coleman, C.M., 2008. Chicken embryo as a model for regenerative medicine. Birth Defects Res C Embryo Today. https://doi.org/10.1002/bdrc.20133

Dady, A., Blavet, C., Duband, J.L., 2012. Timing and kinetics of E- to N-cadherin switch during neurulation in the avian embryo. Developmental Dynamics 241, 1333–1349. https://doi.org/10.1002/dvdy.23813

Dasgupta, S., Cheng, V., Vliet, S.M.F., Mitchell, C.A., Volz, D.C., 2018. Tris(1,3-dichloro-2-propyl) Phosphate Exposure during the Early-Blastula Stage Alters the Normal Trajectory of Zebrafish Embryogenesis. Environ Sci Technol 52, 10820–10828. https://doi.org/10.1021/acs.est.8b03730

de Robertis, E.M., Kuroda, H., 2004. Dorsal-Ventral Patterning and Neural Induction in Xenopus Embryos. Annu Rev Cell Dev Biol 20, 285–308.

Diamanti-Kandarakis, E., Bourguignon, J.P., Giudice, L.C., Hauser, R., Prins, G.S., Soto, A.M., Zoeller, R.T., Gore, A.C., 2009. Endocrine-disrupting chemicals: An Endocrine Society scientific statement. Endocr Rev. https://doi.org/10.1210/er.2009-0002

Dibb, K.M., Clarke, J.D., Horn, M.A., Richards, M.A., Graham, H.K., Eisner, D.A., Trafford, A.W., 2009. Characterization of an extensive transverse tubular network in sheep atrial myocytes and its depletion in heart failure. Circ Heart Fail 2, 482–489. https://doi.org/10.1161/CIRCHEARTFAILURE.109.852228

Ding, J., Deng, T., Ye, X., Covaci, A., Liu, J., Yang, F., 2019. Urinary metabolites of organophosphate esters and implications for exposure pathways in adolescents from Eastern China. Science of the Total Environment 695. https://doi.org/10.1016/j.scitotenv.2019.133894

Ding, J., Xu, Z., Huang, W., Feng, L., Yang, F., 2016. Organophosphate ester flame retardants and plasticizers in human placenta in Eastern China. Science of the Total Environment 554–555, 211–217. https://doi.org/10.1016/j.scitotenv.2016.02.171

Dobin, A., Davis, C.A., Schlesinger, F., Drenkow, J., Zaleski, C., Jha, S., Batut, P., Chaisson, M., Gingeras, T.R., 2013. STAR: Ultrafast universal RNA-seq aligner. Bioinformatics 29, 15–21. https://doi.org/10.1093/bioinformatics/bts635

Dohle, D.S., Pasa, S.D., Gustmann, S., Laub, M., Wissler, J.H., Jennissen, H.P., Dünker, N., 2010. Chick ex ovo culture and ex ovo CAM assay: How it really works. Journal of Visualized Experiments. https://doi.org/10.3791/1620

Du, Z., Wang, G., Gao, S., Wang, Z., 2015. Aryl organophosphate flame retardants induced cardiotoxicity during zebrafish embryogenesis: By disturbing expression of the transcriptional regulators. Aquatic Toxicology 161, 25–32. https://doi.org/10.1016/j.aquatox.2015.01.027

EFRA, 2007. Frequently Asked Questions.

Eriksson, A., Cao, R., Roy, J., Tritsaris, K., Wahlestedt, C., Dissing, S., Thyberg, J., Cao, Y., 2003. Small GTP-binding protein Rac is an essential mediator of vascular endothelial growth factor-induced endothelial fenestrations and vascular permeability. Circulation 107, 1532–1538. https://doi.org/10.1161/01.CIR.0000055324.34758.32

Essaghir, A., Demoulin, J.B., 2012. A minimal connected network of transcription factors regulated in human tumors and its application to the quest for universal cancer biomarkers. PLoS One 7. https://doi.org/10.1371/journal.pone.0039666

Faloon, P., Arentson, E., Kazarov, A., Deng, C.X., Porcher, C., Orkin, S., Choi, K., 2000. Basic fibroblast growth factor positively regulates hematopoietic development. Development 127, 1931–1941.

Farhat, A., Crump, D., Chiu, S., Williams, K.L., Letcher, R.J., Gauthier, L.T., Kennedy, S.W., 2013. In ovo effects of two organophosphate flame Retardants-TCPP and TDCPP-on pipping success, development, mRNA expression, and thyroid hormone levels in chicken embryos. Toxicological Sciences 134, 92–102. https://doi.org/10.1093/toxsci/kft100

Fearnley, C.J., Llewelyn Roderick, H., Bootman, M.D., 2011. Calcium signaling in cardiac myocytes. Cold Spring Harb Perspect Biol 3. https://doi.org/10.1101/cshperspect.a004242

Fernie, K.J., Palace, V., Peters, L.E., Basu, N., Letcher, R.J., Karouna-Renier, N.K., Schultz, S.L., Lazarus, R.S., Rattner, B.A., 2015. Investigating Endocrine and Physiological Parameters of Captive American Kestrels Exposed by Diet to Selected Organophosphate

Flame Retardants. Environ Sci Technol 49, 7448–7455. https://doi.org/10.1021/acs.est.5b00857

Filatova, T.S., Abramochkin, D. v., Shiels, H.A., 2020. Warmer, faster, stronger: Ca2+ cycling in avian myocardium. Journal of Experimental Biology 223. https://doi.org/10.1242/jeb.228205

Fu, Jie, Fu, K., Chen, Y., Li, X., Ye, T., Gao, K., Pan, W., Zhang, A., Fu, Jianjie, 2021. Long-Range Transport, Trophic Transfer, and Ecological Risks of Organophosphate Esters in Remote Areas. Environ Sci Technol. https://doi.org/10.1021/acs.est.0c08822

Gbadamosi, M.R., Abdallah, M.A.E., Harrad, S., 2022. Organophosphate esters in UK diet; exposure and risk assessment. Science of the Total Environment 849. https://doi.org/10.1016/j.scitotenv.2022.158368

Gerthoffer, W.T., 2008. Migration of airway smooth muscle cells. Proc Am Thorac Soc 5, 97–105. https://doi.org/10.1513/pats.200704-051VS

Gerthoffer, W.T., 2007. Mechanisms of vascular smooth muscle cell migration. Circ Res 100, 607–621. https://doi.org/10.1161/01.RES.0000258492.96097.47

Greaves, A.K., Letcher, R.J., 2014. Comparative body compartment composition and in ovo transfer of organophosphate flame retardants in North American Great Lakes herring gulls. Environ Sci Technol 48, 7942–7950. https://doi.org/10.1021/es501334w

Guo, Jiahua, Ito, S., Nguyen, H.T., Yamamoto, K., Tanoue, R., Kunisue, T., Iwata, H., 2018. Effects of prenatal exposure to triclosan on the liver transcriptome in chicken embryos. Toxicol Appl Pharmacol 347, 23–32. https://doi.org/10.1016/j.taap.2018.03.026

Guo, J., Romanak, K., Westenbroek, S., Hites, R.A., Venier, M., 2017. Current-Use Flame Retardants in the Water of Lake Michigan Tributaries. Environ Sci Technol 51, 9960–9969. https://doi.org/10.1021/acs.est.7b01294

Guo, Jiehong, Simon, K., Romanak, K., Bowerman, W., Venier, M., 2018. Accumulation of flame retardants in paired eggs and plasma of bald eagles. Environmental Pollution 237, 499–507. https://doi.org/10.1016/j.envpol.2018.02.056

Hamada, T., Gangopadhyay, J.P., Mandl, A., Erhardt, P., Ikemoto, N., 2009. Defective regulation of the ryanodine receptor induces hypertrophy in cardiomyocytes. Biochem Biophys Res Commun 380, 493–497. https://doi.org/10.1016/j.bbrc.2009.01.152

Hamburger, V., Hamilton, H.L., 1992. A SERIES O F NORMAL STAGES IN THE DEVELOPMENT OF THE CHICK EMBRYO, DEVELOPMENTAL DYNAMICS.

Hao, Y., Zheng, S., Wang, P., Sun, H., Matsiko, J., Li, W., Li, Y., Zhang, Q., Jiang, G., 2021. Ecotoxicology of persistent organic pollutants in birds. Environ Sci Process Impacts. https://doi.org/10.1039/d0em00451k

Hardy, K.M., Yatskievych, T.A., Konieczka, J., Bobbs, A.S., Antin, P.B., 2011. FGF signalling through RAS/MAPK and PI3K pathways regulates cell movement and gene expression in the chicken primitive streak without affecting E-cadherin expression. BMC Dev Biol 11. https://doi.org/10.1186/1471-213X-11-20

Haugen, A.C., Schug, T.T., Collman, G., Heindel, J.J., 2018. Evolution of DOHaD : the impact of environmental health sciences 6, 55–64. https://doi.org/10.1017/S2040174414000580

Heisenberg, C.P., Solnica-Krezel, L., 2008. Back and forth between cell fate specification and movement during vertebrate gastrulation. Curr Opin Genet Dev 18, 311–316. https://doi.org/10.1016/j.gde.2008.07.011

Herranz, N., Pasini, D., Díaz, V.M., Francí, C., Gutierrez, A., Dave, N., Escrivà, M., Hernandez-Muñoz, I., di Croce, L., Helin, K., García de Herreros, A., Peiró, S., 2008. Polycomb Complex 2 Is Required for E-cadherin Repression by the Snail1 Transcription Factor . Mol Cell Biol 28, 4772–4781. https://doi.org/10.1128/mcb.00323-08

Hong, T., Yang, H., Zhang, S.S., Cho, H.C., Kalashnikova, M., Sun, B., Zhang, H., Bhargava, A., Grabe, M., Olgin, J., Gorelik, J., Marbán, E., Jan, L.Y., Shaw, R.M., 2014. Cardiac BIN1 folds T-tubule membrane, controlling ion flux and limiting arrhythmia. Nat Med 20, 624–632. https://doi.org/10.1038/nm.3543

Hong, T.T., Shaw, R.M., 2017. Cardiac t-tubule microanatomy and function. Physiol Rev 97, 227–252. https://doi.org/10.1152/physrev.00037.2015

Hong, T.T., Smyth, J.W., Gao, D., Chu, K.Y., Vogan, J.M., Fong, T.S., Jensen, B.C., Colecraft, H.M., Shaw, R.M., 2010. BIN1 localizes the L-type calcium channel to cardiac T-tubules. PLoS Biol 8. https://doi.org/10.1371/journal.pbio.1000312

Hou, M., Shi, Y., Jin, Q., Cai, Y., 2020. Organophosphate esters and their metabolites in paired human whole blood, serum, and urine as biomarkers of exposure. Environ Int 139. https://doi.org/10.1016/j.envint.2020.105698

Hou, R., Xu, Y., Wang, Z., 2016. Review of OPFRs in animals and humans: Absorption, bioaccumulation, metabolism, and internal exposure research. Chemosphere 153, 78–90. https://doi.org/10.1016/j.chemosphere.2016.03.003

Huang, C., Sheikh, F., Hollander, M., Cai, C., Becker, D., Chu, P.H., Evans, S., Chen, J., 2003. Embryonic atrial function is essential for mouse embryogenesis, cardiac morphogenesis and angiogenesis. Development 130, 6111–6119. https://doi.org/10.1242/dev.00831

Huang, D.W., Sherman, B.T., Lempicki, R.A., 2009. Bioinformatics enrichment tools: Paths toward the comprehensive functional analysis of large gene lists. Nucleic Acids Res 37, 1–13. https://doi.org/10.1093/nar/gkn923

Huang, Q., Wei, L., Bignert, A., Ye, H., Huang, F., Qiu, Y., Bergman, Å., 2019. Organophosphate flame retardants in heron eggs from upper Yangtze River basin, southwest China. Chemosphere 236. https://doi.org/10.1016/j.chemosphere.2019.07.058

Huang, W., Arai, F., Kawahara, T., 2015. Egg-in-cube: Design and fabrication of a novel artificial eggshell with functionalized surface. PLoS One 10. https://doi.org/10.1371/journal.pone.0118624

Isales, G.M., Hipszer, R.A., Raftery, T.D., Chen, A., Stapleton, H.M., Volz, D.C., 2015. Triphenyl phosphate-induced developmental toxicity in zebrafish : Potential role of the retinoic acid receptor. Aquatic Toxicology 161, 221–230. https://doi.org/10.1016/j.aquatox.2015.02.009

Itasaki, N., Nakamura, H., Yasuda, M., 1989. Anatomy and Embryology Changes in the arrangement of actin bundles during heart looping in the chick embryo. Anat Embryol

(Berl) 180, 413–420.

Iyer, N. v, Kotch, L.E., Agani, F., Leung, S.W., Laughner, E., Wenger, R.H., Gassmann, M., Gearhart, J.D., Lawler, A.M., Yu, A.Y., Semenza, G.L., 1998. Cellular and developmental control of O 2 homeostasis by hypoxia-inducible factor 1.

J. Bogue, Y., 1932. THE HEART RATE OF THE DEVELOPING CHICK. J Exp Biol 9, 351–358. https://doi.org/10.1242/jeb.9.4.351

Kanda, K., Ito, S., Koh, D.H., Kim, E.Y., Iwata, H., 2021. Effects of tris(2-chloroethyl) phosphate exposure on chicken embryos in a shell-less incubation system. Ecotoxicol Environ Saf 207. https://doi.org/10.1016/j.ecoenv.2020.111263

Kanehisa, M., Goto, S., Sato, Y., Furumichi, M., Tanabe, M., 2012. KEGG for integration and interpretation of large-scale molecular data sets. Nucleic Acids Res 40. https://doi.org/10.1093/nar/gkr988

Kar, R., Jha, N.K., Jha, S.K., Sharma, A., Dholpuria, S., Asthana, N., Chaurasiya, K., Singh, V.K., Burgee, S., Nand, P., 2019. A “NOTCH” deeper into the epithelial-to-mesenchymal transition (EMT) program in breast cancer. Genes (Basel) 10. https://doi.org/10.3390/genes10120961

Karaman, S., Leppänen, V.M., Alitalo, K., 2018. Vascular endothelial growth factor signaling in development and disease. Development 145. https://doi.org/10.1242/dev.151019

Kerric, A., Okeme, J., Jantunen, L., Giroux, J.F., Diamond, M.L., Verreault, J., 2021. Spatial and temporal variations of halogenated flame retardants and organophosphate esters in landfill air: Potential linkages with gull exposure. Environmental Pollution 271. https://doi.org/10.1016/j.envpol.2020.116396

Khan, M.U., Li, J., Zhang, G., Malik, R.N., 2016. First insight into the levels and distribution of flame retardants in potable water in Pakistan: An underestimated problem with an associated health risk diagnosis. Science of the Total Environment 565, 346–359. https://doi.org/10.1016/j.scitotenv.2016.04.173

Kim, J.W., Isobe, T., Chang, K.H., Amano, A., Maneja, R.H., Zamora, P.B., Siringan, F.P.,

Tanabe, S., 2011. Levels and distribution of organophosphorus flame retardants and plasticizers in fishes from Manila Bay, the Philippines. Environmental Pollution 159, 3653–3659. https://doi.org/10.1016/j.envpol.2011.07.020

Kim, J.W., Isobe, T., Muto, M., Tue, N.M., Katsura, K., Malarvannan, G., Sudaryanto, A., Chang, K.H., Prudente, M., Viet, P.H., Takahashi, S., Tanabe, S., 2014. Organophosphorus flame retardants (PFRs) in human breast milk from several Asian countries. Chemosphere 116, 91–97. https://doi.org/10.1016/j.chemosphere.2014.02.033

Klutstein, M., Nejman, D., Greenfield, R., Cedar, H., 2016. DNA methylation in cancer and aging. Cancer Res. https://doi.org/10.1158/0008-5472.CAN-15-3278

Kölsch, V., Charest, P.G., Firtel, R.A., 2008. The regulation of cell motility and chemotaxis by phospholipid signaling. J Cell Sci 121, 551–559. https://doi.org/10.1242/jcs.023333

Laughner, E., Taghavi, P., Chiles, K., Mahon, P.C., Semenza, G.L., 2001. HER2 (neu) Signaling Increases the Rate of Hypoxia-Inducible Factor 1α (HIF-1α) Synthesis: Novel Mechanism for HIF-1-Mediated Vascular Endothelial Growth Factor Expression. Mol Cell Biol 21, 3995–4004. https://doi.org/10.1128/mcb.21.12.3995-4004.2001

Lee, J.S., Morita, Y., Kawai, Y.K., Covaci, A., Kubota, A., 2020. Developmental circulatory failure caused by metabolites of organophosphorus flame retardants in zebrafish, Danio rerio. Chemosphere 246, 125738. https://doi.org/10.1016/j.chemosphere.2019.125738

Li, X., Xiong, X., Yi, C., 2016. Epitranscriptome sequencing technologies: Decoding RNA modifications. Nat Methods. https://doi.org/10.1038/nmeth.4110

Linask, K.K., VanAuker, M., 2007. A role for the cytoskeleton in heart looping. ScientificWorldJournal 7, 280–298. https://doi.org/10.1100/tsw.2007.87

Liu, C., Zu, J., Baskar, V., Wernery, U., Chang, I.K., 2012. Culture of chicken embryo in interspecific surrogate egg white. Poult Sci 91, 2866–2871. https://doi.org/10.3382/ps.2012-02403

Liu, X., Ji, K., Choi, K., 2012. Endocrine disruption potentials of organophosphate flame retardants and related mechanisms in H295R and MVLN cell lines and in zebrafish.

Aquatic Toxicology 114–115, 173–181. https://doi.org/10.1016/j.aquatox.2012.02.019

Liu, Y., Beyer, A., Aebersold, R., 2016. On the Dependency of Cellular Protein Levels on mRNA Abundance. Cell. https://doi.org/10.1016/j.cell.2016.03.014

Liu, Z., Li, T., Liu, Y., Jia, Z., Li, Y., Zhang, C., Chen, P., Ma, K., Affara, N., Zhou, C., 2009. WNT signaling promotes Nkx2.5 expression and early cardiomyogenesis via downregulation of Hdac1. Biochim Biophys Acta Mol Cell Res 1793, 300–311. https://doi.org/10.1016/j.bbamcr.2008.08.013

Lyons, I., Parsons, L.M., Hartley, L., Li, R., Andrews, J.E., Robb, L., Harvey, R.P., Walter, T., Hall, E., 1995. Myogenic and morpho.genetic defects in the heart tubes of murlne embryos lacking the homeo box gene Nkx2-5. Genes Dev 9, 1654–1666.

Maeda, M., Johnson, K.R., Wheelock, M.J., 2005. Cadherin switching: Essential for behavioral but not morphological changes during an epithelium-to-mesenchyme transition. J Cell Sci 118, 873–887. https://doi.org/10.1242/jcs.01634

Maier, T., Güell, M., Serrano, L., 2009. Correlation of mRNA and protein in complex biological samples. FEBS Lett. https://doi.org/10.1016/j.febslet.2009.10.036

Mangoni, M.E., Traboulsie, A., Leoni, A.L., Couette, B., Marger, L., le Quang, K., Kupfer, E., Cohen-Solal, A., Vilar, J., Shin, H.S., Escande, D., Charpentier, F., Nargeot, J., Lory, P., 2006. Bradycardia and slowing of the atrioventricular conduction in mice lacking CaV3.1/α1G T-type calcium channels. Circ Res 98, 1422–1430. https://doi.org/10.1161/01.RES.0000225862.14314.49

Marcelo, K.L., Goldie, L.C., Hirschi, K.K., 2013. Regulation of endothelial cell differentiation and specification. Circ Res. https://doi.org/10.1161/CIRCRESAHA.113.300506

Marklund, A., Andersson, B., Haglund, P., 2003. Screening of organophosphorus compounds and their distribution in various indoor environments. Chemosphere 53, 1137–1146. https://doi.org/10.1016/S0045-6535(03)00666-0

Marks, A.R., 2013. Calcium cycling proteins and heart failure: Mechanisms and therapeutics. Journal of Clinical Investigation. https://doi.org/10.1172/JCI62834

Martin, M., 2011. Cutadapt removes adapter sequences from high-throughput sequencing reads. EMBnet J 17, 10–12. https://doi.org/https://doi.org/10.14806/ej.17.1.200

Martinsen, B.J., 2005. Reference Guide to the Stages of Chick Heart Embryology 1217–1237. https://doi.org/10.1002/dvdy.20468

Marziano, C., Genet, G., Hirschi, K.K., 2021. Vascular endothelial cell specification in health and disease. Angiogenesis 24, 213–236. https://doi.org/10.1007/s10456-021-09785-7

Melincovici, C.S., Boşca, A.B., Şuşman, S., Mărginean, M., Mihu, C., Istrate, M., Moldovan, I.M., Roman, A.L., Mihu, C.M., 2018. Vascular endothelial growth factor (VEGF) – key factor in normal and pathological angiogenesis. Romanian Journal of Morphology and Embryology 59, 455–467.

Meyer, J., Bester, K., 2004. Organophosphate flame retardants and plasticisers in wastewater treatment plants. Journal of Environmental Monitoring 6, 599–605. https://doi.org/10.1039/b403206c

Mohr, A.M., Mott, J.L., 2015. Overview of microRNA biology. Semin Liver Dis. https://doi.org/10.1055/s-0034-1397344

Moly, P.K., Cooley, J.R., Zeltzer, S.L., Yatskievych, T.A., Antin, P.B., 2016. Gastrulation EMT is independent of P-cadherin downregulation. PLoS One 11. https://doi.org/10.1371/journal.pone.0153591

Monaghan, R.M., Page, D.J., Ostergaard, P., Keavney, B.D., 2021. The physiological and pathological functions of VEGFR3 in cardiac and lymphatic development and related diseases. Cardiovasc Res 117, 1877–1890. https://doi.org/10.1093/cvr/cvaa291

Monclús, L., Lopez-Bejar, M., de la Puente, J., Covaci, A., Jaspers, V.L.B., 2018. First evaluation of the use of down feathers for monitoring persistent organic pollutants and organophosphate ester flame retardants: A pilot study using nestlings of the endangered cinereous vulture (Aegypius monachus). Environmental Pollution 238, 413–420. https://doi.org/10.1016/j.envpol.2018.03.065

Monclús, L., Løseth, M.E., Dahlberg Persson, M.J., Eulaers, I., Kleven, O., Covaci, A., Benskin, J.P., Awad, R., Zubrod, J.P., Schulz, R., Wabakken, P., Heggøy, O., Øien, I.J., Steinsvåg, M.J., Jaspers, V.L.B., Nygård, T., 2022. Legacy and emerging organohalogenated compounds in feathers of Eurasian eagle-owls (Bubo bubo) in Norway: Spatiotemporal variations and associations with dietary proxies (δ13C and δ15N). Environ Res 204. https://doi.org/10.1016/j.envres.2021.112372

Nakagawa, S., Takeichi, M., 1995. Neural crest cell-cell adhesion controlled by sequential and subpopulation-specific expression of novel cadherins. Development 121, 1321–1332.

Nakane, Y., Tsudzuki, M., 1999. Development of the skeleton in Japanese quail embryos. Dev Growth Differ 41, 523–534. https://doi.org/10.1046/j.1440-169x.1999.00454.x

Nakaya, Y., Sheng, G., 2009. An amicable separation: Chick's way of doing EMT. Cell Adh Migr. https://doi.org/10.4161/cam.3.2.7373

Nakaya, Y., Sheng, G., 2008. Epithelial to mesenchymal transition during gastrulation: An embryological view. Dev Growth Differ. https://doi.org/10.1111/j.1440-169X.2008.01070.x

Niessen, K., Fu, Y.X., Chang, L., Hoodless, P.A., McFadden, D., Karsan, A., 2008. Slug is a direct Notch target required for initiation of cardiac cushion cellularization. Journal of Cell Biology 182, 315–325. https://doi.org/10.1083/jcb.200710067

Nowak-Sliwinska, P., Segura, T., Iruela-Arispe, M.L., 2014. The chicken chorioallantoic membrane model in biology, medicine and bioengineering. Angiogenesis. https://doi.org/10.1007/s10456-014-9440-7

Oda, T., Yano, M., Yamamoto, T., Tokuhisa, T., Okuda, S., Doi, M., Ohkusa, T., Ikeda, Y., Kobayashi, S., Ikemoto, N., Matsuzaki, M., 2005. Defective regulation of interdomain interactions within the ryanodine receptor plays a key role in the pathogenesis of heart failure. Circulation 111, 3400–3410. https://doi.org/10.1161/CIRCULATIONAHA.104.507921

OECD, 2016. Avian Acute Oral Toxicity Test. Test Guideline No. 223. Guideline for the testing of Chemicals 1–15.

Orsulic, S., Huber, O., Aberle, H., Arnold, S., Kemler, R., 1999. E-cadherin binding prevents beta-catenin nuclear localization and beta-catenin-LEF-1-mediated transactivation. J Cell Sci 112, 1237–1245.

Pashmforoush, M., Lu, J.T., Chen, H., St Amand, T., Kondo, R., Pradervand, S., Evans, S.M., Clark, B., Feramisco, J.R., Giles, W., Yen Ho, S., Woodrow Benson, D., 2004. Nkx2-5 Pathways and Congenital Heart Disease: Loss of Ventricular Myocyte Lineage Specification Leads to Progressive Cardiomyopathy and Complete Heart Block. Cell 117, 373–386.

Peden-Adams, M.M., Stuckey, J.E., Gaworecki, K.M., Berger-Ritchie, J., Bryant, K., Jodice, P.G., Scott, T.R., Ferrario, J.B., Guan, B., Vigo, C., Boone, J.S., McGuinn, W.D., DeWitt, J.C., Keil, D.E., Keil, D.E., 2009. Developmental toxicity in white leghorn chickens following in ovo exposure to perfluorooctane sulfonate (PFOS). Reproductive Toxicology 27, 307–318. https://doi.org/10.1016/j.reprotox.2008.10.009

Peng, X., Fan, S., Tan, J., Zeng, Z., Su, M., Zhang, Y., Yang, M., Xia, L., Fan, X., Cai, W., Tang, W.H., 2020. Wnt2bb Induces Cardiomyocyte Proliferation in Zebrafish Hearts via the jnk1/c-jun/creb1 Pathway. Front Cell Dev Biol 8. https://doi.org/10.3389/fcell.2020.00323

Perry, M.M., 1988. A complete culture system for the chick embryo. Nature 331, 70–72. https://doi.org/10.1038/331070a0

Pink, D.B.S., Schulte, W., Parseghian, M.H., Zijlstra, A., Lewis, J.D., 2012. Real-time visualization and quantitation of vascular permeability in vivo: Implications for drug delivery. PLoS One 7. https://doi.org/10.1371/journal.pone.0033760

POPRC, 2015. Report of the Persistent Organic Pollutants Review Committee on the work of its eleventh meeting.

Qi, L., Song, W., Li, L., Cao, L., Yu, Y., Song, C., Wang, Y., Zhang, F., Li, Y., Zhang, B., Cao, W., 2016. FGF4 induces epithelial-mesenchymal transition by inducing store-operated calcium entry in lung adenocarcinoma. Oncotarget 7, 74015–74030.

Qi, L., Sun, B., Liu, Z., Cheng, R., Li, Y., Zhao, X., 2014. Wnt3a expression is associated with epithelial-mesenchymal transition and promotes colon cancer progression. Journal of

Experimental and Clinical Cancer Research 33. https://doi.org/10.1186/s13046-014-0107-4

Quijada, P., Trembley, M.A., Small, E.M., 2020. The Role of the Epicardium during Heart Development and Repair. Circ Res. https://doi.org/10.1161/CIRCRESAHA.119.315857

Rauert, C., Schuster, J.K., Eng, A., Harner, T., 2018. Global Atmospheric Concentrations of Brominated and Chlorinated Flame Retardants and Organophosphate Esters. Environ Sci Technol 52, 2777–2789. https://doi.org/10.1021/acs.est.7b06239

Reemtsma, T., García-López, M., Rodríguez, I., Quintana, J.B., Rodil, R., 2008. Organophosphorus flame retardants and plasticizers in water and air I. Occurrence and fate. TrAC - Trends in Analytical Chemistry 27, 727–737. https://doi.org/10.1016/j.trac.2008.07.002

Ribatti, D., 2014. The chick embryo chorioallantoic membrane as a model for tumor biology. Exp Cell Res. https://doi.org/10.1016/j.yexcr.2014.06.010

Richter, A., Valdimarsdottir, L., Hrafnkelsdottir, H.E., Runarsson, J.F., Omarsdottir, A.R., Oostwaard, D.W. van, Mummery, C., Valdimarsdottir, G., 2014. BMP4 promotes EMT and mesodermal commitment in human embryonic stem cells via SLUG and MSX2. Stem Cells 32, 636–648. https://doi.org/10.1002/stem.1592

Risau, W., 1997. Mechanisms of angiogenesis. Nature 386, 671–674.

Risau, W., Sariola, H., Zerwes, H.-G., Sasse, J., Ekblom, P., Kemler, R., Doetschman, T., 1988. Vasculogenesis and angiogenesis in embryonic-stem-cell-derived embryoid bodies. Development 102, 471–478.

Robinson, M.D., McCarthy, D.J., Smyth, G.K., 2010. edgeR: A Bioconductor package for differential expression analysis of digital gene expression data. Bioinformatics 26, 139–140. https://doi.org/10.1093/bioinformatics/btp616

Rodil, R., Quintana, J.B., Concha-Graña, E., López-Mahía, P., Muniategui-Lorenzo, S., Prada-Rodríguez, D., 2012. Emerging pollutants in sewage, surface and drinking water in Galicia (NW Spain). Chemosphere 86, 1040–1049.

https://doi.org/10.1016/j.chemosphere.2011.11.053

Saini, A., Harner, T., Chinnadhurai, S., Schuster, J.K., Yates, A., Sweetman, A., Aristizabal-Zuluaga, B.H., Jiménez, B., Manzano, C.A., Gaga, E.O., Stevenson, G., Falandysz, J., Ma, J., Miglioranza, K.S.B., Kannan, K., Tominaga, M., Jariyasopit, N., Rojas, N.Y., Amador-Muñoz, O., Sinha, R., Alani, R., Suresh, R., Nishino, T., Shoeib, T., 2020. GAPS-megacities: A new global platform for investigating persistent organic pollutants and chemicals of emerging concern in urban air. Environmental Pollution 267. https://doi.org/10.1016/j.envpol.2020.115416

Sampurna, B.P., Audira, G., Juniardi, S., Lai, Y.H., Hsiao, C. der, 2018. A simple ImageJ-based method to measure cardiac rhythm in zebrafish embryos. Inventions 3, 1–11. https://doi.org/10.3390/inventions3020021

Schug, T.T., Janesick, A., Blumberg, B., Heindel, J.J., 2011. Endocrine disrupting chemicals and disease susceptibility. Journal of Steroid Biochemistry and Molecular Biology 127, 204–215. https://doi.org/10.1016/j.jsbmb.2011.08.007

Shaw, R.M., Fay, A.J., Puthenveedu, M.A., von Zastrow, M., Jan, Y.N., Jan, L.Y., 2007. Microtubule Plus-End-Tracking Proteins Target Gap Junctions Directly from the Cell Interior to Adherens Junctions. Cell 128, 547–560. https://doi.org/10.1016/j.cell.2006.12.037

Sheikh, F., Lyon, R.C., Chen, J., 2014. Getting the skinny on thick filament regulation in cardiac muscle biology and disease. Trends Cardiovasc Med. https://doi.org/10.1016/j.tcm.2013.07.004

Sheng, G., 2010. Primitive and definitive erythropoiesis in the yolk sac: A bird's eye view. International Journal of Developmental Biology 54, 1033–1043. https://doi.org/10.1387/ijdb.103105gs

Shibuya, M., Claesson-Welsh, L., 2006. Signal transduction by VEGF receptors in regulation of angiogenesis and lymphangiogenesis. Exp Cell Res 312, 549–560. https://doi.org/10.1016/j.yexcr.2005.11.012

Shiels, H.A., Galli, G.L.J., 2014. The sarcoplasmic reticulum and the evolution of the vertebrate

heart. Physiology 29, 456–469. https://doi.org/10.1152/physiol.00015.2014

Sirenko, O., Grimm, F.A., Ryan, K.R., Iwata, Y., Chiu, W.A., Parham, F., Wignall, J.A., Anson, B., Cromwell, E.F., Behl, M., Rusyn, I., Tice, R.R., 2017. In vitro cardiotoxicity assessment of environmental chemicals using an organotypic human induced pluripotent stem cell-derived model. Toxicol Appl Pharmacol 322, 60–74. https://doi.org/10.1016/j.taap.2017.02.020

Smith, C.L., Baek, S.T., Sung, C.Y., Tallquist, M.D., 2011. Epicardial-derived cell epithelial-to-mesenchymal transition and fate specification require PDGF receptor signaling. Circ Res 108. https://doi.org/10.1161/CIRCRESAHA.110.235531

Sprague, G.L., Sandvik, L.L., Brookins-Hendricks, M.J., Bickford, A.A., Bickford, A.A., 1981. Neurotoxicity of two organophosphorus ester flame retardants in hens. J Toxicol Environ Health 8, 507–518. https://doi.org/10.1080/15287398109530087

Sukparangsi, W., Thongphakdee, A., Intarapat, S., 2022. Avian Embryonic Culture: A Perspective of In Ovo to Ex Ovo and In Vitro Studies. Front Physiol 13. https://doi.org/10.3389/fphys.2022.903491

Sundkvist, A.M., Olofsson, U., Haglund, P., 2010. Organophosphorus flame retardants and plasticizers in marine and fresh water biota and in human milk. Journal of Environmental Monitoring 12, 943–951. https://doi.org/10.1039/b921910b

Tahara, Y., Obara, K., 2014. A novel shell-less culture system for chick embryos using a plastic film as culture vessels. Japan Poultry Science Association 51, 307–312. https://doi.org/10.2141/jpsa.0130043

Tang, D.D., Gerlach, B.D., 2017. The roles and regulation of the actin cytoskeleton, intermediate filaments and microtubules in smooth muscle cell migration. Respir Res 18. https://doi.org/10.1186/s12931-017-0544-7

Terada, R., Warren, S., Lu, J.T., Chien, K.R., Wessels, A., Kasahara, H., 2011. Ablation of Nkx2-5 at mid-embryonic stage results in premature lethality and cardiac malformation. Cardiovasc Res 91, 289–299. https://doi.org/10.1093/cvr/cvr037

Thiery, J.P., Acloque, H., Huang, R.Y.J., Nieto, M.A., 2009. Epithelial-Mesenchymal Transitions in Development and Disease. Cell 139, 871–890. https://doi.org/10.1016/j.cell.2009.11.007

Timmerman, L.A., Grego-Bessa, J., Raya, A., Bertrán, E., Pérez-Pomares, J.M., Díez, J., Aranda, S., Palomo, S., McCormick, F., Izpisúa-Belmonte, J.C., de La Pompa, J.L., 2004. Notch promotes epithelial-mesenchymal transition during cardiac development and oncogenic transformation. Genes Dev 18, 99–115. https://doi.org/10.1101/gad.276304

Tinevez, J.Y., Perry, N., Schindelin, J., Hoopes, G.M., Reynolds, G.D., Laplantine, E., Bednarek, S.Y., Shorte, S.L., Eliceiri, K.W., 2017. TrackMate: An open and extensible platform for single-particle tracking. Methods 115, 80–90. https://doi.org/10.1016/j.ymeth.2016.09.016

Tonomura, Y., Matsushima, S., Kashiwagi, E., Fujisawa, K., Takagi, S., Nishimura, Y., Fukushima, R., Torii, M., Matsubara, M., Matsubara, M., 2012. Biomarker panel of cardiac and skeletal muscle troponins, fatty acid binding protein 3 and myosin light chain 3 for the accurate diagnosis of cardiotoxicity and musculoskeletal toxicity in rats. Toxicology 302, 179–189. https://doi.org/10.1016/j.tox.2012.07.012

Trapnell, C., Pachter, L., Salzberg, S.L., 2009. TopHat: Discovering splice junctions with RNA-Seq. Bioinformatics 25, 1105–1111. https://doi.org/10.1093/bioinformatics/btp120

Trapnell, C., Williams, B.A., Pertea, G., Mortazavi, A., Kwan, G., van Baren, M.J., Salzberg, S.L., Wold, B.J., Pachter, L., 2010. Transcript assembly and quantification by RNA-Seq reveals unannotated transcripts and isoform switching during cell differentiation. Nat Biotechnol 28, 511–515. https://doi.org/10.1038/nbt.1621

van den Eede, N., Dirtu, A.C., Neels, H., Covaci, A., 2011. Analytical developments and preliminary assessment of human exposure to organophosphate flame retardants from indoor dust. Environ Int 37, 454–461. https://doi.org/10.1016/j.envint.2010.11.010

van der Ploeg, P., Uittenboogaard, A., Thijs, A.M.J., Westgeest, H.M., Boere, I.A., Lambrechts, S., van de Stolpe, A., Bekkers, R.L.M., Piek, J.M.J., 2021. The effectiveness of monotherapy with PI3K/AKT/mTOR pathway inhibitors in ovarian cancer: A meta-analysis. Gynecol Oncol 163, 433–444. https://doi.org/10.1016/j.ygyno.2021.07.008

van der Veen, I., de Boer, J., 2012. Phosphorus flame retardants: Properties, production, environmental occurrence, toxicity and analysis. Chemosphere 88, 1119–1153. https://doi.org/10.1016/j.chemosphere.2012.03.067

Verreault, J., Letcher, R.J., Gentes, M.L., Braune, B.M., 2018. Unusually high Deca-BDE concentrations and new flame retardants in a Canadian Arctic top predator, the glaucous gull. Science of the Total Environment 639, 977–987. https://doi.org/10.1016/j.scitotenv.2018.05.222

Vicente-Steijn, R., Kelder, T.P., Tertoolen, L.G., Wisse, L.J., Pijnappels, D.A., Poelmann, R.E., Schalij, M.J., DeRuiter, M.C., Gittenberger-De Groot, A.C., Jongbloed, M.R.M., 2017. RHOA-ROCK signalling is necessary for lateralization and differentiation of the developing sinoatrial node. Cardiovasc Res 113, 1186–1197. https://doi.org/10.1093/cvr/cvx104

Voiculescu, O., Bertocchini, F., Wolpert, L., Keller, R.E., Stern, C.D., 2007. The amniote primitive streak is defined by epithelial cell intercalation before gastrulation. Nature 449, 1049–1052. https://doi.org/10.1038/nature06211

Wagner, G.P., Kin, K., Lynch, V.J., 2012. Measurement of mRNA abundance using RNA-seq data: RPKM measure is inconsistent among samples. Theory in Biosciences 131, 281–285. https://doi.org/10.1007/s12064-012-0162-3

Wang, D., Eraslan, B., Wieland, T., Hallström, B., Hopf, T., Zolg, D.P., Zecha, J., Asplund, A., Li, L., Meng, C., Frejno, M., Schmidt, T., Schnatbaum, K., Wilhelm, M., Ponten, F., Uhlen, M., Gagneur, J., Hahne, H., Kuster, B., 2019. A deep proteome and transcriptome abundance atlas of 29 healthy human tissues. Mol Syst Biol 15. https://doi.org/10.15252/msb.20188503

Wang, H., Jing, C., Peng, H., Liu, S., Zhao, H., Zhang, W., Chen, X., Hu, F., 2022. Parental whole life-cycle exposure to tris (2-chloroethyl) phosphate (TCEP) disrupts embryonic development and thyroid system in zebrafish offspring. Ecotoxicol Environ Saf 248. https://doi.org/10.1016/j.ecoenv.2022.114313

Wang, Q., Liang, K., Liu, J., Yang, L., Guo, Y., Liu, C., Zhou, B., 2013. Exposure of zebrafish

embryos/larvae to TDCPP alters concentrations of thyroid hormones and transcriptions of genes involved in the hypothalamic-pituitary-thyroid axis. Aquatic Toxicology 126, 207–213. https://doi.org/10.1016/j.aquatox.2012.11.009

Wang, X., Zhu, Q., Yan, X., Wang, Y., Liao, C., Jiang, G., 2020. A review of organophosphate flame retardants and plasticizers in the environment: Analysis, occurrence and risk assessment. Science of the Total Environment. https://doi.org/10.1016/j.scitotenv.2020.139071

Weber, D.S., Taniyama, Y., Rocic, P., Seshiah, P.N., Dechert, M.A., Gerthoffer, W.T., Griendling, K.K., 2004. Phosphoinositide-dependent kinase 1 and p21-activated protein kinase mediate reactive oxygen species-dependent regulation of platelet-derived growth factor-induced smooth muscle cell migration. Circ Res 94, 1219–1226. https://doi.org/10.1161/01.RES.0000126848.54740.4A

Wei, G.L., Li, D.Q., Zhuo, M.N., Liao, Y.S., Xie, Z.Y., Guo, T.L., Li, J.J., Zhang, S.Y., Liang, Z.Q., 2015. Organophosphorus flame retardants and plasticizers: Sources, occurrence, toxicity and human exposure. Environmental Pollution 196, 29–46. https://doi.org/10.1016/j.envpol.2014.09.012

Wheelock, M.J., Shintani, Y., Maeda, M., Fukumoto, Y., Johnson, K.R., 2008. Cadherin switching. J Cell Sci. https://doi.org/10.1242/jcs.000455

WHO, 1998. Flame Retardants: Tris (chloropropyl) phosphate and tris (2-chloroethyl) phosphate. Environmental Health Criteria 209, 129.

Wilkinson, D.G., Bhatt, S., Herrmann, B.G., 1990. Expression pattern of the mouse T gene and its role in mesoderm formation. Nature 343, 657–659.

Wong, F., de Wit, C.A., Newton, S.R., 2018. Concentrations and variability of organophosphate esters, halogenated flame retardants, and polybrominated diphenyl ethers in indoor and outdoor air in Stockholm, Sweden. Environmental Pollution 240, 514–522. https://doi.org/10.1016/j.envpol.2018.04.086

Wu, Y., Su, G., Tang, S., Liu, W., Ma, Z., Zheng, X., Liu, H., Yu, H., 2017. The combination of in silico and in vivo approaches for the investigation of disrupting effects of tris (2-

chloroethyl) phosphate (TCEP) toward core receptors of zebrafish. Chemosphere 168, 122–130. https://doi.org/10.1016/j.chemosphere.2016.10.038

Xie, Z., Wang, P., Wang, X., Castro-Jiménez, J., Kallenborn, R., Liao, C., Mi, W., Lohmann, R., Vila-Costa, M., Dachs, J., Dachs, J., 2022. Organophosphate ester pollution in the oceans. Nat Rev Earth Environ 3, 309–322. https://doi.org/10.1038/s43017-022-00277-w

Yamashita, S., Miyagi, C., Carmany-Rampey, A., Shimizu, T., Fujii, R., Schier, A.F., 2002. Stat3 Controls Cell Movements during Zebrafish Gastrulation. Dev Cell 2, 363–375.

Yang, H.-T., Tweedie, D., Wang, S., Guia, A., Vinogradova, T., Bogdanov, K., Allen, P.D., Stern, M.D., Lakatta, E.G., Boheler, K.R., 2002. The ryanodine receptor modulates the spontaneous beating rate of cardiomyocytes during development. Proceedings of the National Academy of Sciences 99, 9225–9230.

Yang, J., Weinberg, R.A., 2008. Epithelial-Mesenchymal Transition: At the Crossroads of Development and Tumor Metastasis. Dev Cell. https://doi.org/10.1016/j.devcel.2008.05.009

Yu, G., Wang, L.G., Han, Y., He, Q.Y., 2012. ClusterProfiler: An R package for comparing biological themes among gene clusters. OMICS 16, 284–287. https://doi.org/10.1089/omi.2011.0118

Zhang, X., Sühring, R., Serodio, D., Bonnell, M., Sundin, N., Diamond, M.L., 2016. Novel flame retardants: Estimating the physical-chemical properties and environmental fate of 94 halogenated and organophosphate PBDE replacements. Chemosphere 144, 2401–2407. https://doi.org/10.1016/j.chemosphere.2015.11.017

Zhong, X., Qiu, J., Kang, J., Xing, X., Shi, X., Wei, Y., 2019. Exposure to tris(1,3-dichloro-2-propyl) phosphate (TDCPP) induces vascular toxicity through Nrf2-VEGF pathway in zebrafish and human umbilical vein endothelial cells. Environmental Pollution 247, 293–301. https://doi.org/10.1016/j.envpol.2018.12.066

Zhou, W., Gross, K.M., Kuperwasser, C., 2019. Molecular regulation of Snai2 in development and disease. J Cell Sci. https://doi.org/10.1242/jcs.235127

Zudaire, E., Gambardella, L., Kurcz, C., Vermeren, S., 2011. A computational tool for quantitative analysis of vascular networks. PLoS One 6. https://doi.org/10.1371/journal.pone.0027385